The Meson Theory of Nuclear Forces and Nuclear Structure

R. Machleidt*
Department of Physics, University of California,
Los Angeles, CA 90024, U.S.A.
and
Los Alamos National Laboratory, MS H850,
Los Alamos, NM 87545, U.S.A.

Prepared for
ADVANCES IN NUCLEAR PHYSICS, Vol. 19
(J. W. Negele and E. Vogt, eds.), Plenum Press, New York;
in press.

April 1988

*Present address: Department of Physics, University of Idaho,
Moscow, Idaho 83843, U. S. A.

Contents

Section 1

Introduction

Tradition cannot be inherited, and if you want it
you must obtain it by great labor.
— T. S. ELIOT, *Tradition and*
the Individual Talent

Nowadays it has become customary in nuclear physics to denote by 'tradition' the approach which considers nucleons and mesons as the relevant degrees of freedom. It is the purpose of this article to review this 'traditional' approach in the area of nuclear forces and their applications to nuclear structure.

The other important sector of nuclear physics in which mesons have revealed their reality, is electron scattering. Meson-exchange currents are indispensable for the quantitative explanation of the electromagnetic properties of nuclei. We will not review this aspect here: it is a comprehensive topic by itself and excellent overviews do exist in the literature (RW 79, FP 87).

The present time appears quite appropriate for a review of the subject. The relevance of subhadronic degrees of freedom for nuclear physics has become a central issue. Therefore, it is important to know how successful the traditional approach really is, and if there are clear indications for its limitations. We will repeatedly refer to this question in the course of the article.

The concret purpose of this review is essentially twofold. One intention is to provide a broad introdution into the field of nuclear forces and the nuclear many body problem with particular emphasis on nuclear matter. On

the other hand, we will also present and discuss the latest results from these two important areas of nuclear physics, and point out the open questions future research should devote to.

Section 2

Historical Overview

History illumines reality, vitalises memory,
provides guidance in daily life.
— CICERO, *De Oratore*

In this section we shall review the history of nuclear forces. Actually, we will do it with more care than subsequent sections require it. It is just an interesting piece of scientific history of our century which deserves some attention.

2.1 The "Hypothetical" Period

The atomic nucleus was discovered by Rutherford in the year of 1911 (Rut 11). The nuclear mass was investigated by Thompson (Tho 13), who also discovered the existence of isotopes. The first nuclear models assumed that the nucleus consisted of A protons and $A - Z$ electrons which seemed to explain the mass number A and the (positive) charge number Z. Apart from the question of how exactly such an object could be kept together by electrostatic forces only, particularly when using quantum mechanics, a clear contradiction to that model occured when it was found that the ^{14}N nucleus obeyed Bose statistics (HH 29, EO 31). According to the above model, however, ^{14}N would consist of 14 protons and 7 electrons which should yield a half-integer total spin and make this nucleus a fermion. In 1932, the neutron was discovered by Chadwick (Cha 32). This suggested that the neutron and the proton were the fundamental constituents of nuclei. On that basis, it appeared compelling to assume the existence of a new

force acting between neutron and proton to bind the nucleus: the *nuclear force* or the *strong force*. Since then, one central problem in physics has been to understand the nature of this force.

A few qualitative features concerning nuclear forces were learned from the binding energies of (particularly, light) nuclei, from which Wigner (Wig 33) concluded that the nuclear force had to be of short range and strong within that range. First theoretical attempts by Heisenberg (Hei 32) and Majorana (Maj 33) introduced the concept of so-called exchange forces which could explain nuclear saturation. Also experiment made further progress: The binding energy of the deuteron, the only two-nucleon bound state, was measured by Chadwick and Goldhaber in 1934 (CG 34). Proton-proton scattering experiments developed rapidly up to about 1 MeV laboratory energy during the 1930's (THH 36). They indicated that the new strong force also acts between two protons, leading to the hypothesis of the *charge independence* of nuclear forces (BCP 36, BF 36). A thorough account of the knowledge and the status of nuclear physics in those early years is given in the excellent review article by Bethe and Bacher (BB 36).

The first more fundamental idea for the origin of the nuclear force was created in 1935. Yukawa (Yuk 35) suggested that a new particle with an "intermediate" mass (compared to the other "elementary particles" known at that time, namely neutron, proton and electron), eventually called *meson* (Bha 39), could be responsible for the interaction energy between proton and neutron. The massive character of the particle to be exchanged between the nuclear constituents would furnish the resulting force with a finite range desirable to account for nuclear saturation. Yukawa's original theory applied to charged scalar bosons (in classical field theory) acting between proton and neutron only, since it was fashioned after Fermi's theory of β decay (Fer 34) in which a charge transfer is involved. Shortly after, Yukawa reconsidered his proposal in the framework of quantized field theory (Yuk 37, YS 37, Yuk+ 38). In the following years, variations and extensions were worked out by him and collaborators (YST 38, Sup 55).

What nobody could possibly foresee at that time: the stage for a half-century struggle of hope and desperation was set. The well-known fundamental interactions in those days were the Coulomb and the gravitational force both having mathematically a very simple form. Naturally, one expected something comparably simple for the nuclear potential, for example just one Yukawa function: $\propto \exp(-\mu r)/r$ (with r the distance between the

two nucleons and $\mu = mc/\hbar$ where m denotes the mass of the exchanged particle). However, even just phenomenologically, the nuclear force shall turn out to be much more complicated — mainly because of its dependence on the spins of the two interacting nucleons. In addition, field theory soon ran into fundamental mathematical difficulties. Both aspects have been seemingly never-ending sources of oppressing problems and startling surprises which, together with some great discoveries and successes, give the history of nuclear forces the touch of a detective novel.

It started encouragingly: In 1937 a "meson" was found in cosmic ray, the muon (NA 37, SS 37). It was interpreted (as we know, incorrectly) as the particle predicted by Yukawa, particularly since its mass ($\approx$ 106 MeV) appeared about right with regard to the range of the nuclear force. Therefore, this discovery aroused considerable interest in Yukawa's idea — and thus, the misinterpretation had a lucky side. Kemmer (Kem 38a) felt inspired to suggest a rich variety of possible meson fields including pseudoscalar, axial-vector and tensor, after Proca, in 1936, had considered already vector fields (Pro 36). Also a "symmetric" theory (the ancient term for a theory using iso-vector bosons, i. e. bosons with three charge states: +, neutral and −) was proposed by Kemmer (Kem 38b) and Bhabha (Bha 38) to account for the known hypothesis of charge independence (see also Yukawa *et al.*, Yuk+ 38). This suggestion was made in spite of the fact that experimentally only charged "mesons" (namely μ^+ and μ^-) were known. In lowest order, these cannot be exchanged between like nucleons and therefore seriously violate charge independence. It was also suggested that the two-meson exchange contribution could counterbalance this substantial inequality. Moreover, in 1939, Kemmer (Kem 39) proposed a new, higher dimensional meson field equation which has experienced some revival in recent times (Cla 86).

Wick (Wic 38) in 1938 provided a plastic picture for how to understand in concret terms the relationship between the mass m of a particle and the range R of the force created by its exchange. As the spontaneous process of "virtual" particle creation violates energy conservation, Heisenberg's uncertainty relation applies:

$$\Delta E \cdot \Delta t \approx \hbar \tag{2.1}$$

where $\Delta E = mc^2$ is the energy required to create the particle neglecting kinetic energy. If the particle moves with at most the speed of light c for a

time $\Delta t \approx R/c$, one obtains for the range

$$R \approx \hbar c/mc^2 \tag{2.2}$$

which is just the Compton wave lenght of the particle. The exponential of a Yukawa function has dropped to $1/e$ at that distance lending further support to the above range estimate. To obtain a range of about 2 fm the mass has to be roughly 100 MeV ($\hbar c \approx 197$ MeV fm).

The discovery of the quadrupole moment and the measurement of the magnetic moment of the deuteron by Rabi and coworkers in 1939 (Kel+ 39, Kel+ 40) motivated immediately more detailed theoretical investigations and the development of more sophisticated models. Thus, it was realized that (isovector) vector fields create a tensor force giving rise to a quadrupolmoment in the deuteron — but with the wrong sign as compared to experiment. The problem was soon overcome by also including pseudoscalar fields. In these "mixed meson theories"[1], in which both pseudoscalar and vector mesons were assumed (with either equal masses as in the work of Møller and Rosenfeld (MR 40) or with a heavier vector boson, see Schwinger (Sch 42)) the problematic r^{-3} singularity in the tensor force was removed. With the Schwinger force about 1/3 of the empirical deuteron quadrupolmoment could be reproduced (JH 44). With regard to the singularity problem, Bethe (Bet 40; see also Rarita and Schwinger, RS 41a) suggested already in 1940 the use of a "cut-off" for small distances r, which could be interpreted as assuming extended meson sources (extended nucleons). This idea and some problems it raised with regard to the relativistic invariance of the theory were examined by Pauli and others. An account of this question as well as many other important issues in the meson theory of those days, like the "strong couplings theory", can be found in the lectures given by Pauli at the MIT in Fall 1944 (Pau 46). Most interestingly, Pauli concluded from the fact that the pseudoscalar "symmetric" theory predicted the right sign for the deuteron quadrupolmoment, that this was most likely the correct theory — long before the pion was found and its spin and parity determined. Also quite early it was recognized, particularly by Breit (Bre 37, BS 38) and Rosenfeld (Ros 45), that vector and scalar fields create a spin-orbit force. Empirical evidence for this was seen in the spectra of light nuclei. Rosenfeld in 1948 (Ros 48):

[1]Kind of early forerunners of the one-boson-exchange potentials, which shall become very fashionable twenty years later.

> The occurence of a rather large spin-orbit coupling in ^5He may be regarded as an indication of the existence of mesons of spin one.

For further details about this "hypothetical" time in meson theory (before the discovery of the pion), we refer the interested reader to the above-mentioned lectures by Pauli (Pau 46) and the field theory text by Wenzel (Wen 49), which offers an informative chapter on this topic. The nuclear physics book by Rosenfeld published in 1948 (Ros 48) contains also many contemporary details.

Experiment finishes this first period: In 1947 Conversi, Pancini, and Piccioni (CPP 47) showed that the muon does not interact strongly with nuclei (and therefore, according to the notation introduced in the early 60's, it is not a meson; it is a *lepton*). That same year, a (real!) meson with a mass of about 140 MeV, the pion, was found in cosmic ray by Occhialini and collaborators (Occ+ 47, LOP 47), and shortly after also in the Berkely cyclotron laboratory (GL 48). In 1949, the Swedish Academy of Science awarded the Nobel prize to Yukawa.

2.2 The Pion as *the* Quantum

Quite understandably, the new reality of a strongly interacting meson motivated vigorous theoretical efforts to describe the nuclear force, now, by *the pion only*. This became the program of the 1950's. Naturally, it started with high expectations and great enthusiasm (but should end in deep disappointment). The success of the renormalization program had just rehabilitated field theory. The pion appeared to be *the* quantum for the strong interaction, in analogy to the role played by the photon in quantum electrodynamics (QED). Considering the overwhelming quantitative successes of QED, there were no limits on the expectations for the strong interaction theory with the pion.

The works of Japanese physicists deserve our special attention for this period, as — in the tradition of Yukawa — they probably contributed the most to the field and, at the same time, may have also been ignored the most — outside their country. In 1951, Taketani, Nakamura, and Sasaki (TNS 51) presented their historic suggestion to subdivide the nuclear force into three regions. The far-sighted character of this proposition becomes evident from the fact that nowadays, particularly in view of "QCD-inspired"

approaches to the nuclear force[2], this subdivision is still physically most meaningful. TNS distinguish a *classical* (long-range, $r \gtrsim 2$ fm; r denotes the distance between the centres of two nucleons), a *dynamical* (intermediate range, 1 fm $\lesssim r \lesssim 2$ fm), and a *phenomenological* or *core* (short-range, $r \lesssim 1$ fm) region. In the classical region the longest range part of the potential, namely, the one-pion-exchange (OPE) is dominant (the pion having the smallest mass of all mesons or multi-pion configurations). In the intermediate range the two-pion-exchange (TPE) is most important, although havier mesons may also become relevant. Finally, in the core region many different processes play a role. There are multi-pion exchanges, heavy mesons of various kinds and — from today's point of view — genuin quark-gluon exchanges. This classification has been of utmost theoretical and practical importance. It allows a step-by-step exploration of the two-nucleon interaction and permits, if necessary and suggested by theory, a different derivation for different parts of the force. Thus it is possible to first calculate the longer range parts of the potential, and correlate the results with empirical information prevailingly sensitive to just that region. In this way, the whole problem — with all its oppressive complexity — does not have to be faced at once. Also, in the light of TNS, the use of extended sources (cut-offs) does not appear so problematic anymore.

In the decade under consideration, the one-pion-exchange became experimentally well established as the long range part of the nuclear force (Sup 56). The evidence came from the analysis of NN scattering data and the deuteron. Speaking in dispersion-theoretic terms (Che 61), the NN scattering amplitude in the non-physical region of the complex $\cos\Theta_{cm}$ plane (with Θ_{cm} the scattering angle in the center-of-mass system) has two symmetrically located poles associated with contributions from one-pion intermediate states. The experimental data is extrapolated to these poles to yield the pion-nucleon coupling constant. This procedure can be applied both near 0^0 and 180^0 for the scattering angle Θ_{cm}. The πN coupling constant obtained in this way agreed with that known from πN scattering (Czi+ 59). An equivalent procedure can be applied in the framework of the (partial-wave) phase-shift analysis. For sufficiently high orbital angular momentum (corresponding to large inter-nucleonic distances) OPE only is assumed. It turned out that the χ^2 for the phase-shift solutions

[2]For an recent review of quarks in nuclear physics see e. g. C. W. Wong (Won 86).

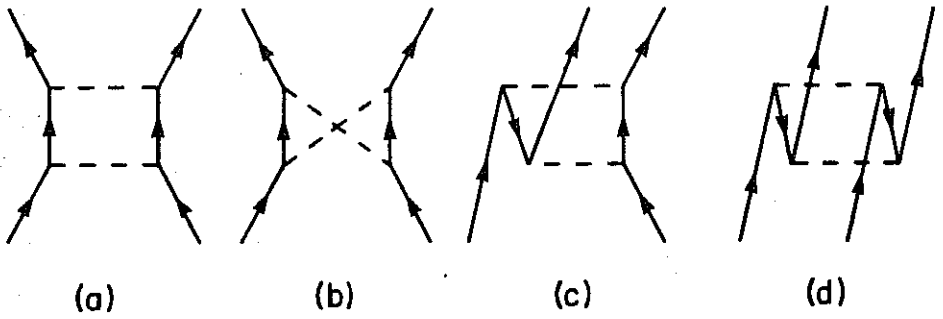

Figure 2.1: **Some two-pion-exchange contributions to the NN interaction. (a) is a box diagram, (b) a crossed box; (c) and (d) contain virtual pairs.** Pair diagrams with crossed pion-exchange are not shown. Full lines denote nucleons, dashed lines pions. The underlying time axis is vertical, pointing upwards into the future.

is a minimum for the correct pion mass and coupling constant (as known from πN scattering) (Bre+ 60, Bre 62). In the case of the deuteron, the quadrupole moment can be well explained by the OPE potential (Iwa+ 56, Sup 56, Won 59, GK 62). Furthermore, the asymptotic D/S state ratio of the deuteron wave functions provides convincing evidence for the OPE tail (Iwa+ 55 and 56, Won 59). In modern times, the different pieces of evidence for the one-pion-exchange have been re-examined by Ericson and Rosa-Clot (ER 83, Eri 84, ER 85). They essentially confirm the arguments used in the olden days, summarized in this paragraph; however, due to the much higher accuracy of the data available in the 1980's, the points can be made much more precise.

As the one-pion-exchange contribution to the nuclear force combined all the pleasant features a physicist may wish from a theory — such as easy to evaluate and most satisfactory in explaining data — so did the two-pion-exchange evolve in an opposite way. It is painful to evaluate and for a long time it had not even been doing well in correlating data. The calculations are not only extremely complicated and tedious, but, in addition, they were beset for a long time by a number of serious ambiguities, which led to quantitatively rather different results causing serious controversies. The many efforts of pion-theoretical potentials of the 1950's are usually

divided into two groups: The Taketani-Machida-Onuma (TMO 52) and the Brueckner-Watson (BW 53) type. In the former case an S-Matrix was evaluated directly from meson field theory, from which in turn a potential was derived. In contrast, the BW method was based on an expansion in the particle number and derived a potential directly. The main differences between the two approaches were that the box-diagrams and the pair terms (i. e. contributions with nucleon-antinucleon intermediate states, see Fig. 2.1) were always included in TMO whereas BW excluded the box from the beginning and could at will leave out the pair terms. For this *pair suppression* there is evidence from low energy πN scattering in S-waves where the pair term leads to by about two orders of magnitude too large a scattering length. Therefore it was suggested that the suppression of virtual pairs might be a general feature of meson theory (BGG 53). This will be put on a better footing by the introduction of chiral symmetry in the next decade (GL 60, Wei 67, Bro 79). Brueckner and Watson also found an almost exact cancelation of the one-pair and the two-pair contribution to the NN interaction (Fig. 2.1c and d). A further source of discrepancies in the pion theories of the 1950's were ambiguities in the subtraction of the iterated OPE, necessary to extract a potential (Kle 58). Apart from a general uncertainty in the results, the spin-orbit force derived from TPE turned out to be too weak — by one order of magnitude — than experimentally needed (HM 62).

A quote by Goldberger from 1960 (Gol 60) may draw the balance for this part of the decade:

> There are few problems in nuclear theoretical physics which have attracted more attention than that of trying to determine the fundamental interaction between two nucleons. It is also true that scarcely ever has the world of physics owed so little to so many. In general, in surveying the field, one is oppressed by the unbelievable confusion and conflict that exists. It is hard to believe that many of the authors are talking about the same problem or, in fact, that they know what the problem is.

The interested reader will find an excellent review of the period of the 1950's in the book by Moravcsik (Mor 63) and in the articles by Phillips (Phi 59) and Hulthén and Sugawara (HS 57); a more comprehensive account is given in Bethe and de Hoffmann (BH 55). The enormous work by Japanese physicists is summarized in two *Supplements* (Sup 56, Sup 67).

Fortunately, there was also another line of research on the nuclear force during the 1950's; and this line, developing in almost complete independence from the theoretical efforts discussed so far, was more successful. The goals were more modest — it was the attempt to give a simple phenomenological description of the nuclear potential.

The basis for the success of the phenomenological line of research on the nuclear force was the substantial progress in the NN scattering experiments of this period. From the properties of nuclear many-body systems precise and detailed information regarding the force cannot be gained. Effective range theory (Bet 49) had made clear that from low energy data one cannot learn much more then what can be parametrized in terms of two numbers, the scattering lenght and the effective range. Therefore, it was obvious that high energy data were required to obtain further insight into the nature of the nuclear force. Moreover, differential cross sections, even at high energy, are good only for a few rather basic and qualitative conclusions.[3] Due to the important spin dependence of the NN interaction, data for many other observables are needed to specify the scattering amplitude (WA 52, Wol 56). In 1954, a first measurement of the polarization by Oxley *et al.* (OCR 54) at Rochester at about 200 MeV laboratory (lab.) energy showed a large result. Fermi (Fer 54) related the strenght of the measured polarization successfully to the spin-orbit coupling postulated in the nuclear shell model of Mayer and Jensen (May 49, HJS 49, MJ 55). *Spin*, the relevance of which was well appreciated and well understood in atomic physics since the 1920's, finally became a broad issue in nuclear physics — to the great benefit of the field. Because of technological advances, also the so-called triple scattering experiments, necessary to measure the more sophisticated spin observables, became feasible around 1957. Thus, in a very extensive set of experiments with polarized protons at 315 MeV lab. energy, Chamberlain and coworkers (Cha+ 57) made measurements on proton-proton scattering at the Berkely 184-inch cyclotron. For the first time, a complete set of observables was measured. The phase shift analysis

[3] Jastrow in 1951 (Jas 51) conjectured from the observation that the differential cross sections of proton-proton (pp) scattering at 340 MeV in the laboratory system (Fig. 5.12) showed an isotropic character that the nuclear force may have a hard core. The symmetry of the angular distribution about 90 degrees observed in neutron-proton (np) differential cross sections (Fig. 5.11) may be attributed to exchange forces of Majorana type in the NN interaction (Serber force) (CH 50).

based essentially on these data performed by Stapp *et al.* (SYM 57) has been of great importance to subsequent developments of phenomenological potentials.

The basic aim of a potential description of the two-nucleon interaction is twofold. One is to provide an economical summary of the data for comparison with potential-like results from theory (e. g. meson theory). The other aim of a phenomenological potential is to serve as an input for nuclear structure calculations.

The most general form a non-relativistic potential may assume, when taking also the spin degree of freedom of the nucleons into account, can be derived from invariance considerations (EW 41, OM 58, GT 60). Restricting to at most linear dependence on the relative momentum of the two nucleons, $\mathbf{p}$, it consists of a *central, spin-spin, tensor, and spin-orbit* term. Permitting also quadratic momentum dependence, adds a *quadratic spin-orbit* term (OM 58). To these operators a function of $\mathbf{r}^2$, $\mathbf{p}^2$ and $\mathbf{L}^2$ is attached (with $\mathbf{L}$ denoting the orbital angular momentum operator). This operator structure — either the more restricted or the extended one — has in general been adopted since for any construction of a non-relativistic NN potential. The attempt to fit the NN scattering data with just the first three terms failed (GCT 57). The next attempt, which included a spin-orbit term, was quite successful.[4] This was the first quantitative NN potential ever constructed — known by the names of Gammel and Thaler, published in 1957 (GT 57). This potential used a so-called hard core (infinite repulsion) at small distances ($r \leq 0.4$ fm) to account for the trend of the $^1S_0$ phase-shift turning negative for lab. energies above 250 MeV. The spin-orbit force turned out to be necessary to describe the observed polarization data and, speaking in terms of phase-shifts, the splittings of the different triplet P-waves. The short ranged character of this part of the force became evident from the fact that F phase shifts do not show much of that splitting anymore. The important role a spin-orbit force may play in nuclei was foreseen already in the late 1930's by Breit (Bre 37, BS 38) and seriously assumed in the late 1940's by Rosenfeld (Ros 48), Mayer (May 49) and Jensen (HJS 49, MJ 55). Another, semi-quantitative, potential was constructed by Signell and Marshak (SM 57, SZM 57) who also used some input from the pion-theoretic potential derived by Gartenhaus (Gar

[4] In 1950, Case and Pais (CP 50) had proposed that a spin-orbit term might help the fit to the high energy pp differential cross section data.

55). The early period of phenomenological studies has been reviewed by Gammel and Thaler (GT 60).

These phenomenological type of potentials have been improved over the years. Other examples for the hard-core type are those constructed by Hamada and Johnston (HJ 62) and by the YALE group (Las+ 62). Both use the five term form mentioned. These models employ a one-pion tail and therefore reproduce the deuteron properties accurately. In the mid 1960's R. V. Reid (Rei 68) developed hard- and soft-core potentials. One of his soft-core versions became the most applied potential in nuclear structure physics in the 1970's. Phenomenological potentials typically use about 30–50 fit parameters.

A quote from an article entitled *What Holds the Nucleus Together* by Hans A. Bethe published in the Scientific American in 1953 (Bet 53) characterises and finishes this decade:

> In the past quarter century physicists have devoted a huge amount of experimantation and mental labor to this problem — probably more man-hours than have been given to any other scientific question in the history of mankind.

Note that another quarter century is still to come, in which the efforts were larger by about one order of magnitude.

2.3 "Dispersive" Approaches

Let us now return to the meson-theoretic work. We are in the year of 1960. This date was characterized by essentially two facts: The failure of the pion field-theoretic program, on the one hand, and a rich phenomenological experience with the nucleon-nucleon interaction (e. g. short-range repulsion and spin-orbit force), on the other. Not surprisingly, this led Breit (Bre 60a,b) and others to revive the old idea of vector-meson exchange (BS 38, Ros 48), which predicts both features just mentioned. Further support came from the electromagnetic properties of the nucleon. Nambu (Nam 57), Sakurai (Sak 60a,b,c) and Frazer and Fulco (FF 59, FF 60) conjectured that vector bosons may play the dominant role in explaining the nuclear form factor. Their supposition was soon confirmed: In 1961, the ρ meson was discovered at Brookhaven in the $\pi^- p \to \pi\pi N$ reaction (Erw+ 61), and

the ω meson was found at Berkeley in $\bar{p}p$ annihilation (Mag+ 61, Käl 64). Both are spin one bosons, the ρ being a 2π and the ω a 3π resonance, with masses around 770–780 MeV.

The discovery of heavy mesons broke the dead-lock situation in the meson theory of the nucleon-nucleon interaction. The first products of the new developments were the one-boson-exchange (OBE) models. These models are based on the old Yukawa idea that the nuclear force is meson mediated. However, one tries to take advantage of the observation that two or several mesons as a group tend to behave as if they formed a single particle with a definite mass and definite intrinsic quantum numbers; in other words, due to the fact that there is also a strong interaction between all mesons, they are correlated or even form a resonance. In fact, it is assumed that the uncorrelated multi-pion exchange is negligible (apart from iterative contributions generated by the unitarizing equation). Note that, in contrast, the calculations of the 1950's were concerned only with the uncorrelated multi-pion exchange.

There are also some very pragmatic reason for the OBE model. First, the evaluation of one-particle exchange processes is essentially straightforward, quite contrary to multi-particle exchanges, as we saw from the history of the 1950's. Second, within the OBE model the NN data can be described with very few parameters (in the order of 10, in contrast to phenomenological potentials which typically need about 30–50). Since the OBE model parameters are meson-nucleon coupling constants and cutoffs, a physical meaning can be attributed to them, at least in principal.

All known OBE models include a large contribution from one or two isoscalar scalar bosons with their mass in the area of 400 to 800 MeV. They provide the necessary intermediate range attraction of the nuclear force. These bosons are supposed to represent 2π-S-wave resonances. Indeed, during the 1960's and the early 70's the Particle Data Group listed in its meson table an alleged isoscalar scalar particle (called σ or ϵ) in the above mass range (PDG 74). This low mass ϵ disappeared from the table in 1976 (PDG 76) in favour of an $\epsilon(1200)$ (which due to its large mass is not useful for providing *intermediate* range attraction). Thus, on this point of the OBE model confirmation did not happen. However, the quantitative success of the model may be understood as an indication that uncorrelated and correlated 2π exchange is in part well simulated by (fictitious) scalar particle exchange. Still, from a more fundamental theoretical view point

this is not satisfactory, and we will come back to this point later.

First OBE potentials (OBEP) were developed by Japanese theorists (HLM 61, Saw+ 62, Sup 67), Bryan and coworkers (BDR 63, BS 64), Wong and collaborators (SW 63, SW 65), and A. E. S. Green and associates (GS 65, GS 67). The improvement of the OBE model continued into the 1970's. In fact, OBEP which use realistic coupling constants and which *accurately* describe all NN scattering data at low energy and the deuteron properties were not provided until the mid 1970's. Such potentials, represented in configuration space (r-space), were constructed by the Nijmegen group (NRS 78) and Sprung and coworkers (TS 73, TRS 75). Finally, the OBE concept was substantially improved by considering three-dimensional relativistic equations based upon the Bethe-Salpeter equation (SB 51) and by working in momentum space to avoid the approximations necessary to obtain analytic r-space expressions (Appendix A.3). Work along this line was done by Schierholz (Sch 72), Thompson and others (Tho 70, GTG 71, BG 72), and the Bonn group (Erk 74, HM 75, HM 76). Finally, Tjon and collaborators solved the full four-dimensional Bethe-Salpeter equation in the ladder approximation (FT 75, FT 77, FT 80, ZT 81).

The work up to 1971 in the field under consideration is well reviewed by Moravcsik (Mor 72) with a complete list of the bibliography of the 1960's. Other good summary articles are the *Supplement* (Sup 67) (in particular the contribution by S. Ogawa *et al.*) and the Proceedings of the First International Conference on the Nucleon-Nulceon Interaction held in Gainsville, Florida, in 1967 (Gre 67), which also reflects some of the enthusiasm of the early OBEP-years.

As mentioned, quite apart from the quantitative success of the OBEP in fitting the NN data, conceptually such models cannot be accepted as a comprehensive theory, as it is hard to believe that the uncorrelated multiparticle exchanges should be totally negligible. The longest range component of such exchanges, and therefore the most important of that kind, is the two-pion exchange (TPE). How to take the TPE more accurately or even "completely" into account, was the other main topic of the 1960's.

Of course, this topic was not new. It was one of the main goals of the 1950's, and it failed at that time. In restrospect, and with the experience aquired during the 1960's, we now understand the reason for this failure: the old program did not consider correlations between the exchanged pions or multi-pion resonances, which — as the OBE model has demonstrated

— play a crucial role. Naturally the new goal was to include all correlated and uncorrelated multi-particle exchanges, particularly for the case of two pions.

In principal, there are two conceptually rather different ways to actually calculate these contributions: by field theory and by dispersion relations. It may be psychologically quite understandable that after the failure of the field-theoretic program of the previous decade, there was not much motivation to try this again. Therefore, during this period there is little work along this line (Mac 67). Fortunately, field theory was not dead for ever and will revive later in the light of a new view, namely, as an effective (non-fundamental) theory.

A completely alternative approach to multi-particle exchange was now pursued which has become known as *dispersion theory* (Che+ 57, Che 61, Man 58, Man 62). As this new approach was born out of a frustration with field theory — with its formidable problems of renormalization, convergence, selection of diagrams (e. g. pair-terms or not), and how to develop a potential concept —, dispersion theory attempts to avoid these shortcomings from the beginning by trying to deal with physically observable quantities only. Lagrangians, Hamiltonians and potentials do not occur anymore. Instead, the new theory deals directly with reaction amplitudes. In fact, it relates different measurable reactions to each other. In this way it provides a framework for a consistency check between such different processes as NN, πN and electron-nucleon scattering (nucleon electromagnetic form factors).

The principal framework of dispersion relations is based on three fundamental assumptions: causality, unitarity, and crossing symmetry. From the first the analyticity of the reaction amplitude is concluded. The third allows to relate processes which differ from each other only by the interchange of some incoming and outgoing particles of the reaction. Due to analyticity, one-particle exchange appears as a pole in the scattering amplitude. This fact can be exploited to extract empirical information about meson masses and, particularly, meson-nucleon coupling constants.

In the early 1960's, Amati, Leader, and Vitale (ALV 60, ALV 63) started work along this line into which soon many groups got involved (Gre 67, Sup 67). An idea of the difficulty of this approach can be obtained from the fact that it took until the end of the decade for quantitative results (Bin 71, BB 71, CDR 72, Vin+ 73). These results showed that, for the intermediate

range, a realistic nuclear potential can be derived using dispersion relations and empirical information from πN and $\pi\pi$ scattering as input. Yet, these efforts were still far from constructing a full, quantitative nuclear potential.

2.4 A Tale of Two Cities

In the course of the 1960's the experimental program of the measurement of NN elastic scattering observables was pursued extensively by many accelerators throughout the world. As a result, by the end of the decade, the Livermore group could come up with a phase-shift analysis of NN scattering up to 425 MeV lab. energy of high quality (MAW 69). This provided an important presupposition for the theoretical work of the 1970's, during which one was finally concerned with the ultimate goal of providing an absolutely quantitative nuclear force which is based on meson theory as much as possible. The work proceeded along the two lines discussed earlier: dispersion theory and field theory. Both approaches finally produced a very quantitative model. Accidentally, most of this work was done in two Central European capitals: Paris and Bonn.

Let us first summarize the final dispersion theoretic efforts. In continuation of the work of Chemtob *et al.* (CDR 72), the Stony Brook Group (JRV 75) constructed a potential in which the dispersion theoretic result for the 2π-exchange was complemented by one-π and one-ω exchange. For short distances the potential was regularized by the eikonal form factor derived by Woloshyn and Jackson (WJ 72). The fit to the NN scattering phase-shifts was semi-quantitative. At about the same time, the Paris group produced a potential based on rather similar theoretical input (Lac+ 75). In the Paris case, the short range part of the NN interaction was treated by an energy-dependent repulsive square-shaped cut-off. For the 2π-exchange contribution to the nuclear potential both groups achieved even quantitative agreement. Further refinements and a convenient representation of the potential was left to the Paris group. Their final version, published in 1980, is parametrized in terms of static Yukawa functions of multiples of the pion mass (Lac+ 80).

Reviews about the dispersion theoretic approach to the nuclear force have been given by Vinh Mau (Vin 79) and by Brown and Jackson (BJ 76). The latter reference contains also many mathematical details.

Finally, let us turn to the field-theoretic attempts. After a decade of prevailing abstinence (see however Mac 67), for reasons explained earlier, the field-theoretic approach was revived by the work of Lomon and Partovi (PL 70). They evaluated the 2π-exchange Feynman diagrams with nucleons in the framework of the relativistic three-dimensional reduction of the Bethe-Salpeter equation (SB 51) proposed by Blankenbecler and Sugar (BS 66). It is a non-static approach to the 2π exchange. The old ambiguity of how to construct and subtract the iterated one-pion-exchange when defining a potential was absent in this work (compare Section 2.2 and TMO 52, BW 53). In subsequent work Lomon and coworkers (PL 72, Lom 76, Lom 80a) studied as well the correlated 2π S-wave contribution. A field-theoretic model similar to that of Lomon and coworkers was developed by Nutt and Wilets (NW 75, Nut 76). They suppressed the pair terms, which were included by Lomon *et al.*.

However, the models discussed so far, left out contributions that are of substantial importance, like meson-nucleon resonances in intermediate states (SH 68) as well as three- and four-pion exchanges. In the mid 1970's the Bonn group started a program directed towards the evaluation of multi-pion exchange diagrams including nucleon resonances. This comprehensive field-theoretic program took about a decade. Step by step, the Bonn group computed all 2π-exchange diagrams including those with virtual Δ-isobar excitations (HM 77, Hol+ 79, Hol+ 81, BHM 81) and, finally, also the relevant diagrams of 3π- and 4π-exchange (Hol+ 78, HM 81, BHM 84). One of the important findings are that, apart from the usual iterative diagrams, the crossed meson-exchanges and the diagrams of π *and* ρ exchange are particularly important for a quantitative description of the NN scattering data and the deuteron properties. The final Bonn model (MHE 87) turns out to be highly quantitative in nature, in spite of the fact that it employs only about a dozen parameters, which — as meson-baryon coupling constants and form factors — have a physical meaning.

There are several reasons for and advantages to a field-theoretic model. First, it determines the off-shell behaviour of the interaction in a well-defined way. As dispersion theory deals with reaction amplitudes, which are always on-shell, the off-shell behaviour remains undetermined in such an approach and is left to guess work or arguments of simplicity (e. g. static Yukawa terms). Furthermore, the set of diagrams provided by a field theoretic model forms a sound basis for a consistent generalization

to many-body forces which may be of interest in the nuclear many-body problem. The evaluation of meson-exchange current corrections to the electromagnetic properties of nuclei requires a precise knowledge of the meson-exchange processes between the nucleons. Field-theoretic models also allow for a consistent extension to intermediate energies including meson production.

2.5 More Recent Developments

As mentioned, in the olden days, meson theory was thought of as a fundamental theory with the mesons being the field quanta in analogy to the photon in QED. Since some time we know that this is not true. The present candidate for a fundamental theory of strong interactions is quantum chromodynamics (QCD) in which the gluons (massless vector bosons like the photon) are the field quanta exchanged between quarks (Ynd 83). On that basis, meson "theory" can be understood as an effective description of quark-gluon dynamics in the low energy regime. Afterall, note that mesons and baryons are the particles seen in experiment. There are theoretical attempts to connect the fundamental theory of QCD with the very successful meson picture at low energy. The Skyrmion model is an example (ZB 86, MZ 86). In other attempts, one tries to derive the NN interaction more or less directly from QCD (see Won 86 for an overview). At present, the predictions are more of a qualitative kind. For quantitative results, the one-pion and two-pion contributions have to be added by hand, as they do not emerge naturally out of QCD inspired models. Knowing that π and 2π are the most important parts of the nuclear force, this defect of present quark model calculations is serious. On the other hand, the short range repulsion seems to arise naturally in a quark model. However, this does not necessarily imply that vector boson exchange has become redundant; omega exchange is equally important for providing the indispensable spin-orbit force, which is not predicted by quark models to the sufficient amount and, in fact, turns out to be unwanted for the baryon spectrum. Quark bag models use typically bag radii in the order of 0.8–1.2 fm (Tho 83). If meson exchanges are cut down at that distance, a quantitative description of the NN data is impossible. In particular data (like the deuteron properties), which can almost exclusively be explained by one-pion-exchange, can by no

means be described with such an extended πNN vertex form factor (Eri 84; and Section 4.2).

Since the mid 1970's, particularly due to the experimental work at the so-called meson factories, a large amount of precision data on NN scattering at intermediate energies (i. e. up to 1–2 GeV in the laboratory frame) has accumulated. These data reveal a spin dependence of NN reactions even richer than at low energies (Bug 85). The inelasticities in that energy range can essentially be explained by the Δ isobar, which nicely complements the findings at low energy where the Δ is indispensable for the realistic explanation of the intermediate range attraction as supplied by the 2π exchange. Most amazingly, at even higher energies (several GeV), at which plausible arguments suggest the disappearance of any pronounced spin effects, large polarizations were measured (FK 81, Kri 85). These recent experimental findings in NN scattering at several GeV present a challenge to the nuclear theoretican of today.

Section 3

Pedagogical Introduction

In this section we will start to look more closely into meson theory. Our goal is to understand, in qualitative terms, what the meson-exchange picture can predict for the NN system. However, first we shall briefly review the empirically known features of the nuclear force. This will later help to better assess the relevance of various meson-exchange contributions.

3.1 Empirical Features of the Nuclear Force

We will summarize below the five most important properties of the nucleon-nucleon interaction. For a more comprehensive treatment of this topic, we refer the reader to the appropriate literature (BW 52, SF 74, Seg 77). The first two books ever written specifically about the two-nucleon system, namely Moravcsik (Mor 63) and Wilson (Wil 63), are still today very useful introductions into the field. Furthermore, there is the book by Brown and Jackson (BJ 76).

1. *Nuclear forces are of short range (finite range).* That their range is shorter than interatomic distances we can conclude from the fact that at the molecular level no forces other than electromagnetic are needed to explain the known phenomena. However, we can put a much more precise and, in fact, much lower limit on the range by studying closely the saturation properties of nuclei. When going from the $A = 4$ nucleus, the helium, upwards to higher A nuclei, one realizes that the binding energy per nucleon remains about constant. The density remains also roughly the same, the radius of heavy nuclei being proportional to $A^{\frac{1}{3}}$. If the nuclear force was of

long range, like e. g. the Coulomb force, the potential energy per particle would increase with A and so would the density. On the other hand, for light nuclei ($A \leq 4$) the binding energy per nucleon does grow with A. The deuteron is bound by 2.2 MeV, ^3H by 8.5 MeV. This fact is best analysed in terms of energy per "bond". Thus, the binding energy per bond is about 2 MeV in the two-nucleon system and 3 MeV for the triton. In ^4He we have $\approx$ 4.5 MeV per bond (28 MeV total). One can then conclude that, when nucleons are pulled closer to each other by more bondes (due to more particles), also the energy per bond increases (up to saturation). From this Wigner (Wig 33), in 1933, conjectured that the nuclear force should be of short range, namely shorter than the deuteron diameter of about 4 fm and roughly equal to the radius of the alpha particle of about 1.7 fm.

2. *The nuclear force is attractive in its intermediate range.* "Intermediate" is meant here relative to the total range of the nuclear force, which we now consider as being subdivided according to TNS (TNS 51) in short, intermediate and long range. The proof for the attractive character of the nuclear force (at least, in a certain range) is provided by the fact of nuclear binding. The range of this attraction can be obtained more precisely by considering the central density of heavy nuclei as known from electron scattering. This density is about 0.17 fm^{-3} (nuclear matter density) which is equivalent to a cube of lenght 1.8 fm for each nucleon. Thus, the average distance between the centers of two nucleons in the interior of a nucleus is about 1.8 fm, in close agreement with our estimate given under item 1. This average distance should be about the range of the attraction. Further evidence for the (partially) attractive character of the nuclear force comes from the analysis of NN scattering data. The S-wave phase shifts are positive (corresponding to attraction) for low energies, see Fig. 3.1. Note that the average momentum of a nucleon in nuclear matter is equivalent to a laboratory energy of about 50 MeV.

3. *The nuclear force has a repulsive core.* Such an assumption could help explaining the saturation properties of nuclear forces and the constant nuclear density. But this aspect is not a compelling proof for a repulsive core, as saturation can also be generated in other ways, namely by "exchange" forces, by Pauli and relativistic effects. In fact, at nuclear matter density the Pauli effect is much more important than the short range repulsion. Historically, a repulsive core was first proposed by Jastrow (Jas 51) to explain the isotropy of proton-proton (pp) differential cross sections (Fig.

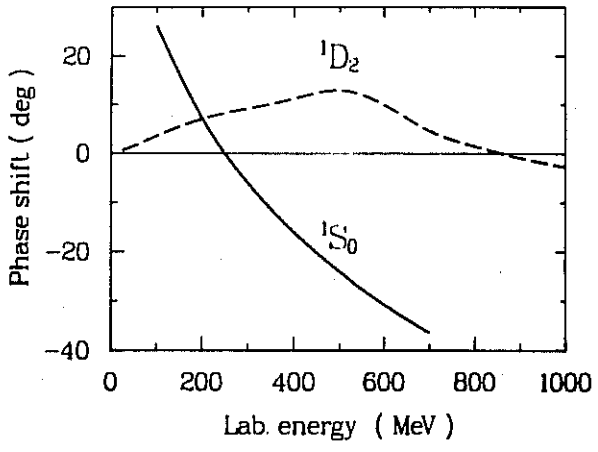

Figure 3.1: NN **phase shifts for the** $^1S_0$ **and** $^1D_2$ **state.** Shown is the energy dependent anlysis by Arndt (Arn 87).

5.12). However, a more precise argument is provided by the behaviour of the $^1S_0$ and $^1D_2$ phase shifts as a function of energy (Fig. 3.1). The latter stays positive (corresponding to attraction) up to about 800 MeV whereas the $^1S_0$ phase shift turns negative (i. e. repulsive) around 250 MeV. Since an S-state (orbital angular momentum $L = 0$, no centrifugal barrier) feels the innermost region of the force, whereas in a D-state ($L = 2$) the nucleons are kept apart by the centrifugal barrier, one may conclude that a repulsion at short range is indicated. The maximum classical orbital angular momentum L_{max} involved in a range R is

$$L_{max} \approx R \cdot p \tag{3.1}$$

where the momentum p of a nucleon in the centre of mass frame of the NN system is related to the laboratory energy, E_{lab}, by

$$E_{lab} = 2p^2/M \tag{3.2}$$

with M the mass of the nucleon. For $E_{lab} = 250$ MeV, where the $^1S_0$ phase-shift turns repulsive, we have $p \approx 1.7$ fm^{-1}. With $L_{max} \lesssim 1$ we obtain

$$R \lesssim 0.6 \text{ fm}. \tag{3.3}$$

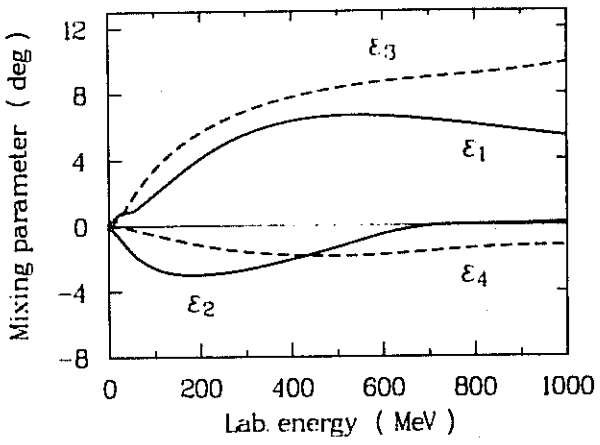

Figure 3.2: **Mixing parameters for $J \leq 4$.** The analysis by Arndt (Arn 87) is shown.

This should represent a fair estimate of the radius of the repulsive core.

4. *There is a tensor force.* The most striking evidence for this fact is seen in the deuteron: the quadrupole moment, the magnetic moment (which requires a D-state contribution), and the asymptotic D/S state ratio. Further evidence is provided by the non-vanishing mixing parameters, ϵ_J, as obtained in a phase-shift analysis of NN scattering data (Fig. 3.2). This parameter is proportional to the transition amplitude from a state with $L = J - 1$ to one with $L = J + 1$ (with J the total angular momentum). Of all operators, by which the most general non-relativistic potential can be represented, only the tensor operator has non-vanishing matrix elements for this transition.

5. *There is a spin-orbit force.* A first indication for this fact was observed in the spectra of nuclei. Note, however, that this refers to the effective nuclear interaction in the many-body system, which is not the same as the free NN interaction, though these two forces are related. Clear evidence came from the first reliable phase-shift analysis at high energy (SYM 57, GT 57). The triplet P-waves resulting from the analysis can only be explained by assuming a strong spin-orbit force, see Fig. 3.3. Speaking in

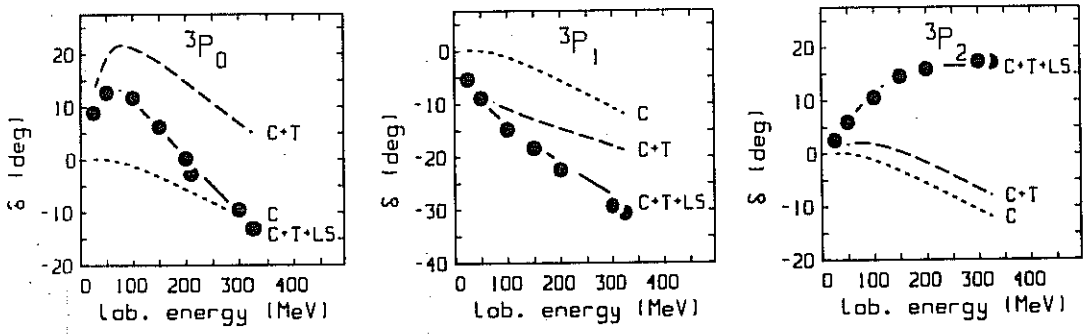

Figure 3.3: NN **phase shifts in triplet** P**-waves.** Shown are predictions using a central force only (C), central plus tensor (C+T), and central plus tensor plus spin-orbit force (C+T+LS). The dots represent energy independent phase shift analyses (Arn+ 83, Dub+ 82).

terms of observables, a strong spin-orbit force is required to explain the polarization, Fig. 3.4.

As we are dealing with the spin dependence of the nuclear force, we should also mentione that there is a spin-spin ($\sigma_1 \cdot \sigma_2$) force, which is, however, not as important as the latter two forces ($\frac{1}{2}\sigma_i$ is the spin operator for nucleon i).

3.2 The Idea of Massive-Particle Exchange

In the 1930's the best established and most striking feature of the nuclear force was its short range nature. For that reason, the first theoretical attempts concentrated on deriving a force of finite range from some more fundamental idea. Yukawa achieved this in 1935 (Yuk 35) by constructing a strict analogy to quantum electrodynamics (QED). His first consideration was carried out in the framework of classical field theory, which we shall now restate.

In QED a field of particles with *zero* mass, the photons, is assumed to fulfill a field equation. In static approximation, the fourth component of

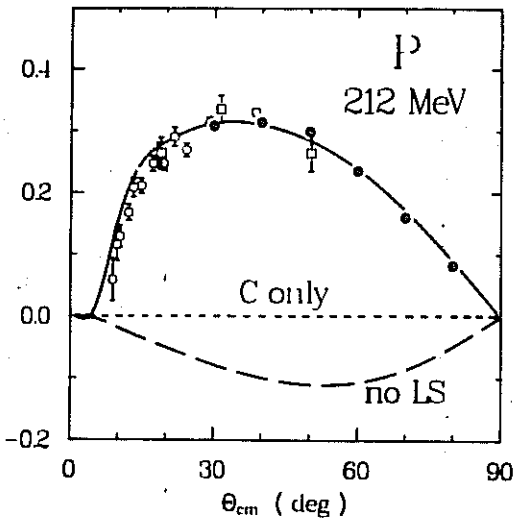

Figure 3.4: **Predictions for the *pp* polarization at 212 MeV lab. energy.** Full line: full nuclear force; dashed: spin-orbit force omitted; dotted: central force only. (Data at 209.1 (open square), 210 (full dot), and 213 MeV (open circle) (BL 82, Arn 87)).

this field satisfies the Laplace equation of classical electrodynamics

$$-\Delta V(\mathbf{r}) = e\delta(\mathbf{r}) \tag{3.4}$$

with Δ the Laplace operator. The solution

$$V(r) = \frac{e}{4\pi}\,\frac{1}{r} \tag{3.5}$$

with $r = |\mathbf{r}|$, is the familiar Coulomb potential.

In analogy, in meson theory a field of particles with *non-zero* mass m, the mesons, is assumed, fulfilling a field equation, which is the Klein-Gordon equation[1]

$$(\Box + m^2)\phi(x) = g\bar{\psi}(x)\psi(x). \tag{3.6}$$

In the approximation that the nucleon (the source of the meson field), represented by $\psi(x)$, is infinitely heavy and fixed at the origin, we obtain

$$(-\Delta + m^2)\phi(\mathbf{r}) = g\delta(\mathbf{r}) \tag{3.7}$$

[1]From now on we will use units $\hbar = c = 1$; notation and conventions as in (BD 64).

satisfied by the "Yukawa potential"

$$\phi(r) = \frac{g}{4\pi}\frac{e^{-mr}}{r}. \tag{3.8}$$

Because of the exponential form, which is a direct consequence of the massive character of the particles, this potential has the desired finite range. For zero mass one recovers the Coulomb potential.

This simple consideration, done in 1935, was the birth of particle physics.

Traditionally the range of a particle exchange is estimated from the Compton wavelength equivalent to the particle's mass

$$R = 1/m. \tag{3.9}$$

In this way, one estimates for the pion (with a mass of 138 MeV) a range of 1.4 fm. This estimate is somewhat small; in fact, the pion just starts to become dominant at that range. That the conventional range estimate is too small, is also true for the heavier mesons. It is due to the fact that we are dealing with large coupling constants: the final nuclear potential is a result of strong interferences of large contributions (see Fig. 3.6 below). Applying a 'fudge' factor of 3 or 4 to the Compton wave length, results in a more realistic estimate of the range.

3.3 Field Theory, Perturbation Theory, and Feynman Diagrams

As discussed, historically, the first meson-theoretic consideration was done in the framework of classical field theory, in which the finite-range character of the potential generated by massive-particle exchange is seen most easily. However, for more advanced considerations, quantized field theory should be applied. This field theory was developed first for QED. When interactions are involved, it is customary to apply perturbation theory, which appears quite reasonable for a coupling constant of 1/137. The interactions, treated perturbatively, are most conveniently represented in terms of Feynman diagrams. Originally, meson theory was believed to represent the theory of strong interactions in analogy to QED. Nowadays, with QCD being the candidate theory for strong interactions, meson theory is viewed

as an effective description which may represent the appropriate approximation to the full and fundamental theory in the low energy regime typical for nuclear physics.

Due to the strong character of the forces we are dealing with, the coupling constants of the interactions of baryons and mesons are large, typically in the order of 10. Therefore, it may be questionable whether a perturbation expansion makes any sense. Nevertheless, it is customary to consider meson-baryon reactions in terms of perturbation theory and in the graphical language of Feynman diagrams.[2] A justification for the use of perturbation theory can be attempted in the light of the Taketani program (TNS 51). Contributions of increasing order, which may become increasingly divergent, are of shorter and shorter range. For the long and intermediate range there is only a finite number of perturbative contributions. Thus, for these ranges there are reasons to be confident in the predictions generated by perturbation theory. At the very short range, due to the extended (quark) structure of hadrons, the meson-exchange picture should break down, anyhow. For that reason, in most meson models, one allows for a partly phenomenological treatment of the short distances by introducing a vertex form factor, which — in a certain sense — takes the extended structure of hadrons effectively into account. Fortunately, since the nuclear force is repulsive at short inter-nucleonic distances, the phenomenology of the very short range is "masked" by a repulsive wall. Thus one may hope that predictions are not very sensitive to the unknown part of the force.

For the above reasons, we will — as customary — discuss meson theory in the framework of perturbation theory. The lowest order contribution to NN scattering is the one-boson-exchange diagram. Fig. 3.5 describes this process in the centre of mass (c.m.) frame of the two interacting particles.

According to Feynman rules (BD 64, IZ 80) the depiction Fig. 3.5 corresponds to the amplitude in analytical form

$$\frac{\bar{u}_1(\mathbf{q}')\Gamma_1 u_1(\mathbf{q}) P_\alpha \bar{u}_2(-\mathbf{q}')\Gamma_2 u_2(-\mathbf{q})}{(q'-q)^2 - m_\alpha^2} \tag{3.10}$$

where P_α over denominator is the meson propagator (represented by the dashed line in the figure; $P_\alpha = i$ for scalar and pseudoscalar exchanges, for

[3] An exception is the old "strong coupling theory" (Pau 46, BH 55) which, however, can only be formulated in the framework of classical field theory.

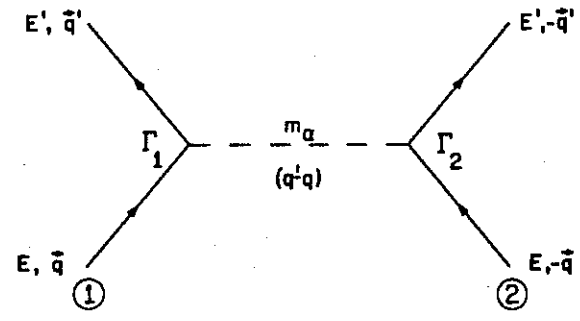

Figure 3.5: **Feynman diagram representing a one-boson-exchange contribution to NN scattering in the c.m. frame.** Full lines denote nucleons, the dashed line a boson with mass m_α.

vector exchange see Appendix A.1) and the Γ_i are the vertices representing the meson-nucleon interactions (as given by corresponding interaction Langrangians). u_i and $\bar{u}_i$ $(= u^\dagger\gamma^0)$ are Dirac spinors and their adjoints representing in- and out-going nucleons, respectively. For simplicity, we have suppressed spin (or helicity) indices. (The four-momentum transfer squared, $(q' - q)^2$, for an on-energy-shell process as well as in the static limit is $-(\mathbf{q}' - \mathbf{q})^2$.)

3.4 Various Boson Fields and their Role in NN

For the NN interaction at low energy there are essentially only three boson fields which are of relevance[3]

- the pseudoscalar (ps) field,
- the scalar (s) field, and
- the vector (v) field.

The modern point of view is to consider these fields as effective (non-fundamental) fields.

[3]For a discussion of other fields and their couplings see (Oga+ 67).

Guided by symmetry principals, simplicity, and physical intuition, the most commonly used interaction Lagrangians which couple these fields to the nucleon are[4]

$$\mathcal{L}_{ps} = -g_{ps}\bar{\psi}i\gamma_5\psi\varphi^{(ps)} \tag{3.11}$$

$$\mathcal{L}_{s} = +g_{s}\bar{\psi}\psi\varphi^{(s)} \tag{3.12}$$

$$\mathcal{L}_{v} = -g_{v}\bar{\psi}\gamma^{\mu}\psi\varphi_{\mu}^{(v)} - \frac{f_v}{4M}\bar{\psi}\sigma^{\mu\nu}\psi(\partial_\mu\varphi_\nu^{(v)} - \partial_\nu\varphi_\mu^{(v)}) \tag{3.13}$$

where ψ denotes the nucleon Dirac spinor field, while $\varphi^{(ps)}$, $\varphi^{(s)}$, and $\varphi_\mu^{(v)}$ are the pseudoscalar, scalar, and vector boson fields, respectively. M is the nucleon mass. In Eq. (3.13) the first term on the r.h.s. is called the vector (v) and the second term the tensor (t) coupling. These two couplings are similar to the interaction of a photon with a nucleon. The first one is analogous to the coupling of the Dirac current to the electromagnetic vector potential, while the second one corresponds to the Pauli coupling of the anomalous magnetic moment. This analogy is not accidental; the vector-meson dominance model for the electromagnetic form factor of the nucleon explains the close relationship (Section 4.2).

Again, these couplings should be viewed as *effective* interactions; in practise, they will be slightly modified ('smeared out') by a vertex form factor (see below). In the light of this view, it is insignificant that the pv and t couplings are non-renormalizable.

Alternatively, for the ps field there is also the so-called pseudovector (pv) or gradient coupling to the nucleon, which is suggested as an effective coupling by chiral symmetry (Wei 67, Bro 79):

$$\mathcal{L}_{pv} = -\frac{f_{ps}}{m_{ps}}\bar{\psi}\gamma^5\gamma^\mu\psi\partial_\mu\varphi^{(ps)}. \tag{3.14}$$

The ps and the pv coupling are equivalent for on-mass-shell nucleons if the coupling constants are related by $f_{ps} = (m_{ps}/2M)g_{ps}$. However, off-shell

[4]Throughout this paper we use the conventions and notations of (BD 64, BD 65, IZ 80); e. g. $\gamma^0 = \begin{pmatrix} 1 & 0 \\ 0 & -1 \end{pmatrix}$, $\gamma^l = \begin{pmatrix} 0 & \sigma^l \\ -\sigma^l & 0 \end{pmatrix}$, with σ^l the usual Pauli matrices; $\gamma_5 = \gamma^5 = i\gamma^0\gamma^1\gamma^2\gamma^3 = \begin{pmatrix} 0 & 1 \\ 1 & 0 \end{pmatrix}$, and $\sigma^{\mu\nu} = \frac{i}{2}[\gamma^\mu, \gamma^\nu]$; Greek indices extend from $0 \to 3$, Latin indices from $1 \to 3$; metric tensor: $g_{00} = +1, g_{ll} = -1, g_{\mu\neq\nu} = 0$.

Table 3.1: **Various meson-nucleon couplings and their contributions to the nuclear force as obtained from one-boson-exchange.**

Coupling	*Bosons (Strength of Coupling)* $I=0$ $[1]$	$I=1$ $[\tau_1 \cdot \tau_2]$	*Characteristics of Predicted Forces* *Central* $[1]$	*Spin-Spin* $[\sigma_1 \cdot \sigma_2]$	*Tensor* $[S_{12}]$	*Spin-Orbit* $[\boldsymbol{L} \cdot \boldsymbol{S}]$
ps	η (weak)	π (strong)	—	**weak,** coherent with v, t	**strong**	—
s	σ (strong)	δ (weak)	**strong, attractive**	—	—	**coherent with v**
v	ω (strong)	ρ (weak)	**strong, repulsive**	weak coherent with ps	opposite to ps	**strong,** coherent with s
t	ω (weak)	ρ (strong)	—	**weak,** coherent with ps	**opposite to ps**	—

I denotes the isospin of a boson. The characteristics quoted refer to $I = 0$ bosons (no isospin dependence). The isovector ($I = 1$) boson contributions, carrying a factor $\tau_1 \cdot \tau_2$, provide the isospin-dependent forces.

the predictions are rather different. Anti-particle contributions (Fig. 2.1c and d) turn out to be huge when using the pseudoscalar coupling wheras they are suppressed by the gradient coupling.

It is now in principal a straightforward (but quite lengthy) task to evaluate the OBE contributions Eq. (3.10) corresponding to the interaction Lagrangians given above. (This is done in all detail in (Mac 86, Section 3.4); see also Appendix A.) This will reveal what each field and coupling predicts for the nuclear force. In Table 3.1 we give an overview. (Note that the features displayed in that table are obtained in the approximation which is considered in Appendix A.3.) Going back to the beginning of this section, we notice that with each of the five most important empirical features of the nuclear force, one can associate at least one boson field which could provide an explanation. This manifests the basic reason why meson-exchange is so appropriate and so successful for the description of the nuclear force.

The predictions from some couplings are seen most clearly in the non-relativistic approximation. In this approximation, the one-boson-exchange

amplitude, Eq. (3.10), for the *ps* and the *pv* coupling reduces to the same expression; it is obtained most straightforward when starting from the *pv* coupling:[5]

$$V_{ps}(\mathbf{k}) = -\frac{g_{ps}^2}{4M^2}\frac{(\boldsymbol{\sigma}_1\cdot\mathbf{k})(\boldsymbol{\sigma}_2\cdot\mathbf{k})}{\mathbf{k}^2+m_{ps}^2} \tag{3.15}$$

$$= -\frac{g_{ps}^2}{12M^2}\{\boldsymbol{\sigma}_1\cdot\boldsymbol{\sigma}_2\frac{\mathbf{k}^2}{\mathbf{k}^2+m_{ps}^2}+\frac{S_{12}(\mathbf{k})}{\mathbf{k}^2+m_{ps}^2}\} \tag{3.16}$$

$$= -\frac{g_{ps}^2}{12M^2}\{\boldsymbol{\sigma}_1\cdot\boldsymbol{\sigma}_2-\boldsymbol{\sigma}_1\cdot\boldsymbol{\sigma}_2\frac{m_{ps}^2}{\mathbf{k}^2+m_{ps}^2}+\frac{S_{12}(\mathbf{k})}{\mathbf{k}^2+m_{ps}^2}\} \tag{3.17}$$

with $\mathbf{k}=\mathbf{q}'-\mathbf{q}$ and

$$S_{12}(\mathbf{k}) = 3(\boldsymbol{\sigma}_1\cdot\mathbf{k})(\boldsymbol{\sigma}_2\cdot\mathbf{k})-\boldsymbol{\sigma}_1\cdot\boldsymbol{\sigma}_2\mathbf{k}^2 \tag{3.18}$$

the tensor operator in momentum space. In Eq. (3.17) we have broken the potential into spin-spin δ-function, spin-spin Yukawa, and tensor force. See Appendix A.3 for the equivalent r-space potential.

For the tensor coupling the corresponding expression is

$$V_t(\mathbf{k}) = -\frac{f_v^2}{4M^2}\frac{(\boldsymbol{\sigma}_1\times\mathbf{k})\cdot(\boldsymbol{\sigma}_2\times\mathbf{k})}{\mathbf{k}^2+m_v^2} \tag{3.19}$$

$$= -\frac{f_v^2}{4M^2}\frac{\boldsymbol{\sigma}_1\cdot\boldsymbol{\sigma}_2\mathbf{k}^2-(\boldsymbol{\sigma}_1\cdot\mathbf{k})(\boldsymbol{\sigma}_2\cdot\mathbf{k})}{\mathbf{k}^2+m_v^2} \tag{3.20}$$

$$= -\frac{f_v^2}{12M^2}\{2\boldsymbol{\sigma}_1\cdot\boldsymbol{\sigma}_2-2\boldsymbol{\sigma}_1\cdot\boldsymbol{\sigma}_2\frac{m_v^2}{\mathbf{k}^2+m_v^2}-\frac{S_{12}(\mathbf{k})}{\mathbf{k}^2+m_v^2}\} \tag{3.21}$$

This consideration clearly shows that these two couplings create tensor forces, which are of opposite sign. The spin-spin forces add up coherently.

[5] Some simple rules of non-relativistic reduction are:

$$i\partial_\mu = i\frac{\partial}{\partial x^\mu} \longmapsto \pm\mathbf{k}$$
$$\gamma^5\gamma^\mu \longmapsto -\boldsymbol{\sigma}\cdot$$
$$\sigma^{\mu\nu} \longmapsto \boldsymbol{\sigma}\times,$$

and replacing Dirac by Pauli spinors.
Furthermore, note that the vertex is i times the interaction Lagrangian stripped off the fields, and that i times the amplitude Eq. (3.10) defines the potential V_α.

The repulsion created by (neutral) vector-boson-exchange can be understood in analogy to the one-photon-exchange between like charges creating a repulsive Coulomb potential. Neutral vector bosons can be visualized as heavy photons. The baryon number plays the role of the electric charge. Consequently, in the nucleon-antinucleon system vector-boson-exchange generates attraction (see Section 8.2). The spin-orbit force produced by vector bosons corresponds to the Thomas term which emerges when the Coulomb potential is employed in the relativistic Dirac equation. Thus, it can only be understood in a relativistic consideration; or, in equivalent terms, the lower component of the Dirac spinor, Eq. (A.14), is crucial for the creation of the spin-orbit force. See Appendix A.3 for the derivation and the explicit expressions for the vector (and also scalar) potential, disclosing the features explained.

The next step is to look into physical manifestations of the fields discussed theoretically so far. For that purpose we give in Table 3.2 the nonstrange mesons below 1350 MeV. In the mass range below the nucleon mass, one finds two pseudoscalar particles, namely $\pi(138)$ and $\eta(550)$, and two vector particles, $\rho(769)$ and $\omega(783)$. The (isoscalar) ω has a strong vector coupling and the (isovector) ρ a strong tensor coupling to the nucleon (see Table 4.1 below). Futhermore, there exists an isovector scalar meson, $\delta(983)$, which, due to its large mass and its small coupling constant, provides only a small contribution. Its isospin-dependent central force can be used to adjust the two S-waves.

Compared to the (isovector) π, the contribution from the (isoscalar) η is very small. This has two reasons: first, the coupling constant of the η is small, a fact which is predicted by the quark model (BJ 76) and confirmed by phenomenological studies analysing NN scattering in terms of forward dispersion relations (GK 80) (Table 4.1 below); second, the mass of the η is substantially larger than the pion mass. Note that the magnitude of one-meson-exchange contributions is roughly proportional to g_α^2/m_α^2, Eq. (3.10). For the reasons given, the η is not important for the NN system. Providing an isospin-independent tensor force, the essential effects of the η are that it lowers the ${}^3P_1$, raises the ${}^3P_0$ phase shifts, and slightly reduces the ${}^3S - D_1$ tensor force. Due to its even larger mass, the $\eta'(958)$ is even less important than the η and in general not taken into account in boson-exchange models.

Summarizing the important contributions of the mesons dicussed so far: the pion as the lightest particle provides the long range force and, due to its

pseudoscalar nature, the tensor force. This tensor force is reduced at short ranges by the ρ meson to a realistic size. (Note that for π and ρ the ps and t potentials given above have to be multiplied by the operator $\tau_1 \cdot \tau_2$ (with $\frac{1}{2}\tau_i$ the isospin operator for nucleon i), since π and ρ are (isospin one) isovector particles; this factor implies a strong isospin dependence for these two potentials.[6]) The ω creates the short range repulsion and the (short-ranged) spin-orbit force. Thus, these three mesons explain already important features of the nuclear force. Still, one important property is unexplained: the intermediate range attraction. A scalar-isoscalar boson with a mass of 500-700 MeV could provide this missing part.

However, the existence of such a boson is not supported by any experimental evidence. The intermediate range attraction is generated by two-particle exchanges, particularly 2π-exchange (see Section 5). Since there is also strong interaction between pions in relative S-wave, there is physical motivation to assume a scalar boson of a mass between 500 and 700 MeV (commonly called σ). Adding this particle to the mesons discussed defines the so-called one-boson-exchange (OBE) model (see Table 3.1 for a qualitative summary and Appendix A for quantitative examples).

Finally, let us say a brief word about the other mesons in Table 3.2. There are a few mesons around 1 GeV, namely the $\phi(1020)$ and the $S^*(975)$. These mesons have a considerable $s\bar{s}$ content (with s denoting the strange quark); their coupling to the nucleon is therefore suppressed according to the Zweig rule (Clo 79). There are many mesons in the area 1200–1300 MeV, e. g. the $f(1274)$ and the $A_1(1275)$. For reasons of chiral invariance the A_1-meson, which is the chiral partner of the ρ, has been considered by some authors (DBS 84). However, there are several good reasons why one should leave out any meson above 1 GeV or so. First, their (short-ranged) contribution is masked to a considerable extent by the strong short-range repulsion originating from ω-exchange. Second, we have to remember that in meson theory, it is necessary to apply so-called form factors (cutoffs) to each meson-nucleon vertex (for more details see next section and Appendix A). Originally this was done for purely mathematical reasons, namely to avoid divergences in the scattering equation. However, nowadays, our knowledge of the (quark) substructure of nucleons and mesons provides a physical reason for this measure. The cutoff masses used are typically in the order 1.2 –

[6]Note that the ρ has also a weak vector coupling leading to (weak, short-ranged) isospin-dependent central and spin-orbit forces.

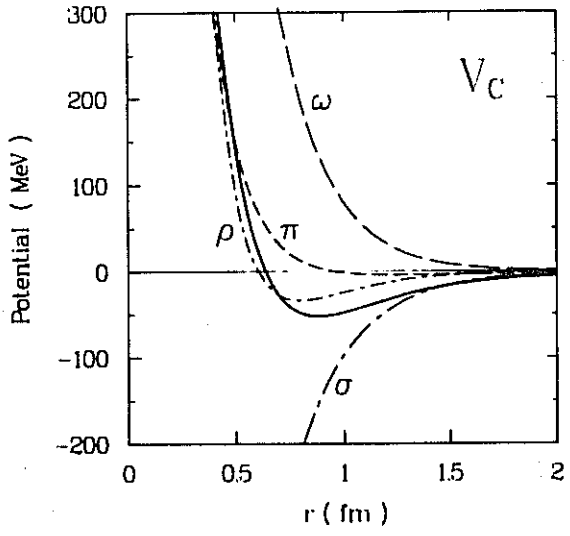

Figure 3.6: **Contributions from single mesons to the even-singlet central potential.** The solid line represents the full potential.

2 GeV. Obviously, it does not make sense to take meson exchange seriously in a region in which modifications due to the extended structure of hadrons come into play; or in other words, the quark structure of hadrons does not leave any room for those very heavy mesons.

To finish this section, we show in concret terms how the four most important bosons, namely π, σ, ρ, and ω, build up the nuclear potential. Figures 3.6-8 demonstrate the role of each meson for the different components of the nuclear force for which the following operator structure is assumed in each spin-isospin state:

$$V(r) = V_C(r) + V_T(r)S_{12} + V_{LS}(r)\mathbf{L}\cdot\mathbf{S} \qquad (3.22)$$

where on the r.h.s. we have the central, tensor, and spin-orbit force. ($\mathbf{S} = \frac{1}{2}(\sigma_1 + \sigma_2)$ is the total spin and S_{12} the r-space tensor operator as defined in Appendix A.3; the total isospin of the two-nucleon system is denoted by T.) In the decompositon Eq. (3.22) the spin-spin force is included in the central term. A quantitative r-space potential is shown in the figures.[7] The

[7]Potential A of Table A.3 is used. This potential and the decomposion Eq. (3.22) is also employed in Fig. 3.3 and 3.4.

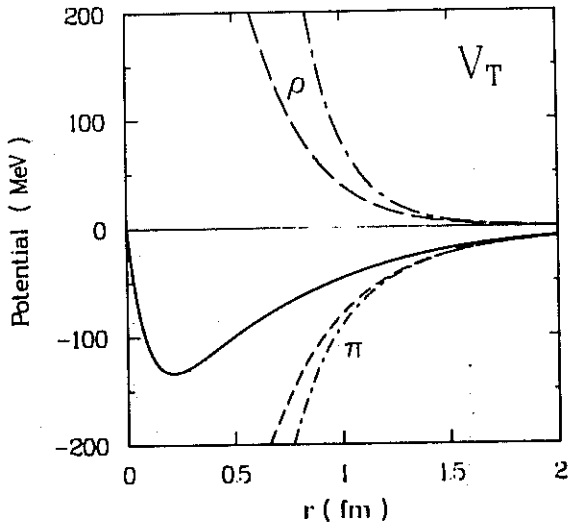

Figure 3.7: **The contributions from π and ρ (dashed) to the $T = 0$ tensor potential.** The solid line is the full potential. The dash-dot lines are obtained when the cutoff is omitted.

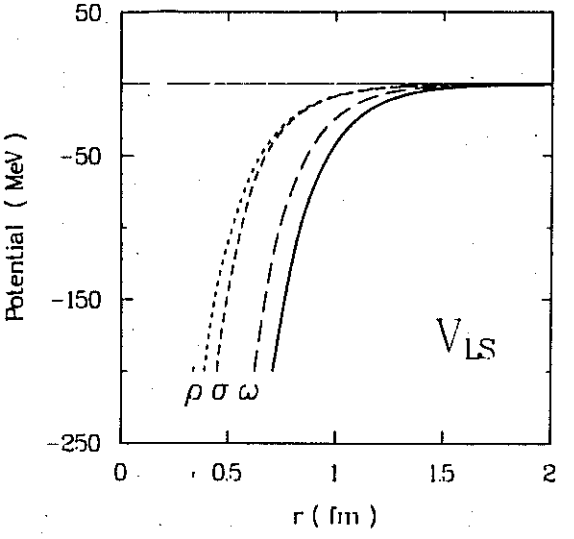

Figure 3.8: **The contributions from single mesons to the $T = 1$ spin-orbit potential, as denoted.** The solid line is the full potential.

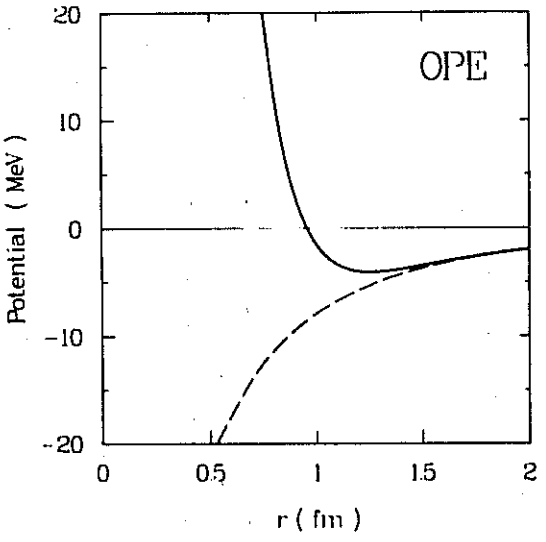

Figure 3.9: **The one-pion-exchange potential in the singlet-even state with cutoff (full line) and without (dashed).**

influence of the cutoff on the potential is demonstrated in some cases (see Figs. 3.7 and 3.9). Note that due to the δ-function in the spin-spin (central) force of the one-pion-exchange, the influence of the cutoff is rather large in this case. It 'smears out' the δ-function. This applies also the rho potential. For σ and ω the effect of the cutoff is much milder; the short-range part of those potentials is just reduced and not reversed in sign.

Table 3.2: **Nonstrange mesons with masses below 1350 MeV and their properties.** [From (PDG 84)]

Name	J^P	I^G	Mass (MeV)	Full width (MeV)	Dominant decay mode
$\pi^\pm$	0^-	1^-	139.57	0	$\mu^\pm\nu$
π^0	0^-	1^-	134.96	0	$\gamma\gamma$
η	0^-	0^+	548.8	0.001	$\gamma\gamma, 3\pi^0$
ρ	1^-	1^+	769	154	2π
ω	1^-	0^-	782.6	9.9	3π
η'	0^-	0^+	957.6	0.3	$\eta\pi\pi$
S^*	0^+	0^+	975	33	$2\pi, K\bar{K}$
δ	0^+	1^-	983	54	$\eta\pi, K\bar{K}$
ϕ	1^-	0^-	1020	4	K^+K^-
B	1^+	1^+	1234	150	$\omega\pi$
f	2^+	0^+	1274	178	2π
A_1	1^+	1^-	1275	315	$\rho\pi$
D	1^+	0^+	1283	26	$\eta\pi\pi, 4\pi$
ϵ	0^+	0^+	1300	200–600	2π
A_2	2^+	1^-	1318	110	$\rho\pi$

Notation: spin J, parity P, isospin I, G-parity G.

Section 4

The One-Boson-Exchange Model

As we have seen in the previous section, the exchanges of single pseudoscalar, scalar, and vector mesons provide all principal features necessary to describe the nuclear force. The model which exploits this fact the most is the so-called one-boson-exchange (OBE) model. To provide intermediate range attraction, indispensable for a nuclear potential to be realistic, the OBE model 'invents' a scalar-isoscalar boson, commonly denoted by σ (or ϵ). Mass and coupling constant of the σ are essentially free parameters and fit to the NN data. On the background of more realistic considerations (Section 5), it will turn out that such a σ boson represents a simple parametrization of the 2π-exchange contribution to the NN interaction. The fact that there is strong interaction between pions in relative S-wave provides a physical argument for that approximation. Considering how complicated the 'true' 2π-exchange is and how simply a single scalar-meson exchange can be calculated, the quantitative success of the OBE model is most impressive. Presumably, this explains the popularity of the model. Since particle-exchange is described by relativistic quantum field theory, it is most appropriate and consistent to work in a relativistic framework (Section 4.1). In Section 4.2 we will demonstrate for some cases the relationship between the meson parameters and the predicted properties of the two-nucleon system.

4.1 Covariant Equations

Two-nucleon scattering is described covariantly by the Bethe-Salpeter (BS) equation (SB 51).[1] In operator notation it may be written as

$$\mathcal{M} = \mathcal{V} + \mathcal{V}\mathcal{G}\mathcal{M} \tag{4.1}$$

with $\mathcal{M}$ the invariant amplitude for the two-nucleon scattering process, $\mathcal{V}$ the sum of all connected two-particle irreducible diagrams and $\mathcal{G}$ the relativistic two-nucleon propagator. As this four-dimensional integral equation is very difficult to solve (FT 75), so-called three-dimensional reductions have been proposed, which are more amenable to numerical solution. These approximations to the BS equation are also covariant and satisfy relativistic elastic unitarity. However, the three-dimensional reduction is not unique, and in principal infinitely many choices exist (Yae 71). Typically they are derived by replacing Eq. (4.1) by two coupled equations:

$$\mathcal{M} = \mathcal{W} + \mathcal{W}g\mathcal{M} \tag{4.2}$$

and

$$\mathcal{W} = \mathcal{V} + \mathcal{V}(\mathcal{G} - g)\mathcal{W} \tag{4.3}$$

where g is a covariant three-dimensional propagator with the same elastic unitarity cut as $\mathcal{G}$ in the physical region. In general, the second term on the r.h.s. of Eq. (4.3) is dropped to arrive at a substantial simplification of the problem.

It is convenient to work in the c. m. frame (Fig. 4.1), where we can write the BS equation as (notation and conventions of (BD 64, BD 65, IZ 80))

$$\mathcal{M}(q';q|P) = \mathcal{V}(q';q|P) + \int d^4k \mathcal{V}(q';k|P)\mathcal{G}(k|P)\mathcal{M}(k;q|P) \tag{4.4}$$

with

$$\mathcal{G}(k|P) = \frac{i}{(2\pi)^4}\frac{1}{(\frac{1}{2}\not{P} + \not{k} - M + i\epsilon)^{(1)}}\frac{1}{(\frac{1}{2}\not{P} - \not{k} - M + i\epsilon)^{(2)}} \tag{4.5}$$

$$= \frac{i}{(2\pi)^4}\left[\frac{\frac{1}{2}\not{P} + \not{k} + M}{(\frac{1}{2}P + k)^2 - M^2 + i\epsilon}\right]^{(1)}\left[\frac{\frac{1}{2}\not{P} - \not{k} + M}{(\frac{1}{2}P - k)^2 - M^2 + i\epsilon}\right]^{(2)} \tag{4.6}$$

[1] An excellent survey of the theory of the Bethe-Salpeter equation is given in (Nak 69).

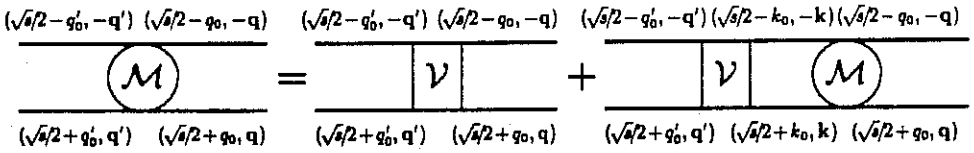

Figure 4.1: **Kinematics of the Bethe-Salpeter equation in the c. m. frame.**

where q, k, and q' are the initial, intermediate, and final relative four-momenta, respectively (with e. g. $k = (k_0, \mathbf{k})$), and P is the total four-momentum in the c. m. frame: $P = (\sqrt{s}, \mathbf{0})$ with $\sqrt{s}$ the total energy; $\not{k} = \gamma^\mu k_\mu$. The superscripts refer to particle (1) and (2). In general, we suppress spin (or helicity) and isospin indices.

Based on a suggestion by Blankenbecler and Sugar (BbS) (BS 66),[2] given originally for spinless particles, one possible choice for g is, when stated in manifestly covariant form (PL 70)

$$\begin{aligned} g_{BbS}(k,s) &= -\frac{1}{(2\pi)^3}\int_{4M^2}^{\infty}\frac{ds'}{s'-s-i\epsilon}\delta^{(+)}[(\frac{1}{2}P'+k)^2-M^2] \\ &\quad\times\delta^{(+)}[(\frac{1}{2}P'-k)^2-M^2] \\ &\quad\times[\frac{1}{2}\not{P}'+\not{k}+M]^{(1)}[\frac{1}{2}\not{P}'-\not{k}+M]^{(2)} \end{aligned} \tag{4.7}$$

with $\delta^{(+)}$ indicating that only the positive energy root of the argument of the δ-function is to be included, placing the particles on the positive mass shell. The propagator g_{BbS} has the same discontinuity across the right-hand cut as $\mathcal{G}$, and therefore preserves the unitarity relation satisfied by $\mathcal{M}$. Integration yields the reduced expression

$$g_{BbS}(k,s) = \delta(k_0)\bar{g}_{BbS}(\mathbf{k},s) \tag{4.8}$$

[2] A similar equation has been proposed by Logunov and Tavkhelidze (LT 63) for application in optical potential scattering from nuclei.

with

$$\bar{g}_{BbS}(\mathbf{k},s) = \frac{1}{(2\pi)^3}\frac{M^2}{E_k}\frac{\Lambda_+^{(1)}(\mathbf{k})\Lambda_+^{(2)}(-\mathbf{k})}{\frac{1}{4}s - E_k^2 + i\epsilon} \tag{4.9}$$

where

$$\Lambda_+^{(i)}(\mathbf{k}) = (\frac{\gamma^0 E_k - \boldsymbol{\gamma}\cdot\mathbf{k} + M}{2M})^{(i)} \tag{4.10}$$

$$= \sum_{\lambda_i} u(\mathbf{k},\lambda_i)\bar{u}(\mathbf{k},\lambda_i) \tag{4.11}$$

represents the positive-energy projection operator for nucleon i with $u(\mathbf{k})$ a positive-energy Dirac spinor of momentum $\mathbf{k}$; λ_i denotes either the helicity or the spin projection of the respective nucleon, and $E_k = \sqrt{M^2+\mathbf{k}^2}$. The projection operators imply that virtual anti-nucleon contributions are suppressed.[3] It has been shown in (FT 80, ZT 81) that these contributions are small when the pseudovector coupling is used for the pion.

Assuming $\mathcal{W} = \mathcal{V}$, we replace in Eq. (4.4) $\mathcal{G}$ by g_{BbS} yielding

$$\mathcal{M}(0,\mathbf{q}';0,\mathbf{q}|\sqrt{s}) = \mathcal{V}(0,\mathbf{q}';0,\mathbf{q}) + \int d^3k\,\mathcal{V}(0,\mathbf{q}';0,\mathbf{k})\bar{g}_{BbS}(\mathbf{k},s)\mathcal{M}(0,\mathbf{k};0,\mathbf{q}|\sqrt{s}) \tag{4.12}$$

in which the both nucleons in intermediate states are equally far off their mass shell. Note that there is four-momentum conservation at each vertex, and that in the initial state the nucleons are on their mass-shell ($q_0 = 0$, Fig. 4.1). The total c.m. energy is

$$\sqrt{s} = 2E_q. \tag{4.13}$$

With this we obtain, simplifying our notation

$$\mathcal{M}(\mathbf{q}',\mathbf{q}) = \mathcal{V}(\mathbf{q}',\mathbf{q}) + \int \frac{d^3k}{(2\pi)^3}\mathcal{V}(\mathbf{q}',\mathbf{k})\frac{M^2}{E_k}\frac{\Lambda_+^{(1)}(\mathbf{k})\Lambda_+^{(2)}(-\mathbf{k})}{\mathbf{q}^2 - \mathbf{k}^2 + i\epsilon}\mathcal{M}(\mathbf{k},\mathbf{q}). \tag{4.14}$$

Taking matrix elements between positive-energy spinors yields an equation for the scattering amplitude

$$\mathcal{T}(\mathbf{q}',\mathbf{q}) = V(\mathbf{q}',\mathbf{q}) + \int \frac{d^3k}{(2\pi)^3}V(\mathbf{q}',\mathbf{k})\frac{M^2}{E_k}\frac{1}{\mathbf{q}^2 - \mathbf{k}^2 + i\epsilon}\mathcal{T}(\mathbf{k},\mathbf{q}), \tag{4.15}$$

[3] For a choice which includes antiparticle intermediate states see e. g. F. Gross (Gro 69).

where, as before, spin (helicity) and isospin indices are suppressed. Within the OBE model, the quasi-potential V is a sum of OBE amplitudes (see Appendix A), which is also denoted as the ladder approximation. Defining

$$\hat{T}(\mathbf{q}',\mathbf{q}) = \sqrt{\frac{M}{E_{q'}}}T(\mathbf{q}',\mathbf{q})\sqrt{\frac{M}{E_q}} \tag{4.16}$$

and

$$\hat{V}(\mathbf{q}',\mathbf{q}) = \sqrt{\frac{M}{E_{q'}}}V(\mathbf{q}',\mathbf{q})\sqrt{\frac{M}{E_q}}, \tag{4.17}$$

which has become known as "minimal relativity" (BJK 69, PL 70, BJ 76), we can rewrite Eq. (4.15) as

$$\hat{T}(\mathbf{q}',\mathbf{q}) = \hat{V}(\mathbf{q}',\mathbf{q}) + \int \frac{d^3k}{(2\pi)^3}\hat{V}(\mathbf{q}',\mathbf{k})\frac{M}{\mathbf{q}^2-\mathbf{k}^2+i\epsilon}\hat{T}(\mathbf{k},\mathbf{q}) \tag{4.18}$$

which has the form of the non-relativistic Lippmann-Schwinger equation. A potential, that has been defined within an equation that is formally identical to the (non-relativistic) Lippmann-Schwinger equation, can be applied to conventional (non-relativistic) nuclear structure physics in the usual way. This is the practical advantage of using Eqs. (4.16-18). Furthermore, relations and methods familiar from non-relativistic momentum space calculations can now be used (HT 70).

The BbS propagator is the most widely used approximation. Another choice, that has been frequently applied, is the version suggested by Thompson (Tho 70), which reads in reduced form

$$g_{Th}(k,s) = \delta(k_0)\frac{1}{(2\pi)^3}\frac{M^2}{2E_k^2}\frac{\Lambda_+^{(1)}(\mathbf{k})\Lambda_+^{(2)}(-\mathbf{k})}{\frac{1}{2}\sqrt{s}-E_k+i\epsilon}. \tag{4.19}$$

This propagator yields the equation

$$T(\mathbf{q}',\mathbf{q}) = V(\mathbf{q}',\mathbf{q}) + \int \frac{d^3k}{(2\pi)^3}V(\mathbf{q}',\mathbf{k})\frac{M^2}{2E_k^2}\frac{1}{E_q-E_k+i\epsilon}T(\mathbf{k},\mathbf{q}). \tag{4.20}$$

Since both nucleons are equally off-shell in the BbS or Thompson equation, the exchanged bosons tranfer three-momentum only, i. e. the meson propagator is (for a scalar exchange)

$$\frac{i}{-(\mathbf{q}'-\mathbf{q})^2-m_\alpha^2}; \tag{4.21}$$

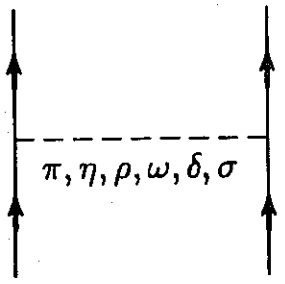

Figure 4.2: **The one-boson-exchange (OBE) model for the nuclear force.** Full lines denote nucleons.

this is also referred to as a static (or non-retarded) propagator.

Many more choices for g have been suggested in the literature. Some imply retardation-like terms in the meson propagators; for example in the case of the equations proposed by (Sch 72 and Erk 74) the meson propagator is

$$\frac{i}{(E_{q'} - E_q)^2 - (\mathbf{q}' - \mathbf{q})^2 - m_\alpha^2}. \tag{4.22}$$

However, it has been shown (Mac 82) that the term $(E_{q'} - E_q)^2$ in this propagator has an effect which is opposite to the one obtained when treating meson retardation properly. In spite of its suggestive appearance and in spite of early believes (Erk 74), the meson propagator Eq. (4.22) has nothing to do with genuine meson retardation and, therefore, cannot be recommended. This remark applies to the scattering of two particles of equal mass. If one particle is much heavier than the other one, it may, however, be appropriate to put one particle (namely the heavier one) on the mass shell, as done in the equations of (Gro 69, Sch 72, Erk 74).

A thorough discussion of the Bethe-Salpeter equation and/or a systematic study of a large family of possible relativistic three-dimensional reductions can be found in (Nak 69, WJ 73, BJ 76). Tjon and coworkers have compared results obtained by solving the full four-dimensional Bethe-Salpeter equation applying a full set of OBE diagrams with those from the

BbS and some other three-dimensional equations; for BbS they find only small differences as compared to full BS (FT 80, ZT 81).

For further formal developments, necessary to do calculations, see (MHE 87, Appendix E).

4.2 Meson Parameters and Two-Nucleon Properties

In this subsection we discuss an example of a relativistic momentum-space one-boson-exchange potential (OBEP). The model is shown in Fig. 4.2. This potential is constructed in the framework of the BbS equation. For analytic information see the previous subsection and Appendix A.

In Table 4.1, the coupling constants of this OBEP, which are to a certain extent best-fit parameters with regard to the NN data, are given and compared to information from other sources. Empirical sources are πN scattering, NN phase shift analysis, NN forward dispersion relations, and the nucleon electromagnetic form factor. Furthermore, there is the quark model (flavour $SU(3)$) in which hadron-meson coupling constants are related to a smaller set of quark-meson coupling constants; see (BJ 76, Appendix B to Chapter X) for details. From Table 4.1 it is seen that the best-fit parameters of the OBEP are in good agreement with those from empirical sources. This indicates that there is some reality to the model. The predictions for the low energy and deuteron parameters are given in Table 4.2. The phase shifts are shown in Section 5.4 (Fig. 5.10 and Table 5.2) together with those from more 'advanced' meson-exchange models. It is amazing, how this simple model with its few parameters is able to do such an excellent job of describing the two-nucleon data up to about 400 MeV lab. energy. (Phase shifts up to 1 GeV lab. energy are shown in Fig. 7.9.)

The constraint of fitting the two-nucleon data confines most meson parameters (coupling constants and cutoff masses) quite narrowly. This is in particular true for the vector bosons ω and ρ. Apart from the (repulsive) $^1S_0$ phase shifts at higher energies, the ω is most important for the triplet P-waves. This is understandable, since the ω provides most of the LS force which is crucial for those P waves (Fig. 3.3). Therefore, the P-waves represent the heaviest constraint on the ω coupling constant (and cutoff). The

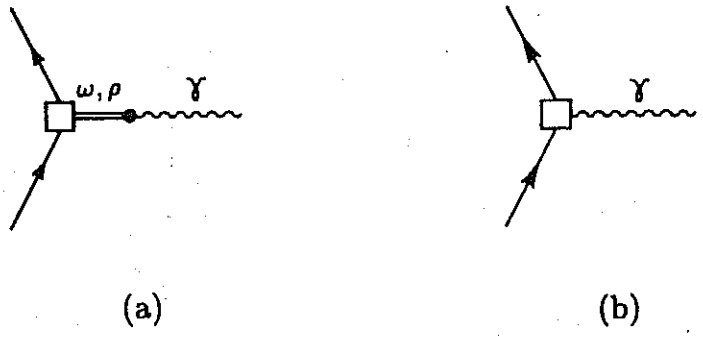

Figure 4.3: **Diagrams describing the interaction of nucleons with the electromagnetic field.** The open square represents the intrinsic form factor of the nucleon.

ρ is most influential for $^3P_0$ and $^3D_1$, with a stronger ρ decreasing the $^3P_0$ and raising the $^3D_1$ phase shifts (for the latter partial wave, particularly, at higher energies). There is also some sensitivity to the ρ in the $^3P_2$. Thus, in particular these three partial waves fix the rho coupling (and cutoff mass).

Note that vector bosons are also closely connected with the electromagnetic properties of the nucleon by the so-called vector dominance model (IJL 73), in which one assumes that the photon couples to the nucleon through a vector boson (Fig. 4.3a). In this way the extended structure of the electromagnetic form factor (which is essentially described by the vector boson mass, slightly modified by an intrinsic form factor involved in the strong coupling of the vector boson to the nucleon) as well as the anomalous magnetic moments of the nucleon are explained. These moments are related to the ratio f/g of the tensor/vector coupling of the vector bosons to the nucleon. In the strict interpretation of the model, this ratio should be 3.7 for the ρ meson which describes the (anomalous) Pauli isovector form factor. The larger value, $f_\rho/g_\rho \approx 6$, which is used in meson-exchange models for the nuclear force and which is also supported by empirical information from dispersion analyses (HP 75, Gre 77) seems to violate the vector dominance assumption. However, this can be understood in a simple way by assuming that there is also a direct vector coupling of the photon

to the nucleon, Fig. 4.3b (rather than all of the coupling going through the ρ meson) (IJL 73). Furthermore, the vector dominance model implies for the ω, which describes the Pauli isoscalar form factor, $f_\omega/g_\omega = -0.12$; this is a negligibly small value. Therefore most meson-exchange models for the nuclear force use $f_\omega = 0$. Knowing the γ-vector meson coupling constant (from the e^+e^- and $\mu^+\mu^-$ decay of vector mesons), also the vector coupling constant, g_v, can be extracted from the electromagnetic form factor of the nucleon (Höh+ 76), see Table 4.1.

In the OBEP, the form factor for the vector bosons is a dipole per vertex, i. e. each vertex is multiplied by

$$\left(\frac{\Lambda_\alpha^2 - m_\alpha^2}{\Lambda_\alpha^2 + \mathbf{k}^2}\right)^{n_\alpha} \tag{4.23}$$

with $n_\alpha = 2$. ($\mathbf{k} = \mathbf{q}' - \mathbf{q}$ denotes the three-momentum transfer.) The cutoff mass is $\Lambda_\alpha = 1.85$ GeV. This is in close agreement with fits to the electromagnetic form factor of the nucleon for which a dipole is preferred and from which a value for the cutoff mass in the order of 2 GeV is obtained (IJL 73). In Fig. 4.3 this form factor is denoted by the small open square ('intrinsic form factor').

The ω coupling constant used in the OBEP is larger than obtained from the (flavour $SU(3)$) quark model which predicts

$$\frac{g_\omega^2}{4\pi} = 9 \times \frac{g_\rho^2}{4\pi} \approx 9 \times 0.55 \approx 5. \tag{4.24}$$

Meson models typically use

$$\frac{g_\omega^2}{4\pi} = 10 - 25. \tag{4.25}$$

Note that the difference between the coupling constant at the meson pole, $g_\alpha^2/4\pi$, and at zero momentum transfer, $g_\alpha^2(\mathbf{k}^2 = 0)/4\pi$,[4] which is as large as a factor of two or so for the heavy bosons (cf. Table 4.1), is simply due to the ansatz for the form factor Eq. (4.23), which is used for reasons of simplicity. It is not the case for all form factors. For example, the so-called eikonal form factor (WJ 72, HM 76) does essentially not change between

[4]Defining $g_\alpha(\mathbf{k}^2) \equiv g_\alpha \times [\frac{\Lambda_\alpha^2 - m_\alpha^2}{\Lambda_\alpha^2 + \mathbf{k}^2}]^{n_\alpha}$, which implies $g_\alpha(-m_\alpha^2) = g_\alpha$.

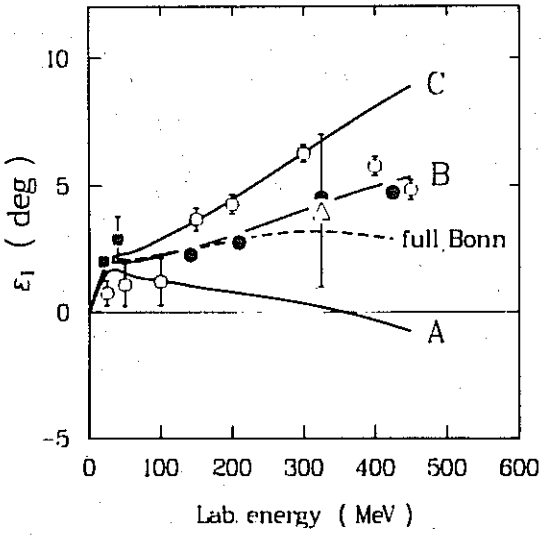

Figure 4.4: **The ϵ_1 mixing parameter for three potentials which differ by their πNN form factor (full lines).** The symbols represent phase shift analyses: open circles (Arn 87), full circles (Dub+ 82), full squares (FK 87), open triangle (Chu+ 88).

the pole and the physical region. Consequently, in meson models which use the eikonal form factor (HM 76) the coupling constants at the meson pole have values which are very close to those obtained at zero momentum tranfer when monopole or dipole form factors are used. Therefore, for a discussion of the coupling constants of the heavy mesons, the "strength" of the coupling in the physical region as represented by the value of the coupling at zero momentum transfer is more relevant than the value at the meson pole. (This does not apply to the pion.) Taking the points just mentioned into account, there is sufficient agreement between the OBEP vector coupling constants and the empirical information from dispersion theory. However, compared to the quark model the OBEP omega coupling is definitely larger (by about a factor of two). A possible reason for this may be that in meson models ω-exchange effectively parametrizes some short range repulsion coming from quark-gluon exchanges at short distances.

The σ parameters (coupling constant and mass) of the OBEP agree surprisingly well with empirical information as obtained from forward dis-

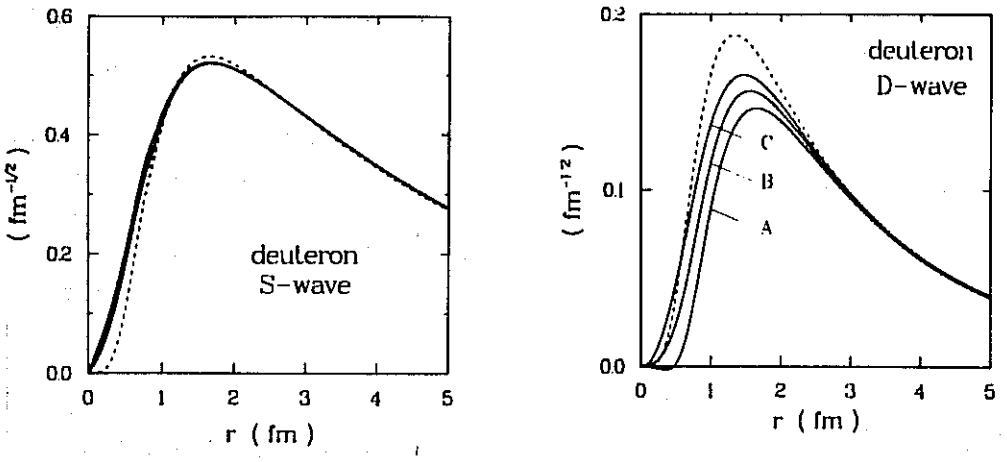

Figure 4.5: **Deuteron wave functions as determined by three potentials which differ by their πNN form factor (full lines).** The S-waves of the three potentials are not distinguishable in the figure. The dashed line shows the waves as predicted by the Reid soft-core potential.

persion relations by Grein (Gre 77).

The πNN coupling constant determines in an essential way the quadrupole moment of the deuteron and its asymptotic D/S state ratio. The value for this coupling constant as obtained from πN scattering is very consistent with those deuteron properties. This fact is one of the strongest arguments for the reality of the one-pion-exchange in nuclear physics (ER 83, Eri 84, ER 85).

There is, however, some lattitude in the πNN form factor. For the pion we use per vertex a factor of monopole form, i. e. Eq. (4.23) with $n_\alpha = 1$. If $\Lambda_\pi \gtrsim 1.3$ GeV, the NN data relevant to low energy nuclear physics can be reproduced. Such a form factor influences the OPE potential just for $r \lesssim 1$ fm, see Fig. 3.9 where $\Lambda_\pi = 1.3$ GeV is used. Concerning NN scattering parameters, this cutoff has the strongest influence on the mixing parameter ϵ_1. In Figure 4.4 we show this ϵ_1 as predicted by potentials using different choices for Λ_π, see Table 4.3. (The dashed line in that figure is from (MHE 87).) The other NN phase parameters predicted by these three potentials

are almost identical (namely like those of Potential B which are shown in Section 5.4).

The other quantities which are sensitive to Λ_π are the quadrupole moment, the asymptotic D/S state ratio, and the %-D-state of the deuteron (P_D), see Table 4.3. This is well reflected in the deuteron waves shown in Fig. 4.5.[5] Notice that the differences between the various waves occur only for $r \lesssim 2$ fm. Typically, the deuteron waves as predicted by meson-theoretic potentials are softer than those derived from phenomenological models (the dashed deuteron wave is from the Reid soft-core potential (Rei 68) with $P_D = 6.5$ %). This is partly due to the strong ρ-coupling (without ρ one obtains $P_D \approx 6.6$ %) and the πNN form factor (Table 4.3), and partly due to (*non-local*) relativistic effects contained in the potential. The strong influence of the πNN form factor on the quantities discussed is not surprising, since the one-pion-exchange provides the nuclear tensor force (slightly damped at short range by ρ-exchange). Cutting off the pion, cuts down the tensor force.

Differences in the strength of the tensor force as reflected in different deuteron D-state probabilities, have rather substantial consequences for the predicted properties of the nuclear few- and many-body problem (see Section 9). The energy of the bound three-nucleon system favours a low P_D (Section 11.1). Including relativistic saturation effects, the empirical saturation properties of nuclear matter can be described correctly when a weak tensor force (low P_D) potential is applied (Section 10.5). There are empirical indications from forward deuteron photodisintegration (AF 77, Lom 77) and from electron-deuteron scattering (Lom 80b) that the P_D should be small ($P_D \approx 4.5$ %). Because of the large impact which the tensor force has on nuclear structure calculations, it is worthwhile to think about further reactions involving the deuteron which might be sensitive to the short-range ($r \lesssim 2$ fm) deuteron waves.

As mentioned, a value of 1.3 GeV is a lower limit for Λ_π. The problems which occur for a quantitative description of the NN data when smaller values are used are demonstrated in Fig. 4.6 for some phase parameters. In one case a monopole form factor with a cutoff mass of 0.78 GeV is used ('0.78'); in the other case denoted by 'CBFF' the cloudy bag form factor

[5]Tables and a parametrization of these deuteron waves are given in Appendix C.

(Tho 83)

$$\frac{3j_1(kR)}{kR} \tag{4.26}$$

is applied, with $R = 0.8$, j_1 the spherical Bessel function, and $k = |\mathbf{k}|$. The two choices are roughly equivalent as the cutoff parameters can be related by $\Lambda_\pi = \sqrt{10}/R$. From the fact that the effect of these two form factors is about the same one can conclude that the principal range of a form factor is most important, whereas its detailed analytical structure does not have a large impact on NN processes. (The full line in Fig. 4.6 is from the OBEP with $\Lambda_\pi = 1.7$ GeV.) It is clearly seen that particularly the mixing parameters and the $^3D_1$ and $^3P_1$ phase shifts are beyond any quantitative description. Furthermore, for the case '0.78' one obtains for the deuteron quadrupole moment 0.238 fm^2, for the D/S state ratio 0.0233, and for D-state probability 2.4%. This example demonstrates that such pion form factors are unrealistic in the NN system.

To finish this section, we show in Fig. 4.7 the contributions of single mesons to the phase shifts. Note that in that figure the difference between the curve '$\pi+\omega+\sigma$' and the full curve (full OBEP) is due to ρ, η and δ, where ρ is the largest contribution. Furthermore, in Fig. 4.8 we demonstrate how single mesons contribute to a neutron-proton (np) differential cross section. (In the case denoted by 'no ρ' also the small contributions from η and δ are omitted.) Note that all contributions are iterated in the scattering equation. These figures may help to further assess the relevance of each meson for the nuclear force.

Table 4.1: **Meson parameters of a relativistic one-boson-exchange potential (OBEP) and from other sources.**

	OBEP			*OTHER SOURCES*	
	m_α	$g_\alpha^2/4\pi$	$g_\alpha^2(\mathbf{k}^2=0)/4\pi^a$ $[f_\alpha/g_\alpha]$	Coupl. const.	Method (Ref.)
π	138.03	14.4	14.21	14.28 ± 0.18	πN scattering (KP 80);
				14.52 ± 0.40	NN forward d.r. (Kro 81);
				14.25	phase-shift an. (Dub+ 82);
				14.5	phase-shift an. (Arn+ 83).
η	548.8	3	2.25	≈ 0	NN forward d.r. (GK 80);
				$\lesssim 5$	flavour $SU(3)$ (BJ 76).
ρ	769	0.9	0.42	0.6 ± 0.1	fit to $N\bar{N} \to \pi\pi$ p.w.
			[6.1]	$[6.6 \pm 1.0]$	(HP 75);
				0.55	NN forward d.r.
				[6.0]	(Gre 77).
ω	782.6	24.5	11.13	$24 \pm 5 \pm 7$	nucleon e.m. form factors
			[0.0]	$[\leq 0.2]$	(Höh+ 76);
				12.0	NN forward d.r.
				[0.0]	(Gre 77);
				8.1 ± 1.5	NN forward d.r.
				$[0.14 \pm 0.20]$	(GK 80);
				5.7 ± 2.0	fixed-s d.r. (HO 84);
				≈ 5	flavour $SU(3)$ (BJ 76).
δ	983	2.488	1.43	–	–
σ [b]	550	8.9437	7.51	14	with m_σ=670 MeV,
	(720)	(18.3773)	(13.92)		NN forward d.r. (Gre 77).

Abbreviations: analysis (an.), dispersion relations (d.r.), partial waves (p.w.).
The [tensor/vector] ratio of the vector-boson coupling constants is always quoted in square brackets.
The OBEP is defined within the relativistic three-dimensional Blankenbecler-Sugar reduction of the Bethe-Salpeter equation and uses the pseudo-scalar coupling for π and η.
[a] $g_\alpha(\mathbf{k}^2) \equiv g_\alpha F_\alpha(\mathbf{k}^2)$, $F_\alpha(\mathbf{k}^2) = [(\Lambda_\alpha^2 - m_\alpha^2)/(\Lambda_\alpha^2 + \mathbf{k}^2)]^{n_\alpha}$;
the cut-off parameters Λ_α and n_α are given in Table A.1 (Potential B).
[b] The σ parameters given in parenthesis apply to the OBEP for $T = 0$ NN states.

Table 4.2: **Deuteron and low energy scattering parameters as predicted by the relativistic OBEP defined in Table 4.1 (Theory) and from experiment (Experiment)**

	Theory	Experiment[a]	References
Deuteron			
Binding energy $-\epsilon_d$ (MeV)	2.2246	2.224575(9)	LA 82
D-state probability P_D (%)	4.99	–	–
Quadrupole moment Q_d (fm^2)	0.278 [b]	0.2860(15)	RV 75, BC 79
		0.2859(3)	ER 83, BC 79
Magnetic moment μ_d (μ_N)	0.8514 [b]	0.857406(1)	Lin 65
Asymptotic S-state A_S (fm$^{-1/2}$)	0.8860	0.8846(8)	ER 83
Asymptotic D/S-state D/S	0.0264	0.0271(8)	GKT 82
		0.0272(4)	Bor+ 82
		0.0256(4)	RK 86
Root-mean-square radius r_d (fm)	1.9688	1.9635(45)	Bér+ 73
		1.9560(68)	SSW 81, KMS 84
		1.953(3)	Kla+ 86
Neutron-proton low-energy scattering (scattering lenght a, effective range r):			
$^1S_0$: a_{np} (fm)	–23.75	–23.748(10)	Dum+ 83
r_{np} (fm)	2.71	2.75(5)	Dum+ 83
$^3S_1$: a_t (fm)	5.424	5.419(7)	Hou 71, Dil 75, KMS 84
$r_t = \rho(0,0)$ (fm)	1.761	1.754(8)	Hou 71, Dil 75, KMS 84

[a] The figures in parentheses after the values give the one-standard-deviation uncertainties in the last digits.
[b] The meson-exchange current contributions to the moments are not included in the theoretical values.

Table 4.3: **Deuteron properties for three different choices of the pion cutoff mass Λ_π.**

Potential	Λ_π (GeV)	$g_\pi^2/4\pi$	P_D (%)	Q_d	D/S
A	1.3	14.7	4.4	0.274	0.0263
B[a]	1.7	14.4	5.0	0.278	0.0264
C	3.0	14.2	5.6	0.281	0.0266

See Appendix A (Table A.1) for more details about the potentials.
[a] Potential B is presented in Table 4.1.

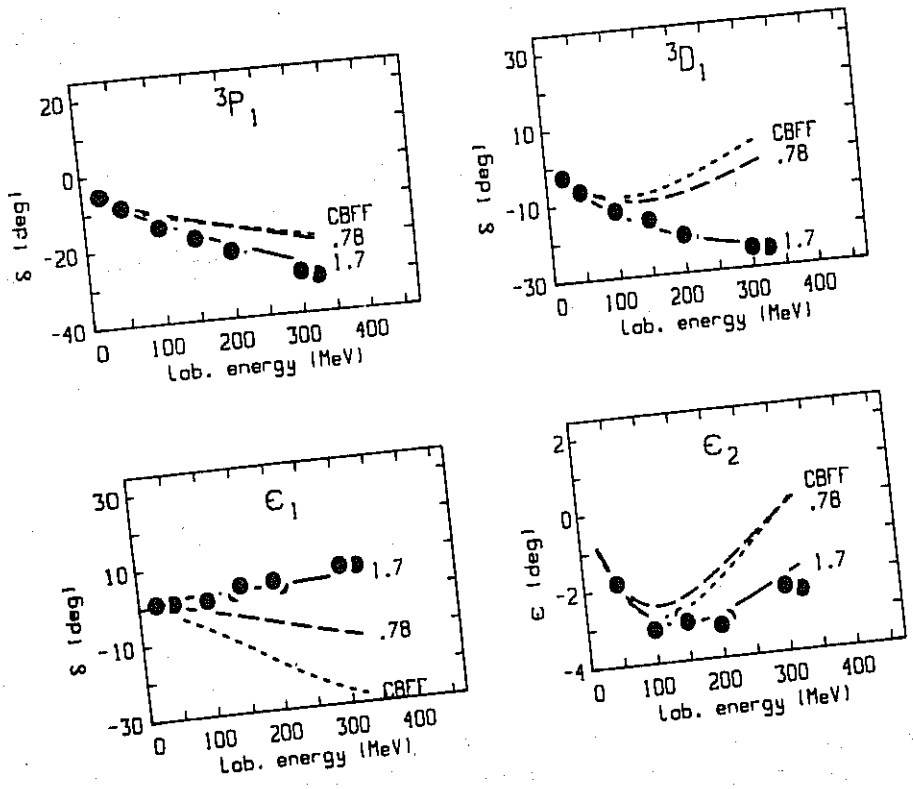

Figure 4.6: **Some phase shifts and mixing parameters as obtained for some extreme choices for the πNN form factor (dashed lines).** Explanations are given in the text. The dots represent energy independent phase shift analyses (Dub+ 82, Arn+ 83).

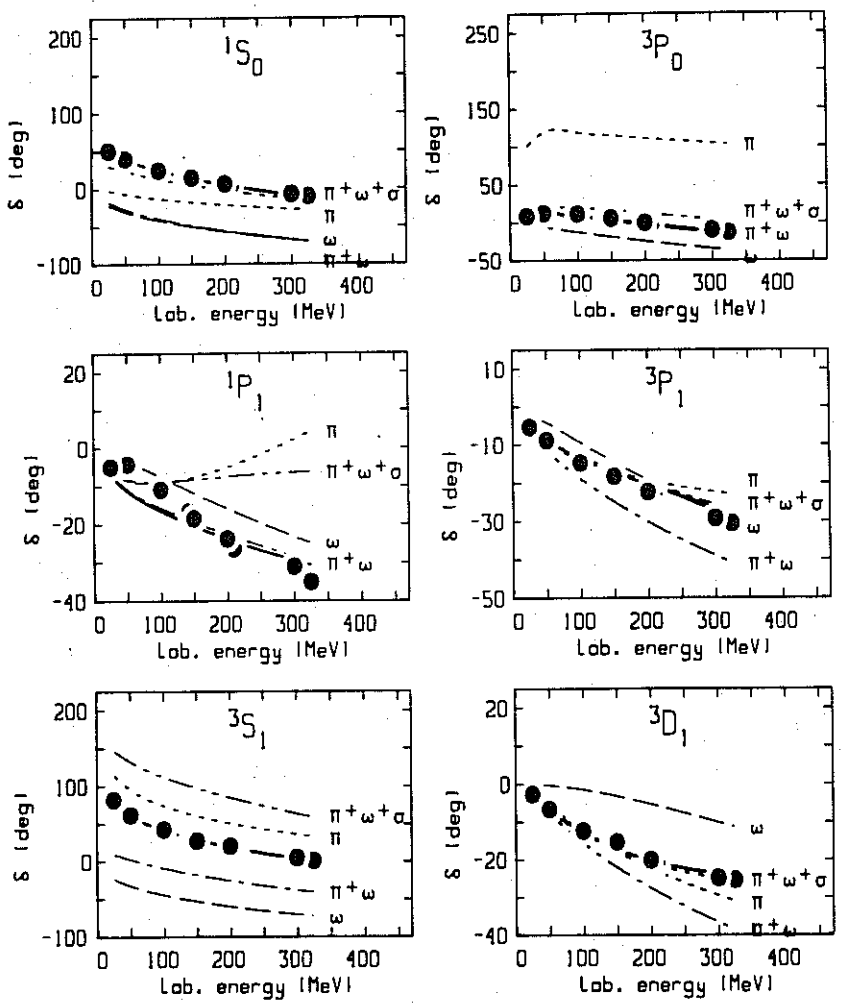

Figure 4.7: **Contributions of single mesons to phase shifts of NN scattering as denoted.** The full line is the prediction by the full OBEP (Table 4.1). The dots represent energy independent phase shift analyses (Dub+ 82, Arn+ 83).

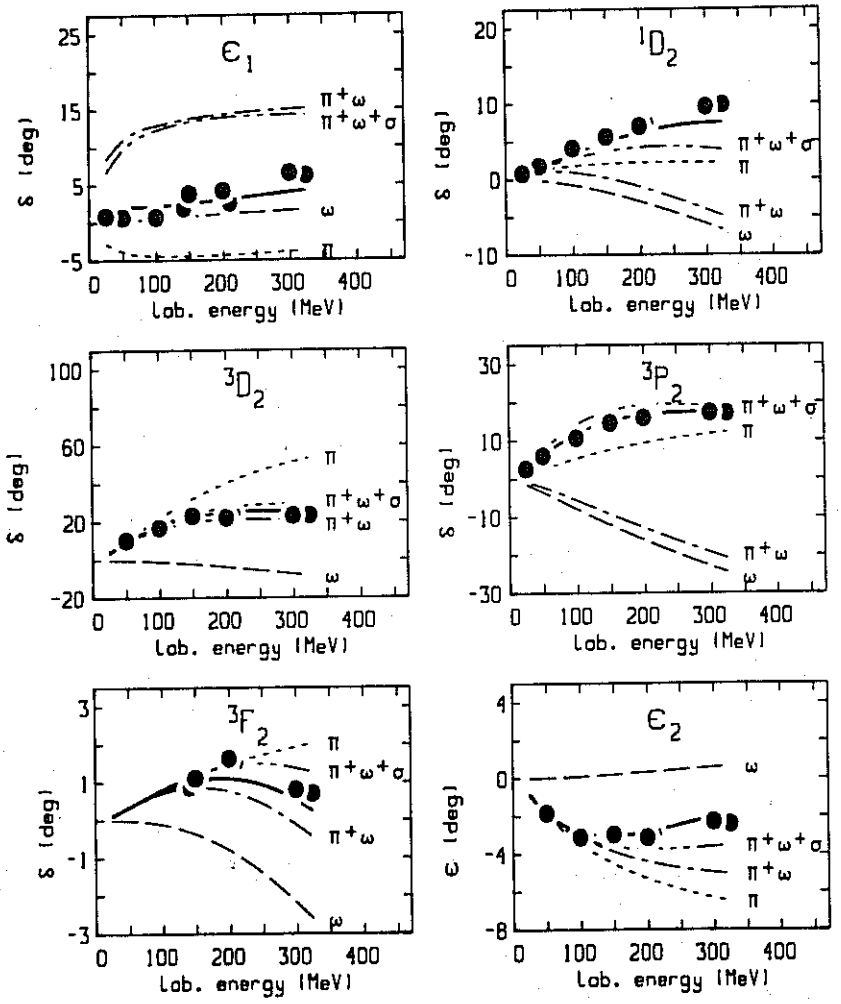

Figure 4.7: continued.

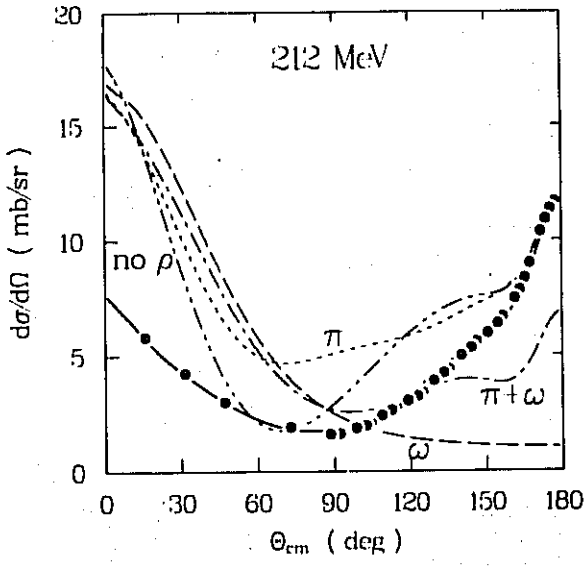

Figure 4.8: **Contributions of single mesons to the np differential cross section at 212 MeV lab. energy as denoted.** The full line represents the prediction by the full OBEP (Table 4.1). The full dots are the experimental data (Arn 87, BL 82).

Section 5

Advanced Meson-Exchange Models

In spite of its impressive quantitative success, the one-boson-exchange model has some principal deficiencies. The weakest point of the model is the fictitious σ boson which provides the intermediate range attraction. This part of the nuclear force is more realistically described by the exchange of two pions. Therefore, attempts to improve the theory have concentrated primarily on models for the 2π-exchange (Subsection 5.1). Besides this, there are other two-meson exchange contributions of importance, in particular the $\pi\rho$ diagrams (Subsection 5.2). In the last two parts of this section we will perform a comparison of meson-theoretic predictions with experimental data.

5.1 Models for the 2π Exchange

As mentioned, essentially two approaches have been used to derive the 2π-exchange potential: dispersion relations and field theory. Subsequently, we will sketch both briefly.

5.1.1 The Dispersion-Theoretic Approach

Figure 5.1 describes schematically the dispersion-theoretic picture of the 2π-exchange. In this approach one assumes that the total diagrams (a)

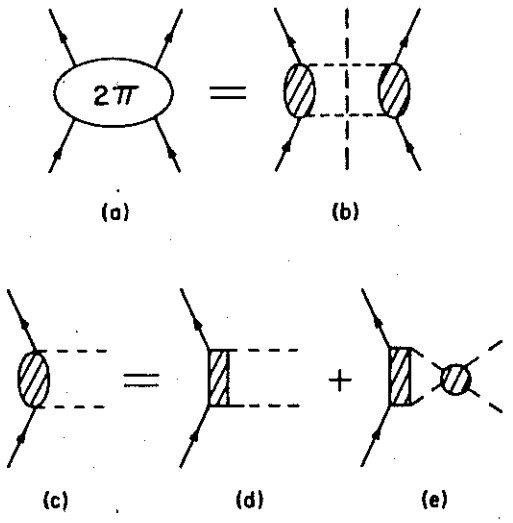

Figure 5.1: **The 2π-exchange contribution to the NN interaction as viewed by dispersion theory** and explained in the text. Full lines represent nucleons, dashed lines pions.

can be analysed in terms of two 'halves' (b). The hatched ovals stand for all possible processes which two pions and a nucleon can undergo. This is made more explicit in (d) and (e). The hatched boxes represent all possible baryon intermediate states including the nucleon. (Note that there are also crossed exchanges which are not shown.) The shaded circle stands for $\pi\pi$ scattering. Quantitatively, these processes are taken into account by using empirical information from πN and $\pi\pi$ scattering (e. g. phase shifts) which represents the input for such a calculation. Dispersion relations then provide an on-shell NN amplitude, which — with some kind of plausible prescription — is represented as a potential.

The Paris potential (Lac+ 80) is constructed along this line complemented by one-pion-exchange (OPE) and ω-exchange. For further details we refer the interested reader to the pedagogical article by Vinh Mau (Vin 79).

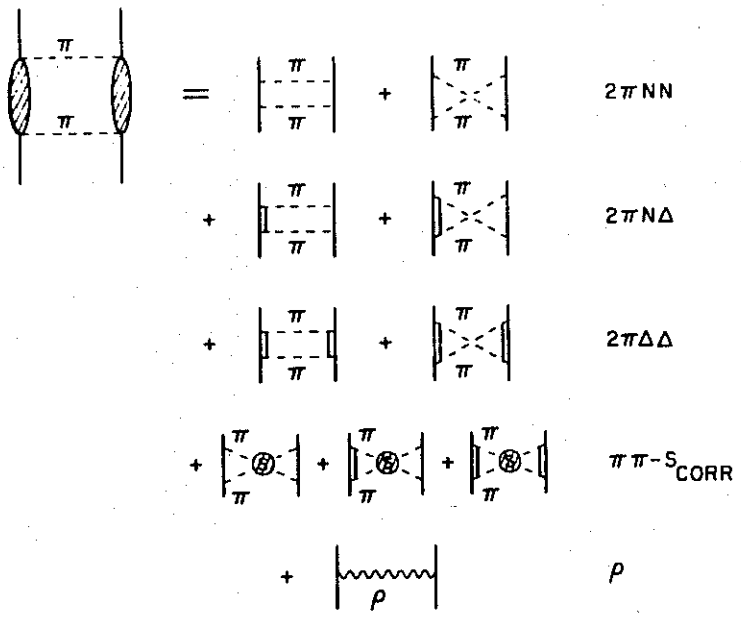

Figure 5.2: **Field-theoretic model for the 2π-exchange.** Full lines represent nucleons, double lines isobars, and dashed lines pions. The hatched circles are $\pi\pi$ correlations.

5.1.2 A Field-Theoretic Model

Alternatively, a field-theoretic model can be developed. It has the advantage that the 'potential' (i. e. the set of all irreducible diagrams, the kernel of the scattering equation) is given *a priori* on and off the energy shell. Furthermore, the effects of the medium which occur, when the potential is inserted into a many-body environment, can be calculated with such a model (Section 10.2-3). In Section 7 we will see that a field-theoretic model can be extended to intermediate energies in a straightforward way and allows for an explanation of the inelasticities in NN scattering.

Figure 5.2 shows an example for a field-theoretic model for the 2π-exchange [from (MHE 87)]. To be realistic, this model includes contributions from isobars as well as from $\pi\pi$ correlations. This can be understood

in analogy to the dispersion relations picture Fig. 5.1. In general, only the lowest-lying πN resonance, the so-called Δ isobar (spin 3/2, isospin 3/2, parity +, mass 1232 MeV), is taken into account. The contributions from other resonances have proven to be small for the low-energy NN processes under consideration. A field-theoretic model treats the Δ isobar as an elementary (Rarita-Schwinger) particle. The Lagrangians, describing the interactions involved, are given in Appendix A and B.

In the model shown, contributions from baryon-antibaryon intermediate states ('pair terms') are omitted ('suppressed'). Using the pseudovector (gradient) coupling for the πNN vertex (which is suggested as an effective coupling by chiral symmetry (GL 60, Wei 67, Bro 79)), these pair contributions have been shown to be small (FT 80, ZT 81). Also, there are large cancelations between one- and two-pair contributions (Fig. 2.1c and d). The latter point was noticed already in the early 1950's (BW 53) and has been recently confirmed (Hip 88). Furthermore, there are plausible arguments based on the quark model which suggest that the baryon-antibaryon vertex may be considerably suppressed as compared to the corresponding baryon-baryon vertex (Bro 84).

The six upper diagrams of Fig. 5.2 represent uncorrelated 2π exchange. The crossed (non-iterative) two-particle exchanges (second diagram in each row) are important. They guarantee the proper (very weak) isospin dependence due to characteristic cancelations in the isospin dependent parts of box and crossed box diagrams. Furthermore, their contribution is about as large as that from the corresponding box diagrams (iterative diagrams); therefore, they are not negligible. Moreover, it has turned out that the quantitative description of the two-nucleon phase shifts, particularly, in low angular momentum partial waves is considerably improved when the crossed diagrams are included. This valuable experience is a further indication for the reality of the model.

We note that in the particular model under consideration the diagrams are evaluated in a non-static approach using time-ordered perturbation theory (see Section 10.2-3 for more details). For diagrams of two-particle exchange, including baryon-resonance intermediate states and suppressing pair terms, this method is more approriate than convariant perturbation theory (which leads to characteristic problems when isobars are included, see (PL 70)). Furthermore, the application of the model in the many-body system is considerably facilitated in the time-ordered approach. In this

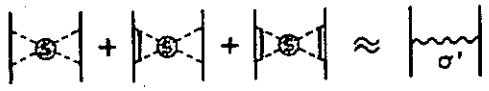

Figure 5.3: **Correlated 2π-S-wave exchanges defining σ'.**

approach, meson retardation (baryon recoil) is naturally included which has turned out to be crucial to obtain realistic contributions from the various diagrams. In the static approximation corresponding diagrams are by factor of two or so bigger furnishing unphysically large contributions which cause problems in describing the NN data.

In addition to the processes discussed, also correlated 2π exchange has to be included (lower two rows of Fig. 5.2). Quantitatively, these contributions are about as large as those from the uncorrelated processes. The correlated $(I = 1, J = 1)$ 2π-P-wave contribution is described by the exchange of a ρ meson which is a proper resonance with a known width. The $(I = 0, J = 0)$ 2π-S-wave correlations, which do not lead to a resonance, have been examined by Durso *et al.* (DJV 80). They showed that these contributions can be well approximated by the exchange of a scalar-isoscalar boson (called σ') with a broad mass distribution and a well-defined coupling constant (see Fig. 5.3). For the $\pi\pi$-S-wave interaction the authors of (DJV 80) use empirical information from $\pi\pi$ scattering. Thus, the σ' of Fig. 5.3 is a well-defined, realistic and quantitative contribution (in contrast to the OBE model σ which is an adjustable parameter).

To properly examine and analyse contributions to the nuclear force, one must always think in terms of ranges (TNS 51). The 2π-exchange is of long/intermediate range. Therefore, to check its reality, we have to look into NN partial waves of high angular momentum ($J \geq 4$) where the centrifugal barrier keeps the two nucleons at an intermediate distance. This is done in Fig. 5.4.[1] The full line in that figure contains all 2π-exchange

[1]In this figure, as throughout this article, 'bar' phase shifts as defined in (SYM 57) are used for NN scattering below the inelastic threshold.

contributions discussed (Fig. 5.2) plus OPE and ω-exchange. (Note that due to its short range nature, the ω contribution is negligibly small in most partial waves shown.) It is clearly seen that the phase shifts in these high partial waves are described very satisfactorily. Note that the difference between the dash-dot line (OPE) and the full line is essentially the effect of the 2π exchange. Obviously there is quite some spin- and L-dependence which is correctly described by the model.

In Fig. 5.5 we show for the case of the ${}^3F_4$ partial wave the effects of the single diagrams of the model Fig. 5.2. It is clearly seen that box and crossed box diagrams[2] are about equally large and that correlated and uncorrelated contributions are equally important. Diagrams involving isobars are typically appreciably larger than those with nucleon intermediate states only. Note that the $N\Delta\pi$ coupling (squared) is about four times as large as the corresponding $NN\pi$ coupling (squared) ($f^2_{N\Delta\pi}/4\pi \approx 0.23 - 0.35$, $f^2_{NN\pi}/4\pi = 0.08$).

We mentioned the dispersion theoretic approach to the problem under consideration. Quite obviously, one may now ask the curious question: how do both approaches compare in quantitative terms? To answer this question, we show in Fig. 5.6 predictions from both types of approaches in some higher partial waves. Dotted lines represent the predictions from dispersion theory (with label P'73 from (Vin+ 73), label P'80 from (Lac+ 80)). Apart from some scatter in the dispersion theoretic results, which may be due to changes in the empirical πN input over the years and/or some uncertainties in the analytic continuations involved in the derivation, the agreement appears to be sufficient.

5.2 $\pi\rho$ Contributions

So far we have considered only higher angular momentum partial waves of NN scattering (long/intermediate ranges). When we turn now to lower partial waves, shorter ranged contributions must come into play. There are, of course, the vector mesons ρ and ω, which — as discussed — are very important. However, there are also two-meson exchange contributions of

[2]For a precise definition of iterative and non-iterative diagrams see Fig. 10.9, where diagram 1 – 4 are iterative and 5 – 12 non-iterative; note that the stretched box diagrams (5 and 6) provide very small contributions.

comparable range. One important set of such diagrams is shown in Fig. 5.7. It is constructed in analogy to the uncorrelated part of the 2π exchange model. It turns out that the diagrams of $\pi\rho$ exchange, shown in Fig. 5.7, are absolutely crucial for a quantitative description of lower partial waves, in particular P-waves. We demonstrate this fact in Fig. 5.8 where in the case of the dashed and the dotted curves the $\pi\rho$ contributions are omitted (the two curves differ by the π-cutoff mass which is denoted in units of GeV). It is clearly seen that in particular $^3P_1$ changes drastically to unphysical values without the repulsive $\pi\rho$ diagrams. The $\pi\rho$ contributions have obviously a strong spin dependence which is needed to appropriately suppress the rather large 2π-exchange contributions at short distances. Note that also the crossed $\pi\rho$ exchanges are included which — as in the case of the 2π exchange — considerably improve the quantitative results.

The repulsive character of the $\pi\rho$ diagrams can be understood from the fact that the tensor forces created by single π and single ρ exchange are of opposite sign (Section 3.4 and Appendix B), which together with the negative intermediate two-baryon propagator results in a positive contribution. The spin-spin forces of π and ρ, which are of equal sign, lead to attraction for the $\pi\rho$ combination that is, in general, typically smaller than the contribution emerging from the tensor forces (except in $^3P_0$, Fig. 5.8).

We mentione that the $\pi\rho$ contributions are still sizable in D-waves. Thus, their repulsive effect leads to a much better agreement with the empirical phase shifts, particularly, in $^3D_2$ and $^3D_3$. The latter two partial waves are overestimated in most meson-exchange models (Lac+ 80, NRS 78).

It had been conjectured (Dur+ 77) that, because of its repulsive nature, the $\pi\rho$ contributions could take over part of the role the ω plays in OBE models. However, ω exchange does not have the drastic spin-dependence that we have just seen for $\pi\rho$ diagrams (Fig. 5.8). Therefore, these two contributions are not simply interchangable. The fact is: when an explicit field-theoretic model for the 2π exchange is used, the corresponding diagrams of $\pi\rho$ exchange are needed to arrive at a realistic total contribution from the sum of both sets of diagrams. A strong ω is required in addition (see Table 5.1), for the usual reasons which apply to just any meson model for the nuclear force (for a detailed discussion and a quantitative demonstration of these points see (MHE 87)).

5.3 Other Two-Meson Exchange Contributions

Once certain two-meson exchanges involving also heavy mesons have turned out to be important, one should (at least for reasons of consistency) look into other diagrams of that kind. In Fig. 5.9 we give an overview. The diagrams discussed so far are located above and left of the dashed line. Systematic investigations have shown that further diagrams contribute amazingly little (MHE 87). Important for this result is an appropriate grouping of the diagrams (which are individually already small). In which way diagrams should be grouped together, is indicated by the arrows in Fig. 5.9. In this way, an increasing cancelation occurs between the different sets of diagrams when proceeding to the lower right of that figure. Thus, some kind of 'convergence' of the diagrammatic expansion is observed 'empirically'.

We finally mentione that there is a non-negligible contribution from crossed $\pi\sigma$ exchange which increases the tensor force. This allows for a more consistent choice of the πNN and the $\pi N\Delta$ form factors (namely closer to each other), which in most models including isobars differ in an unreasonable way.

5.4 Results

In this section we have stressed the fact of the two alternative meson-theoretic approaches to the nuclear force. Accidentally, for each of the two approaches there exists one carefully constructed example: the Paris potential (dispersion theory, Lac+ 80) and the Bonn potential (field theory, MHE 87).

We give the coupling constants used in both models (and for OBEP) in Table 5.1, which demonstrates an amazing agreement in spite of the substantial differences in the details of the models. The $N\Delta$ coupling constants used in the Bonn model are based on relations derived from the quark model (BW 75)

$$f^2_{N\Delta\pi} = \frac{72}{25} f^2_\pi \tag{5.1}$$

with

$$f_\pi = g_\pi \frac{m_\pi}{2M}, \tag{5.2}$$

and

$$f^2_{N\Delta\rho} = \frac{f^2_{N\Delta\pi}}{f^2_\pi}[g_\rho(1 + f_\rho/g_\rho)m_\rho/2M]^2 \tag{5.3}$$

using the notation $f_\pi \equiv f_{NN\pi}$.

An alternative source for the $\pi N\Delta$ coupling constant is the empirical width of the Δ which implies $f^2_{N\Delta\pi}/4\pi = 0.35$. The smaller value for that coupling as predicted by the quark model (namely ≈ 0.23) is reasonable when crossed diagrams are included (as in the case of the Bonn model) to avoid double counting. The larger value obtained from the Δ width is appropriate in models which include box-type diagrams only, like coupled channel models (see Section 7 and Appendix B).

Concerning the low energy scattering parameters and the deuteron properties, the Paris and the Bonn potential essentially reproduce accurately the experimental values as given in Tables 4.2 and 6.1. There is a difference in the singlet scattering length (and effective range) between the two potentials, since the Paris potential fits pp data (for $T = 1$) while for the Bonn potential there exists a np (MHE 87) and a pp version (see footnote to Table 6.2 below). Furthermore, the two potentials differ in their predictions for the D-state probability of the deuteron (Paris: 5.77 %, Bonn: 4.25 %). The low %-D-state as predicted by Bonn is mainly due to the inclusion of meson retardation in that field-theoretic model.

The explicit field-theoretic form of the Bonn potential allows to determine for the deuteron the probabilities of having configurations other than just two nucleons. They are (with the probability given in parenthesis): $\Delta\Delta$ (0.62 %), $\Delta\Delta\pi\pi$ (0.29 %), $N\Delta\pi\pi$ (0.44 %), $NN\pi\pi$ (0.30 %), $NN\pi$ (1.32 %). The total probability of having anything but just two nucleons is 3.94 %.[3]

In Figs. 5.10-12 and Table 5.2 we show some predictions from the two models for NN phase shifts and observables in comparison.[4] It is seen in the figures and the table that the two models reproduce the data in general with very high precision. (Predictions from the OBEP of Section 4 are included in the figures by the dotted line; note that this dotted curve is omitted whenever it is very close to the full line.) Furthermore, both predictions are so close that in most cases it is impossible to distinguish

[3]The values given here are more accurate than the previous ones (MHE 87).

[4]The Paris $T = 1$ np potential is the pp potential without Coulomb effects (Arn 87).

between them. The only exception are some np spin observables at 325 MeV where, however, the experimental errors are rather large. *This demonstrates in an impressive way, how extraordinarily quantitative meson theory is for the low-energy NN interaction.*

5.5 Off-Shell Aspects

In the previous subsection we have clearly seen that the on-shell predictions of present-day meson models show very little differences. With on-(energy)-shell it is meant that the total energy of the two nucleons in the initial and final state of the reaction is the same. This is, of course, always the case in elastic two-nucleon scattering.

On the other hand, the behaviour of the nuclear potential off the energy shell does play a role in various sectors of nuclear physics, for example in pion production and in the nuclear many-body problem. In virtual intermediate states the nucleons violate energy conservation; such states enter nuclear structure calculations, in general, in a different way as compared to the two-nucleon problem in free space (see Section 9.4).

Due to the differences in the derivation of models for the nuclear force, there are indeed differences off-shell. Dispersion relations yield a scattering amplitude on-shell. However, by defining a potential some kind of off-shell prescription enters the derivation silently. Like the Reid potential (Rei 68), the Paris potential is parametrized in terms of static Yukawa functions which define the potential on- and off-shell. In the fieldtheoretic approach, the set of irreducible diagrams defining a quasi-potential is given *a priori* on- and off-shell. Because of these substantial differences in the origin of the off-shell part of the potentials, it is interesting to see if noticable differences occur. Therefore, in Fig. 5.13 we show half-shell K matrices as derived from the Bonn (full line), Paris (dashed), and the Reid (dotted) potential. The $^1S_0$ and the $^3P_1$ partial waves are considered. The on-shell point is denoted by the full dot. It is clearly seen that for $^1S_0$ there exist, indeed, drastic off-shell differences between the potentials. In the case of the P-wave, however, these differences are already strongly reduced.

NN Bremsstrahlung ($NN\gamma$), i. e. the reaction

$$N + N \longrightarrow N + N + \gamma,$$

is one way of investigating the off-shell behaviour of the NN interaction. Due to the production of a photon, the corresponding nucleons are put off their energy shell. Some processes contributing to $NN\gamma$ are shown in Fig. 5.14. Note that there are also other, so-called internal mechanisms, like rescattering and meson current contributions, which are not shown. However, for pp Bremsstrahlung these internal processes contribute only at a higher order of the photon momentum and are, therefore, expected to be small (Fea 87, WF 86, Mor 72, Sig 69, SC 63).

In Fig. 5.15 we show a cross section and an analysing power measured in a TRIUMF experiment on $pp\gamma$ (Kit+ 86). The theoretical calculations have been done by H. W. Fearing *et al.* (Fea 87, WF 86). (The short-dashed curve in that figure is obtained in the soft-photon approximation, the dotted curve in an on-shell approximation.) The differences between the predictions from different potentials are very small. On the background of the half-off-shell K-matrices just considered, this result appears amazing in the first moment. However, more detailed investigations (Fea 87) have shown that the $^1S_0$ partial wave contributes little in this process. The main contributions are coming from P-waves, in which, as we have seen, the off-shell differences are already rather small. On the background of this experience one should try to think about reactions which are more sensitive to the S-wave contribution. It would be worthwhile to check-out on the theoretical side if $np\gamma$ might be a candidate.

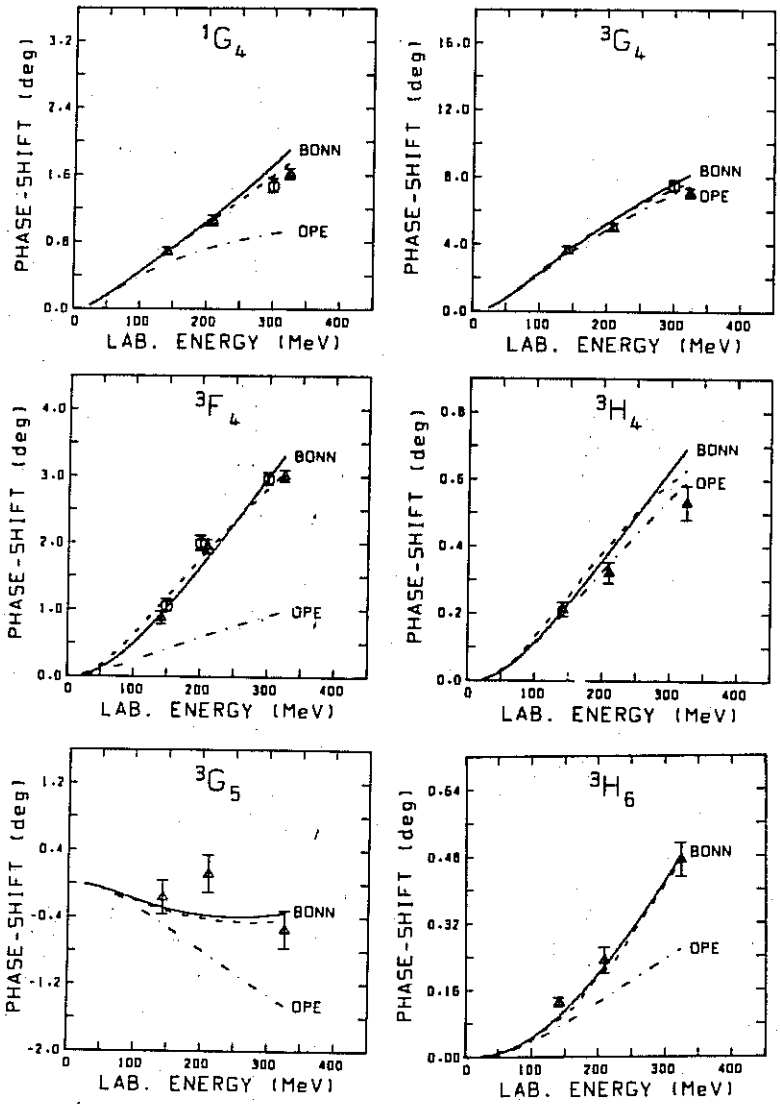

Figure 5.4: **Higher partial wave phase-shift predictions from a field-theoretic model for the 2π exchange** complemented by OPE and ω exchange (full line). The single pion contribution (OPE) is given by the dash-dot line. Phase-shift analyses are represented by the dashed line, octagons (Arn+ 83), and triangles (Dub+ 82).

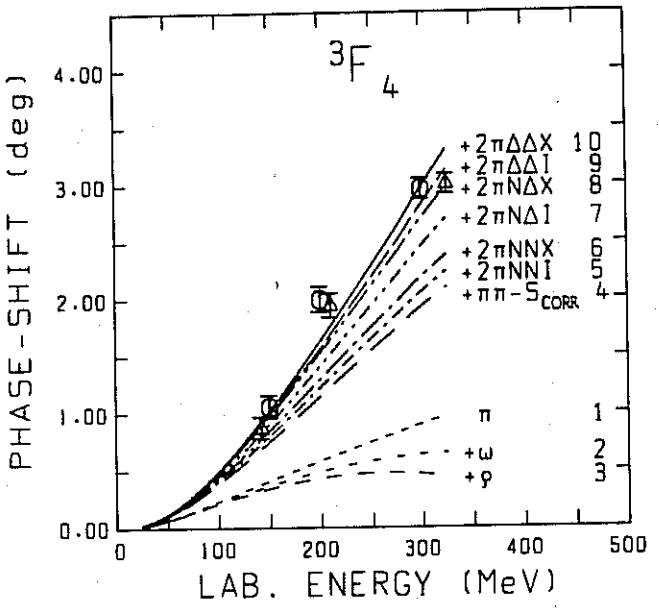

Figure 5.5: **The effects from the individual diagrams of the field-theoretic 2π-exchange.** The contributions are added up successively in the denoted order. The notation is explained in Fig. 5.2. 'I' stands for iterative contribution, 'X' for non-iterative.

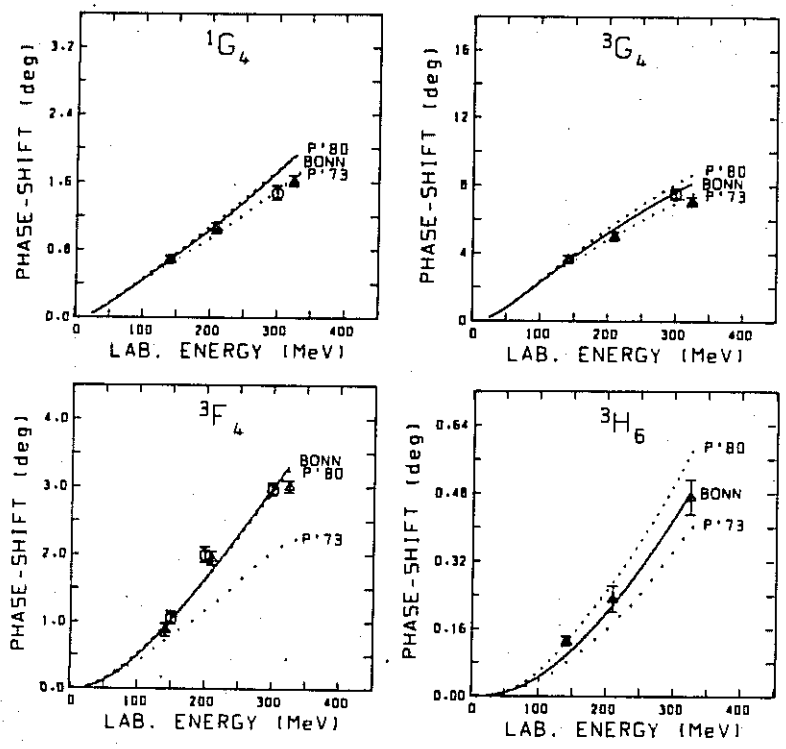

Figure 5.6: **Comparison of predictions from a field-theoretic model (full line) and from dispersion relations calculations (dotted lines) of the 2π exchange.** Shown are NN phase shifts.

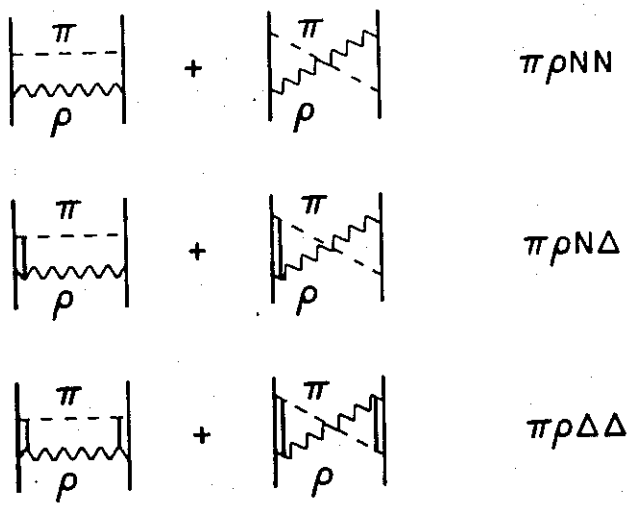

Figure 5.7: $\pi\rho$ **contributions to the** NN **interaction.**

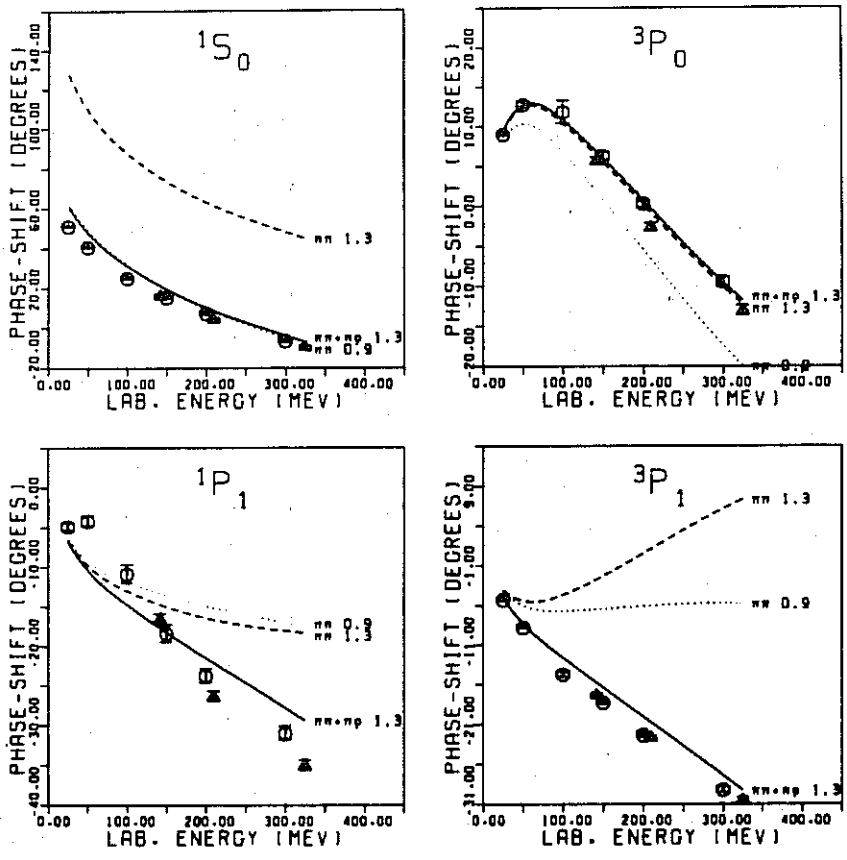

Figure 5.8: Effect of the $\pi\rho$ diagrams on lower partial waves. The full line contains the $\pi\rho$ contributions, which are omitted in the dashed and dotted line. The number in the curve label quotes the pion cutoff mass used in units of GeV.

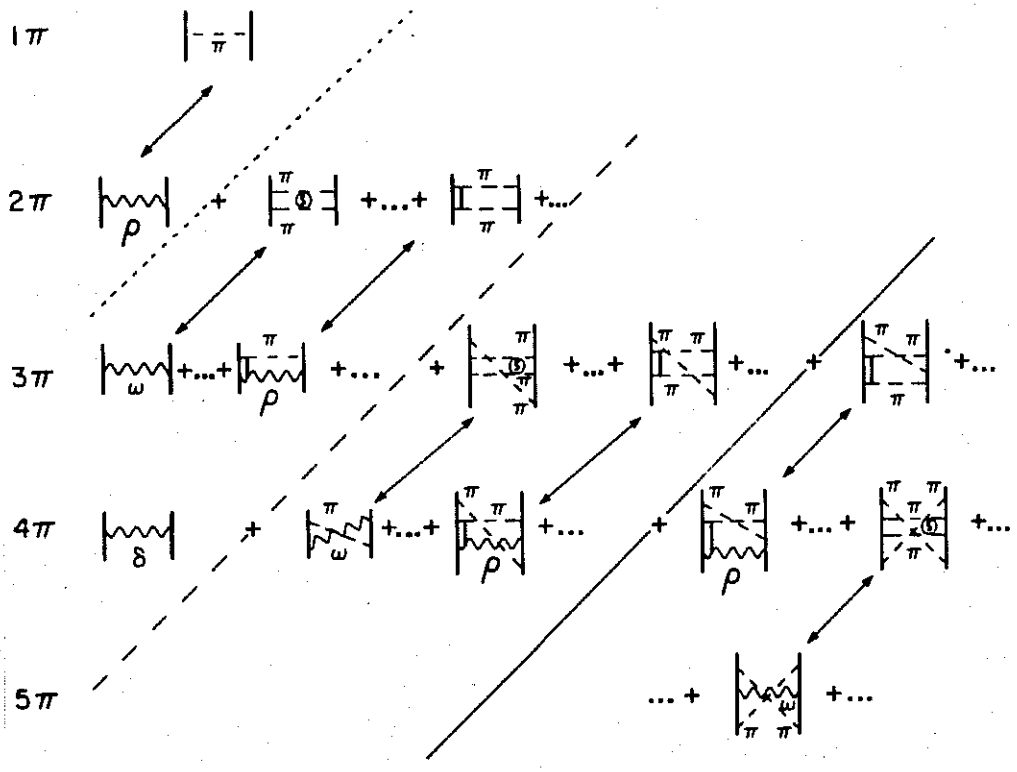

Figure 5.9: **Diagrammatic expansion of the meson-theoretic NN interaction.** Explanations are given in the text.

Table 5.1: **Meson-baryon coupling constants used in different meson-theoretic NN potentials.**

	OBEP [a]	*Paris* [b]	*Bonn* [c]	Λ_α (GeV)
$NN\pi$	14.21 (14.4)	14.43	14.08 (14.4)	1.3
$NN\eta$	3 (2.25)	0	0	–
$NN\rho$	0.42 [6.1] (0.9)	0.55 [6.6]	0.41 [6.1] (0.84)	1.4
$NN\omega$	11.13 [0.0] (24.5)	11.75 [–0.12]	10.6 [0.0] (20)	1.5
$NN\sigma^d$	7.51 (8.94)	–	4.56 (5.69)	2
$NN\delta$	1.43 (2.49)	0	1.62 (2.82)	2
NNA_1	0	14	0	–
$N\Delta\pi$	–	–	0.218 (0.224)	1.2
$N\Delta\rho$	–	–	4.86 (20.45)	1.4

For models which apply a form factor, $g_\alpha^2(\mathbf{k}^2 = 0)/4\pi$ and $(g_\alpha^2/4\pi)$
are given — the latter in round parenthesis —
(and correspondingly for the $N\Delta$-vertices using $f_{N\Delta\alpha}$).
For vector mesons, the tensor/vector ratio is quoted in square brackets.
The cutoff masses in the last column refer to the full Bonn model
(with $n_\alpha = 1$, except for $n_{N\Delta\rho} = 2$).
See Table 4.1 for definitions and a comparison to coupling constants from other sources.
[a] Section 4. [b] (Lac+ 80). [c] Full Bonn Model (MHE 87).
[d] The σ-mass is 550 MeV for both OBEP and Bonn.

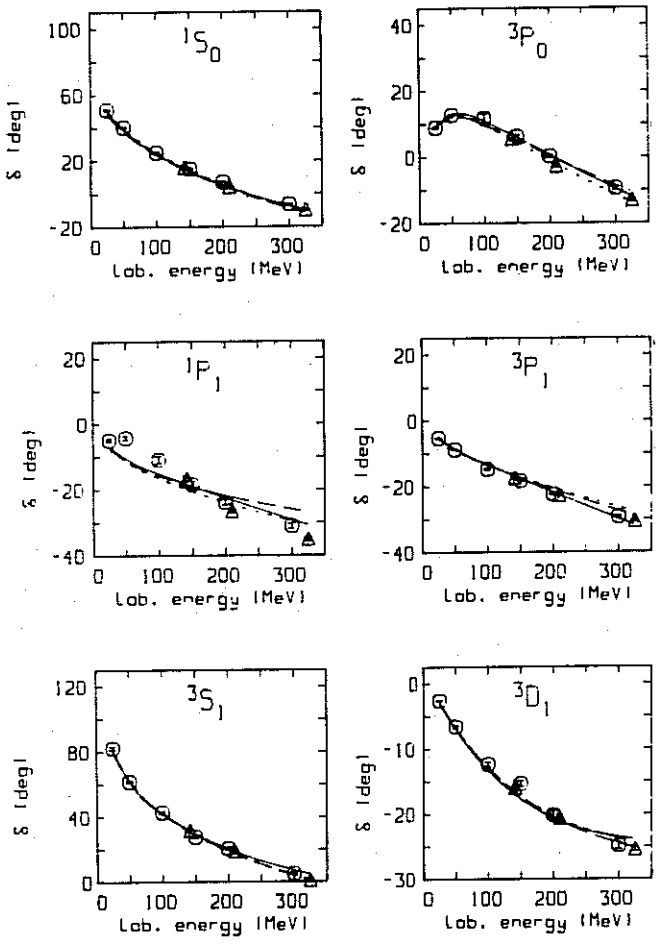

Figure 5.10: *np* **phase parameters as predicted by the Bonn (full line), the Paris potential (dashed), and the OBEP of Section 4 (dotted).** The octagons (Arn+ 83) and triangles (Dub+ 82) represent phase shift analyses.

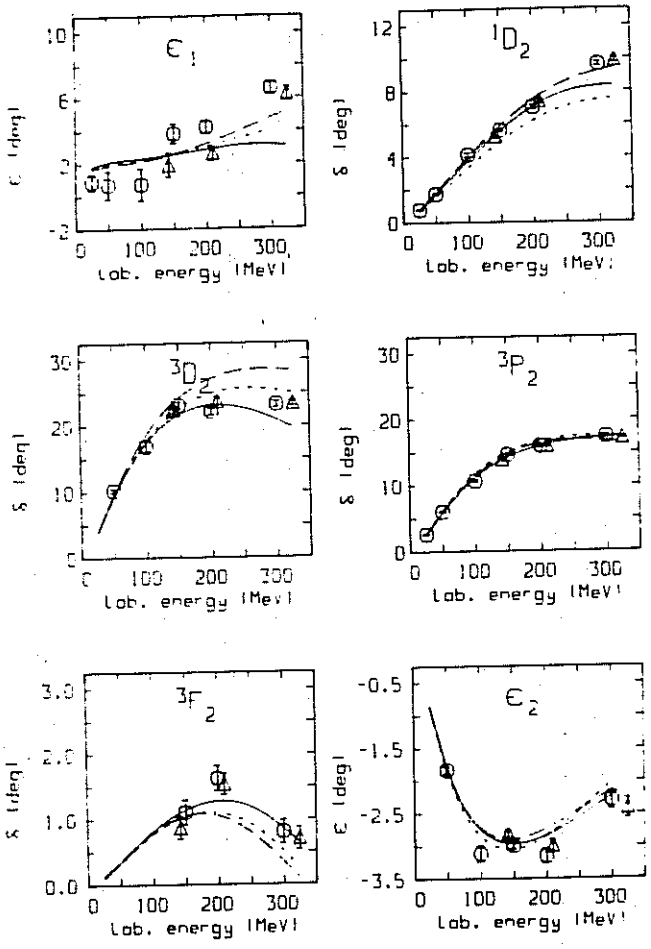

Figure 5.10: continued.

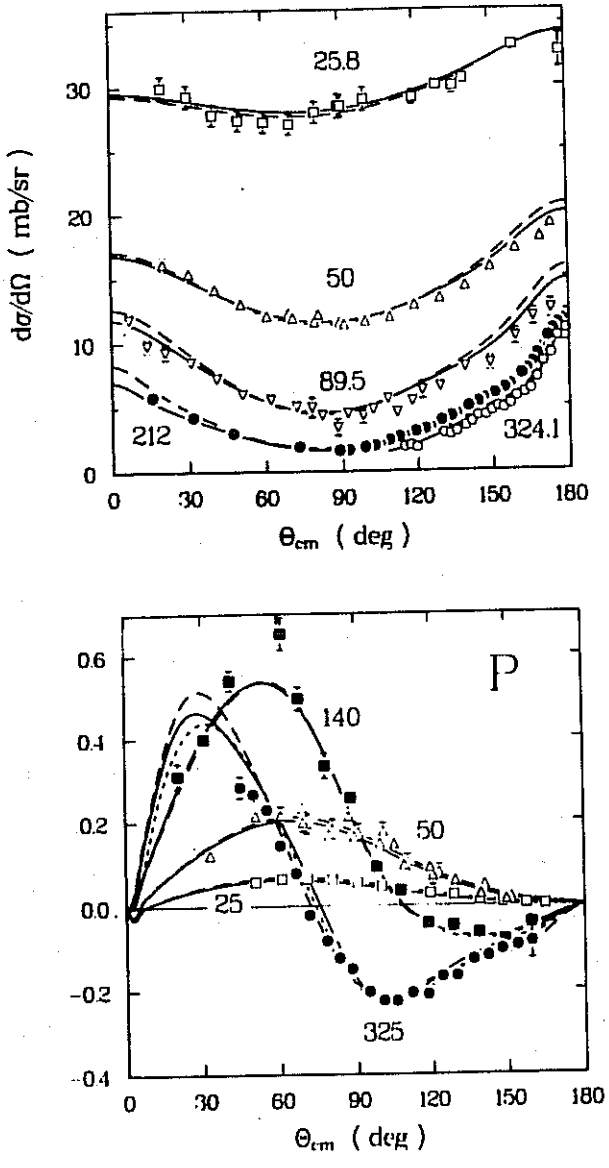

Figure 5.11: **Some *np* observables.** Lab. energies and observables as denoted. The curves representing predictions from different potentials are defined as in Fig. 5.10. For references to the experimental data see (Arn 87, BL 82). For notation see (Hos 68).

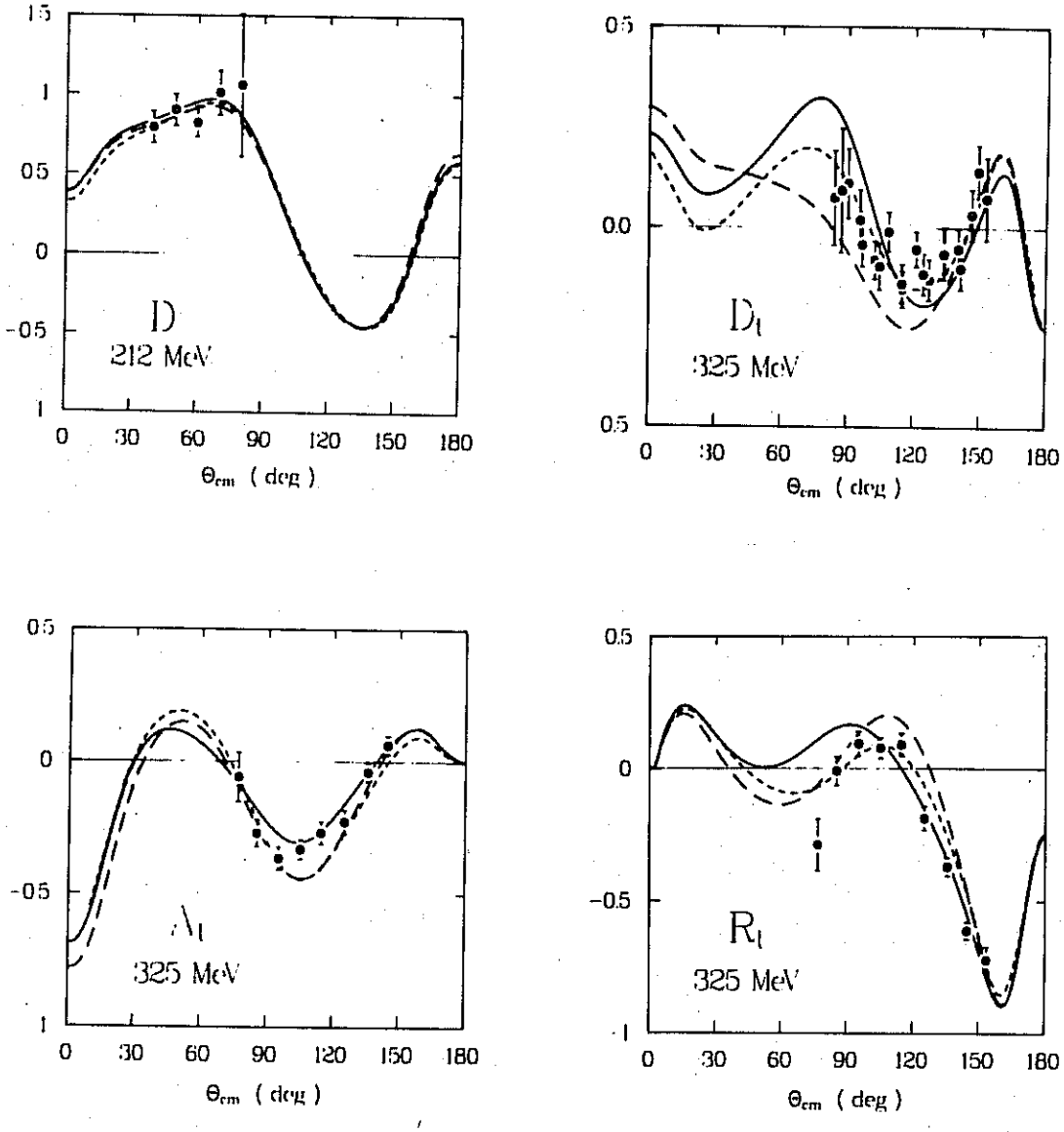

Figure 5.11: continued.

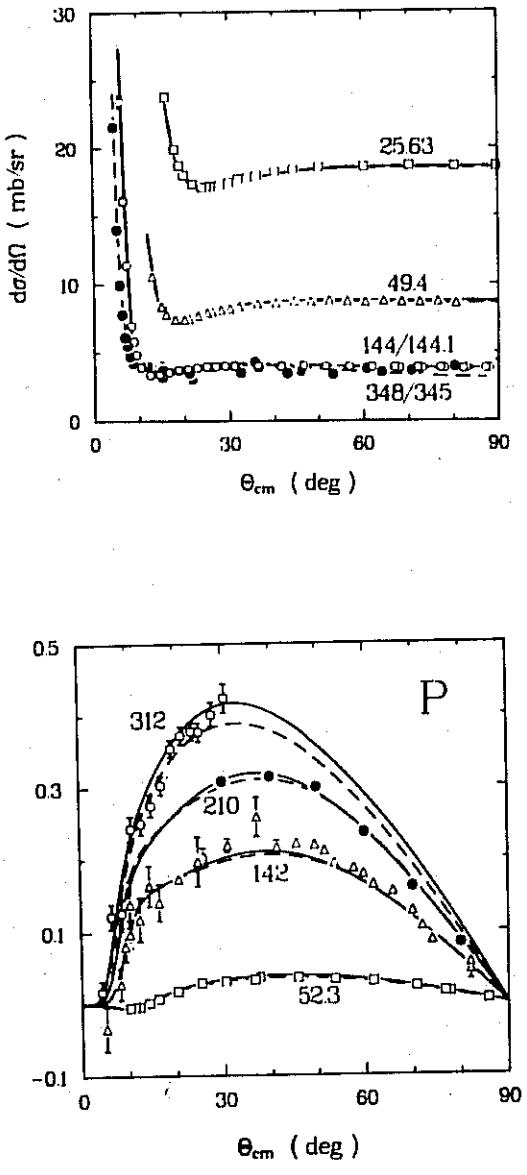

Figure 5.12: **Some *pp* observables,** notation as in Fig. 5.11.

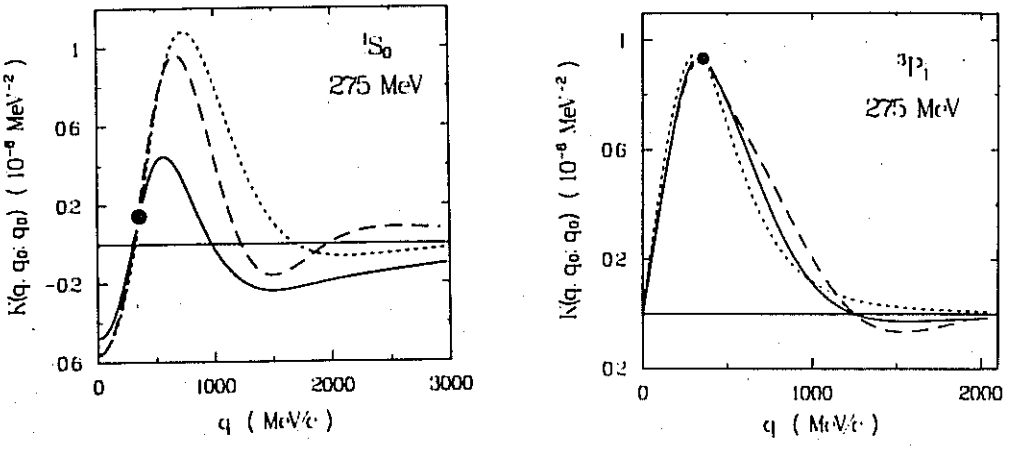

Figure 5.13: **Half-off-shell K-matrices at 275 MeV lab. energy** as derived from the Bonn (full line), the Paris (dashed), and the Reid (dotted) potentials. The on-shell point is given by the dot.

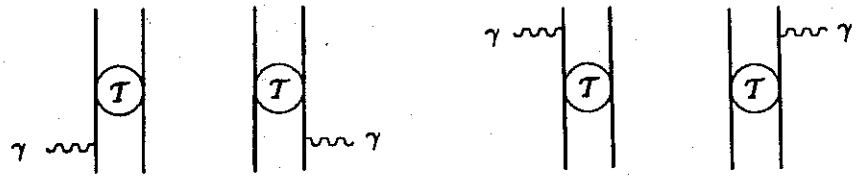

Figure 5.14: **Processes contributing to NN Bremsstrahlung taken into account by Fearing** *et al.* (Fea 87, WF 86). $\mathcal{T}$ represents the NN $\mathcal{T}$-matrix.

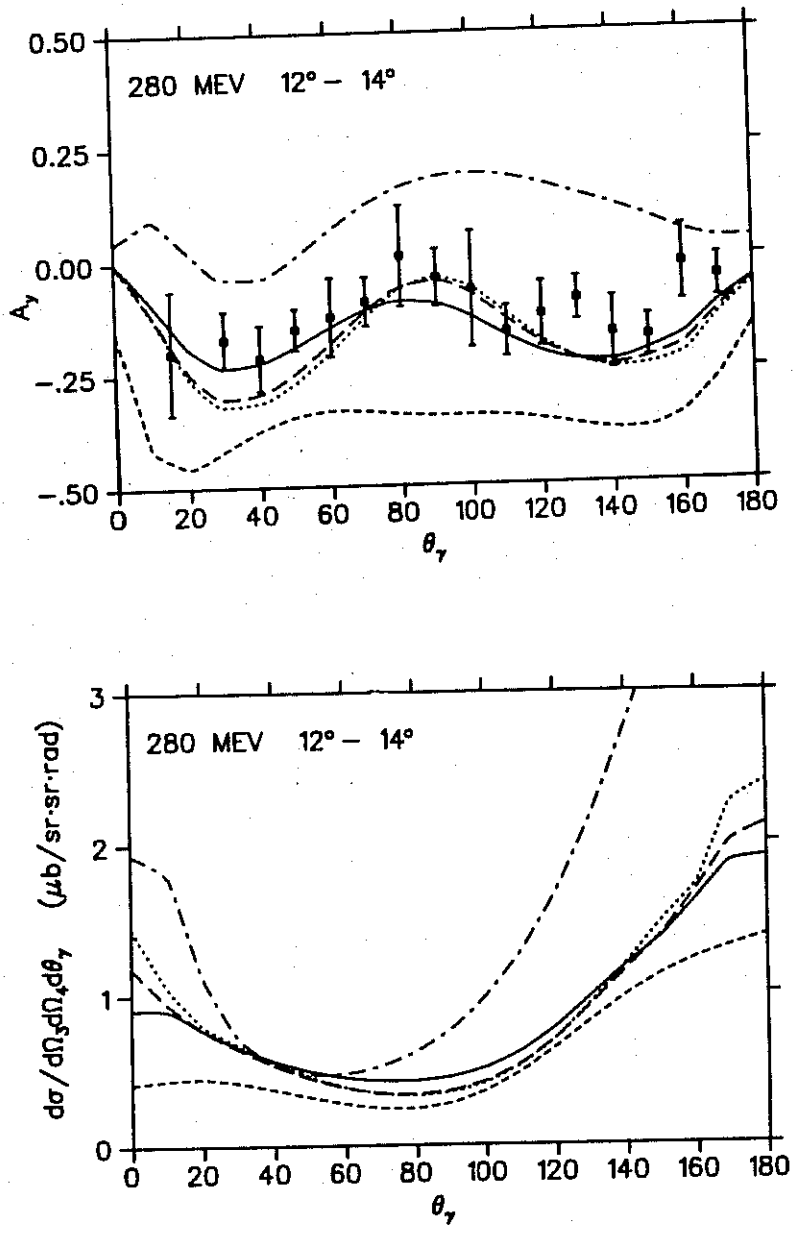

Figure 5.15: $pp\gamma$ **analysing power,** A_y**, and cross section** obtained using the Bonn (solid line), Paris (long dash), and Reid (dotted) potential. The lab. energy is 280 MeV. Data from (Kit+ 86). [From (Fea 87)]

Table 5.2: **Neutron-proton phase shifts (in degrees) for various lab. energies (in MeV) from different meson-theoretic NN potentials.**

State	Model	25	50	100	150	200	300
	OBEP	50.72	39.98	25.19	14.38	5.66	−8.18
$^1S_0$	*Paris*	48.38	38.12	23.88	13.38	4.84	−9.01
	Bonn	50.03	39.15	24.36	13.72	5.30	−7.62
	OBEP	9.34	12.24	9.80	4.57	−1.02	−11.48
$^3P_0$	*Paris*	9.21	11.93	9.83	5.32	0.48	−8.52
	Bonn	9.57	12.79	10.88	6.02	0.66	−9.66
	OBEP	−7.21	−11.20	−16.44	−20.45	−23.85	−29.41
$^1P_1$	*Paris*	−7.11	−10.95	−15.72	−19.08	−21.73	−25.92
	Bonn	−6.90	−10.48	−15.11	−18.88	−22.41	−29.17
	OBEP	−5.33	−8.77	−13.47	−17.18	−20.49	−26.38
$^3P_1$	*Paris*	−5.27	−8.64	−13.44	−17.35	−20.91	−27.30
	Bonn	−5.17	−8.53	−13.38	−17.62	−21.73	−29.87
	OBEP	80.32	62.16	41.99	28.94	19.04	4.07
$^3S_1$	*Paris*	80.35	62.28	42.26	29.24	19.25	3.91
	Bonn	80.30	62.19	42.27	29.64	20.31	7.06
	OBEP	−2.99	−6.86	−12.98	−17.28	−20.28	−23.72
$^3D_1$	*Paris*	−2.95	−6.77	−12.85	−17.22	−20.42	−24.52
	Bonn	−3.03	−6.98	−13.25	−17.64	−20.62	−23.43
	OBEP	1.76	2.00	2.24	2.58	3.03	4.03
ϵ_1	*Paris*	1.69	1.89	2.14	2.59	3.21	4.76
	Bonn	1.82	2.08	2.29	2.54	2.82	3.19
	OBEP	0.68	1.58	3.34	4.94	6.21	7.49
$^1D_2$	*Paris*	0.78	1.85	4.00	5.90	7.47	9.19
	Bonn	0.72	1.72	3.76	5.62	7.04	8.32
	OBEP	3.88	9.29	17.67	22.57	24.94	25.36
$^3D_2$	*Paris*	3.96	9.60	18.64	24.19	27.15	28.54
	Bonn	3.88	9.27	17.41	21.68	23.09	20.84
	OBEP	2.62	6.14	11.73	14.99	16.65	17.40
$^3P_2$	*Paris*	2.61	5.97	11.34	14.68	16.39	16.74
	Bonn	2.54	5.89	11.14	14.24	15.93	17.22
	OBEP	0.11	0.34	0.77	1.04	1.10	0.52
$^3F_2$	*Paris*	0.11	0.36	0.79	1.05	1.06	0.49
	Bonn	0.11	0.35	0.81	1.14	1.28	0.87
	OBEP	−0.86	−1.82	−2.84	−3.05	−2.85	−2.02
ϵ_2	*Paris*	−0.87	−1.80	−2.73	−2.90	−2.74	−2.14
	Bonn	−0.85	−1.77	−2.74	−2.97	−2.84	−2.23

Section 6

Charge Dependence

6.1 Introduction

Historically, it was first assumed that the nuclear force was acting between neutron and proton only and not between like nucleons (Hei 32, Maj 33, Yuk 35), i. e. a strong charge-dependence was supposed. The isospin formalism, introduced by Heisenberg in 1932 (Hei 32), was not meant to imply a new invariance law. In 1936, the hypothesis of the charge independence of the nuclear force (BCP 36, BF 36, CC 36) was stated in the form that the interaction between nucleons in the same spin-angular momentum state is the same for pp, np, and nn. Charge symmetry (the equality of the strong force between pp and nn) was conjectured already by Feenberg and Knipp in 1935 (FK 35) and applied by Share (Sha 36). Share recognized that the binding energy difference between ^3H and ^3He, ΔB, is closely related to the issue of charge symmetry. For ^3He he obtained a Coulomb energy $\mathcal{E}_{Coul} = 700$ keV. The experimental value for the binding energy difference was $\Delta B_{exp} = 807 \pm 92$ keV. Thus, with the precision of those days the charge-symmetry breaking (CSB) difference was

$$\Delta B_{exp} - \mathcal{E}_{Coul}(^3He) = 107 \pm 92 \text{ keV}. \tag{6.1}$$

This provided no clear evidence for CSB; however, as we know today, it pointed already into the right direction (cf. Table 6.3 below). We mentione this point in some detail, as it is an important issue still today, particularly with higher precision data available.

With regard to the historical background sketched above, it may not be surprising that ever since the hypothesis of isospin symmetry was formulated, there was suspicion that it might be (slightly) broken. Therefore, the charge-dependence of the nucleon-nucleon interaction has been the subject of intense investigations both experimentally and theoretically since several decades. Nevertheless, still today, many — even basic — questions are unsettled. This applies to the experimental as well as the theoretical state of the art in the field.

On the theoretical side, it was a general believe for a long time that all charge dependence, including the mass differences between the charge states of particles, is ultimately of electromagnetic origin, even though one could not calculate this quite convincingly. This point of view has been modified by the quark model and QCD. Here isospin is broken by the quark masses which is not necessarily an electromagnetic effect. However, since the mass difference between the up (u) and down (d) quark is presumably small,

$$m_u - m_d \approx M_n - M_p \approx 1.3 \text{ MeV} \ll M_N \approx 1 \text{ GeV}, \qquad (6.2)$$

isospin invariance is a good assumption for most purposes.

The subject of charge-dependence has been reviewed extensively in the literature (Wil 69, Noy 72, Bli 73, HM 79). Therefore, we will discuss here only a few points, we believe to be of particular interest.

6.2 Empirical Evidence

The empirical evidence for the charge-dependence of nuclear forces comes mainly from few-body systems. The NN scattering length in the $^1S_0$ state plays a special role. As there exists an almost bound state in that partial wave, the (negative) scattering length is extremely sensitive to small changes in the strength of the force. Whereas the np and the pp scattering lengths, a_{np} and a_{pp}^E, respectively, can be obtained from the corresponding low energy two-body data, the nn scattering lenght, a_{nn}, poses a difficult experimental problem due to the fact that direct nn scattering is presently not feasible. The experiments performed to extract this scattering length can be subdivided into those with either two or three nucleons in the final state. An example for the former type of experiment is the reaction $\pi^- d \to nn\gamma$. A three-body final state with two neutrons is obtained in

Table 6.1: **Empirical singlet S-state low energy NN scattering parameters.**

	a (fm)	r (fm)	Reaction	References
np	-23.748 ± 0.010	2.75 ± 0.05	np	Dum+ 83
nn	-18.5 ± 0.4	2.80 ± 0.11	$\pi^- d \to \gamma nn$	TG 87
	-18.8 ± 1.0	—	$nd \to pnn$	Koo+ 87, Sla 87
pp^a	-7.813 ± 0.004	2.78 ± 0.02	pp	Dum+ 83, Swa 87

Given are the scattering length a and the effective range r.
[a]With electromagnetic effects, commonly denoted by a_{pp}^E and r_{pp}^E.

the reaction $nd \to nnp$. In the 1970's it was claimed that a value of $a_{nn} = -16.4 \pm 1.2$ fm was obtained from the analysis of a large number of results from both types of experiments (HM 79). Recently, however, an experimental value of

$$a_{nn} = -18.5 \pm 0.5 \text{ fm} \tag{6.3}$$

has been recommended — again based on data from both types of experiments (Sla 87). The terrible fight with this quantity as well as the huge uncertainty it was beset with for a long time, is reflected well in the review article by Henley (Hen 69). These uncertainties indicate only a part of the tremendous difficulties involved in these experiments. In Table 6.1 we summarize the most recent empirical values for low energy scattering in the $^1S_0$ state.

Also of interest are the pp parameters without direct electromagnetic effects. However, their extraction is model dependent. Therefore, we give in Table 6.2 the values obtained by applying four different NN potentials. Assuming that the potentials in that table represent a true variety of real-

Table 6.2: *pp* **low energy scattering parameters in the absence of the Coulomb field for various** *pp* **potentials.**

Potential	a_{pp} (fm)	r_{pp} (fm)	Reference
Reid	−17.1	2.80	Rei 68
SSC	−17.58	2.855	KS 69
Paris	−17.3[a]	2.88[a]	Lac+ 80
Bonn[b]	−17.23	2.866	MHE 87

[a]Values given in (Lac+ 80) for *nn* corrected for the $p-n$ mass difference.
[b]Fit to the empirical *pp* scattering parameters including the Coulomb force ($a_{pp}^C = -7.817$ fm, $r_{pp}^C = 2.788$ fm) by using $g_{\sigma'}^2 = 5.6043$.

istic potentials, one may conclude

$$a_{pp} = -17.3 \pm 0.3 \text{ fm}. \tag{6.4}$$

This value is less negative than the corresponding one for *nn*, Eq. (6.3), which implies that the *nn* interaction is slightly more attractive than the *pp* interaction.

The equality between *nn* (or *pp*) and *np* nuclear interactions is known as *charge independence*. The data quoted in Table 6.1 show that this is slightly, but clearly broken. With $\bar{a} = \frac{1}{2}(a_{nn} + a_{pp}) = -17.9 \pm 0.6$ fm, we define the charge-independence breaking (CIB) in the singlet scattering length as

$$\Delta a_{CIB} = \bar{a} - a_{np} = 5.85 \pm 0.6 \text{ fm}. \tag{6.5}$$

The term *charge symmetry* is customary for the equality of the forces

Table 6.3: CSB contributions to the ^3H - ^3He binding energy difference ΔB. [From (Bra+ 88a)]

	ΔB (keV)	Reference
Static Coulomb	687	Bra+ 88a
Finite size effects[a]	−39	Bra+ 88a
CSB strong force	59	Bra+ 88a
$n - p$ mass difference in kinetic energy	12	BCS 78
Second order perturbation corrections	−6	PFG 80
Other electromagnetic effects	29	BCS 78
Total	742	
(Experiment)	(764)	

[a] i. e. taking into account the proton electromagnetic form factors.

between nn and pp; its violation is not so clear. On the basis of the numbers given above, one may presently assume for the charge-symmetry breaking in the singlet scattering length

$$\Delta a_{CSB} = a_{pp} - a_{nn} = 1.2 \pm 0.6 \text{ fm}. \tag{6.6}$$

Information about charge-symmetry breaking can also be inferred from binding energy differences of so-called mirror nuclei. The most studied case is the ^3H – ^3He mirror pair. Experimentally the difference between the binding energies of these two three-nucleon systems is found to be 764 keV. Model-independent calculations of the Coulomb energy difference, based on the experimental knowledge of the three-nucleon electromagnetic form factors, amount to about 640 keV. More careful studies which also include the effect of the $n - p$ mass difference on the kinetic energy, the effect of exchange currents on the electromagnetic form factors and the

spin and momentum dependent parts of the electromagnetic interaction increase the theoretical estimate to 683 ± 29 keV (BCS 78). A charge-asymmetric difference of 81 ± 29 keV remains with regard to the empirical value. Recently, it has been shown (CB 87, Bra+ 88a) that this remaining discrepancy can be explained by a CSB force which is consistent with the asymmetry in the singlet scattering length, Eq. (6.6). This explanation is plausibel, since there is a neutron pair in ^3H, whereas there is a pair of protons in ^3He. Assuming that the interaction between two neutrons is more attractive than between two protons, more binding energy is provided for ^3H as compared to ^3He (see Table 6.3 for precise numbers).

In heavier nuclei, Nolen and Schiffer (NS 69) found that the calculated energy differences between mirror nuclei were systematically too small as compared to experiment. This is referred to as the Nolen-Schiffer or Coulomb anomaly. However, Negele (Neg 71 and 74) showed for the $^{41}Ca-^{41}Sc$ mirror pair that a small charge asymmetry in the nuclear force, corresponding to $\Delta a_{CSB} = 0.8$ fm, could account for the remaining binding energy difference. This asymmetry is consistent with the present empirical evidence, Eq. (6.6).

6.3 Some Results from Theory

As discussed, from the point of view of theory, nowadays one believes that the charge-dependence of strong forces is due to the difference in the quark masses and to electromagnetic effects. Based on these more fundamental causes, important sources for CIB and CSB are:

- The mass splittings between the charge states of hadrons of the same species, in particular, the π meson, the ρ meson, the nucleon and the Δ isobar (Figs. 6.1-3).
- Irreducible pion-photon exchange (Figs. 6.4-5).
- Electromagnetic meson mixing (Fig. 6.6).

6.3.1 Meson Mass splitting

Early, the mass difference between the charged and neutral pion was recognized as an important source for charge dependence. (Note that meson

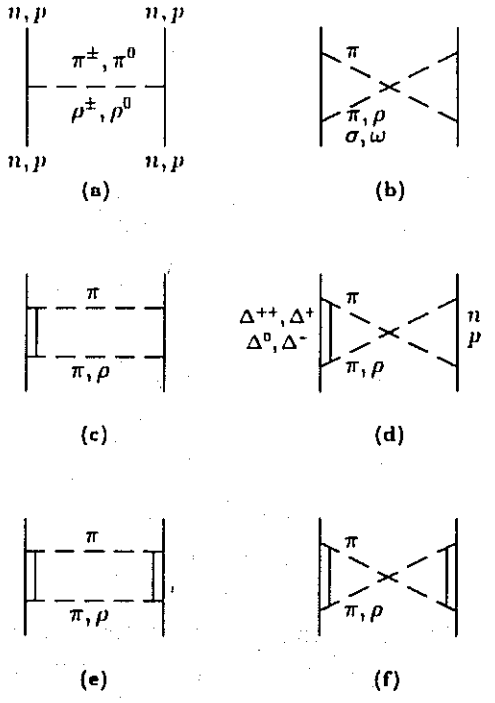

Figure 6.1: **One- and two-meson exchange diagrams contributing to CSB and CIB.** For all mesons and baryons the different charge states have to be considered. This is indicated in some cases.

mass splitting does not break charge symmetry.) This mass splitting is precisely known and amounts to 4.6 MeV (cf. Table 3.2), which is about 3% of the total pion mass; this is a large fraction. Taking into account this mass difference in the one-pion-exchange (OPE) part of the nuclear potential, Fig. 6.2, produces about 50% of Δa_{CIB}. Between two protons (two neutrons) only the lighter π^0 can be exchanged (with an isospin factor of 1), which makes the (repulsive) OPE potential in $^1S_0$ stronger as compared to the np case, in which also the heavier charged pions are exchanged (with an isospin factor of 2 for $\pi^\pm$ and a factor (-1) for π^0).[1]

Recently, there have been systematic investigations of the charge-depen-

[1]As pointed out in Section 3.4, the strength of OBE contributions is roughly proportional to g_α^2/m_α^2.

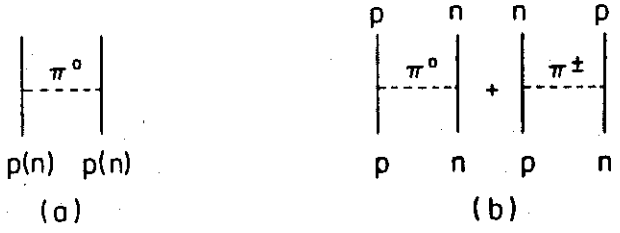

Figure 6.2: **One-pion exchange contributions to (a) pp (nn), and (b) pn scattering.**

dence of the 2π-exchange (TPE) contribution to the NN interaction (EM 83, CM 86). The model for the 2π-exchange used in the work of (CM 86) is shown in Fig. 6.1 with dashed lines representing pions only. The pion mass difference was taken into account in all diagrams shown (the indicated mass splitting between the different charge states of baryons was not taken into account). For part of the contributions, namely those with $N\Delta$ intermediate states, Fig. 6.1c and d, we show all charge-dependent diagrams explicitly in Fig. 6.3. A crucial point in the findings of (CM 86) is that there are substantial cancelations between the charge-dependent effects from box and crossed box diagrams *and* from the contributions involving one and two Δ isobars. Without these cancelations, the result would be completely unrealistic. Thus, for example, a pure box model for the 2π exchange would describe CIB incorrectly; the same is true for a model which takes only single Δ excitation into account. These results are another strong indication that the inclusion of crossed diagrams is important to obtain the correct isospin dependence of the nuclear force. The isovector parts of box and crossed box diagrams (see MHE 87, Appendix B) have opposite sign and, therefore, cancel to a large extend leading to a rather weak over-all isospin dependence (cf. Section 5.1).

In an alternative study by Ericson and Miller (EM 83) the 2π-exchange model of Lomon and Partovi (PL 70) was used. In spite of the substantial differences in the details of the models, the results are very similar, namely about 1 fm for the charge dependent effect on the scattering length. One

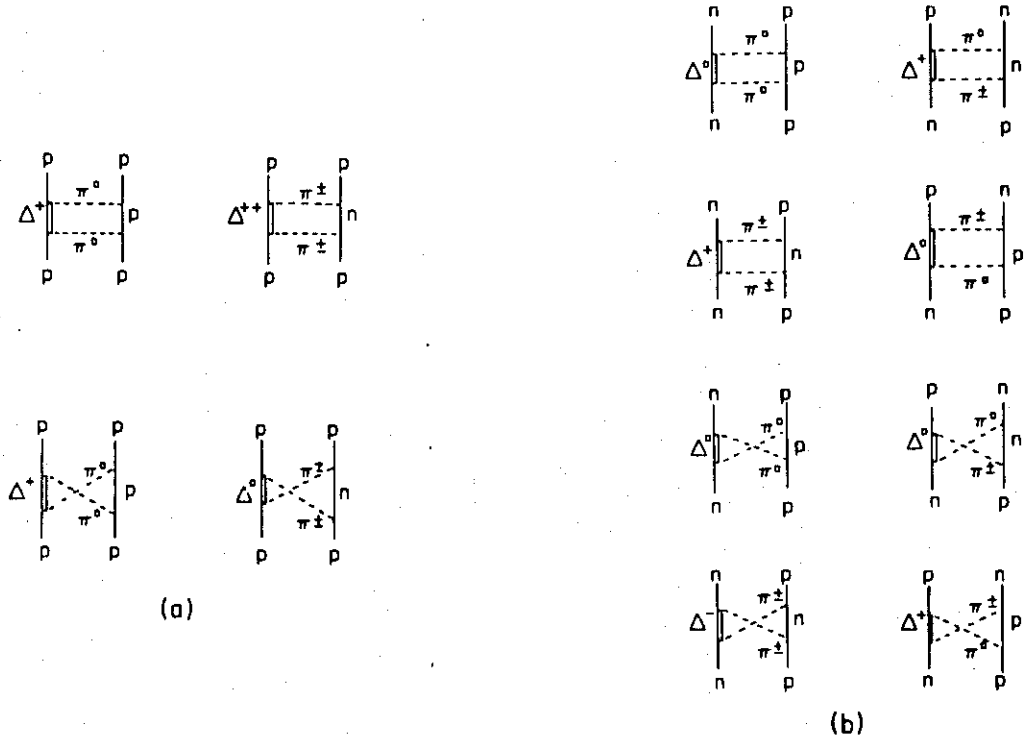

Figure 6.3: 2π-**exchange contributions with** $N\Delta$ **intermediate states to (a)** pp **and (b)** np **scattering.**

essential reason for the close agreement is that also in the model by Partovi and Lomon (PL 70) crossed pion exchanges are taken into account. Together with the OPE contribution and further contributions from $\pi\rho$, $\pi\sigma$, and $\pi\omega$ exchanges (Fig. 6.1b) this explains about 80% of the CIB in the $^1S_0$ scattering lenght (Table 6.4).

We mentione that there may be charge dependence in the coupling constant of the pion or other isovector mesons. For example, if charge independence of the *ps* coupling constant is assumed (as done in the results quoted), the *pv* coupling constant, Eq. (3.14), must be charge dependent. Furthermore, radiative corrections to the πN coupling constant may cause charge dependence since those contributions depend on the charge of the

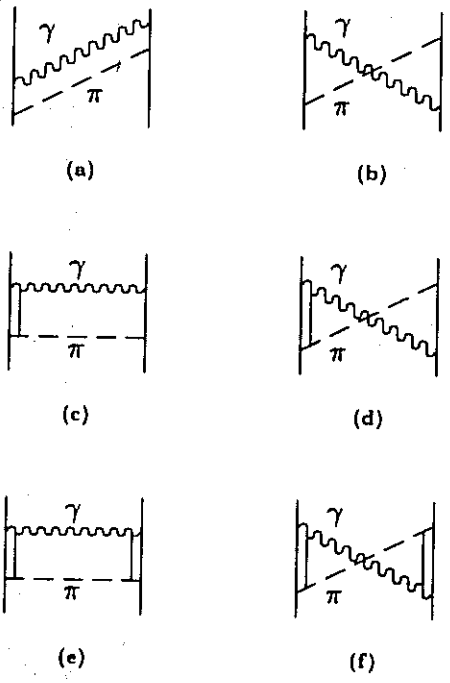

Figure 6.4: **Irreducible pion-photon exchanges contributing to CSB and CIB.**

meson as well as of the nucleon (HM 79). However, there is presently no clear empirical evidence for any difference between the $\pi^0 N$ and the $\pi^\pm N$ coupling constants, though vigorous research on this subject is in progess (Swa 87). Furthermore, in (EM 83) it is found that the effect from a possible charge dependence of the πN coupling constant would be small due to strong and systematic cancelations between OPE and TPE contributions.

There may be mass splitting also for other iso-vector mesons, e. g. the ρ meson — a meson which plays an important role in the meson theory of the NN interaction. However, the present empirical value for the mass difference between the neutral and charged ρ is 0.3 ± 2.2 MeV (PDG 84). This means that the evidence is not clear. Furthermore, a mass splitting has to be compared with the total mass of the particle which is 769 MeV in

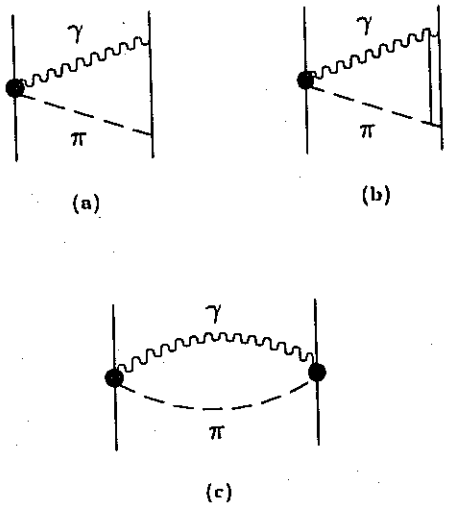

Figure 6.5: **Irreducible pion-photon exchange involving the gauge term (full dot).**

this case. Therefore, even 2.5 MeV, which is the upper limit of the empirical value for the ρ-mass splitting, would amount to only about 0.3% (1/10 of what we have in the case of the pion). Therefore, one can exspect only a very small effect, if any.

6.3.2 Baryon Mass splitting

Mass splitting of baryons, especially nucleons, causes CIB and CSB (see the indications in Figs. 6.1-3). The $n-p$ mass difference, which is well-known to be 1.3 MeV, affects the kinetic energy of the nucleons and, thus, leads to more attraction for two (heavier) neutrons relative to two protons. This effect is small (about 0.3 fm for the scattering length) as the nucleon mass splitting is only 0.14%. A larger effect could be expected from the 2π exchange. This large and intermediate-ranged contribution to the nuclear force involves nucleons and nucleon resonances in intermediate states, in particular the $\Delta(1236)$ resonance.

From the 2π exchange, Riska and Chu (RC 74) obtain $\Delta a_{CSB} \approx -2$ fm. A recent estimate by Coon and Scadron (CS 82b) is +0.3 fm. The

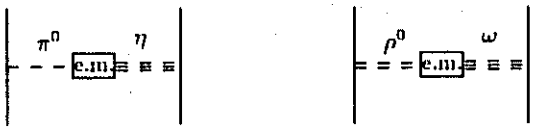

Figure 6.6: **CSB forces from electromagnetic meson mixing.**

discrepancy between these two results is probably due to substantial differences in the models used for the 2π exchange. In any case, more systematic work is clearly needed, in which also the important $\pi\rho$ diagrams should be included. The model of Fig. 6.1 could provide a sound basis, since it has been shown that this model describes the low energy NN interaction very accurately (MHE 87 and Section 5).

6.3.3 Electromagnetic Processes

Irreducible meson-photon exchange can contribute to both CSB and CIB. The pion being the lightest meson, $\pi\gamma$ exchange leads to the longest ranged charge-dependent force of that kind. It has been studied in the literature. However, again, there is little agreement between different authors. For example, Riska and Chu (RC 74) estimate the CSB effect on the scattering length difference to be only a small fraction of a fermi, whereas Banerjee (Ban 75) obtains $a_{CSB} = -1.31$ fm. In Figs. 6.4 and 6.5 we show several meson-photon exchanges which contribute to CSB as well as CIB. Some diagrams have been examined explicitly. In the work of Chemtob (Che 75) diagrams (c) – (f) of Fig. 6.4 have been found to be small. S. N. Yang has considered the diagrams of Fig. 6.5 (Yan 84). It is expected that diagrams (a) and (b) of Fig. 6.4 provide the largest contribution to CSB and CIB. Estimates of the CIB effect from these diagrams done so far vary by as much as 50% depending on the author (Che 75, Ban 75, EM 83). A full and systematic investigation is still needed.

There are also the $\rho\gamma$ diagrams corresponding to Fig. 6.4 with the π replaced by the ρ. To our knowledge, they have never been studied.

Finally, electromagnetic mixing of neutral mesons with the same spin

Table 6.4: **Charge-independence breaking (CIB) contributions to the singlet S-state scattering length.**

	Δa_{CIB} (fm)		References
OPE	2.80 ± 0.1		CM 86
2π	0.85 ± 0.1		CM 86
	$[0.88 \pm 0.1]$		[EM 83]
$\pi\rho$, $\pi\sigma$, $\pi\omega$	0.79 ± 0.2		CM 86
$\pi\gamma$	1.10 ± 0.4	?	Che 75, Ban 75, EM 83
Total	5.54 ± 0.5		
(Empirical)	(5.85 ± 0.6)		

and parity, but different isospin is another source for CSB (see Fig. 6.6). In that figure, the box labeled 'e.m.' represents the electromagnetic transition matrix element responsible for the mixing. Empirical information, for example for the case of $\rho - \omega$ mixing, is obtained from the branching ratio for the decay of the ω into 2π which is about 2 ± 0.8 % (PDG 85, CB 87). The most studied examples are $\pi - \eta(\eta')$ and $\rho - \omega$ mixing. Coon and coworkers (CSM 77, CS 82b) find only negligible effects from $\pi - \eta$ and $\pi - \eta'$ mixing; however, a contribution of about 1 fm to a_{CSB} is obtained from the mixing of ρ_0 and ω meson. This contribution alone essentially explains the present empirical evidence.

6.3.4 Summary and Outlook

Theoretical estimates for CSB and CIB in the singlet scattering lengths, which we believe to be the best available at the present time, are given in Table 6.4 and 6.5. Numbers which are uncertain are commented by a question mark indicating that a comprehensive and reliable calculation is

Table 6.5: **Charge symmetry breaking (CSB) contributions to the singlet S-state scattering length.**

	Δa_{CSB} (fm)		References
$n-p$ mass difference in kinetic energy	0.30 ± 0.10		Hen 69
$n-p$ mass difference in 2π	0.30 ± 0.10	?	CS 82b
$\rho^0-\omega$ mixing	0.74 ± 0.35		CS 82b
$\pi^0-\eta$, $\pi^0-\eta'$ mixing	≤ -0.03		CS 82a
$\gamma\pi^0$ exchange	0.19 ± 0.04	?	RC 74,Che 75
Total	1.53 ± 0.5		
(Empirical)	(1.20 ± 0.60)		

still needed.

The examples for CSB discussed so far involve Coulomb corrections. However, there is one system for which such corrections do not enter, namely the np system. In a recent measurement at TRIUMF (Abe+ 86) the difference in the analysing power for polarized protons and neutrons in np scattering at 477 MeV has been measured by determining the difference in the zero crossing angle of the analysing power, which makes the measurement insensitive to the polarization calibration. The experimental result is well explained by a calculation by Miller *et al.* (MTW 86) in which only conventional mechanisms are taken into account (the dominant contributions are: the effect of the $n-p$ mass difference on the πNN vertex and single-photon exchange).

In summary, as far as reliable calculations and precise experimental data exist, the phenomena of CSB and CIB can be explained quantitatively using mesons and baryons only and no exotic ingredients. However, as mentioned repeatedly, in some sectors there are still tremendous uncertainties, both

on the theoretical and the experimental side, which should be cleared up in the near future.

There are many more examples for CSB and CIB and, furthermore, there other symmetries, like parity conservation and time reversal, which are or might be slightly violated in the two- or many-nucleon system. Appropriate meson-baryon Lagrangians describing such interactions can be constructed. As we cannot cover these topics here, we refer the interested reader for recent reviews to the papers by Simonius (Sim 83, Sim 87).

Section 7

Nucleon-Nucleon Scattering above the Inelastic Threshold

In former sections we have seen that meson theory works excellently for the description of the NN interaction in the low energy regime typical for traditional nuclear physics including many subtle features like charge dependence and others. It is now natural to raise the question: what happens at higher energies? At about 300 MeV in the lab. system, meson production starts, i. e. increasing inelasticity begins to enter the picture. Is it still possible to describe these phenomena in terms of nucleons and mesons? One can well argue that the appearance of *real* mesons is a *real* test of meson theory. In fact, this point indicates some of the fundamental relevance of intermediate energy physics (i. e. hadronic physics up to energies of about 1-2 GeV in the lab. frame); it has been part of the basic motivation for the development of the meson factories in the past. On the other hand, there can be no doubt that the meson model has to break down at certain higher energies, namely when the substructure of hadrons reveals itself in a crucial way. This does certainly happen at energies of several tens of GeV, as it was at those energies (of electron scattering) that the parton structure of hadrons was discovered first — at SLAC in the late 1960's. However, our feeling today is that this substructure might show up already at much lower energies. Now, when does that precisely happen? Presently, we do not know. Indeed, this basic question is part of the motivation for the so-called *Kaon Factories* which are planned as successors for some existing meson facilities. Today, a few polarization data from NN scattering

at energies of several GeV exist already. They show large and unexspected spin effects posing a serious challenge to theory.

7.1 At Intermediate Energies

7.1.1 Overview

Since the mid 1970's, the so-called meson factories, in particular, TRIUMF,[1] LAMPF,[2] SIN,[3] and SATURN have measured systematically elastic and inelastic NN scattering up to about 1 GeV lab. energy. Today, the pp phase-shifts are determined well up to 1 GeV, and the np phase-shifts likewise to 500 MeV and tentatively at 800 MeV. Our understanding of inelasticity has progressed particularly since 1980. Extensive data on $pp \to d\pi^+$ have been taken such that the six amplitudes for this process are known with confidence up to 800 MeV. Intensive work on $pp \to pn\pi^+$ is in progress.[4]

In previous sections we have seen that a characteristic feature of the nuclear potential at low energies is its rich spin structure. We also saw that the exchange of various mesons typically offers such a rich spin dependence. However, in recent years it has turned out that above the inelastic threshold this spin structure is even richer, so rich that even new phenomena like dibaryons (baryon-baryon resonances) have been suggested for their explanation. The excitation of one $\Delta(1232)$ at about 600 MeV lab. energy puts the most decisive signature on the elastic and inelastic scattering parameters. Pion production proceeds essentially through this process. Therefore, one pion production is dominant up to 1 GeV, though the threshold for two pions is at about 600 MeV. At low energy, we found that the virtual excitation of the Δ isobar is indispensable for a realistic description of the intermediate range attraction of the nuclear force as provided by the 2π exchange (Section 5). This ingredient of the nuclear force is now found to be equally crucial at intermediate energies — for pion production as well as for the explanation of characteristic structures in the elastic scattering

[1] TRI-University Meson Facility, Vancouver, Canada.

[2] Los Alamos Meson Physics Facility, Los Alamos, New Mexico, U.S.A..

[3] Schweizerisches Institut für Nuklearforschung, Villigen, Switzerland.

[4] For recent reviews of the status of NN physics up to 1 GeV see Bugg (Bug 81 and 85).

parameters. This fact provides further support of and confidence in the basic ingredients of meson models used in nuclear physics.

Inelasticity plays the central role in NN scattering at intermediate energies. It is closely related to the controversial and exciting issue of dibaryon resonances. Furthermore, it poses a clear structure on elastic scattering. The most important 'conventional' inelasticity in the energy regime under consideration is the $NN \rightarrow N\Delta$ threshold at 600 MeV (GV 83). Because of isospin conservation it can occur in isospin $T = 1$ two-nucleon states only. Double Δ excitation, possible for both isospin zero and one, has its threshold above 1 GeV. $N\Delta$ excitation appears first in $^1D_2$ with $L_{N\Delta} = 0$, where $L_{N\Delta}$ denotes the relative orbital angular momentum between nucleon and delta. $L_{N\Delta} = 1$ contributes to $^3F_3$ showing its distinct signature typically at a slightly higher energy compared to $^1D_2$ because of the higher angular momentum. This angular momentum also contributes to $^3F_2$, $^3P_2$, $^3P_1$, and $^3P_0$, however not so pronounced. At still higher energies $L_{N\Delta} = 2$ folds into $^1G_4$ and $^1S_0$. Below Δ production , i. e. below 425 MeV, $pp \rightarrow d\pi^+$ is the main source for inelasticity which appears first in $^3P_1$ and $^1D_2$.

During the past decade, speculations on the possible existence of dibaryon resonances have blossomed considerably. Presently, there is no firm evidence for such exotic states. However, the possibility cannot be excluded that conventional resonances (i. e. $N\Delta$ or $\Delta\Delta$ bound or virtual states) might exist in association with inelastic thresholds.

The excitement started when, in pp scattering, Auer *et al.* (Aue+ 77 and 78) at the Argonne ZGS[5] observed peaks in

$$\Delta\sigma_L^{tot} \equiv \sigma_{tot}(\rightrightarrows) - \sigma_{tot}(\rightleftarrows), \tag{7.1}$$

the difference in total cross sections measured with longitudinally polarized beam and target with spin parallel or opposed (for more details see the reviews by Fernow and Krisch (FK 81) and (Yok 80, BLS 80)). A similar peak has been found (Bie+ 78) in

$$\Delta\sigma_T^{tot} \equiv \sigma_{tot}(\uparrow\uparrow) - \sigma_{tot}(\uparrow\downarrow), \tag{7.2}$$

the corresponding measurement with transverse spin orientations (FK 81), see Fig. 7.1. Hidaka *et al.* (Hid+ 77) proposed that the peak around

[5]Zero Gradient Synchrotron, Argonne National Laboratory, Argonne, Illinois, U.S.A.

550 MeV is due to a $^1D_2$ resonance and the inverted peak in $\Delta\sigma_L^{tot}$ around 800 MeV to a $^3F_3$ resonance. Indeed, phase shift analyses of elastic data have revealed counter-clockwise loopings in the Argand diagrams of $^1D_2$ and $^3F_3$ (and also of $^3P_2$ and $^1G_4$), Fig. 7.2. It was suggested these might be manifestations of new degrees of freedom, such as the dibaryon resonances suggested by the quark bag model (MAS 78).

If one calls these structures resonances is pretty much a matter of taste and interpretation.[6] One may be stubborn and say if something looks like a resonance in an Argan plot, it is a resonance. However, in this way not much of the real physics is disclosed. In a more conservative approach, one would first try to explain things as far as possible by conventional means. In fact, it turns out that the threshold $NN \to N\Delta$ gives at least qualitatively the observed resonance-like structures; in particular, it leads typically to half-loops in the controversal partial waves. The explanation of the observed structures in $\Delta\sigma_L^{tot}$ and $\Delta\sigma_T^{tot}$ can then be given as follows: The $^1D_2$ NN partial wave contributes positively to both cross-section differences with weight $(2J+1)$; $^3F_3$ contributes only to $\Delta\sigma_L^{tot}$ with a negative sign and a weight of $(2J+1)$; finally $^3P_2$ contributes negatively to both observables. The shapes are then explained by the inelastic threshold in $^1D_2$ which appears typically at lower energy than in $^3F_3$ and $^3P_2$.

Theoretical models explain the cross section differences up to the degree of quality to which they reproduce the phase shift analysis, especially in the three critical partial waves mentioned. In fact, this is where almost all models share common deficiencies. Due to the dependence on a delicate balance between, particularly, $^1D_2$, $^3F_3$ and $^3P_2$, small deviations in the predictions of a model from the phase shift analysis in these partial waves are 'blown up' in the predictions for the cross section differences (compare Fig. 7.1 and 7.9). This magnifying effect essentially explains the poor fit of the spin-dependent total cross section differences by theory (Fig. 7.1). Note, however, that qualitatively the energy-dependent structures are reproduced correctly.

[6] For a thorough discussion of the issue of dibaryons see the recent review by Locher *et al.* (LSS 86).

7.1.2 Status of Theory

On the theoretical side, one can distinguish between two frameworks: coupled two-body channels and three-body equations.

The *coupled channel* method was started by A. M. Green in the early 70's. The original purpose was to calculate the medium effects on the nuclear force when inserted into nuclear or neutron matter due to isobar degrees of freedom (GH 74, GN 75, Gre 79). Later, this work was extended to higher energies (GNS 78, GS 79). In this approach one solves a system of coupled equations for the T-matrix:

$$T_{ij} = V_{ij} + \sum_{k=1}^{3} V_{ik} g_k T_{kj} \tag{7.3}$$

where the V_{ij} are the so-called transition potentials with i and $j = 1, 2$ or 3, and 1, 2 and 3 corresponding to NN, $N\Delta$ and $\Delta\Delta$, respectively; g_k is the appropriate two-baryon propagator. The coupled channel typically generates diagrams of box shape, the most important ones (for the creation of the intermediate range attraction as well as for the production of inelasticity) being shown in Fig. 7.3.

Existing models differ essentially in two details: first, by the transition potentials used, which can be either relativistic (FT 84 and 86, HM 87, Els 86, Els+ 87) or non-relativistic (Lom 82, Lee 83 and 84, PSZ 87); second, by the imaginary part in the propagator g_k, for which either some reasonable *ad hoc* assumption based on the empirical Δ width is made (GNS 78), or the self-energy of the Δ (and in some cases of the nucleon), see Fig. 7.4, is calculated more or less properly (FT 84, HM 87, Els 86, Els+ 87). Apart from a real contribution which is readjusted to the empirical mass, this produces an imaginary part for the Δ mass (the 'width') which explains most of the inelasticity in the energy range under discussion. This is quite understandable since in the self-energy diagrams, Fig. 7.4b, the Δ is coupled strongly to its πN decay channel. Another source for inelasticity is the nucleon self-energy, Fig. 7.4a, which provides only a very small contribution;[7] however, it is the only one in $T = 0$ up to $\Delta\Delta$ production. This is why the inelasticitiy in $T = 0$ states is so small for low energies (see

[7]This can be understood from a comparison of the coupling constants — $f^2_{NN\pi}/4\pi \approx 0.08$ while $f^2_{N\Delta\pi}/4\pi \approx 0.35$ — and the fact that the nucleon is not a resonance.

Fig. 7.9). Furthermore, there is inelasticity coming from the pion propagator (dashed lines denoted by 'π' in Fig. 7.3), since the pion can be real above threshold. This effect can be taken into account only by non-static theories (propagators). It has turned out that this inelasticity is important for $^3F_3$ (see below), while it is irrelevant in all other states.

Nowadays, all realistic models of the coupled channel type use π *and* ρ exchange for transitions from two-nucleon states to states involving Δ.[8] Examples are given in Appendix B. The coupled channel method is suitable to compute phase shifts and inelasticity parameters for NN scattering. The $NN \to N\Delta$ $\mathcal{T}$-matrix can be exploited to predict pion-production observables; if the πd channel is included, e. g. $pp \to \pi d$ spin observables can be calculated.

The original motivation for the approach using *three-body equations* was to describe elastic scattering of pions from deuterons in a realistic way (AAY 68, Aar 77, AT 74, AM 83). The enormous work done by several groups (RT 77, FLM 80, KS 80, KS 81, Gar 82, Gar 87) differs in details and in philosophy. In some of the work (BA 81, BL 81, Rin 83), the major emphasis has so far been on the $pp \to d\pi$ reaction. Kloet and Silbar (KS 80, KS 81) and Sammarruca (Sam 88) have concentrated on calculating spin observables for the three-body final state, $NN \to NN\pi$ (Dub+ 81, DKS 82, DKS 87).

All approaches and models mentioned have in common that they involve only known mesons and baryons together with the usual effective meson-baryon interactions, i. e. they do not use dibaryons or any other exotic input. Resonance-like structures, if predicted, emerge simply through conventional meson-baryon dynamics (Figs. 7.1-2). Total cross sections as predicted by the three rather different theoretical models, which were applied for Fig. 7.1, are displayed in Fig. 7.5.

Furthermore, in Figs. 7.6–7.10 we show more predictions from two coupled-channel models (full line and dashed). Both models use relativistic transition potentials to Δ states with π and ρ exchange and a full relativistic OBEP (with reduced σ) for the $NN \to NN$ potential. The model by (Els+ 87) (dashed line) also includes nucleon renormalization (Fig. 7.4a) and uses a non-static pion propagator which — as discussed — leads to a characteristic signature in the $^3F_3$ phase parameters (Fig. 7.9). The better

[8]Note that due to the Δ-isospin of $\frac{3}{2}$ only isovector bosons can be exchanged.

fit of the P-waves by Model I (full line) is essentially due to a larger ω coupling and the neglect of the N-renormalization; the larger inelasticity produced by this model may be related to the neglect of the momentum dependence in the Δ-bubble (Fig. 7.4b). Note that 2π production starts around 600 MeV. Model I predicts all ϵ parameters up to 1 GeV (Fig. 7.10) correctly including the difficult ϵ_1 and ϵ_2.

In general, all models are able to reproduce *qualitatively* the special tendencies in $^1D_2$ and $^3F_3$, regardless the details of the theory. On the other hand, with regard to *quantitative* predictions there are (about the same) deficiencies in all models. As far as $^1D_2$ is concerned, it seems that the inclusion of the πd channel improves the inelasticity below 600 MeV (Sam 88). In general, all conventional models tend to underestimate it above Δ threshold. For $^3F_3$ the quantitative predictions of all models are in general worse: the phase shift does not show enough attraction around 650 MeV, while the inelasticity is poor just about everywhere.

The total cross sections for pp and np are in general reproduced well up to 2 GeV (Fig. 7.5); the inelastic cross sections are presumably too small, particularly above 1 GeV. This is not astonishing since other resonance than the Δ must play a role in that energy region which are omitted in the present models. The $N^*(1470)$ has been included by Lee (Lee 84), who finds only a small effect; there are, however, many more resonances (PDG 84). pp polarization up to about 650 MeV is described well (Fig. 7.6),[9] while the np polarization is predicted only qualitatively correctly (Fig. 7.7). The np differential cross section at 640 MeV is reproduced accurately by Model I (Fig. 7.8). The predictions we show in Figs. 7.6–7.10 for two examples of coupled channel models only are representative for those from any other existing model in the field.

Predictions by OBEP (dotted line) are also shown in the figures; by comparing them with the coupled channel results, the characteristic structures produced when Δ-isobars are included in the theory can be observed (of course, OBEP does not generate any inelasticities).

Summarizing the results, we like to stress that conventional models of mesons and baryons are so far able to explain a substantial amount of data on NN scattering at intermediate energies. The agreement is in some

[9]The energies of the experimental data displayed in Figs. 7.6-8 are always sufficiently close to the denoted energy of the predictions, such that the comparison is meaningfull.

cases only of a qualitative kind; however, none of the available models is 'complete' taking all possible hadronic contributions into account. For example, crossed two-pion exchange which had proven to be crucial at low energies (Section 5), has not been included in any model yet. However, above threshold the inclusion of such diagrams would imply that four-body unitarity must be satisfied. This is a huge task. As mentioned, also baryon resonances other than the Δ should be considered. Thus, missing agreement by present models can very well be due to approximations and restrictions used. Consequently, for the energies under consideration, there is in the moment no need to invoke new (quark) substructures (like exotic dibaryons) to explain the present data. However, it is highly desirable that the present models are substantially improved such that clear conclusions with regard to the origin of the present quantitative problems can be drawn. Likewise, more reliable and 'complete' hadronic models would allow for more conclusive insight into the question of the necessity and possible role of non-hadronic ingredients in nuclear physics at intermediate energies.

7.2 The GeV Region

Data on total and differential cross sections for proton-proton scattering at energies of several GeV and more are available since the 1950's, as this reaction has been used in particle production. These data can be explained in terms of a simple optical model (Ser 63) which by itself does not reflect much excitement. Therefore, these observables of NN scattering do not provide much insight into the NN interaction at high energies.

The picture changed completely with the event of high energy polarized proton beams. Pioneering work was done by the Michigan group at the Argonne ZGS in the early 1970's (see the review by Fernow and Krisch (FK 81) for an overview). Subsequently this group and others performed numerous experiments that studied spin effects in high energy strong interaction physics using polarized proton beams in the energy range of 1-12 GeV/c incident lab. momentum. These high energy polarization experiments present a benchmark, comparable to the Chamberlain experiments around 1957 (Cha+ 57). As the old experiments were decisive for our understanding of some important features of the nuclear force (spin-orbit force), the recent experiments could have a strong impact on our present

thinking. It may go so far that we have to change our present view of QCD.

For elastic pp scattering, the analysing power A, the spin-spin correlation parameter A_{nn}, and the ratio of spin-parallel and spin-antiparallel cross sections at 6 and 12 GeV/c have been measured (FK 81). The amazing result in all cases are strikingly large spin effects.

Hulthage and Myhrer (HM 84) have shown that the NN polarisation data obtained at the Argonne ZGS (Die+ 75, Yok 80) for $p_{lab} \approx 2$ GeV/c can be explained in terms of vector boson exchange using conventional choices for the coupling constants. Note that for the given lab. momentum, the c.m. momentum is $\approx$ 770 MeV/c which is about the mass of the omega and the rho meson. Thus, vector boson exchange provides the correct LS strenght even at these high energies.

At even higher energies, i. e. 12 GeV/c ZGS energy and, more recently, 28 GeV/c at the Brookhaven AGS[10], the polarization data pose a serious theoretical problem. Particularly the sharp rise in the data on A at high $p_\perp$ is quite unexspected (Kri 85). Assuming quark independence, the conventional quark model of the nucleon predicts $A \approx 0$ for those high momenta. This is certainly a challenging theoretical problem for the future.

[10]Alternating Gradient Synchrotron, Brookhaven National Laboratory, Upton, New York, U.S.A..

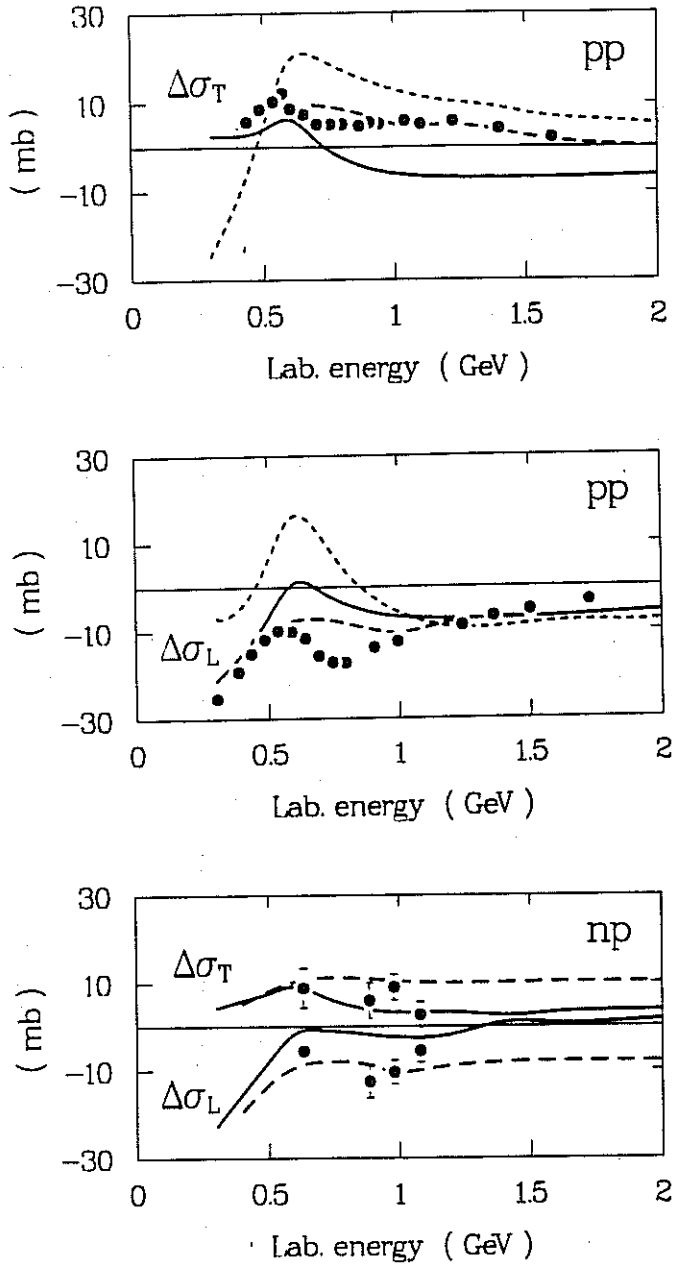

Figure 7.1: **Total longitudinal and transvers cross section differences for *pp* and *np* scattering as denoted.** The solid curve represents the prediction from the coupled channel Model I (of Appendix B), dashed from H. Lee (Lee 84), and dotted from Kloet und Silbar (KS 81). For data see (Arn 87).

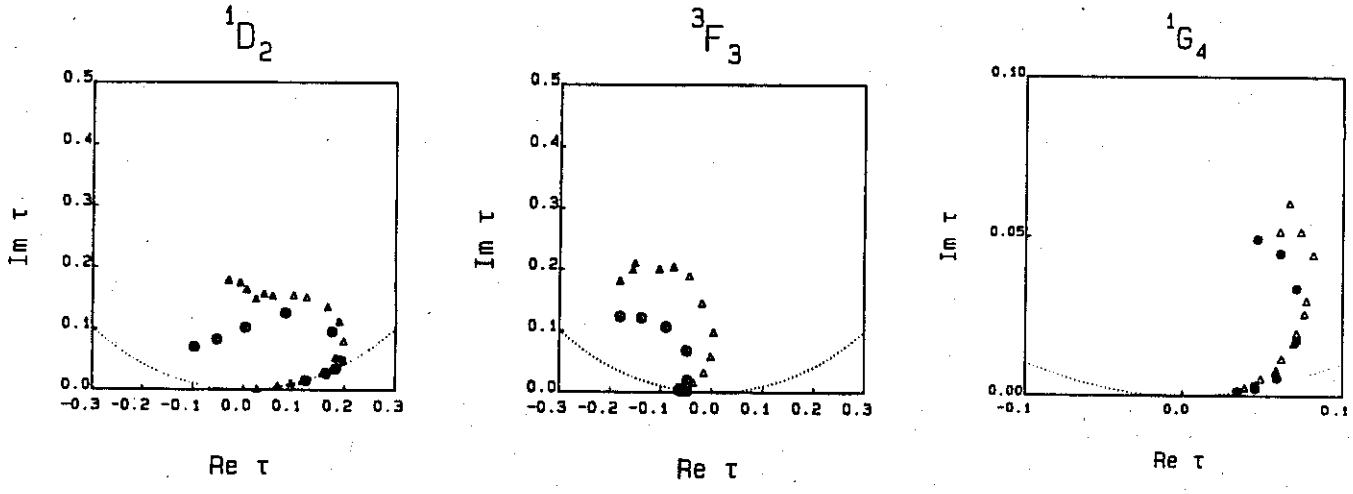

Figure 7.2: **Argand diagrams for three NN partial waves as denoted.** The full dots are the predictions by (Els+ 87), open triangles from the data analysis by Arndt (Arn 87).

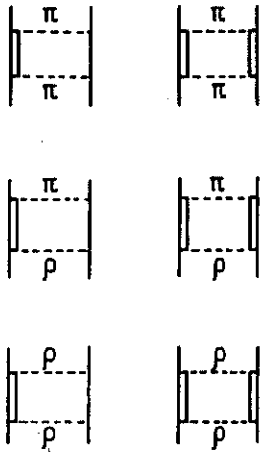

Figure 7.3: **Some diagrams involving Δ isobars (double lines) generated in a coupled channel model using π- and ρ-exchange transition potentials.**

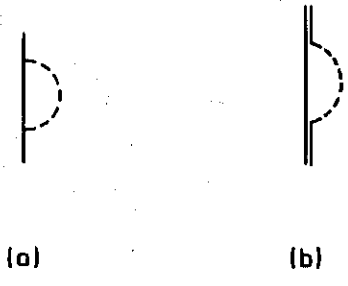

Figure 7.4: **(a) Nucleon and (b) Δ isobar self-energy diagram** involving the pion (dashed line).

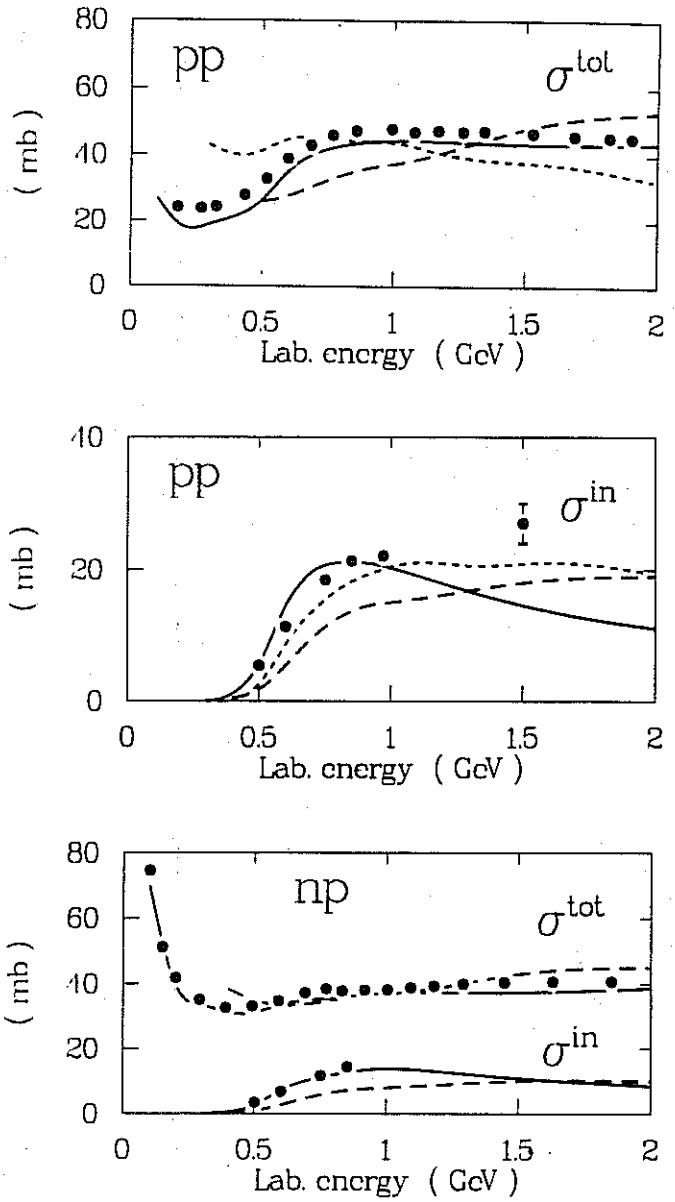

Figure 7.5: **Total and inelastic cross sections, σ^{tot} and σ^{in}, respectively, for pp and np scattering as denoted.** Theoretical curves as in Fig. 7.1. For data see (Bl 82, Arn 87).

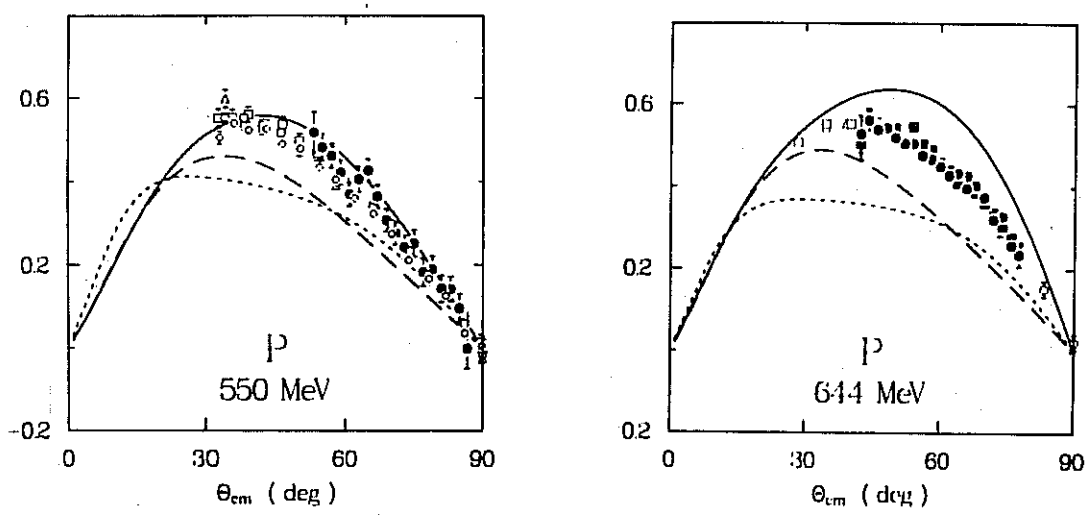

Figure 7.6: Predictions for the *pp* polarization at 550 and 644 MeV lab. energy. Full curve from the coupled channel Model I (of Appendix B), the dashed from (Els+ 87), and the dotted curve from the OBEP of Section 4. Full symbols denote data from SATURN, open symbols SIN or LAMPF data (BL 82, Arn 87).

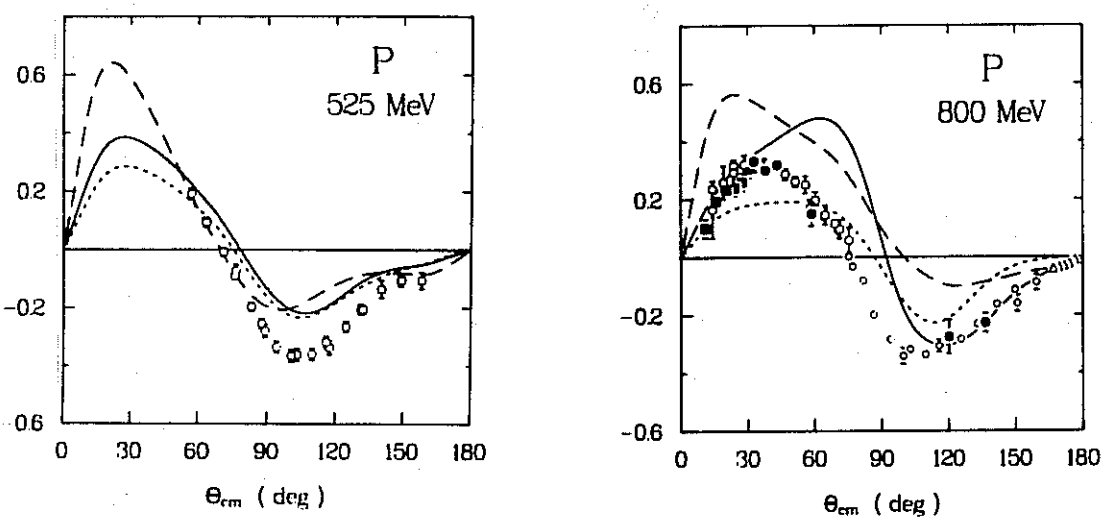

Figure 7.7: Predictions for the *np* polarization at 525 and 800 MeV lab. energy. Notation as in Fig. 7.6.

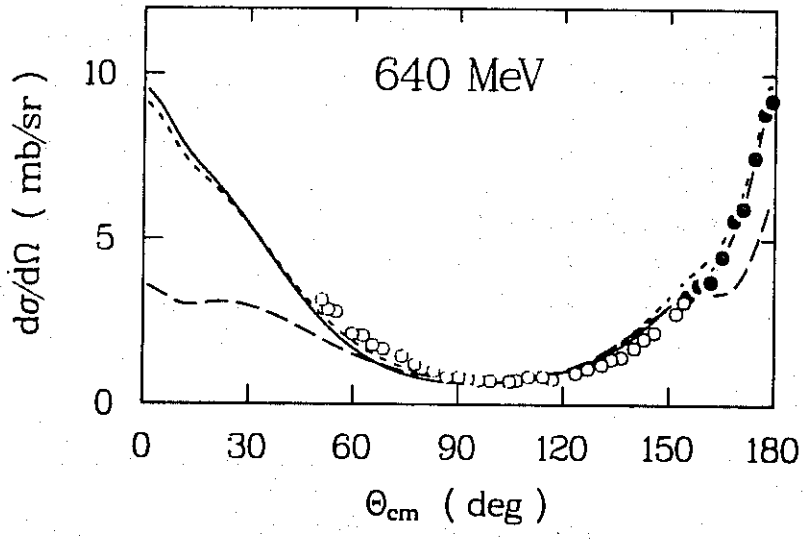

Figure 7.8: **Predictions for the np differential cross section at 640 MeV lab. energy.** Notation of curves as in Fig. 7.6.

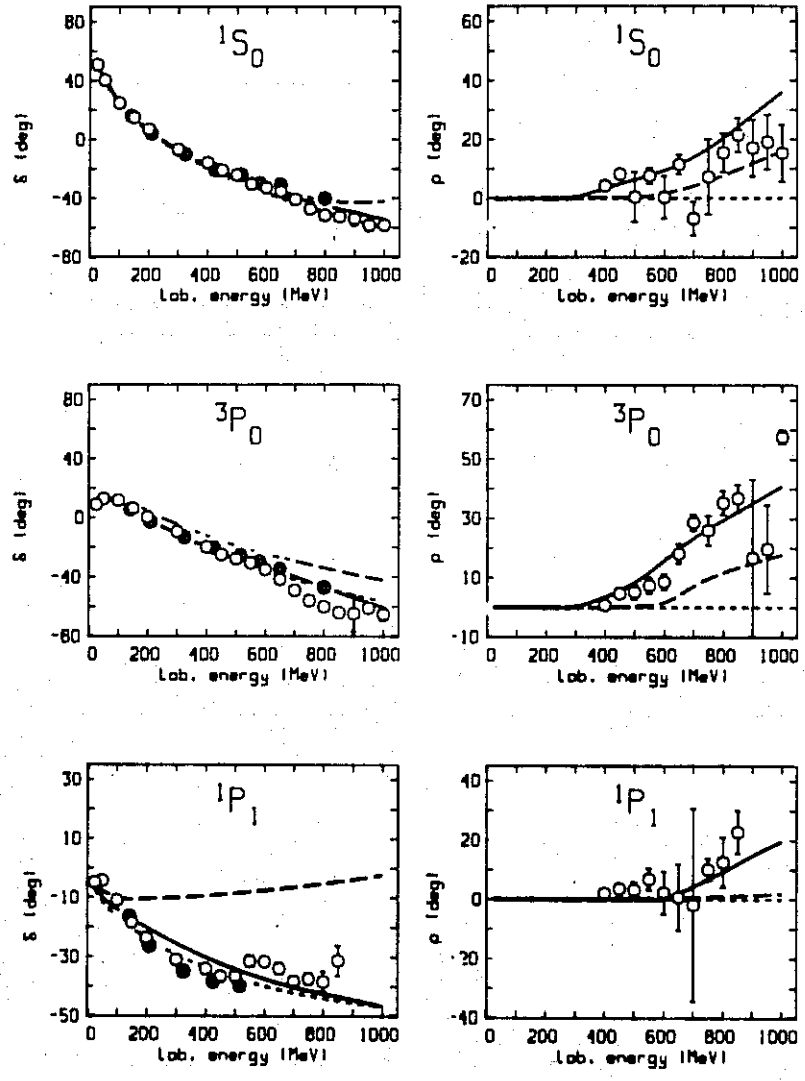

Figure 7.9: **Isospin zero and one phase parameters of NN scattering.** Definition of curves as in Fig. 7.6. The phase shift analysis by Arndt *et al.* (Arn+ 83) is represented by open circles, the one by Bugg and coworkers (Dub+ 82) by full dots. Arndt-Roper conventions are used (Arn+ 83).

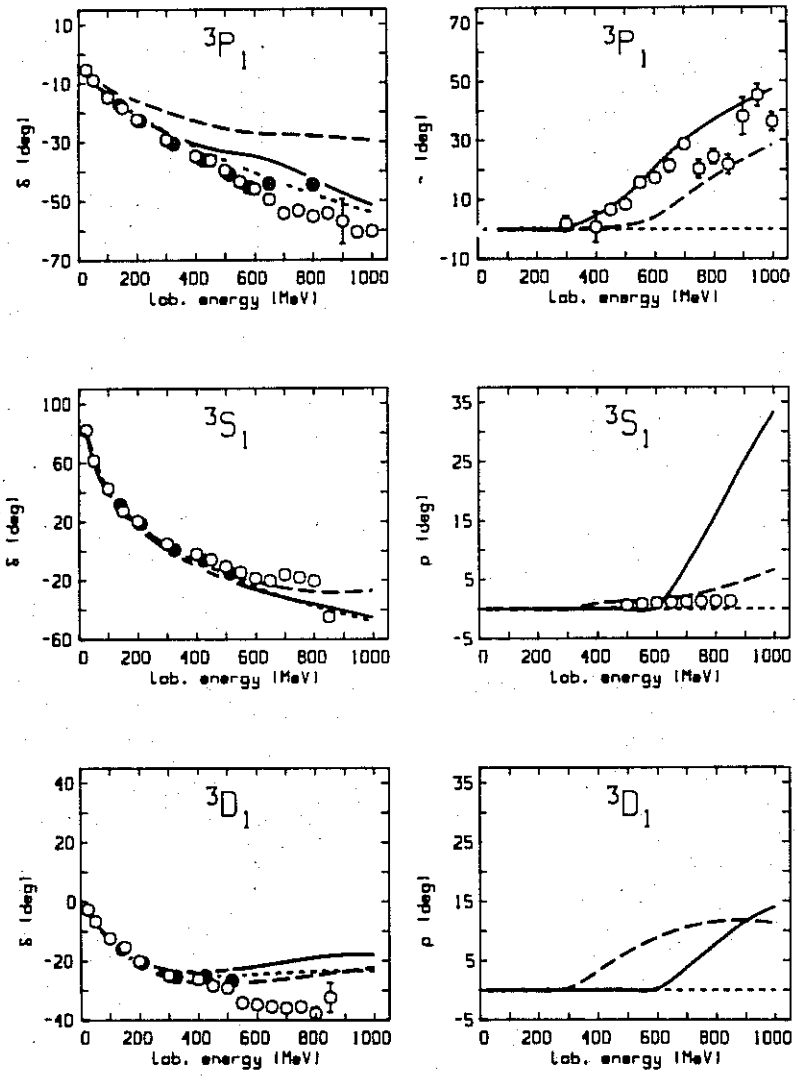

Figure 7.9: continued.

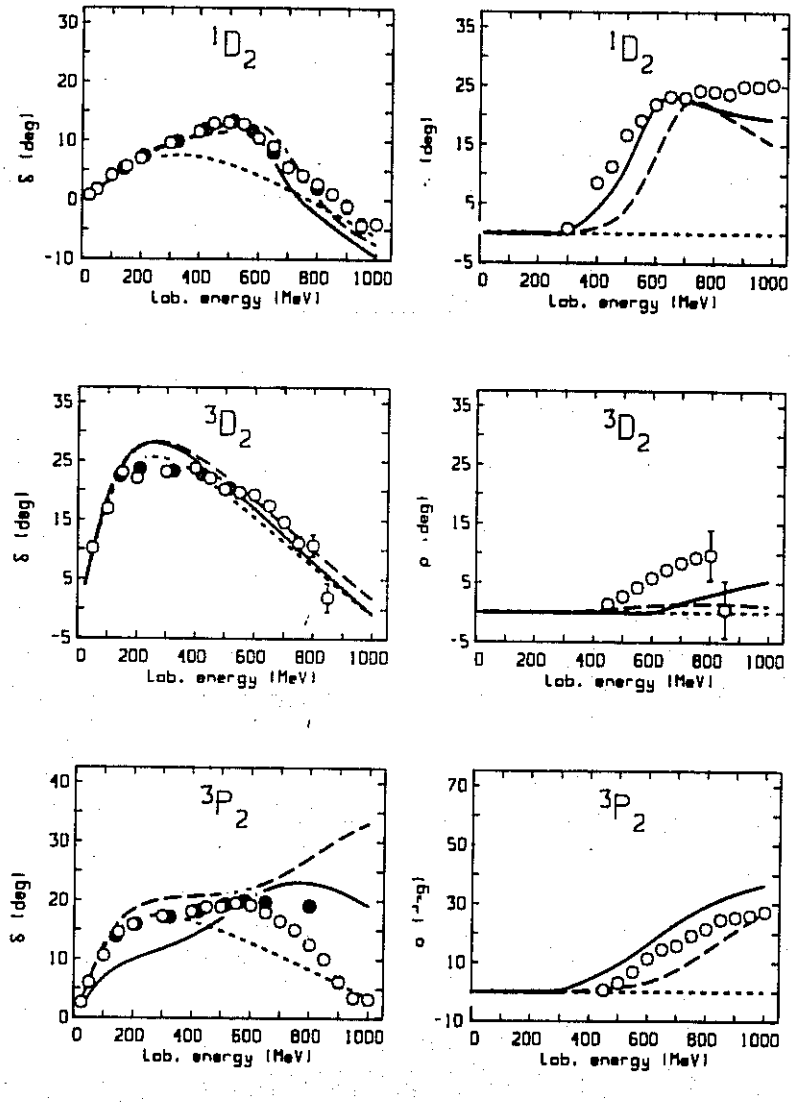

Figure 7.9: continued.

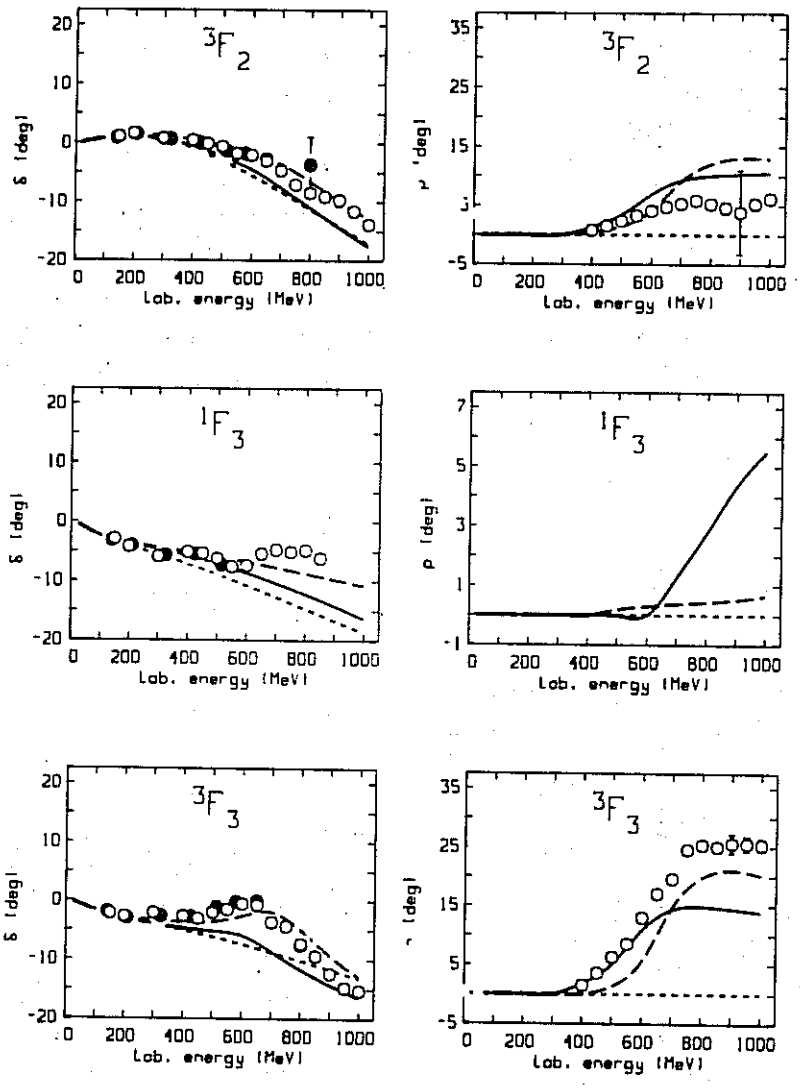

Figure 7.9: continued.

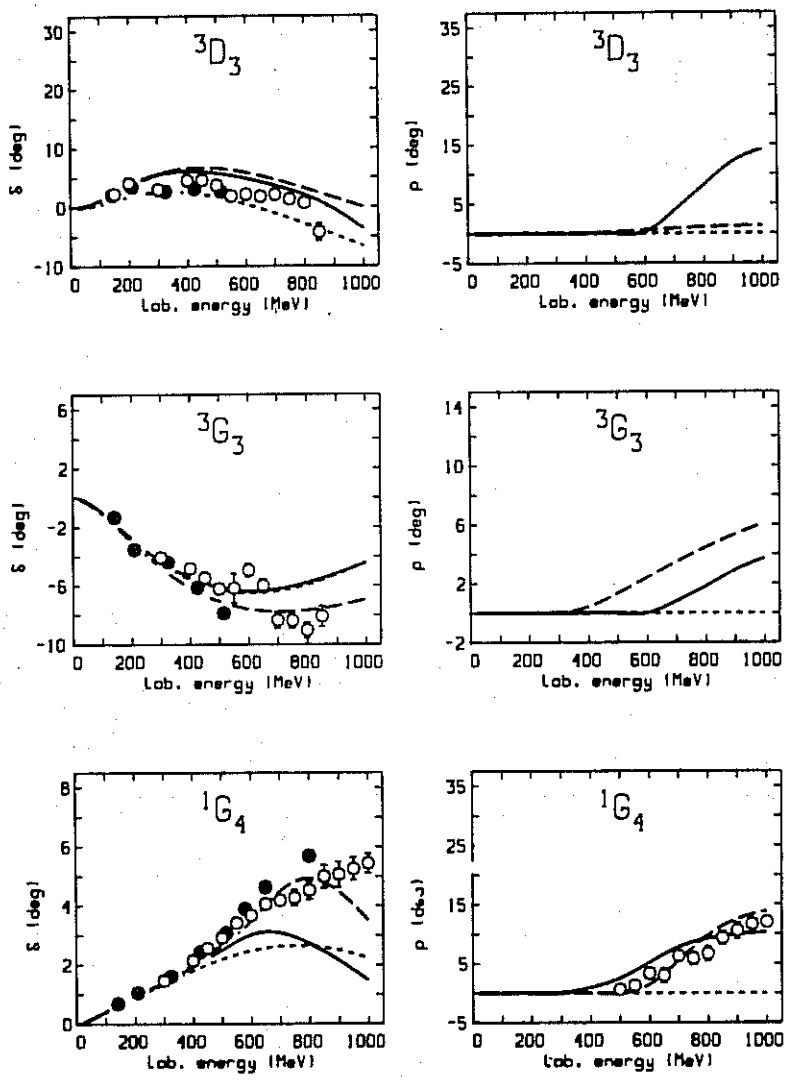

Figure 7.9: continued.

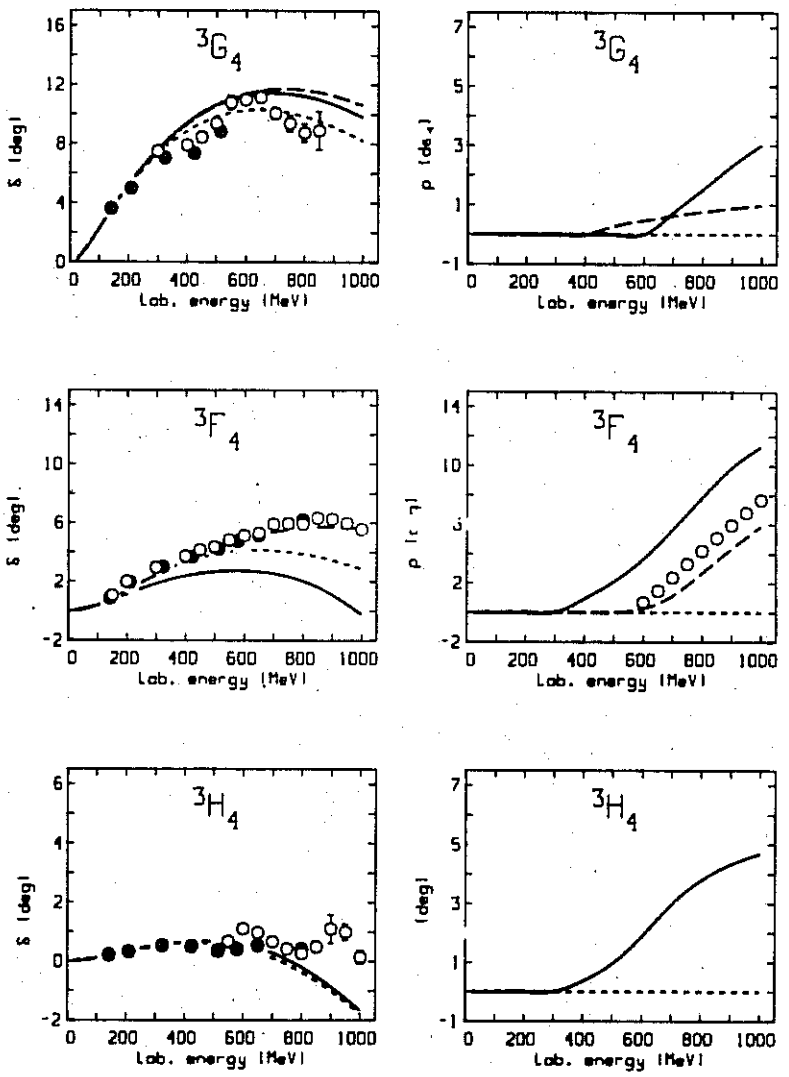

Figure 7.9: continued.

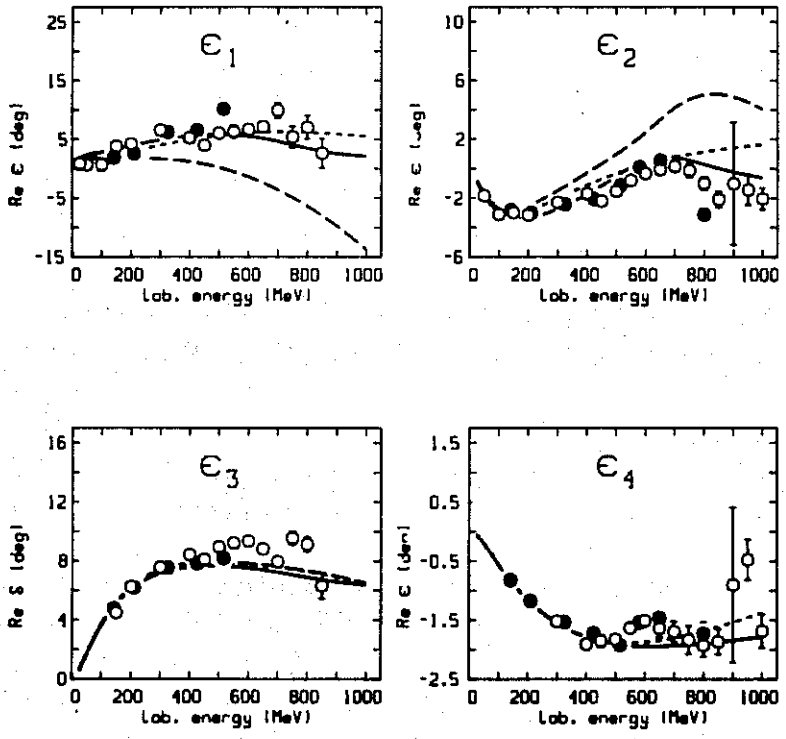

Figure 7.10: Real part of the mixing parameters for $J \leq 4$. Notation as in Fig. 7.9.

Section 8

Some Related Hadronic Interactions

In the 1950's it became clear that the nuclear force is not the only strong interaction in nature. Nowadays, the unified description of strong interactions including the mass spectrum of hadrons is attempted by QCD. On the background of this fundamental theory, meson theory plays the role of an effective quantitative model for the low energy regime. The Skyrmion model or lattice QCD may provide the justification for this approximation. The amazingly quantitative character of meson theory for the case of the nucleon-nucleon system has been demonstrated convincingly in previous sections. Most work presented for NN uses field-theoretic perturbation theory starting from certain well-defined effective meson-baryon interaction Lagrangians. These interactions have implications for other meson-baryon and baryon-baryon processes. Therefore, it is natural to ask the question: How about these other related strong interaction processes at low energy — does the meson model make equally realistic and even quantitative predictions as in the case of NN? The answer to this question is important with regard to the credibility of the whole concept of meson theory. If meson theory works for NN and fails everywhere else, one should better forget about it and use equally well any other mathematical ansatz for the nuclear potential which fits the data. However, the success of the meson-exchange currents in describing the electromagnetic properties of nuclei is another independent piece of evidence for the relevance and for the reality of mesons in nuclear physics. Hadronic reactions other than NN provide further sup-

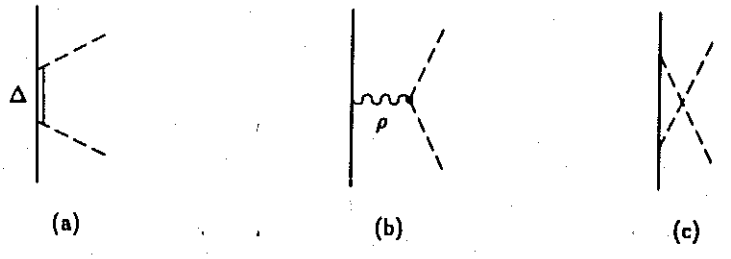

Figure 8.1: **Diagrams contributing to the πN interaction.** The full line denotes a nucleon, the dashed a pion.

port. There are some key processes of strong interactions which have drawn particular interest, for example πN, ΛN, ΣN, and $N\bar{N}$. Whereas the relationship between πN and NN is of direct nature, the interaction with hyperons can be related via flavour $SU(3)$; for the real part of the $N\bar{N}$ interaction G-parity provides a bridge. In this section we will briefly discuss some of these examples.

8.1 Pion-Nucleon Scattering

The 'elementary' meson-baryon interactions, from which we have built the NN interaction in previous sections, has implications for meson-nucleon scattering. The πN system is of particular interest; comprehensive and precise data exist on πN scattering, phase-shift analyses are available. The key question from the theoretical view point is if, what we have assumed in the case of NN, is consistent with what is known about πN. When dispersion relations are used, we have no problem with that question, as the consistency is built into the theory.

The situation is different for an approach which uses Lagrangian field theory. In analogy to the model for the 2π exchange discussed in Section 5 (Fig. 5.2), we display in Fig 8.1 diagrams which contribute to πN scattering. Appropriate assumptions for the $\rho\pi\pi$ vertex can be made (FS 80). All other vertices also occur in the NN model and are therefore fixed. In

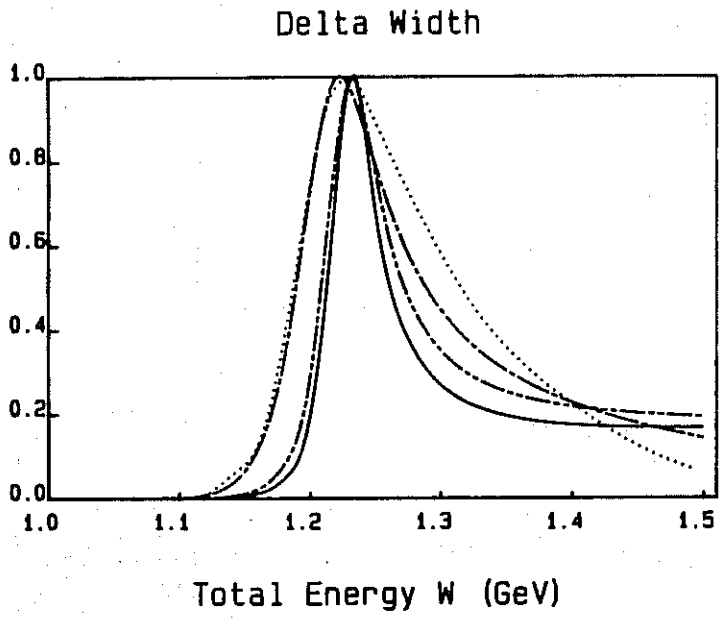

Figure 8.2: **Imaginary part of the πN T-matrix in the P_{33} partial wave versus the total energy, W, of the πN system.** Solid line: contribution from diagram Fig. 8.1a; dash-dot-dot: diagram Fig. 8.1a+b; dash-dot: all diagrams of Fig. 8.1. [From (Els 86)]

Fig. 8.2 we show results for the P_{33} partial wave of πN scattering. The individual contributions from the various diagrams are shown explicitly. A σ-contribution (analogous to the ρ-diagram, Fig. 8.1b), which is not shown, raises the amplitude above resonance further bringing it close to the empirical curve. (The dotted line in Fig. 8.2 represents the empirical result from Höhler *et al.* (Höh+ 79)). It is clearly seen, how the individual contributions build up the complete amplitude step by step. Thus, it is possible to describe consistently πN, $\pi\pi$ (FS 80), and NN within one fieldtheoretic model.

An important issue is the πNN and $\pi N\Delta$ vertex cutoff Λ_π. Models for the NN interaction use typically $\Lambda_\pi \gtrsim 1$ GeV. Below that value a quantitative reproduction of the low energy NN data — in particular the deuteron data — is impossible (Section 4). On the other hand, models for πN frequently apply a substantially lower value for that parameter,

namely $\Lambda_\pi \approx 0.4$ GeV. However, such models use only the Δ pole graph, Fig. 8.1a. The substantial discrepancy between these two choices for the cut-off parameter poses a serious problem. Figure 8.2 indicates the possible solution of that problem. When *all* contributions to the πN process are taken into account which are *consistently* implied by the fieldtheoretic model for NN, a quantitative description of the P_{33} amplitude is, indeed, possible using the *same* parameters as in NN. It is also clearly seen that the direct Δ contribution alone applying the large cutoff parameter from NN would provide a completely insufficient description of that amplitude.

We note that the present discussion, as far as the πN system is concerned, applies only to the P_{33} partial wave. For a recent discussion of the S-waves and the P_{11} we refer the interested reader to the papers by Jennings and coworkers (CJ 86b, Coo+ 87) and by Pearce and Afnan (PA 86), respectively.

8.2 The $N\bar{N}$ Potential

As a Dirac particle, the nucleon has an anti-particle state, the anti-nucleon ($\bar{N}$). Soon after the experimental discovery of the anti-proton in the Berkeley Bevatron in 1955 (Cha+ 55) the interaction between anti-nucleons and nucleons at low energy was studied extensively (for summaries of this early work see Seg 58 and Mcc 60). On the theoretical side it was realized that in the framework of meson theory the NN and the $N\bar{N}$ interactions are most intimately related by the so-called G-parity rule (IH 56, BC 58). According to this rule, a NN potential given by

$$V_{NN} = \sum_\alpha V_\alpha \tag{8.1}$$

with V_α a well-defined t-channel meson-exchange contribution (see Section 3.4), implies the $N\bar{N}$ potential

$$V_{N\bar{N}} = \sum_\alpha G_\alpha V_\alpha \tag{8.2}$$

where G_α denotes the G-parity of the exchanged meson(s). For a system α consisting of n_α pions the G-parity is

$$G_\alpha = (-1)^{n_\alpha}. \tag{8.3}$$

This transformation can also be defined quite generally (IZ 80) implying a definite G-parity for every meson and system of mesons. Considering the six bosons usually applied in one-boson-exchange models (Section 3 and 4, Appendix A), namely π, η, σ, ρ, ω, and δ, the contribution from three of them switches sign, namely π, ω, and δ.[1] As a consequence, the one-omega-exchange, which provides the short range repulsion in the NN interaction, is attractive in the $N\bar{N}$ system and adds to the attraction from 2π exchange. Thus, the $N\bar{N}$ potential is strongly attractive at short distances and does not have a repulsive core. This implies an enhancement of the $N\bar{N}$ cross section as compared to NN (BC 58). To give an example, at 230 MeV lab. energy the total (elastic) cross section for neutron-proton scattering is 39 mb; at that same energy the cross sections for proton-antiproton scattering are, total: 137 mb, elastic: 50 mb, and charge exchange (i. e. $p\bar{p} \to n\bar{n}$): 11 mb.

The close connection between the NN and the $N\bar{N}$ potential, encouraged early hopes that an analysis of the $N\bar{N}$ observables could provide additional constraints on the meson exchange model of the NN force (Phi 67, BP 68). However, in practice the usefulness of the G-parity rule is limited to the long and intermediate range part of the potential. At short distances, the annihilation is dominant in $N\bar{N}$, a feature which has no analogue in the NN system at low energies. Since the $N\bar{N}$ system has zero baryon number, it can dissolve into mesons, the mean multiplicity of pions being about five for the low energies under consideration. The annihilation cross section is large, about twice as large as the elastic.

In early work, either boundary models ("black spheres") or purely phenomenological potentials were used to describe the annihilation.[2] For example, Bryan and Phillips (BP 68) and Dover and Richard (DR 80) assume a complex potential of local Woods-Saxon form with no spin- and isospin-dependence:

$$U_{N\bar{N}}^{(ann)}(r) = -\frac{V_0 + iW_0}{1 + \exp(\frac{r-R}{a})} \tag{8.4}$$

with V_0 and W_0 real constants and R and a parametrizing the range. This is added to $V_{N\bar{N}}$, Eq. (8.2), to obtain the total optical potential for low

[1] Note that the decay of the η meson into three pions is of electromagnetic nature, therefore the η is not a strong 3π resonance; $G_\eta = +1$, $G_\delta = -1$ (PDG 84), cf. Table 3.2.

[2] For a useful survey of the theoretical studies during the early period see the review by Phillips (Phi 67).

energy $\bar{N}N$ scattering:

$$U_{N\bar{N}}^{(tot)} = U_{N\bar{N}}^{(ann)} + V_{N\bar{N}} \tag{8.5}$$

The parameters of the absorptive potential, as obtained from phenomenological studies, are typically of the following orders:

$$\begin{array}{rcrcl} 0 & \leq & V_0 & \leq & 21 \text{ GeV} \\ 0.5 \text{ GeV} & \leq & W_0 & \leq & 62 \text{ GeV} \\ 0 & \leq & R & \leq & 0.8 \text{ fm} \\ & & a & \approx & 0.2 \text{ fm} \end{array} \tag{8.6}$$

where the larger ranges are in general associated with the smaller V_0 and W_0 and vice versa; in this way the strenght of the absorptive potential around 1 fm is about the same in all cases, namely in the order of 100 MeV. For example, using the (G-parity transformed) OBEP of Section 4 complemented by the annihilation potential Eq. (8.4) with $V_0 = 0$, $W_0 = 8.3$ GeV, $R = 0$, and $a = 0.2$ fm, one reproduces the present low energy $N\bar{N}$ cross section data (MMM 87).[3]

The strenght and the range of the annihilation potentials, necessary to fit the data, are difficult to understand from the theoretical point of view (DR 80). The W_0 necessary in the case of a short-ranged annihilation potential appears rather large; on the other hand, if a more reasonable value of W_0 is applied, e. g. in the order of 1 GeV, a long range has to be used ($R \approx 1$ fm) for which the theoretical interpretation poses some problem.

In the traditional picture, in which nucleon and antinucleon annihilate into mesons, the range of the annihilation is essentially determined by baryon-exchange. This argument suggests a range for the absorptive potential in the order of $(2M)^{-1}$ (Mar 61). The most consistent work along this line of thought has been done by the Paris group (Côt+ 82). From detailed calculations of annihilation diagrams with two meson intermediate states, they derive an annihilation potential which is energy-, spin-, and isospin-dependent and which is of the short range indicated. In other work the annihilation range is in general much longer, in the order of 0.5-1 fm (DR 80). This is also true for the work by the Nijmegen group (TSS

[3]The annihilation parameters used in this model are the same as in the Bryan-Phillips potential (BP 68) in which the OBEP of Bryan-Scott (BS 64 and 69) is applied.

84), who developed a coupled channel model and assume spin- and isospin-dependence.

From a more modern point of view, $N\bar{N}$ annihilation should be a good test of quark/gluon dynamics at short distances. The crucial question is if a connection between the microscopic and the phenomenological forms of the annihilation potentials can be established. Quark rearrangement and quark annihilation into gluons has been considered (GN 84, TMM 85). In spite of the considerable work already done, the theory for this part of the $N\bar{N}$ interaction is still in its infancy. Much more work is needed in the future for which more precise data could provide a welcome guideline for the theoretical efforts.

The long and intermediate range $N\bar{N}$ potential is on safer grounds (if one believes in meson theory). It has become customary and it is, in fact, revealing, to discuss the contributions to this part of the potential under the aspect of *coherence* (BDR 79, DR 79). As explained in Section 3.4, in the meson-exchange picture the central forces are provided essentially by the σ and the ω. These have opposite sign for the NN system, while they add up to a strong short range attraction for $N\bar{N}$. The spin-orbit forces created by these two bosons add up in NN; they cancel in the $N\bar{N}$ system, for which, therefore, a weak LS force is predicted by meson theory. The tensor forces provided by π and ρ exchange are of opposite sign in NN and add up coherently in $N\bar{N}$. Consequently the real part of the $N\bar{N}$ potential shows substantial qualitative differences from that for NN, namely a much stronger central attraction, no repulsive core, a much weaker spin-orbit force and a stronger tensor force, particularly at short range (compare Figs. 3.6-8). In particular, spin-observables are sensitive to these characteristic differences between NN and $N\bar{N}$. Except for very few and rough measurements of the polarization there are no data available on spin observables for $N\bar{N}$. To measure those will be a worthwhile experimental program for the future. The effect of coherent meson-exchange contributions in the medium and long range show up drastically in predictions for spin observables, particularly in the charge exchange channel. For example, the $N\bar{N}$ polarization is extremely sensitive to the tensor force (DR 82), in contrast to NN where the spin-orbit force plays the dominant role for the polarization (GT 57), see Fig. 3.4. Therefore, a careful mesurement of $N\bar{N}$ spin observables could provide a constraint on the strenght of the various

Yukawa couplings in a meson exchange model. LEAR[4] may provide such data in the near future. Thus, early hopes (Phi 67, BP 68) may finally be justified.

As we learned in Section 5, a more refined meson theory uses an explicit model for the 2π exchange and necessarily has to include the $\pi\rho$ diagrams. These contributions replace the fictitious σ boson customary in one-boson-exchange models. This refinement of the meson-exchange model for NN has consequences for $N\bar{N}$. First, the explicit 2π exchange is more attractive than a σ boson, particularly at short ranges. Second, the $\pi\rho$ exchanges which are repulsive in NN, thus reducing the short range attraction provided by 2π, turn attractive in the $N\bar{N}$ system, due to the G-parity rule ($\pi\rho$ is a three-pion exchange). Thus, a refined meson model predicts substantially more short range attraction for the $N\bar{N}$ potential than one-boson-exchange models do. As a consequence, the amazingly large values for V_0 and W_0 (Eqs. (8.4 and 8.6)) needed by present models may considerably reduce.

There is another exciting point about the $N\bar{N}$ system, namely the possibility of $N\bar{N}$ bound states or resonances, so-called baryonia. More precisely speaking, hadronic states which, while massive and mesonic, would be strongly coupled to the baryon-antibaryon channel and relatively weakly coupled to standard mesonic channels, are referred to as baryonium states. Both experimentally and theoretically the speculations have been flourishing during the past decade. However, presently the situation is rather unclear. From the theoretical point of view, such states appear quite likely, because of the strong short range attraction in the real part of the $N\bar{N}$ potential as obtained from meson theory. However, it has been questioned if such narrow structures survive the strong annihilation potential (MT 76), the answer depending most sensitively on the annihilation radius. Furthermore, quantitative studies show a large sensitivity to the uncertain short range part of the force. Theoretical considerations based upon potential models are treated in (BDR 79, DR 79, Sha 78). QCD inspired work is reviewed in (MRV 80). On the experimental side, early indications for baryonium states (KT 75, Pav+ 78) have not been confirmed. For a recent summary and for more hope see Dover (Dov 84, Dov 86).

In summary, meson theoretic potentials complemented by a (phenomen-

[4]Low Energy Antiproton Ring, CERN, Geneva, Switzerland.

logical) absorptive part can describe present $N\bar{N}$ data well. However, more precise data, particularly of spin observables, are needed to learn more about the microscopic annihilation mechanism and the spin structure of the real potential which differs in a characteristic way from the real NN potential. Also, any more precise knowledge of the annihilation part of the potential will put constraints on the real (meson-theoretic) part and, thus, another more precise test of meson theory would be provided.

8.3 Strange Nuclear Interactions

The relationship between NN and YN (where Y stands for a hyperon) is not as simple as in the case of πN or $N\bar{N}$. The Lagrangians we have used in conjunction with the NN problem bear no direct relationship to the hyperon fields. However, if one believes that quarks are the ultimate building blocks of hadrons, then flavour $SU(3)$ implies relations between meson-baryon coupling constants. Thus, when a meson-nucleon coupling constant has been fixed by NN data, the corresponding meson-hyperon coupling constant can be predicted. Models following these guidelines have been developed, particularly, by the Nijmegen group (NRS 73, NRS 79). The result of this work is that the existing YN data can, indeed, be desribed quantitativly in that framework.

However, the present ΛN and ΣN data are not very precise. More reliable experimental information is desirable. This would be a worthwhile program for future kaon factories.

Also the (effective) interaction of hyperons in nuclei (hypernuclei) has been studied for many years. Meson-exchange models have been fairly successful in describing the binding energy of a Λ in a nucleus. However, there are some cases in which a remarkable discrepancy between theory and experiment exists. The case of ${}^{5}_{\Lambda}He$ is particularly outstanding. Conventional models predict too much binding energy. There are suggestions that this nucleus could be used to study the deconfinement of baryons in the nucleus (Yam 87).

Another challenging issue is the spin-orbit coupling of hyperons with nucleons. This coupling comes out weaker (by about a factor 2-3) as compared to the nuclear force if the meson picture is applied (BW 81, Bro 81). It is due to a weaker σ and ω coupling as predicted by $SU(3)$. Whereas for

the Λ this prediction is in agreement with experiment, there appears to be a discrepancy in the case of Σ hypernuclei. Present data (Ber+ 85) can be interpreted such that the ΣN spin-orbit force should be at least as large as that of NN, in contrast to predictions from meson models (Bro 81). However, the interpretation of the data is controversial (Dov+ 86). Predictions using quark models contradict each other (Gal 85). In some quark model estimates a large ΣN spin-orbit force is, indeed, obtained (Pir 79). The exciting point about this issue is that a decision between the meson and the quark model by experiment could in principal be possible. However, in view of the present controversies on the experimental as well as on the theoretical side, it is too early to draw any conclusions.

Section 9

Nuclear Matter I — Conventional

With this section we start the discussion of nuclear structure aspects using meson-theoretic forces. After dealing in length with the two-nucleon system, it might appear natural to consider next further *few*-nucleon problems. Nevertheless, we will turn now to the system of infinitely many nucleons, i. e. nuclear matter. The reason for this big step is that there are substantial mathematical simplifications in the nuclear matter problem as compared to finite nuclei. They are due to the translational invariance of the system: first, the single-particle wave functions are known to be plane waves (instead of, for example, solutions of the Faddeev equations — for the three-body problem, or self-consistent Hartree-Fock wave functions — for heavier nuclei); second, momentum conservation eliminates certain classes of diagrams and yields equations which are diagonal in momentum space. Because of these practical advantages, more systematic work has been done for nuclear matter than for any finite nucleus. This is particularly true for considerations including sub-nucleonic degrees of freedom, which are one of the final goals of this and the following section.

9.1 Introduction

By definition, *nuclear matter* refers to an infinite uniform system of nucleons interacting via the strong force without electromagnetic interactions. This hypothetical system is supposed to approximate conditions in the interior

of a heavy nucleus. We shall assume equal neutron and proton density, that is, we will consider symmetric nuclear matter. This many-body system is characterized by its energy per nucleon as a function of the particle density.

Empirical information on the minimum of that curve — the saturation point — is deduced by extrapolation from the properties of finite nuclei. Based on the liquid drop model for the nucleus, the semi-empirical Bethe-Weizäcker mass formula provides a value for the energy via its volume term (Wei 35, BB 36). An extended version of that formula, which takes shell effects into account, was given by Myers and Swiatecki (MS 69). A collection of contemporary mass formulas by many different authors can be found in the Atomic Data and Nuclear Data Tables (NDT 76). From the charge distribution of heavy nuclei as determined in electron scattering, the saturation density can be deduced by taking into account corrections due to the Coulomb repulsion and the surface tension (Bra 64). Alternatively, both the saturation energy and density can be deduced from Hartree(-Fock) or Thomas-Fermi calculations with phenomenological effective forces fitted to the ground state properties of closed shell nuclei (Neg 70, CS 72, FN 73, DG 80, WHW 83, Dut+ 86, HS 81, SW 86). Thus, nuclear matter is determined to saturate at a density

$$\rho_0 = 0.17 \pm 0.02 \text{ fm}^{-3} \tag{9.1}$$

and energy per particle

$$\mathcal{E}/A = -16 \pm 1 \text{ MeV}. \tag{9.2}$$

Other parameters related to the particle density are the interparticle spacing r and the Fermi momentum k_F which are defined by

$$4\pi r^3/3 = 1/\rho \tag{9.3}$$

and

$$\rho = 2k_F^3/(3\pi^2). \tag{9.4}$$

The equilibrium values for these quantities corresponding to the above given ρ_0 are

$$r_0 = 1.13 \pm 0.04 \text{ fm} \tag{9.5}$$

$$k_F^{(0)} = 1.35 \pm 0.05 \text{ fm}^{-1} \tag{9.6}$$

Also of interest is the incompressibility or compression modulus[1] of saturated nuclear matter

$$K = k_F^2 \frac{\partial^2(\mathcal{E}/A(k_F))}{\partial k_F^2} \Big|_{k_F=k_F^{(0)}} . \tag{9.7}$$

From empirical information deduced from the systematics of the isoscalar monopol vibrations (breathing modes) in nuclei (You+ 77, BGB 76, Bla 80), one obtains

$$K = 210 \pm 30 \text{ MeV}. \tag{9.8}$$

The fission barrier heights of actinides have been shown to depend sensitively on the compression modulus (BGH 85). With an incompressibility consistent with the value quoted above, one was for the first time able to reproduce the experimental barrier heights (Bar+ 82). A recent analysis of the differences in the charge density distributions of ^{208}Pb, on the one hand, and ^{207}Pb or ^{206}Pb, on the other, essentially confirms the above given value as a lower bound (Cav+ 87, CS 86b). It has been pointed out, however, that in this type of analysis there is a large sensitivity to the effective mass and to pair correlations which casts some uncertainty on this method for extracting K (Bar+ 86). In many-body calculations using density-dependent phenomenological forces fit to the groundstate properties of closed-shell nuclei, values for the compressions modulus are obtained which agree with Eq. (9.8) (DG 80, WHW 83).

It is the objective of nuclear matter theory to explain these empirical properties miscrocopically.

9.2 History of the Conventional Many-Body Problem

Historically, the first nuclear matter calculations were performed by Heisenberg's student, Hans Euler, in 1937 (Eul 37). This was just two years after Weizäcker (Wei 35) had suggested the semi-empirical mass formula. Euler applied an attractive potential of Gaussian shape in second order perturbation theory.

[1] More popular is the incorrect term of *compressibility*.

Modern studies began in the early 1950's after a repulsive core in the nuclear potential had been conjectured (Jas 51). It was obvious that conventional perturbation theory was inadequate to handle such singular potentials (e. g. a hard-core potential would give an infinite contribution in each order). Therefore, special methods had to be developed. This program was initiated by Brueckner and coworkers (BLM 54, Bru 54, BL 55, Bru 55), who applied — for the groundstate problem of nuclei — methods similar to those developed by Watson (Wat 53) for multiple scattering. Later, a formal basis for this new approach was provided by Goldstone (Gol 57) who — using perturbation theoretical methods — established the so-called linked cluster expansion. The physics behind this new approach was revealed, in particular, by Bethe (Bet 56). The success of Brueckner theory in practical calculations stems from the fact that certain classes of linked diagrams can be summed in closed form up to infinite orders defining the so-called reaction matrix G. All quantities are then formulated in terms of this G which — in contrast to the bare nuclear potential — is smooth and well-behaved.

About at the same time when this new perturbation theory was formulated, an alternative approach was suggested. Jastrow (Jas 55) recommended the use of trial wave functions to be applied in a variational problem. However, the complexity of the problem which evolves when spin, isospin, tensor and spin-orbit correlations are included (all required in a realistic case) discouraged physicists from seriously pursuing this approach in the 1950's. When the discovery of pulsars (neutron stars) in the late 1960's suggested the consideration of highly dense matter, interest in the Jastrow approach was revived, as it is believed to be more reliable at high densities than Brueckner theory.

The first numerical calculations applying Brueckner theory were performed in 1958 by Brueckner and Gammel (BG 58) using the Gammel-Thaler potential (GT 57). In the following decade, substantial advances were made in the physical understanding of Brueckner theory due to Hans Bethe and his collaborator (BBP 63, Day 67, RB 67, Bra 67, Bra 70, Bra 77); furthermore, practical methods of (approximately or exactly) solving the equation involved were developed (MS 60, KD 69) which gave rise to first remarkable success (KB 66). Systematic and accurate calculations were finally performed around 1970 (Sie 70, Coe+ 70, HT 70, Bet 71, Spr 72). An alternative formulation of Brueckner theory, the so-called coupled

cluster or $\exp(S)$ method, was developed by Coester and Kümmel (Coe 58, CK 60, KLZ 78, BK 87).

In the middle 1970's the nuclear many-body community was shaken by an apparent discrepancy between results from Brueckner theory and the variational approach. This indicated clearly that both theories had to be re-examined and more consistent calculations had to be performed. For Brueckner theory this was done in particular by Ben Day (Day 78, 81a, 81b). The variational approach was pursued mainly by Pandharipande and Wiringa (PW 79). As a result of this enormous work, in the early 1980's, quantitatively very close predictions were obtained from the two different many-body approaches using realistic NN potentials (LP 81, DW 85). Consequently, it is believed today that both many-body approaches are reliable for densities typical for low energy nuclear physics.

9.3 Conventional Theories

Conventional many-body theories are based on the *simplest* model for the atomic nucleus: point nucleons obeying the non-relativistic Schrödinger equation interact through a two-body potential that fits low energy NN scattering data and the properties of the deuteron. There are several reasons for starting a many-body study within this model. First, one wants to know if under such restrictive assumptions, the prediction for the saturation point of nuclear matter is unique. If this is not the case, i. e. if the predictions vary for different potentials, then one might ask a second question: namely, is there at least one potential which does predict nuclear matter saturation correctly? Such a potential could then be used as a standard model for nuclear physics: NN scattering and nuclear structure could be understood in terms of the same underlying two-body force. Third, if such a potential cannot be found, the results may be understood as an indication that the simplest model is inadequate and extensions are necessary, such as the inclusion of many-body forces, meson and isobar degrees of freedom, relativistic effects, the sub-structure of hadrons etc..

Thus, in this section we consider a system of A identical nucleons (in a large box of volumn Ω) which obey the non-relativistic Schrödinger equation. The Hamiltonian of the system is the sum of the kinetic energies of all the particles plus the sum of the two-body interactions between them,

i. e.

$$H = \sum_{i=1}^{A} T_i + \sum_{i<j}^{A} V_{ij} \tag{9.9}$$

The problem to be solved is to calculate the groundstate energy per particle, $\mathcal{E}/A$, as a function of the particle density, $\rho = A/\Omega$. The minimum of this curve will give the saturation values to be compared with the empirical ones.

In the *variational method* one chooses a trial many-body wave function of the form

$$\Psi = F\Phi \tag{9.10}$$

and attempts to minimize the variational energy

$$\mathcal{E}_{var} = \frac{\langle \Phi | F^\dagger H F | \Phi \rangle}{\langle \Phi | F^\dagger F | \Phi \rangle} \tag{9.11}$$

which should provide an upper bound for the groundstate energy. Here, Φ denotes the non-interacting Fermi gas wave function. For a central two-body potential, $V(r)$, the correlation operator F is usually chosen to be the product of two-body correlation functions $f(r_{ij})$,

$$F = \prod_{i<j}^{A} f(r_{ij}). \tag{9.12}$$

The $f(r_{ij})$ are parametrized in some form and — due to the repulsive core — should go to zero for small r_{ij}. At large r_{ij}, $f(r_{ij})$ is required to approach unity. For a realistic nuclear force the ansatz for the correlation functions has to be generalized. Tensor force, spin-orbit force and other correlations have to be taken into account. $\mathcal{E}_{var}$ can be evaluated exactly by Monte Carlo methods or approximately by means of cluster expansions. The most popular expansion uses the method of hypernetted chains. For more details about this many-body approach and its calculational techniques we refer the interested reader to the reviews by Day (Day 78) and by Pandharipande and Wiringa (PW 79).

The Brueckner-Bethe-Goldstone method (in short: *Brueckner theory*) is based on the Goldstone expansion (Gol 57) which is a linked-cluster perturbation series for the groundstate energy of a many-body system. The Hamiltonian is rewritten as

$$H = H_0 + H_1 \tag{9.13}$$

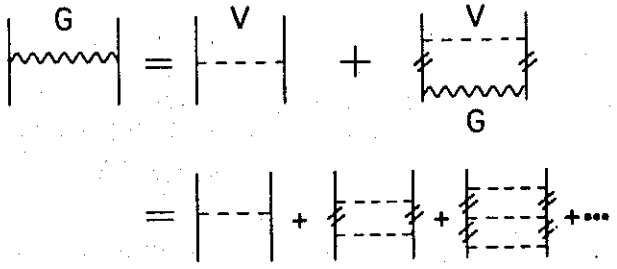

Figure 9.1: **Diagramatic representation of the Brueckner integral equation and G-matrix.** Intermediate nucleon lines are particle states, the double slash indicating the change of the propagator in the medium (as compared to the corresponding T-matrix equation).

with the unperturbed Hamiltonian

$$H_0 = \sum_{i=1}^{A}(T_i + U_i) \tag{9.14}$$

and the perturbation

$$H_1 = \sum_{i<j}^{A} V_{ij} - \sum_{i=1}^{A} U_i. \tag{9.15}$$

Here, U is a single-particle potential that is at our disposal. Since the total Hamiltonian does not involve U, the final result should in principal be independent of U. However, as the energy is calculated as an expansion in powers of H_1, the convergence of that expansion will depend on the choice of U. Thus, it is attempted to choose U such that the energy expansion converges rapidely enough to be useful for practical calculations.

Because of the strong repulsion between nucleons at short distances, the Golstone expansion is first rewritten in terms of the reaction matrix G which sums all possible rescattering of two interacting nucleons into unoccupied states. This infinite sum of ladder graphs, represented graphically in Fig. 9.1, is evaluated by solving the Brueckner (Bethe-Goldstone) integral equation

$$G(w) = V + V\frac{Q}{w - H_0}G(w) \tag{9.16}$$

Figure 9.2: **Lowest order (two-hole line) contributions** in the Brueckner-Goldstone expansion with (a) the direct and (b) the exchange diagram.

where the Pauli operator Q projects onto unoccupied states. Physically, defining the correlated wave function ψ in terms of the uncorrelated wave function ϕ

$$G\phi = V\psi, \tag{9.17}$$

implying

$$\psi = \phi + \frac{Q}{w - H_0} G\phi, \tag{9.18}$$

the ladder sum builds into ψ the short-range correlations induced by the repulsive core. In free space, G reduces to the familiar $\mathcal{T}$-matrix, and ψ simply corresponds to the exact scattering wave function defined by the potential V.

A perturbation expansion in powers of G is not convergent, but the cluster diagrams can be grouped instead according to the number of independent hole lines (see Fig. 9.2 for two-hole line and Fig. 9.3 for some three-hole line diagrams[2]). Formal arguments for the convergence of the hole-line expansion have been given by Brandow (Bra 67). Accordingly, a n-hole-line diagram should be proportional to κ^{n-1}, where κ measures the probability that there is an unoccupied state below the Fermi surface. This *wound integral* is defined by

$$\kappa = \rho \int |\phi - \psi|^2 d\tau. \tag{9.19}$$

In lowest order (two-hole line contribution, see Fig. 9.2), the energy per nucleon in nuclear matter at a density equivalent to a Fermi momentum k_F

[2]Wavy lines represent G-matrices, dashed lines with a cross U-interactions. Upward directed arrows denote occupied states above the Fermi sea (particles), and downward directed arrows denote unoccupied states in the Fermi sea (holes).

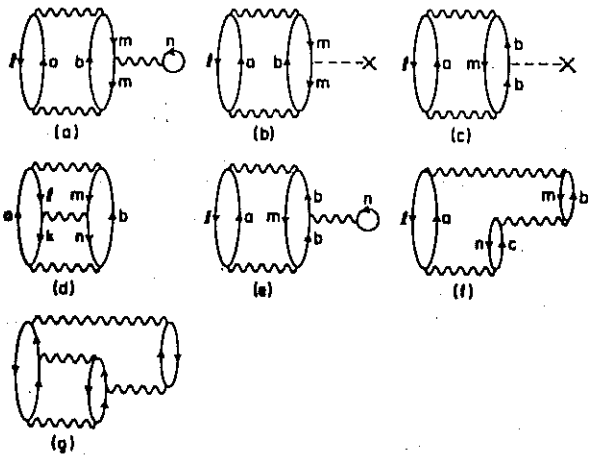

Figure 9.3: **Some three-hole line (three-body cluster) diagrams** that contribute to the energy of nuclear matter. Exchange diagrams are not shown.[Reproduced from (Day 78).]

is given by

$$\frac{\mathcal{E}}{A} = \frac{1}{A}\sum_{m\leq k_F}\langle m|T|m\rangle + \frac{1}{2A}\sum_{m,n\leq k_F}\langle mn|G(w)|mn-nm\rangle \tag{9.20}$$

with

$$w = e(m) + e(n) \tag{9.21}$$

and

$$e(m) = T(m) + U(m) \tag{9.22}$$

the single particle energy. The choice for U suggested by (BBP 63, Bra 66) is

$$U(m) = \begin{cases} \sum_{n\leq k_F}\langle mn|G(w)|mn-nm\rangle & m < k_F \\ 0 & m > k_F \end{cases} \tag{9.23}$$

which produces a gap at the Fermi surface (*standard choice*). Alternatively, a *continuous choice* for U can be made (JLM 75, 76) by defining

$$U(m) = Re\sum_{n\leq k_F}\langle mn|G(w)|mn-nm\rangle \tag{9.24}$$

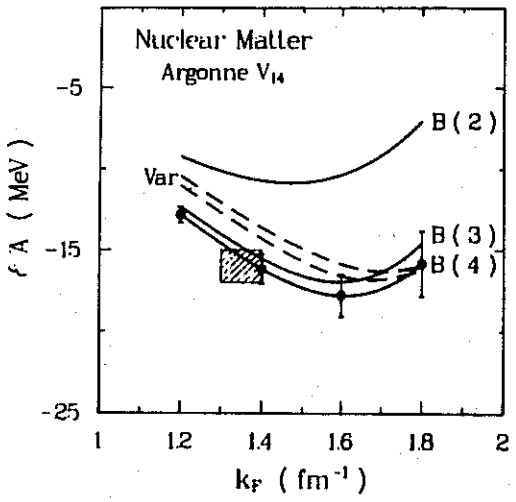

Figure 9.4: **Energy per nucleon, $\mathcal{E}/A$, in nuclear matter versus the Fermi momentum, k_F, using the Argonne V_{14} potential (WSA 84)** [from (DW 85)]. Full lines (B) represent results from Brueckner-Bethe theory, dashed lines (Var) show variational energies. The shaded box denotes the empirical saturation area.

for all states m below *and* above the Fermi surface. In both definitions the starting energy is chosen to be $w = e(m) + e(n)$ ('on-shell').

Further details about Brueckner theory can be found in several excellent books and review articles (Day 67, Bet 71, Spr 72, SF 74, Köh 75, JLM 76, Day 78, Neg 82). The formulae involved in Brueckner calculations in a more explicit form and methods for their numerical treatment are presented in (HT 70).

The convergence of Brueckner results in terms of the hole-line expansion is demonstrated Fig. 9.4 for the case of the Argonne V_{14} potential (WSA 84); the number of hole lines taken into account are given in parenthesis; the error bars show the estimated uncertainty. The energies as obtained by two variational methods are also shown; they are estimated to have about the same uncertainty as the Brueckner curve (all results are from (DW 85)). Within these uncertainties there appears to be agreement between the two many-body approaches. We will interpret this fact as a reason to

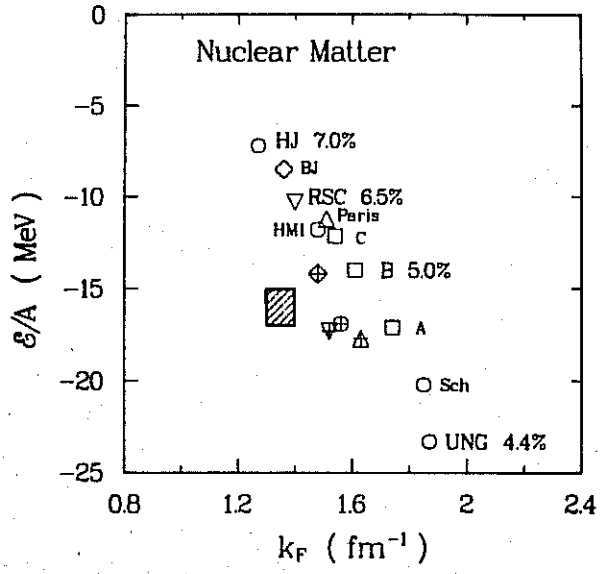

Figure 9.5: Nuclear matter saturation as predicted by a variety of NN potentials (see Table 9.1). Open symbols are saturation points obtained in the two-hole line approximation, symbols with a cross denote corresponding predictions with 3- and 4-hole lines included.

be confident in both theories at nuclear matter densities. As Brueckner theory is more versatile with regard to the types of potentials which can be applied, and as it also allows — in a straight-forward way — for extensions of conventional many-body theory (see Section 10), we will subsequently use Brueckner theory only.

9.4 Results and Problems

Let us now return to the physics questions we raised earlier. Are the nuclear matter predictions for all realistic potentials about the same and if not what are the variations? In other words: Does the fact that all realistic potentials fit the two-nucleon data accurately (and almost identically) imply that they predict identical results for the many-body system?

Table 9.1: **Nuclear matter saturation properties as predicted by various NN potentials.**

Potential	Reference	$P_D^{(d)}$ (%)	κ (%)	$\mathcal{E}/A$ (MeV)	k_F (fm^{-1})
HJ	HJ 62	7.0	21	−7.2	1.27
BJ	BJ 74	6.6	—	−8.5 [−14.2]	1.36 [1.48]
RSC	Rei 68	6.5	16	−10.3 [−17.3]	1.40 [1.52]
V_{14}	WSA 84	6.1	12 [19]	−10.8 [−17.8]	1.47 [1.62]
Paris	Lac+ 80	5.8	11	−11.2 [−17.7]	1.51 [1.63]
HM1	HM 75	5.8	11	−11.8 [−16.9]	1.48 [1.56]
Sch	Sch 72	4.9	8	−20.2	1.85
UNG	UNG 73	4.4	5	−23.3	1.87
C	Table A.1	5.6	8.1 (14.4)	−12.1 (−16.2)	1.54 (1.55)
B	Table A.1	5.0	6.6 (12.5)	−14.0 (−18.0)	1.61 (1.62)
A	Table A.1	4.4	5.4 (11.1)	−17.1 (−20.7)	1.74 (1.75)

Given are the saturation energy, $\mathcal{E}/A$, and Fermi momentum, k_F, as obtained in the two-hole line approximation using the standard (the continuous) choice for the single particle potential. Results including 3- and 4-hole line contributions are given in square brakets.
The woundintegral κ is given at $k_F = 1.35$ fm^{-1}.
$P_D^{(d)}$ is the predicted %-D-state of the deuteron.

The answer to these questions is displayed in Figs. 9.5 and 9.6 and Table 9.1. It can be summarized as follows: There are substantial differences in the predictions both for the saturation energy and density. Qualitatively, all potentials predict the right sign and order of magnitude; however, no potential predicts nuclear matter saturation correctly. In fact, the irony of the fate is that, in spite of rather large variations in the predictions, these variations take a course which is such that the empirical area is exactly avoided. It has become customary to denote this phenomenon by the Coester band (Coe+ 70). This Coester band structure of the results has also been confirmed by systematic calculations using phase-shift equivalent potentials (Coe+ 70, ACS 70, HT 71). From Fig. 9.5 it is also seen that the inclusion of 3- and 4-hole line contributions leads to a new 'improved'

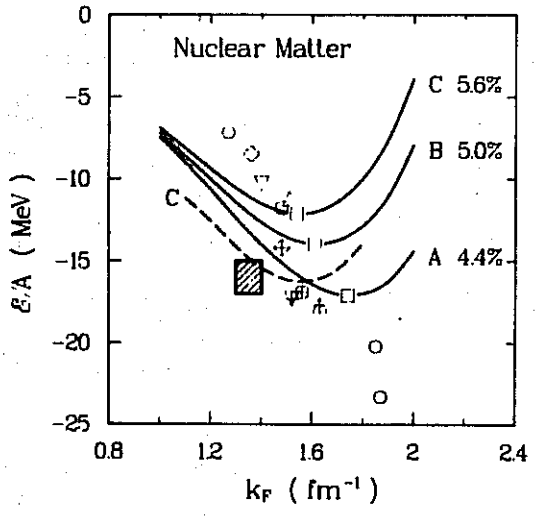

Figure 9.6: **Same as Fig. 9.5 with some saturation curves drawn explicitly.** For full lines the standard choice for the single particle potential is used; the dashed line is obtained with the continuous choice.

Coester band; however, the improvement is obviously insufficient to explain the empirical saturation point. In all calculations of Fig. 9.5 the standard choice for the single particle potential is used. However, what we just discussed is also true for calculations which employ the continuous choice (see dashed curve in Fig. 9.6 which is for Potential *C*). It is also seen from Fig. 9.6 that a lowest order calculation using the continuous choice (dashed curve) resembles much of the results from standard calculations which include 3- and 4-hole line contributions. This fact was first pointed out by the Liège-Strasbourg group (GL 79, Mah 79).

The variations in the nuclear matter predictions are generally attributed to off-shell differences in the potentials (see also the discussion in Section 5.5). This off-shell behaviour of a potential contributes slightly differently in nuclear matter as compared to free two-nucleon scattering. The reason for this is the Pauli projector and energy denominator in which the Brueckner

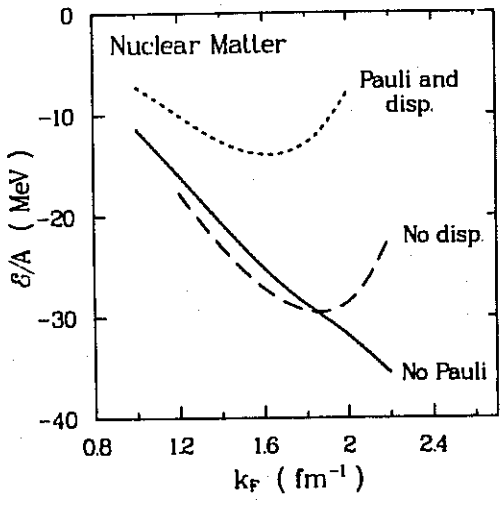

Figure 9.7: **The essential conventional saturation mechanisms in nuclear matter.** Explanations are given in the text.

equation, Eq. (9.16), differs from the corresponding equation for free two-nucleon scattering, namely the Lippmann-Schwinger equation:

$$\mathcal{T}(w_f) = V + V\frac{1}{w_f - T + i\epsilon}\mathcal{T}(w_f) \tag{9.25}$$

where w_f denotes the free (purely kinetic) energy of the two interacting nucleons (in contrast to w in Eq. (9.16) which includes a single particle potential U due to the nuclear medium). The bulk of the G-matrix (and analogously for the $\mathcal{T}$-matrix) is obtained in the approximation

$$G(w) \approx V_C + \mathcal{V}_T\frac{Q}{w - H_0}\mathcal{V}_T \tag{9.26}$$

where V_C denotes the central force and $\mathcal{V}_T = V_T S_{12}$ the tensor force component in the nuclear potential applied. If the tensor force is large, the attractive second order term is large. Note now, that all quantitative nuclear potentials are fit to essentially the same NN data which are related to the on-shell $\mathcal{T}$-matrix. Therefore, a potential with a weaker V_T (implying a small second order term in Eq. (9.25)) needs a stronger (attractive) central

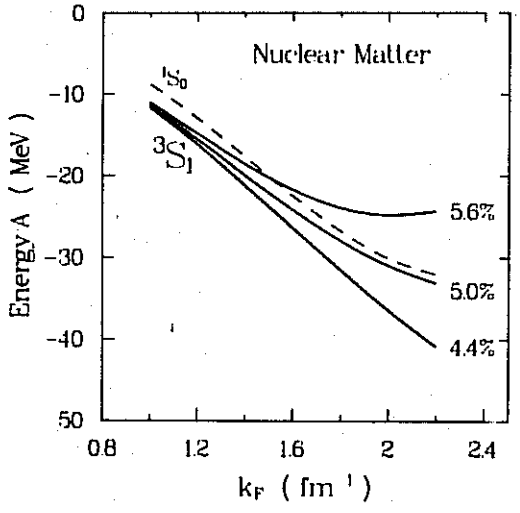

Figure 9.8: $^3S_1$ **contributions to the nuclear matter energy as a function of density** for three potentials which differ by the strength of their tensor force (the %-D-state is denoted). The $^1S_0$ contribution (dashed line) is given for comparison.

force to arrive at the same on-shell T-matrix values as a potential with a stronger tensor force. When we enter now nuclear matter, the Pauli projector (which is absent in the Lippmann-Schwinger equation) and a larger energy denominator (due to the single-particle potential in the many-body environment) reduces the second order term as compared to the free case. These two effects are commonly referred to as the *Pauli* and *dispersion (disp.)* effect (see Fig. 9.7 and Table 9.2). This reduction of the attractive second order term increases with density, where the Pauli effect is typically stronger density dependent than the dispersion effect (see Fig. 9.7). The larger the second order term (i. e. the larger V_T), the larger the absolute reduction.

This explains the outstanding role which the tensor force plays for *nuclear saturation*, and it also explains the differences in the predictions by potentials which differ in the strength of the tensor force. A simple measure for the strength of the tensor force is the prediction for the D-state admixture in the deuteron, as the transition from a $^3S_1$ to a $^3D_1$ state can only

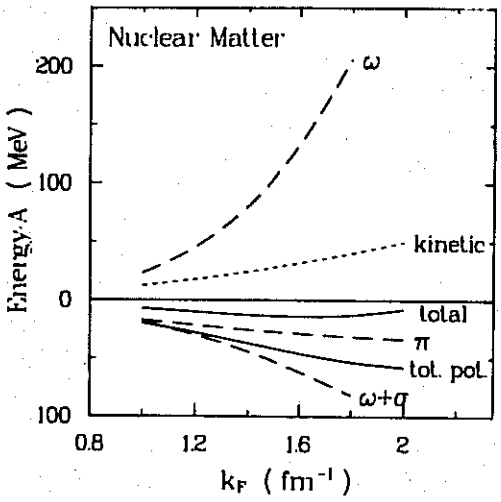

Figure 9.9: **Some contributions from single mesons to the nuclear matter potential energy.** Potential B is used.

proceed via a tensor force. Another measure is the wound integral κ for analogous reasons (see Table 9.1 and 9.3). Therefore, in Fig. 9.5 and 9.6 we give in some cases the %-D-state of the deuteron as predicted by that same potential. It is clearly seen that the binding energy predictions follow the strength of the tensor force, with larger tensor forces implying less binding energy. Deviations from this rule are essentially due to differences in the fit of the NN phase shifts; e. g. the fact that potential UNG and potential A differ by about 5 MeV in spite of identical deuteron D-state predictions can be traced to substantial differences in the fit of the P-waves, with potential A fitting modern phase shift analyses accurately. As the Potentials A, B, and C have (almost) identical fits, the accurate $P_D^{(d)}$ systematic of nuclear matter results is most reliably seen in Fig. 9.6 by comparing curves A, B, and C.

For the $^3S_1$ G-matrix element, for which the influence of the tensor force is the largest compared to all other states, we demonstrate this effect for three potentials differing by their deuteron %-D-state predictions in Fig. 9.8.

Apart from the tensor force there are also other causes for saturation.

The most trivial one is the Pauli principle giving rise to an average kinetic energy per nucleon in nuclear matter of $0.3k_F^2/M$ which increases with density (see Fig. 9.9). The sum of the P-wave contributions is repulsive (see Table 9.2) and increases with density. However, this is largely canceled by the attractive D-wave contributions. Therefore the main contribution to the binding energy comes from the S-waves including the effect of saturation (due to $^3S_1$). Finally, there is the repulsive core which should give saturation automatically. However, this comes into play only when the average distance between two nucleons is in the order of the core radius of about 0.5 fm. This distance is equivalent to about eight times nuclear matter density. Accordingly, this effect is small at the empirical saturation density. Essentially, the hard core prevents a collaps at very high densities (Bet 71).

The role of some single mesons in providing binding energy and saturation is demonstrated in Fig. 9.9. The total potential energy (tot. pot.), the average kinetic energy (kinetic), and the total energy (total) per nucleon are also shown. All meson-exchanges considered are iterated in the Brueckner equation. The π-curve plus kinetic energy saturates, whereas this is not true for $\omega + \sigma$. Again, the tensor force provided by the pion is the reason for this difference.

In summary, we have seen — in particular from Fig. 9.7 — that conventional many-body theory provides powerful saturation mechanisms. However, we have also seen (from Fig. 9.5) that this conventional saturation is insufficient to completely and accurately explain the empirical nuclear saturation. In fact, the standard problem of the conventionally treated nuclear many-body system is: if the binding energy of the system is about correct, the saturation density is too large, — and if the density is correct, the system is underbound.

When it was realized that there was a fundamental problem in obtaining a good fit to the ground state properties of nuclear matter and finite nuclei in a parameter-free approach, several suggestions were made to either overcome or simply elude the problem. Density-dependent effective forces was one of these suggestions, which revived an old idea advanced by Skyrme in the 1950's (Sky 59). In this approach one introduces a phenomenological density dependence into the two-body force in the medium. This was done either ad hoc (Skyrme forces, see e. g. Bar+ 82) or orientated towards a Brueckner G-matrix originally obtained from a free potential (Neg 70, CS

72, FN 73, MEH 74, MMF 75, MHN 75). These interactions were then adjusted to reproduce the empirical saturation properties of nuclear matter by introducing some suitable parameters. However, these effective forces and their adjustable parameters takes us away from the goal of calculating nuclear properties in a parameter-free theoretical sceme. We feel that a fundamental understanding of nuclear structure is only achieved when we are able to explain the properties of nuclear many-body systems in terms of the fundamental NN interaction as we know it from studies of free space NN scattering (Sections 4 and 5). In the following section we will further pursue this goal.

Table 9.2: **Partial wave contributions to the energy per nucleon in nuclear matter (in MeV) with and without conventional saturation effects.**

State	With Pauli and dispersion effects	No dispersion effect	No Pauli effect
$^1S_0$	−16.51	−17.51	−18.02
$^3P_0$	—3.53	−3.64	−3.59
$^1P_1$	4.55	4.29	4.35
$^3P_1$	10.27	9.69	9.91
$^3S_1$	−18.89	−25.52	−23.40
$^3D_1$	1.50	1.47	1.20
$^1D_2$	−2.36	−2.38	−2.37
$^3D_2$	−3.90	−4.03	−4.01
$^3P_2$	−7.14	−7.86	−7.42
$^3F_2$	−0.55	−0.55	−0.56
$^1F_3$	0.84	0.83	0.83
$^3F_3$	1.54	1.53	1.53
$^3D_3$	0.27	0.13	0.23
$^3G_3$	0.21	0.20	0.20
$J \geq 4$	−1.08	−1.10	−1.09
Total potential energy	−34.78	−44.44	−42.22
Kinetic energy	22.67	22.67	22.67
Total energy	−12.11	−21.77	−19.54

For Potential B at $k_F = 1.35$ fm^{-1} in the two-hole line approximation using the standard choice for the single particle potential. (This is also used in Fig. 9.7.)

Table 9.3: **Contributions to the wound integral in nuclear matter (in %) for three different potentials** (defined in Table A.1)

	A	*B*	*C*
$^1S_0$	1.0 (1.2)	1.0 (1.2)	1.0 (1.3)
$^3S_1$	0.5 (1.5)	0.6 (1.3)	0.8 (1.4)
$^3S_1 - {}^3D_1$	2.2 (4.9)	3.3 (6.5)	4.7 (8.4)
Total	5.4 (11.1)	6.6 (12.5)	8.1 (14.4)

At $k_F = 1.35$ fm^{-1} using the standard (the continuous) choice for the single particle potential.

Section 10

Nuclear Matter II — Beyond Convention

Profound skepticism is favorable to conventions,
because it doubts that the criticism of conventions
is any truer than they are.
— G. SANTAYANA,
On My Friendly Critics

The results of the previous section have shown that the conventional model for the nucleus is probably insufficient to quantitatively describe the nuclear ground state. Therefore, it seems necessary to go beyond the conventional scheme. This is the task we will try to undertake in this section — after giving first an overview (Subsection 10.1) of possible extensions proposed in the literature.

10.1 Possible Extensions

We have seen that it is not really possible to explain the saturation properties of nuclear matter quantitatively in the framework of the conventional model, i. e. assuming a non-relativistic Hamiltonian with a two-body potential obtained from the study of NN scattering in free space. To predict simultaneously the correct saturation density and binding energy seems an impossible task. The fatal trend is that the saturation density is always substantially too high for reasonable energies. As nuclear matter — an infinitely extended nucleus without Coulomb interactions — does not exist in

reality, one may think of attributing the failure to the hypothetical nature of the system as such. Calculations in finite nuclei, however, have shown that in those realistic systems the exactly analogous problems appear: either the predicted radius is reasonable, but the binding energy substantially underestimated, or *vice versa* (the second case corresponding to an overestimated saturation density); see (KLZ 78) and Section 11. The conclusion that the conventional model might be – in part – insufficient is suggested by these facts. Realizing the outstanding simplicity of the conventional model, it seems obvious to suspect that it is just too "narrow" — or with other words, that suppressed degrees of freedom may play a non-negligible role. So, the time has come to think about appropriate and reasonable extensions of the underlying assumptions.

To get some structure into the upcoming considerations, we list in Table 10.1 four items relevant to the nuclear many-body problem. The assumptions made in the conventional approach are given in column two. Column three states some obvious ideas leading beyond convention. Of course, there is no claim of completeness concerning that table. Also, the distinction between the various points is not clear-cut, since the extension of one item often has consequences for others. We will discuss now some of the points.

In recent years the relevance of the *quark-structure of hadrons* for nuclear physics has become a major issue. Attempts have been made to take the composite structure of nucleons explicitly into account in the nucleus. In some work this is done by considering six-quark bags for the short range part of the NN interaction (HKM 83, CM 87). In other studies the nucleons dissolve completely in the nucleus — instead of an A-nucleon nucleus a confined $3A$-quark system is considered (FM 77, Pet 84); however, there are problems in getting a bound nucleus in this way. In a less radical approach, nucleons dissolve only partly (Gol+ 87). Some of these moderate considerations yield remarkable effects (CM 87, Gol+ 87). However, due to the complexity of the calculations and the approximations involved, the results presently available are by no means of a final nature. Certainly more work has to be done and will be done in the near future.

More systematic investigations have been pursued in the traditional framework of hadronic physics. In Sections 4–7 we have seen how well the nuclear force can be understood in terms of meson-exchanges. Nevertheless the usual procedure in nuclear physics is to "freeze" these mesons out as soon as they have finished their job of creating the nuclear force.

Table 10.1: **Basic assumptions underlying the nuclear many-body problem**

Item	*Simplest assumption*	*Possible extension(s)*
Degrees of freedom	Nucleons only	Mesons, Isobars, Quarks and gluons
Hadron structure	Point structure	(Quark) sub-structure
Interaction(s)	(Static, instantaneous) two-body potential	Non-static interactions, Many-body forces
Dynamical equation	Non-relativistic Schrödinger equation	Relativistic Dirac equation

Obviously, this is inconsistent. Therefore, in a first step beyond convention one should consider *meson degrees of freedom* explicitly in the nuclear many-body system. This point gets strong support from studies of electron scattering in which the role of these additional degrees of freedom in the nucleus have been clearly established. The intrinsic magnetic moments of proton and neutron differ substantially from the Dirac value for structureless particles. As discussed in Section 4.2, the emission and absorption of vector mesons by an isolated nucleon makes the major contribution to the anomalous magnetic moment. In the many-nucleon system, the exchange of charged mesons between nucleons gives rise to additional contributions to the nuclear electromagnetic current. One of the significant achievements of nuclear physics in the past 20 years has been the unambigous isolation and identification of these exchange-current contributions to the electro-

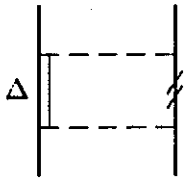

Figure 10.1: **Two-meson exchange diagram involving one Δ isobar.** The double slash on the intermediate nucleon line indicates the change of that propagator in the medium.

magnetic properties — in particular, of light nuclei (RW 79, SHS 83, HGB 83, LG 86, FP 87).

Furthermore, we have seen in Section 5 and 7 that the excited states of the nucleon play an important role in a genuine and realistic meson-exchange model for the nuclear force. The lowest-lying pion-nucleon resonance, the Δ(1232) isobar, is essential for NN scattering at low and intermediate energies. It provides a large part of the intermediate range attraction and of the inelasticity above pion-production threshold. Again, being aware of how crucial this degree of freedom is for the two-body interaction, we should not "freeze it out" in the many-body problem. The Δ *degree of freedom* leads to serious consequences in the nuclear many-body system. Due to the presence of the medium, the propagation of the Δ and the nucleon is altered in nuclear matter, Fig. 10.1. This gives rise to Pauli and dispersion effects in addition to those predicted by ordinary Brueckner theory with static forces. These effects are both repulsive and contribute to saturation. Following a suggestion by G. E. Brown, the influence of the Δ on nuclear saturation was first studied by Green and Schucan (GS 72) in perturbation theory. More consistent and systematic studies of these effects were done in the course of the 1970's by several groups (GH 74, GN 75, DC 76, HM 77). This early work has been reviewed by A. M. Green (Gre 79). As mentioned, the items in Table 10.1 are not all independent — the Δ degree of freedom can also be understood as taking, to a certain extend, the quark structure of the baryon into account, by considering a quark-spin flip.

The idea of nuclear *many-body forces* is almost as old as the meson hypothesis for the two-nucleon force (PH 39, Ros 48). This is not surprising: If mesons mediate the force between two nucleons, then, in a many-nucleon

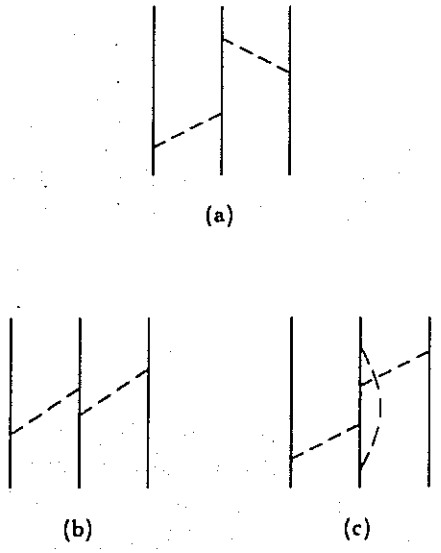

Figure 10.2: **Three-nucleon diagrams, (a) is a three-nucleon correlation, (b) and (c) are three-nucleon force contributions.**

environment, they must give rise to many-body force contributions in various ways (see e. g. Fig. 10.2b and c). Nevertheless only in recent years the concept of many-body forces has drawn substantial interest, since it has become apparent that two-body forces, used in a non-relativistic framework, do not quantitatively describe the properties of nuclei (Section 9). This failure is frequently interpreted as an indication for the need of many-body forces.

Generally speaking, a n-body force is an irreducible function of the coordinates or momenta of n particles, e. g. an irreducible Feynman diagram which cannot be generated by merely iterating two-body interactions. To give some examples: the diagram depicted in Fig. 10.2a does not represent a three-nucleon force contribution; this diagram can be generated by simply iterating two-nucleon interactions; it is a three-nucleon *correlation*. In contrast, the diagrams b and c of Fig. 10.2 represent three-nucleon *forces*.

When discussing three- or many-body forces, caution is in place: the

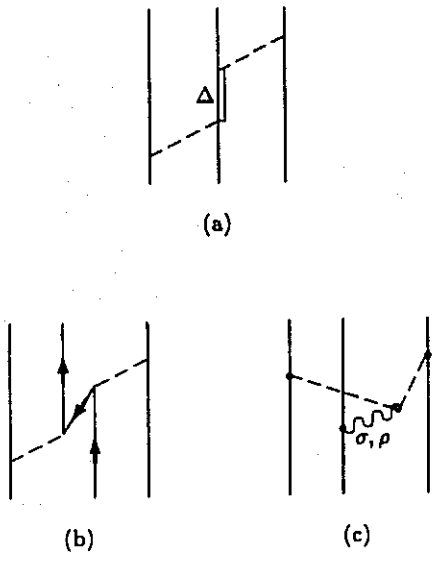

Figure 10.3: **Various three-nucleon force diagrams.** Full lines (nucleons) are upward directed if not noted otherwise.

distinction between many-body *forces* and many-body *correlations* is neither unique nor fundamental. It depends on the model space applied or, in other words, on the degrees of freedom treated explicitly. For example, the diagram Fig. 10.3a is a genuine three-body force in a model space which consists of nucleon states only. In an extended Hilbert space which includes Δ isobar states, Fig. 10.3a represents just a three-particle correlation. A similar consideration applies to diagram b of Fig. 10.3: In a genuin relativistic theory (three-body Bethe-Salpeter equation) this diagram does not represent a three-body force. Thus, most many-body forces are artificially created by freezing out degrees of freedom. In this respect they are merely artefacts of the particular theoretical framework applied. Because of this model dependence of the terminology, it is useful to introduce an operating definition for *n-nucleon forces* which we will take to be the following: forces that depend in an irreducible way on the coordinates or momenta of *n nucleons* when only *nucleon* degrees of freedom are taken into account

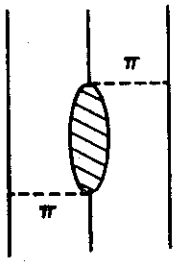

Figure 10.4: **2π-exchange three-nucleon force.** The shaded oval represents the πN amplitude with the forward propagating Born term subtracted.

(FGP 84).

The classical example of a three-body force is the electromagnetic force of Primakoff and Holstein (PH 39). It arises from the creation of particle-antiparticle pairs (similar to Fig. 10.3b) which in a non-relativistic Schroedinger equation is represented by a three-body potential term. Applying the meson theory of the nuclear force, which — at that time — had just been suggested by Yukawa in analogy to the electromagnetic interaction, Primakoff and Holstein proposed the first three-nucleon force in that same paper.

The three-body force which received a lot of attention during the past 20 years is the two-pion exchange diagram shown in Fig. 10.4. The essential ingredient is apparently the πN scattering amplitude. The crucial question is how to model this amplitude in the energy region of interest for the three-body diagram. There are essentially two approaches in the literature. One method uses the observed on-mass-shell properties as physical input and extrapolates the amplitude off-mass-shell by using current algebra and PCAC (BGG 68, CSB 75, MR 79, Coo+ 79, CG 81). Alternatively one can develop a field-theoretic model. Some of the important diagrams of such a

model are displayed in Fig. 10.3;[1] additional diagrams are b and c of Fig. 10.2. These diagrams are to be viewed in analogy to those building up the πN amplitude in a field-theoretic model for πN scattering (Section 8.1). It is perhaps instructive to note that the same dichotomy exists for the 2π-exchange contribution to the NN potential (Section 5.1). The Stony Brook (JRV 75, BJ 76) and Paris (Vin 79, Lac+ 80) group adopted the dispersion theoretic approach in which as much πN and $\pi\pi$ data are used as possible, together with theoretical constrains on the πN amplitude. Alternatively, the Bonn group built a field-theoretic model for the NN interaction which takes isobars explicitly into account (see MHE 87 and Section 5).

There has been a great deal of discussion concerning which of the two approaches is to be preferred. Each has advantages and disadvantages. Whereas the former (Fig. 10.4) suggests completeness of the amplitude, it cannot take into account the medium effects on this diagram and on the corresponding two-body force diagrams. Furthermore, the uncertainty of what to choose for the πNN cutoff parameter in Fig. 10.4 can affect the size of the resulting contribution to the energy per nucleon by a factor 2 to 3. On the other hand, the present field-theoretic models take only the diagram Fig. 10.3a into account which depicts an intermediate Δ isobar. However, in this case there is no uncertainty with regard to the parameters, as they are taken from the corresponding NN model which is constrained by the NN data. Moreover, it has been shown that the contribution from this three-body diagram (Fig. 10.3a) and the medium effects on the corresponding two-body diagram (Fig. 10.1) cancel to a large extent (see Subsection 10.3 and 10.4). Therefore, the consistent and simultaneous treatment of corresponding two- and three-body force contributions, which is the more fundamental approach and which the field-theoretic model allows for, results in a net contribution that is small compared to just one isolated three-body force contribution. Furthermore, it is crucial for the diagrams of Figs. 10.4 and 10.3a to include also the exchange of a ρ meson (ECM 85); this is particularly straightforward in the field-theoretic approach (DFM 82, Müt 84).

The three-body force diagrams discussed so far, are only a small subset of all possibilities. For others that have been recently discussed in the literature, we refer the interested reader to the work of Keister and Wiringa

[1] A diagram of the type Fig. 10.3a was first considered by Fujita and Miyazawa in 1957 (FM 57).

(KW 86) and the Stony Brook group (BB 75, Nym 79, JRK 83, Ain+ 87). These latter studies are also closely related to relativistic effects in the nuclear many-body problem which we will discuss in Subsection 10.5.

This brief survey of some possible extensions of the conventional model may have given us some idea of the complexity of the problem. It is particularly important to stress that the various contributions and effects are not all independent from each other. To avoid double counting or a distorted representation of just one of the effects, it is essential to proceed consistently and carefully.

10.2 Meson Degrees of Freedom

Ever since the meson hypothesis was formulated, it was (at least in principal) clear that the full nuclear many-body problem should include nucleons *and* mesons. Nevertheless, traditionally only nucleons have been considered, these interacting via a static two-body potential. Even in cases where the two-nucleon force was derived from meson theory, the mesons were usually "forgotten" as soon as the nuclear force was constructed. "Meson theory" was merely used to provide a suitable ansatz for the two-body potential with a convenient parametrization in terms of mass and coupling parameters. Thus, the dynamical presence of the mesons was ignored. Obviously, from a more fundamental point of view, this is not satisfactory.

Apart from some early studies of which we mention the work by Schiff (Sch 51) and by Duerr (Due 56), historically, the possible role of mesons in the nuclear many-body problem was considered more seriously by a larger part of the nuclear physics community when two *empirical* events/developments apparently called for it. The discovery of pulsars (neutron stars) in the late 1960's suggested the existence of neutron matter with a high density — about ten times the one of saturated nuclear matter. At about that same time, progress in the heavy ion physics experimental program stimulated speculations over higher density nuclear matter giving rise to new phenomena like pion condensation. It is questionable wether in these systems of high density — implying higher average momenta — the principal assumptions the usual approach is based upon are still valid. However, even for nuclear matter at normal densities it is legitimate to ask whether mesonic degrees of freedom could cause subtle, but remarkable effects; af-

ter all, the "failure" of conventional many-body theory consists only in a rather small deviation from the empirical properties.

Motivated by these and similar thoughts, during the past two decades, several groups have attempted to develop a many-body theory for nucleons and mesons. We mentione here the work by Dover and Lemmer (DL 68, DL 69), Brown, Puff and Wilets (BPW 70, Wil 79), Bolsterli (Bol 71), Danos and Gillet (Dan 71, DG 79), Walecka and Chin (Wal 74, Chi 77), and Schütte (Sch 74). As it is beyond the scope of this article to discuss all these comprehensive studies, we refer the interest reader to the excellent review literature cited. Substantial applied work has been done in the framework suggested by Schütte providing a rich choice of quantitative results. Therefore we will discuss his ideas in more detail.

The approach by Schütte (Sch 74) is field-theoretic in nature, thus treating baryons and mesons *a priori* on an equal footing. However, a principal problem of every field-theoretic many-body theory is how to take into account the effects of the many-body environment on the particles and their interactions (e. g. the single-particle energies in the medium, propagation in the medium, etc.). This is difficult to do in a covariant way. Therefore, Schütte suggested to use time-ordered ("old-fashioned") perturbation theory[2], which is similar to the usual perturbation theory of ordinary quantum mechanics. Thus, methods familiar from non-relativistic many-body theories can be applied.

Now, we will outline the principals for a many-body theory in which the Hilbert space consists of baryon and meson states (for more details see MHE 87, Appendices A–C). The starting point is a field-theoretic Hamiltonian for mesons and baryons which is represented in the language of second quantization[3]:

$$h = t + W \tag{10.1}$$

where

$$t = t^{(B)} + t^{(m)} \tag{10.2}$$

[2]See e. g. the field theory text by Schweber (Sch 61), Chapters 11 and 13.

[3]Our notation deviates here substantially from the usual, in which one would write $H = H_0 + H_I$ instead of Eq. (10.1). However, to avoid confusion with the notation introduced in Section 9 for the non-relativistic theory, we will use a small letter for the field-theoretic Hamiltonian.

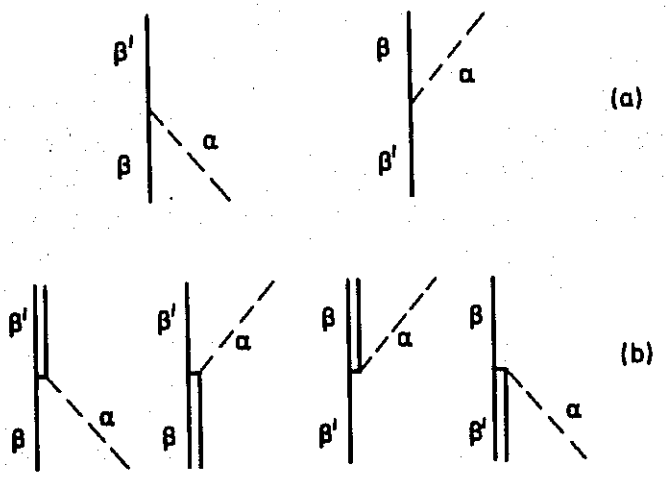

Figure 10.5: **Meson-nucleon-nucleon (a), and meson-nucleon-isobar (b) vertices.** Single lines denote nucleons, double lines isobars, and dashed lines mesons.

represents the free, unperturbed Hamiltonian for baryons

$$t^{(B)} = t^{(N)} + t^{(\Delta)} + \ldots = \sum_{\beta} E_\beta b^\dagger_\beta b_\beta \tag{10.3}$$

and mesons

$$t^{(m)} = t^{(\pi)} + t^{(\rho)} + \ldots = \sum_{\alpha} \omega_\alpha a^\dagger_\alpha a_\alpha. \tag{10.4}$$

The $b^\dagger_\beta, b_\beta$ and $a^\dagger_\alpha, a_\alpha$ are the creation, annihilation operators for baryons (fermions) and mesons (bosons) satisfying the usual commutation relations. The summation index β stands for all baryons (nucleons, isobars etc.) taken into account and all the quantum numbers characterizing their states (e. g. spin, isospin, momentum, parity). The index α has the corresponding meaning for mesons. E_β and ω_α are the relativistic free energies for baryons and mesons, respectively. The interaction part of the Hamiltonian is denoted by W. It describes the interaction between mesons and baryons

$$W = W^{(NN\pi)} + W^{(NN\rho)} + \ldots + W^{(N\Delta\pi)} + \ldots = \sum_{\beta\beta'\alpha} W_{\beta\beta'\alpha} b^\dagger_{\beta'} b_\beta a_\alpha + h.c. \tag{10.5}$$

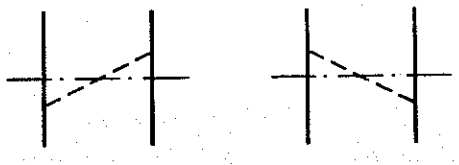

Figure 10.6: **One-boson-exchange diagrams in time-ordered perturbation theory.** The horizontal, dash-dot lines indicate the states involved in the meson propagators which — in a many-body environment — are affected by the medium.

with *h.c.* standing for the hermitian conjugate. These interactions are displayed graphically in Fig. 10.5. They are related to the interaction Lagrangians $\mathcal{L}_I$ (see Appendix A and B for a summary) in the usual way:

$$W^{(I)} = -\int d^3x [\mathcal{L}_I - \frac{\partial \mathcal{L}_I}{\partial \dot{\varphi}^{(\alpha)}_{(\mu)}} \dot{\varphi}^{(\alpha)}_{(\mu)}]_{x_0=0} \tag{10.6}$$

where $\varphi^{(\alpha)}_{(\mu)}$ is a meson field and the dot stands for the time derivative (see MHE 87 for more explicit expressions).

Applying time-ordered perturbation, the lowest order contribution to the two-nucleon system caused by the Hamiltonian Eq. (10.1) is of second order

$$V(z) = W \frac{1}{z - t + i\epsilon} W \tag{10.7}$$

(z denotes the relativistic free energy of the two interacting nucleons in the c.m. frame, see Eq. (10.26) below). This corresponds to the diagrams shown in Fig. 10.6, and can be understood as an one-boson-exchange "quasi-potential". The OBE diagrams up to infinite orders, the so-called ladder diagrams, can be summed up most conveniently by an equation of the Lippmann-Schwinger type which employes this quasi-potential

$$T(z) = V(z) + V(z) \frac{1}{z - t + i\epsilon} T(z) \tag{10.8}$$

where T denotes the T-matrix, which is related to the S-matrix by

$$\langle\beta_1'\beta_2'|S|\beta_1\beta_2\rangle = \langle\beta_1'\beta_2'|\beta_1\beta_2\rangle - 2\pi i\delta(E_{\beta_1'} + E_{\beta_2'} - E_{\beta_1} - E_{\beta_2})\langle\beta_1'\beta_2'|T|\beta_1\beta_2\rangle \tag{10.9}$$

with the states defined as in Eq. (10.22) below.

These are the basic ingredients for the scattering of two free nucleons, in a simple model which does not include other baryons and takes into account only iterative OBE diagrams. More elaborate models and the role of other baryons will be discussed in Section 10.3.

Let us now go back to the nuclear many-body problem. It is our concern to proceed consistently in the field-theoretic framework for mesons and baryons, which we have just set up and applied to free NN scattering. To take the many-body environment adequately into account, we rewrite our Hamiltonian Eq. (10.1), in analogy to Eq. (9.13), as follows:

$$h = h_0 + h_1 \tag{10.10}$$

with the unperturbed Hamiltonian

$$h_0 = t + U \tag{10.11}$$

and

$$h_1 = W - U \tag{10.12}$$

the perturbation. More explicitly we have

$$h_0 = h_0^{(B)} + h_0^{(m)} \tag{10.13}$$

where

$$h_0^{(B)} = t^{(B)} + U^{(B)} = \sum_\beta \epsilon_\beta\, b_\beta^\dagger b_\beta \tag{10.14}$$

is the unperturbed Hamiltonian for baryons and

$$h_0^{(m)} = t^{(m)} + U^{(m)} = \sum_\alpha \tilde{\omega}_\alpha\, a_\alpha^\dagger a_\alpha \tag{10.15}$$

the corresponding one for mesons. Here, we will assume $U^{(m)} = 0$, i. e. $h_0^{(m)} = t^{(m)}$ and $\tilde{\omega}_\alpha = \omega_\alpha$; other choices have been considered in (MH 85). The single baryon potential in the nuclear medium is

$$U^{(B)} = \sum_\beta U_\beta\, b_\beta^\dagger b_\beta, \tag{10.16}$$

implying

$$\epsilon_\beta = E_\beta + U_\beta. \tag{10.17}$$

The explicit choice for this single particle potential is given below.

A second order term in the perturbation is

$$\bar{V}(\bar{z}) = W \frac{1}{\bar{z} - h_0} W \tag{10.18}$$

which describes a one-meson-exchange in the nuclear medium; it is to be compared with the free exchange Eq. (10.7) (see also Fig. 10.6)). In analogy to conventional Brueckner theory (Sect. 9.3), we have the following Bethe-Goldstone equation in the medium

$$\bar{G}(\bar{z}) = \bar{V}(\bar{z}) + \bar{V}(\bar{z}) \frac{Q}{\bar{z} - h_0} \bar{G}(\bar{z}) \tag{10.19}$$

with Q the usual Pauli operator which projects onto unoccupied two-nucleon states. In lowest order, the energy is given by

$$\frac{\mathcal{E}}{A} = \frac{1}{A} \sum_{\beta \le k_F} E_\beta + \frac{1}{2A} \sum_{\beta_1, \beta_2 \le k_F} \langle \beta_1 \beta_2 | \bar{G}(\bar{z}) | \beta_1 \beta_2 - \beta_2 \beta_1 \rangle - M \tag{10.20}$$

with

$$\bar{z} = \epsilon_{\beta_1} + \epsilon_{\beta_2}, \tag{10.21}$$

M the mass of the physical nucleon, and

$$|\beta_1 \beta_2\rangle = b^\dagger_{\beta_1} b^\dagger_{\beta_2} |0\rangle \tag{10.22}$$

where $|0\rangle$ denotes the vacuum.

Again, in analogy to conventional Brueckner theory, we use for the single particle potential the definition

$$U_\beta = Re \sum_{\beta' \le k_F} \langle \beta \beta' | \bar{G}(\epsilon_\beta + \epsilon_{\beta'}) | \beta \beta' - \beta' \beta \rangle. \tag{10.23}$$

Applying this definition for nucleon states below and above the Fermi surface is denoted by the *continuous choice*. Alternatively, Eq. (10.23) may be employed for states below the Fermi surface only, using a vanishing potential above; this choice is equivalent to the *standard choice*. To a good approximation, the single particle energy at one density can be parametrized in terms of two constants, $\tilde{M}$ and U_0, by using the ansatz

$$\epsilon_\beta = E_\beta + U_\beta = (\tilde{M}^2 + \mathbf{p}_\beta^2)^{\frac{1}{2}} - \tilde{M} + M + U_0 \tag{10.24}$$

with $\mathbf{q}_\beta$ the particle 3-momentum.

Equations (10.18) to (10.24) represent the calculational scheme for the energy in nuclear matter in lowest order in G when the dynamical presence of mesons is taken into account. How does this compare with the usual scheme which applies static two-body forces (Section 9)? The main difference is that in the approach just presented, the meson propagators change in a characteristic way in the many-body environment as compared to free two-nucleon scattering. This can be clearly seen by comparing Eq. (10.7) with Eq. (10.18): the free propagator $[z-t]^{-1}$ is replaced by $[\bar{z}-h_0]^{-1}$ in the medium. We can evaluate the size of this effect on the energy in nuclear matter by defining the following G-matrix

$$G(\bar{z}) = V(z) + V(z)\frac{Q}{\bar{z}-h_0}G(\bar{z}) \tag{10.25}$$

with

$$z = E_{\beta_1} + E_{\beta_2} \tag{10.26}$$

and $\bar{z}$ as defined before in Eq. (10.21), and replacing $\bar{G}$ in Eq. (10.20) by G. The difference in these two types of calculations gives an idea of the effect of the medium on meson propagation.

Results for the two types of calculations are shown in Fig. 10.7.[4] It is seen that the medium affects the meson propagators such that the binding energy is slightly reduced (about 2 MeV at nuclear matter density). This quenching of the attraction can be understood by comparing the contributions to the energy from second order in the quasi-potential. (Note that the Born term in the 'Brueckner equation' (10.19) is not altered in the medium.) We will consider the relevant propagators only, ignoring vertices: Without the medium effects we have

$$\sum_{\beta_1',\beta_2'\geq k_F} \left| \frac{1}{E_{\beta_1} - E_{\beta_1'} - \omega_\alpha} \right|^2 /(\bar{z} - \epsilon_{\beta_1'} - \epsilon_{\beta_2'}). \tag{10.27}$$

With medium effects this changes to

$$\sum_{\beta_1',\beta_2'\geq k_F} \left| \frac{1}{\epsilon_{\beta_1} - \epsilon_{\beta_1'} - \omega_\alpha} \right|^2 /(\bar{z} - \epsilon_{\beta_1'} - \epsilon_{\beta_2'}). \tag{10.28}$$

[4] OBEPT defined in (MHE 87, Appendix B, Table 8) is applied using the standard choice for the single-particle potential.

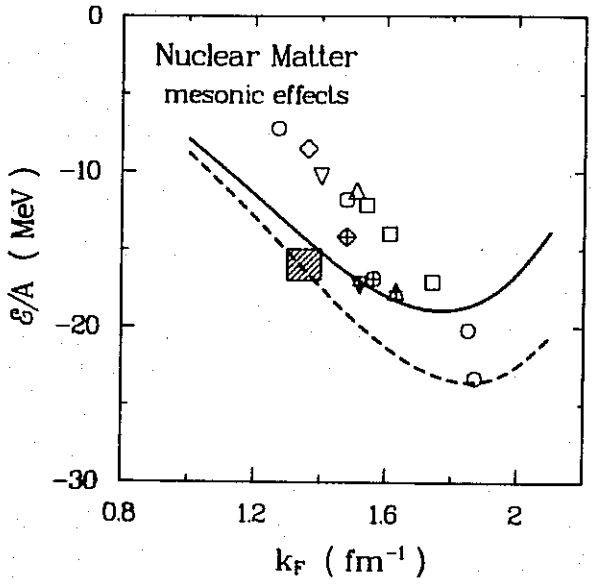

Figure 10.7: **Mesonic effects in nuclear matter for the case of an one-boson-exchange potential.** The full curve includes the medium effects on meson propagation, whereas in the dashed curve these effects are suppressed.

Due to the single particle potential, the energy-denominator in the medium, $\Delta\epsilon = |\epsilon_{\beta_1} - \epsilon_{\beta_1'} - \omega_\alpha|$, is larger than in the vacuum, $\Delta E = |E_{\beta_1} - E_{\beta_1'} - \omega_\alpha|$. This reduces the (attractive) second order contribution in the many-body environment (Kot+ 75, KMS 76). This effect is analogous to the dispersion effect in ordinary Brueckner theory (Sect. 9.4); it is, however, much smaller. Relatively speaking, it is largest for the $^3S_1$ contribution, as it affects the pion propagator the most (since of all mesons, the pion has the smallest mass), which in turn weakens the tensor force. The density-dependence of this mesonic effect is such that the saturation point moves along the Coester band and not off it (Fig. 10.7).

10.3 Isobar Degrees of Freedom

In the previous subsection we established the basic formalism for taking into account degrees of freedom other than the nucleon. As a first example we chose the simple OBE model and considered meson degrees of freedom

explicitly. We saw how the nuclear force can be influenced when inserted into a nuclear many-body surrounding: the meson propagator is altered. The quantitative effect we found in the simple case of OBEP was quite moderate. However, this cannot be the full story. The most important feature of the nuclear force for the nuclear groundstate properties is its intermediate range attraction. Within the OBE model this is described by a σ boson with a mass of about 500–700 MeV. We know that this particle does not exist in nature. It is merely introduced as a convenient parametrization for the rather complex processes involved in the exchange of two pions.

However, here we are concerned with subtleties like the role of subnucleonic degrees of freedom in the many-body problem. For such distinguished effects a model of appropriate sophistication is needed, otherwise there would be no credibility to the results. Therefore, we will now include explicit two-meson-exchanges in our consideration and avoid fictitious bosons. In Section 5 we discussed a model for the NN interaction which contains all relevant two-meson-exchange diagrams. These diagrams (of the kernel) can be classified according to the baryons which occur in the intermediate states; namely, either nucleons only, or one nucleon and one isobar, or isobars only. For the case of two nucleons in intermediate states, the two-meson-exchange diagrams have to be irreducible (i. e. of the stretched or crossed box type); otherwise there would be double counting, as the reducible (iterative) diagrams are generated by the Lippmann-Schwinger, respectively Brueckner equation. As shown in Section 5, the stretched and crossed box diagrams with NN intermediate states are in general not large; furthermore, there are characteristic cancelations between these diagrams. Consequently the net contribution is rather small and so are the medium effects coming from these diagrams.

More important are the diagrams which involve isobars. They contribute substantially to the nuclear force, particularly in the intermediate range. Accordingly, their medium effects may turn out to be large. Therefore, we shall present in more detail the structure of diagrams involving isobars. This will clearly reveal the various ways in which the contribution from these diagrams may be modified in the nuclear medium.

The lowest order in which isobars can contribute to the NN interaction is the fourth order in the interaction Hamiltonian W (which corresponds to a two-meson exchange). The general structure of the fourth order per-

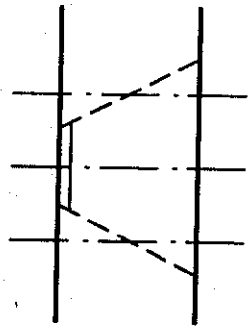

Figure 10.8: **Two-meson exchange diagram with one intermediate Δ state.** The horizontal, dash-dot lines indicate the states involved in the propagators which — in nuclear matter — are affected by the many-body medium.

turbation is for the case of free scattering

$$V^{(4)}(z) = W\frac{1}{z-t+i\epsilon}W\frac{1}{z-t+i\epsilon}W\frac{1}{z-t+i\epsilon}W \qquad (10.29)$$

with W as given in Eq. (10.5). The irreducible part of these diagrams contributes to the "kernel" $V(z)$ of the scattering equation (10.8). When inserted into the many-body problem the contribution $V^{(4)}(z)$ is altered in a characteristic way; namely it is replaced by

$$\bar{V}^{(4)}(\bar{z}) = W\frac{Q}{\bar{z}-h_0}W\frac{Q}{\bar{z}-h_0}W\frac{Q}{\bar{z}-h_0}W \qquad (10.30)$$

where the Pauli operator Q projects nucleons onto unoccupied nucleon states.

One can distiguish between two ways in which the medium exercises influence:

- The Pauli projector Q cuts out the lower part of the nucleon spectrum in intermediate states; this leads to the so-called *Pauli effect.*
- The propagator $[z-t+i\epsilon]^{-1}$ is replaced by $[\bar{z}-h_0]^{-1}$; the effect caused by this replacement has become known as *dispersion (disp.) effect.*

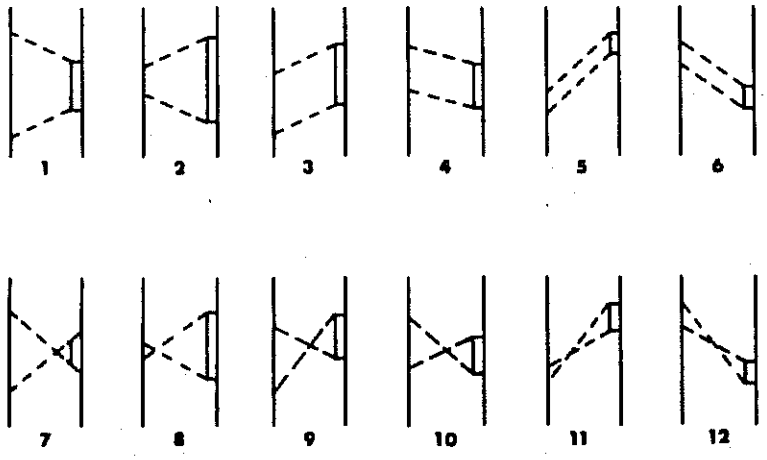

Figure 10.9: **Time-ordered diagrams with $N\Delta$ intermediate states.**

Both effects reduce the absolute size of the diagram. Thus, for an attractive diagram there is a net repulsive effect, and *vice versa*.

The dispersion effect occurs in both the meson and the baryon propagators. This is demonstrated graphically for the case of one $N\Delta$ box diagram in Fig. 10.8. In Fig. 10.9 we show all diagrams (i. e. all time orderings) which exist for the case of $N\Delta$ intermediate states. There are also the corresponding diagrams with $\Delta\Delta$ intermediate states and the non-iterative ones (corresponding to diagram 5–12 of Fig. 10.9) with two intermediate nucleons. We will take into account all these diagrams involving π and ρ exchange and the medium effects caused by them in nuclear matter.

In Figure 10.10 we present results employing the field-theoretic model just sketched.[5] As expected, the medium effects are substantially larger than for the simple OBE model. The essential reason for this is the quenching of the intermediate range attraction as mediated by the 2π-exchange involving isobar intermediate states. Note that also the (repulsive) $\pi\rho$ diagrams are included (for which the medium effect causes a net attrac-

[5]The model and its parameters are given in (MHE 87, Appendix B, Table 9). It is also explained in Section 5. In the nuclear matter calculations, the continuous choice for the single baryon potential is used.

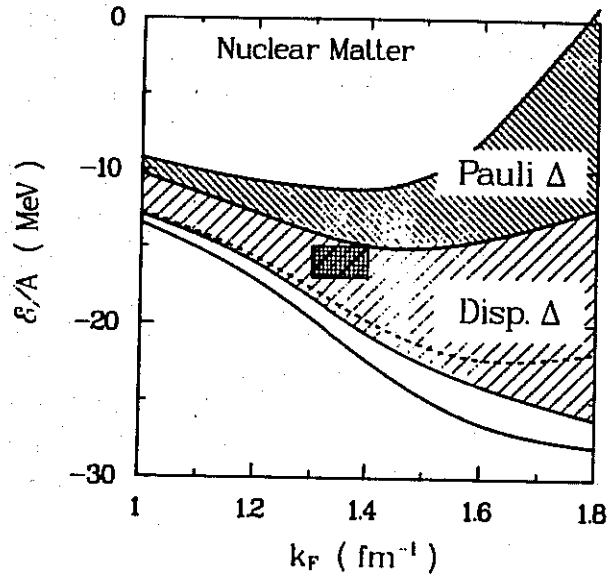

Figure 10.10: **Meson and Δ-isobar effects in nuclear matter,** as explained in the text.

tion). However, since the sum of 2π and $\pi\rho$ diagrams is attractive, the 2π-exchange being dominant at intermediate range, the net medium effect is repulsive. It is clearly seen that dispersion and Pauli effects are about equally important, the latter typically increases more strongly with density. The non-iterative diagrams contribute about as much to the medium effects as the box (iterative) diagrams. This is quite understandable, since we saw in Section 5 that iterative and non-iterative diagrams contribute about equally to the NN interaction.

The shaded areas in Fig. 10.10 represent the (repulsive) medium effects from diagrams involving Δ isobars (the Pauli effect occurs, of course, only in diagrams with $N\Delta$ intermediate states). The bottom line is obtained when no medium effects are taken into account. The white area between the lowest two full lines represents the total medium effect from all diagrams (i. e. iterative and non-iterative) with only NN intermediate states. The dashed line is obtained for the medium effect on only the iterative diagrams with NN intermediate states.

The density-dependence of the effects due to Δ degrees of freedom (particularly, the Pauli effects) is only slightly stronger than that of conventional saturation mechanisms, bringing the saturation point not markedly off the Coester band (DC 76, HM 77, MG 78, HA 78, Ana+ 78, Ana+ 79, Gre 79, MH 80).

Further detailed quantitative information is given in Tables 10.2-7, which are self-explanatory. The wound integral in nuclear matter at $k_F = 1.35$ fm^{-1} from NN, $N\Delta$, and $\Delta\Delta$ intermediate states is $\kappa_{NN} = 10.2\%$, $\kappa_{N\Delta} = 3.2\%$, and $\kappa_{\Delta\Delta} = 4.6\%$, respectively, amounting to a total wound of 18% (note that the continuous choice for the single baryon potential is used in all calculations of this subsection). In the given $\kappa_{N\Delta}$ and $\kappa_{\Delta\Delta}$ the contributions from the crossed box diagrams are included which are about as large as the ones from the box diagrams. The probability for exciting a nucleon to a delta isobar in nuclear matter is $P_\Delta = \frac{1}{2}\kappa_{N\Delta} + \kappa_{\Delta\Delta} = 6.2\%$.

10.4 Many-Body Forces

Many-body forces can originate from various sources. In Section 10.1 we gave an overview of some possible three-nucleon force contributions. We also pointed out that many of these contributions are beset by large uncertainties. For example, consider the diagram Fig. 10.4 representing the presently most popular three-body force, — the contribution from this diagram to the energy per particle in nuclear matter or the energy of the three-nucleon system differs by up to a factor of three depending on which parameters are used for its evaluation, or the details of the model employed, or the person who did the calculation. This is unsatisfactory. What is obviously needed here, is some kind of physical guidance. Now, what would be a reasonable guideline? Well, it appears to be quite self-evident that the two-body and the many-body forces should be consistent with each other. Finally all these interactions between nucleons go back to the same effective meson-baryon interactions as given e. g. by the interaction Hamiltonian Eq. (10.5). The parameters of these vertices cannot change depending on whether one, two, or three nucleons happen to be in the neighbourhood (except we plan to take six- or nine-quark effects into account). In the two-nucleon case, the experimental data to be described quantitatively by the meson-exchanges, constrain the coupling constants and vertex form fac-

Table 10.2: **Energy per nucleon in nuclear matter (in MeV) with effects due to meson and isobar degrees of freedom.**

Effects included at k_F (fm^{-1})	1.0	1.2	1.4	1.6	1.8
All Pauli and dispersion effects (including Δ diagrams)	−9.23	−10.70	−11.27	−7.92	+0.95
All dispersion effects [a] (including Δ diagrams)	−10.26	−12.79	−14.93	−14.51	−12.39
All Pauli and dispersion effects in iterative and non-iterative diagrams with only NN intermediate states	−12.92	−16.03	−20.67	−23.99	−26.10
Mesonic dispersion effects in iterative diagrams with only NN intermediate states	−12.76	−15.67	−19.78	−22.26	−21.79
No medium effects on the NN interaction [b]	−13.48	−17.13	−22.39	−26.45	−27.90

[a] The (small) Pauli effects in the non-iterative diagrams with only NN intermediate states are also included.
[b] This curve saturates at $k_F = 1.8$ fm^{-1}; the result at $k_F = 2.0$ fm^{-1} is −26.29 MeV.

tors almost uniquely (see Section 4). With these parameters there is no uncertainty in the three-body force diagram of Fig. 10.3a.

Our experience with the theory of the two-nucleon interaction may lend us also some guidance in another aspect of the problem: Which three-body force contribution may be important and which not? In Section 5 we saw that diagrams involving the Δ-isobar in intermediate states give rise to substantial contributions. We also noticed that diagrams with two intermediate Δ's are about as important as those with just one. Furthermore, the exchange of a ρ meson as "counterpart" to π-exchange for the excitation and de-excitation of a Δ-isobar is of outstanding significance. A reasonable three-body force calculation should keep all these experiences from the NN problem in mind. One can expect that the diagram of Fig. 10.3a will give a large contribution. However, for the reasons just discussed,

Table 10.3: **Partial-wave contributions to the energy per nucleon in nuclear matter (in MeV) at $k_F = 1.35$ fm^{-1} with effects due to meson and isobar degrees of freedom.**

Effects included	All Pauli and dispersion effects [a]	All dispersion effects [a]	All effects in NN diagrams [b]	Mesonic disp. in iterative NN diagrams [c]	No medium effects
$^1S_0$	−14.25	−14.98	−16.65	−16.78	−17.33
$^3P_0$	−3.46	−3.70	−3.76	−3.64	−3.67
$^1P_1$	3.97	3.96	3.99	4.12	4.13
$^3P_1$	10.17	9.76	9.77	9.37	9.31
$^3S_1$	−20.73	−21.49	−24.36	−22.78	−24.35
$^3D_1$	1.43	1.38	1.38	1.34	1.34
$^1D_2$	−2.22	−2.37	−2.38	−2.56	−2.56
$^3D_2$	−4.00	−3.98	−3.97	−3.96	−3.97
$^3P_2$	−5.68	−6.32	−6.80	−7.08	−7.14
$^3F_2$	−0.53	−0.54	−0.54	−0.56	−0.56
$^1F_3$	0.82	0.81	0.81	0.81	0.81
$^3F_3$	1.52	1.49	1.49	1.47	1.47
$^3D_3$	0.16	0.10	0.10	0.09	0.07
$^3G_3$	0.20	0.20	0.20	0.20	0.20
$J \geq 4$	−1.04	−1.08	−1.08	−1.10	−1.10
Total potential energy	−33.64	−36.75	−41.81	−41.06	−43.36
Kinetic energy	22.36	22.36	22.36	22.36	22.36
Total energy	−11.28	−14.40	−19.45	−18.71	−21.00
$\bar{M}/M$	0.700	0.704	0.676	0.650	0.648
U_0 (MeV)	−75.6	−81.8	−93.6	−93.9	−98.6

[a] including Δ diagrams.
[b] i. e. all Pauli and dispersion effects in iterative and non-iterative diagrams with only NN intermediate states.
[c] i. e. mesonic dispersion effects in iterative diagrams with only NN intermediate states.

Table 10.4: **Parameters for the self-consistent single-particle potential in nuclear matter including all medium effects.**

k_F (fm^{-1})	1.0	1.2	1.4	1.6	1.8
$\tilde{M}/M$	0.799	0.757	0.689	0.619	0.591
U_0 (MeV)	−52.0	−66.0	−79.9	−93.6	−104.2

See Eq. (10.24) for definition.

besides π-exchange the ρ meson should be included and the excitation of more than just one Δ should be considered. As we are dealing with strong short-ranged forces, correlations have to be taken into account.

A calculation which takes all these essential aspects into consideration has, indeed, been done, namely by Dickhoff, Faessler, and Müther (DFM 82, Müt 84). Diagrams which are the subject of their study are shown in Fig. 10.11, using now the graphical many-body language appropriate for this problem (compare Section 9). Speaking in terms of the hole-line expansion, Fig. 10.11 shows the three-hole line contributions of the ring diagram type — however, now with the inclusion of isobar degrees of freedom. According to the definition of a many-nucleon force given in Section 10.1, the ring diagrams involving isobars are to be understood as contributions from many-body forces. The weavy line in the Figure represents a G-matrix derived from the corresponding transition potential which takes π and ρ exchange into account. The results obtained by the Tübingen group (DFM 82) are shown in Table 10.8 and Fig. 10.12.

The top line in Fig. 10.12 denoted by "(2)", which is the starting point of our quantitative considerations in this subsection, repeats the final result of the previous subsection; it is obtained in lowest order Brueckner theory (two-hole line approximation) and includes all medium effects as discussed. Now, to this curve the attractive contributions from the N and Δ rings

Table 10.5: Landau parameters at various densities of nuclear matter with all effects due to meson and isobar degrees of freedom.

k_F (fm^{-1})	density	f_0	f_0'	g_0	g_0'
1.0	$0.4\rho_0$	−1.38	0.62	0.12	0.66
1.35	ρ_0	−1.01	0.41	0.07	0.70
1.7	$2\rho_0$	−0.51	0.24	0.06	0.75

Based on the nuclear matter G-matrix, the effective particle-hole interaction at the Fermi surface is calculated, which, multiplied by the density of states $(k_F M)/(\hbar^2\pi^2)$, is parametrized by $\mathcal{F} = f + f'\boldsymbol{\tau}_1 \cdot \boldsymbol{\tau}_2 + g\boldsymbol{\sigma}_1 \cdot \boldsymbol{\sigma}_2 + g'\boldsymbol{\sigma}_1 \cdot \boldsymbol{\sigma}_2\boldsymbol{\tau}_1 \cdot \boldsymbol{\tau}_2$. From an expansion of the parameters in terms of Legendre polynominals, P_l, we give in the table the coefficient for $l = 0$. For more details see (Müt 84, NKS 84).

Table 10.6: **Landau parameters at $k_F = 1.35$ fm^{-1} with effects due to meson and isobar degrees of freedom.**

	f_0	f_0'	g_0	g_0'
All medium effects	–1.01	0.41	0.07	0.70
All dispersion effects	–1.14	0.40	0.07	0.71
No medium effects	–1.41	0.44	0.08	0.77

See footnote of Table 10.5.

Table 10.7: **Energy per particle, $\mathcal{E}/A$, Fermi momentum, k_F, and kompression modulus, K, at saturation for nuclear matter with effects due to meson and isobar degrees of freedom.**

	$\mathcal{E}/A$ (MeV)	k_F (fm^{-1})	K (MeV)
All medium effects	–11.28	1.37	135
All dispersion effects	–15.00	1.48	143
No medium effects	–27.90	1.80	248

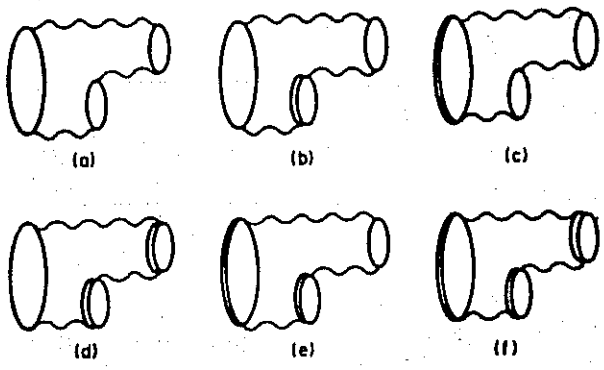

Figure 10.11: **Ring diagrams of third order in nuclear matter including Δ-isobar excitations.** [Reproduced from (Müt 84).]

of third order, displayed graphically in Fig. 10.11, are added to arrive at the curve labelled "(3) N Δ". In Table 10.8 it is clearly seen that the contributions from ring diagrams including Δ excitations are much larger than those which involve nucleons only. The Tübingen group went further and evaluated also the N and Δ rings of fourth order, see Table 10.8 and curve "(4) N Δ" of the Figure. Again, the contributions are much larger when Δ are included.

Finally, using several approximations, the Tübingen group summed up the N and Δ rings up to infinite orders in closed form. This result (with the rings up to fourth order subtracted) is represented by the lowest shaded area of Fig. 10.12 denoted by "?". Divergence for higher density appears to be suggested. However, some caution is in place with regard to this last result. First, several approximations had to be done to make this calculation feasible. Secondly, the calculation implies pion condensation to occur at densities where it has experimentally not been observed. Therefore, further investigations will be necassary before final conclusions can be drawn concerning rings of very high order.

The bottom dashed line of Fig. 10.12 is the result from the previous

Table 10.8: **Contributions from third and fourth order ring diagrams in nuclear matter at various densities.** [From (DFM 82)]

k_F (fm^{-1})	1.0	1.2	1.4	1.6
Third order				
Nucleons only	+0.08	−0.60	−0.84	−1.70
Δ included	−0.35	−1.63	−2.85	−5.22
Fourth order				
Nucleons only	−0.60	−0.34	−0.27	−0.34
Δ included	−0.76	−0.89	−1.81	−4.15
Total	−1.10	−2.52	− 4.66	-9.37

The third order ring with nucleons only
is shown in Fig. 10.11a.

subsection when no medium effects were included. Note that this starting point of our considerations (of medium effects and many-body forces) and the final result we here arrived at (after a lot of up and down in-between) are very close.

In summary of this and the previous subsection, isobar degrees of freedom have essentially *two* consequences in nuclear matter:

- *medium effects* on the two-nucleon interaction and
- *many-body force* contributions.

Both are *large* effects/contributions — but, of *opposite* sign. In a consistent treatment of degree(s) of freedom either both effects occur simultaneously, or none of them occurs. One of these two effects alone, in isolation, does not exist in reality. Therefore, to take into account only one of them (for instance, only the three-body force contributions, ignoring the

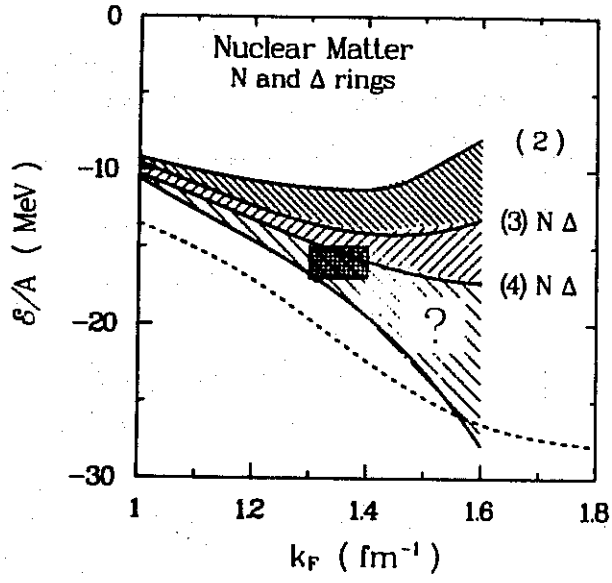

Figure 10.12: **Contributions from ring diagrams to the energy per particle in nuclear matter.** The order of the ring diagrams taken into account is given in parenthesis. [From (DFM 82, Müt 84)]

medium effects on the corresponding two-body diagrams) yields a substantially distorted picture. In fact, the almost cancelation between these two effects/contributions may be the deeper reason why, ultimately, many-body forces may not play a great role in nuclear physics; it may also be the reason why the traditional two-body force picture has been (and is) by and large rather successful.[6]

10.5 Relativistic Effects

In the 1970's a new (relativistic) approach to proton-nucleus scattering was developed by Clark and coworkers (Cla+ 73), which has become known as Dirac phenomenology. A Dirac equation is solved which contains a strong (attractive) scalar and (repulsive) vector potential. The most significant

[6]The cancelation of the two effects discussed here for nuclear matter, has also been found in corresponding calculations for the three-nucleon system by the Hannover group (HSS 83), giving support to the conjecture that this might in general be true for the nuclear ground state.

result of this new method is the quantitative fit of spin observables, which are only poorly described by the Schroedinger equation.

Inspired by these successes in the area of scattering, a relativistic extension of Brueckner theory has been suggested by Shakin *et al.* (Ana+ 83), frequently called the *Dirac-Brueckner* approach. In analogy to the new ideas in scattering, the essential point is to use the Dirac equation for the single-particle motion in nuclear matter

$$(\not{p} - M - U)\tilde{u}(\mathbf{p}, s) = 0 \tag{10.31}$$

or in Hamiltonian form

$$(\boldsymbol{\alpha} \cdot \boldsymbol{p} + \beta M + \beta U)\tilde{u}(\mathbf{p}, s) = \epsilon_p \tilde{u}(\mathbf{p}, s)$$

with

$$U = U_S + \gamma^0 U_V \tag{10.32}$$

where U_S is an attractive scalar and U_V (the time-like component of) a repulsive vector field. (Notation as in (BD 64); $\beta = \gamma^0$, $\alpha^l = \gamma^0\gamma^l$.) As discussed in Section 3.4, in analogy to the creation of the Thomas term by the Coulomb potential, a vector field inserted into a Dirac equation generates a spin-orbit force. As such a spin-orbit term is typically proportional to M^{-2} (see Eqs. (A.22, A.25)), the reduction of the nuclear mass by the scalar field, leading to the replacement $M \to \tilde{M}$ with $\tilde{M}$ defined in Eq. (10.34) below, causes an enhancement of the spin-orbit force. This is the basic reason for the success of this approach in nucleon-nucleus scattering.

The fields, U_S and U_V, are in the order of several hundred MeV and strongly density dependent (numbers will be given below). In nuclear matter they can be determined self-consistently. The resulting fields are in close agreement with those obtained in the Dirac phenomenology of scattering.

The solution of Eq. (10.31) is

$$\tilde{u}(\mathbf{p}, s) = \sqrt{\frac{\tilde{E}_p + \tilde{M}}{2\tilde{M}}} \begin{pmatrix} 1 \\ \frac{\boldsymbol{\sigma} \cdot \boldsymbol{p}}{\tilde{E}_p + \tilde{M}} \end{pmatrix} \chi_s \tag{10.33}$$

with

$$\tilde{M} = M + U_S, \tag{10.34}$$

$$\tilde{E}_p = \sqrt{\tilde{M}^2 + \mathbf{p}^2}, \tag{10.35}$$

and χ_s a Pauli spinor. Normalization as in Eq. (A.10).

As in conventional Brueckner theory, the basic quantity is a G-matrix, which satisfies an integral equation. In this relativistic approach, a relativistic three-dimensional equation is chosen, which is applied to nuclear matter in strict analogy to free scattering. The Thompson equation, Eq. (4.20), is particularly convenient (BM 84, HM 87). For this equation we have in nuclear matter

$$\bar{G}(\mathbf{q}',\mathbf{q};\mathbf{P},\bar{z}) = \bar{V}(\mathbf{q}',\mathbf{q}) + \int \frac{d^3k}{(2\pi)^3}\bar{V}(\mathbf{q}',\mathbf{k})\frac{\bar{M}^2}{\bar{E}^2_{P+k}}\frac{Q(\mathbf{k},\mathbf{P})}{\bar{z}-2\bar{E}_{P+k}}\bar{G}(\mathbf{k},\mathbf{q};\mathbf{P},\bar{z}) \tag{10.36}$$

with

$$\bar{z} = 2\bar{E}_{P+q}. \tag{10.37}$$

$\mathbf{P}$ is one half the c.m. momentum, and $\mathbf{q}, \mathbf{k}$ and $\mathbf{q}'$ are the initial, intermediate and final relative momenta of the two particles interacting in nuclear matter, respectively. We suppress the k_F dependence as well as spin (helicity) and isospin indices. For $|\mathbf{P} \pm \mathbf{q}|$ and $|\mathbf{P} \pm \mathbf{k}|$ the angle average is used. Further treatments of Eq. (10.36) can follow the lines established from conventional Brueckner theory, as e. g. the use of the angle averaged Pauli projector etc.. Numerically the equation can be solved by standard methodes of momentum space Brueckner calculations (HT 70).

The essential difference to standard Brueckner theory is the use of the potential $\bar{V}$ in Eq. (10.36). Indicated by the tilde, this meson-theoretic potential is evaluated by using the spinors Eq. (10.33) instead of the free spinors Eq. (A.14) (which are obtained as solutions of Eq. (10.31) for $U \equiv 0$) applied in scattering (and conventional Brueckner theory), see Appendix A.1. Since U_S (and $\bar{M}$) are strongly density dependent, so is the potential $\bar{V}$. $\bar{M}$ decreases with density. The essential effect in nuclear matter is a suppression of the (attractive) σ-exchange; this suppression increases with density, providing additional saturation. It turns out (see figures below) that this effect is so strongly density-dependent that *the empirical saturation and incompressibility* can be reproduced. Furthermore, the prediction for the Landau parameter f_0 is considerably improved without deteriorating the other parameters (see table below). Note that all conventional saturation effects discussed in Section 9 (which, as we saw, are quite sizable) are also contained in this calculations. Thus, the relativistic effect is just a small, but important correction to the conventional result (Tables and

figures below will quantify these points.)

The single-particle potential

$$U(m) = \frac{\tilde{M}}{\tilde{E}_m}\langle m|U|m\rangle = \frac{\tilde{M}}{\tilde{E}_m}\langle m|U_S + \gamma^0 U_V|m\rangle = \frac{\tilde{M}}{\tilde{E}_m}U_S + U_V \qquad (10.38)$$

is the many-body self-energy which is defined in terms of the G-matrix in formally the usual way

$$U(m) = \sum_{n\le k_F} \frac{\tilde{M}^2}{\tilde{E}_n\tilde{E}_m}\langle mn|\tilde{G}(\tilde{z})|mn-nm\rangle \qquad (10.39)$$

from which the constants U_S and U_V are determined. Note that the ansatz Eq. (10.32) is an approximation, since the scalar and vector fields are in principal momentum dependent; however, it has been shown that this momentum dependence is very weak (HM 87, Mac 86).

Finally the energy in nuclear matter is obtained in lowest order (Brueckner-Hartree-Fock approximation) by

$$\frac{\mathcal{E}}{A} = \frac{1}{A}\sum_{m\le k_F}\frac{\tilde{M}}{\tilde{E}_m}\langle m|\boldsymbol{\gamma}\cdot\boldsymbol{p}_m + M|m\rangle + \frac{1}{2A}\sum_{m,n\le k_F}\frac{\tilde{M}^2}{\tilde{E}_m\tilde{E}_n}\langle mn|\tilde{G}(\tilde{z})|mn-nm\rangle - M \qquad (10.40)$$

In Eqs. (10.39-40) we use

$$\tilde{z} = \tilde{E}_m + \tilde{E}_n. \qquad (10.41)$$

Note that in Eqs. (10.38-40) the states $|m\rangle$ and $|n\rangle$ are represented by Dirac spinors of the kind Eq. (10.33) and an appropriate isospin wavefunction, $\langle m|$ and $\langle n|$ are the adjoint Dirac spinors $\bar{u} = u^\dagger\gamma^0$; $\tilde{E}_m = \sqrt{\tilde{M}^2 + \mathbf{p}_m^2}$. The first term on the r.h.s. of Eq. (10.40) — the 'kinetic energy' — is in more explicit form

$$\frac{1}{A}\sum_{m\le k_F}\frac{M\tilde{M} + \mathbf{p}_m^2}{\tilde{E}_m}. \qquad (10.42)$$

The single particle energy is

$$\epsilon_m = \frac{\tilde{M}}{\tilde{E}_m}\langle m|\boldsymbol{\gamma}\cdot\boldsymbol{p}_m + M|m\rangle + U(m) \qquad (10.43)$$

$$= \tilde{E}_m + U_V. \qquad (10.44)$$

(Compare Eq. (10.24).)

In Figs. 10.13-15 and Tables 10.9-12 we show results (BM 88) which are essentially self-explanatory.[7]

The suppression of the σ contribution can be understood in simple terms by considering the covariant one-σ-exchange amplitude, Eq. (A.8), for $\mathbf{q}' = \mathbf{q}$ and $\lambda_i = \lambda_i'$, in which case, due to the covariant normalization of the Dirac spinors Eq. (A.10), the numerator becomes **1**. Since the physical states of the nucleons in nuclear matter are normalized by $u^\dagger u = 1$, the sigma (as any other) contribution gets a 'renormalization' factor $(\tilde{M}/\tilde{E})^2$ (see second term on the r.h.s. of Eq. (10.40)) which decreases with decreasing $\tilde{M}$ (i. e. increasing density). A corresponding consideration for the time-like (γ_0) component of ω-exchange would lead to no changes for that contribution. However, due to the exchange term there is a small enhancement of the repulsion created by the ω with density. The repulsive relativistic effect seen in Table 10.10 for the P-wave contributions is essentially due to σ suppression together with a signature of ω spin-orbit force enhancement. The change of the $^1S_0$ contribution is so small, because of a cancelation of effects due to σ and ρ. The repulsive effect in $^3S_1$ is essentially due to a suppression of the twice iterated one-pion exchange for reasons quite analogous to the sigma suppression.

It has been shown that when the fictitious σ boson is replaced by genuine 2π-exchange, the relativistic effects in nuclear matter are about the same as those obtained within the OBE model (which is applied in the calculations presented here) (MB 85).

From the numbers given in Table 10.9 it is seen that the relativistic effect on the energy per nucleon, $\Delta(\mathcal{E}/A)_{rel}$ (i. e. the difference between the relativistic and non-relativistic calculation), is well fitted by the ansatz

$$\Delta(\mathcal{E}/A)_{rel} \approx 2 \text{ MeV} \times (\rho/\rho_0)^{8/3}, \tag{10.45}$$

which is suggested by an estimate by Brown *et al.* (Bro+ 87).

The representation of nucleons by Dirac spinors with a reduced mass, $\tilde{M}$, can be interpreted, as taking virtual nucleon-antinucleon excitations in the many-body environment (many-body Z-graphs) effectively into account (Bro+ 87), see Fig. 10.16. This can be made plausible by expanding the

[7] In all cases the Potential B defined in Table A.2 is used, except for Fig. 10.13 in which all three potential of Table A.2 are applied.

spinor Eq. (10.33) in terms of (a complete set of) spinor solutions of the free Dirac equation which will necessarily also include solutions representing negative energy (antiparticle) states (Ana+ 83).

There exists a comprehensive literature on this matter to which we refer the interested reader for alternative presentations of this and related subjects (CS 86a, SW 86, HS 87, HM 87).

In summary, the only effect, we presently know of, that is able to account quantitatively for the remaining descrepancy between the empirical nuclear saturation and the predictions from conventional many-body theory, is the relativistic effect as obtained in the Dirac-Brueckner approach. However, this approach in its current form does not represent a theory. Consequently, several critical questions can be raised (Neg 85, CJ 86a, Thi 86, Bro+ 87); for an informative summary of the present discussion see the recent review by Wallace (Wal 87). Future investigations should devote to the question if a relativistic many-body theory can be formulated which the Dirac-Brueckner approach would be a consequence of (for instance, in a certain, well-defined approximation). First attempts into this direction have been undertaken by Schütte (Sch 83).

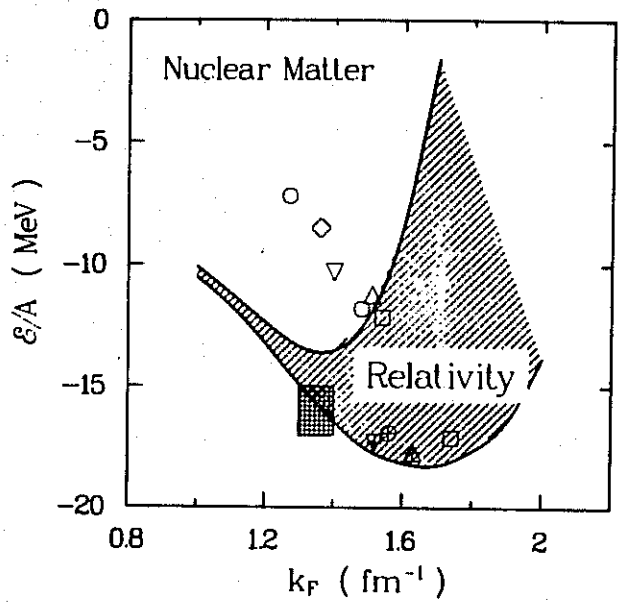

Figure 10.13: **The repulsive relativistic effect in nuclear matter as obtained in a Dirac-Brueckner-Hartree-Fock calculation.** Conventional saturation points are displayed in the background.

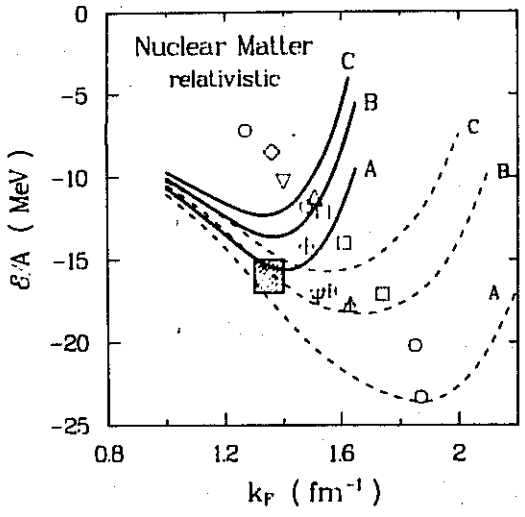

Figure 10.14: **Results from calculations with a family of relativistic potentials revealing a new Coester band which meets the empirical area;** full lines: relativistic, dashed lines: non-relativistic calculations.

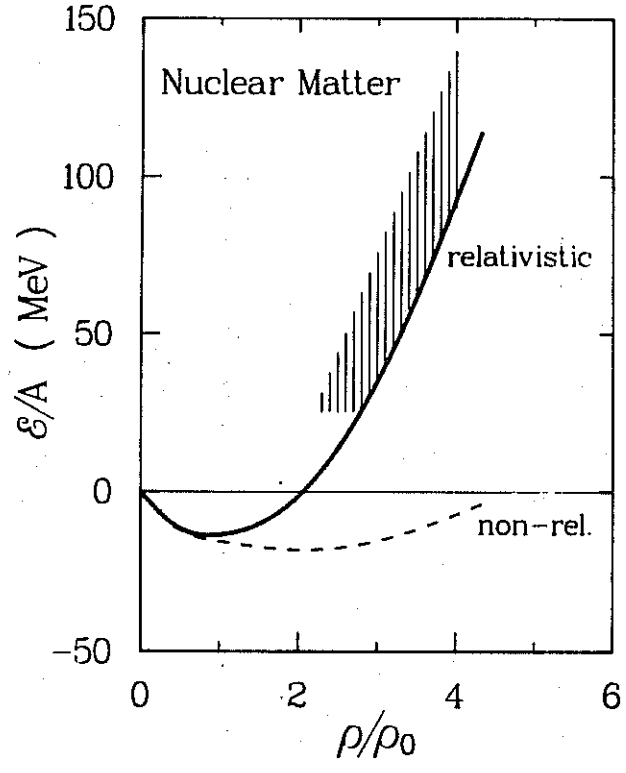

Figure 10.15: **Dirac-Brueckner results for nuclear matter (solid line) at higher densities.** The shaded area represents empirical information as deduced from pion production in heavy ion collisions (Sto+ 82, Har+ 85).

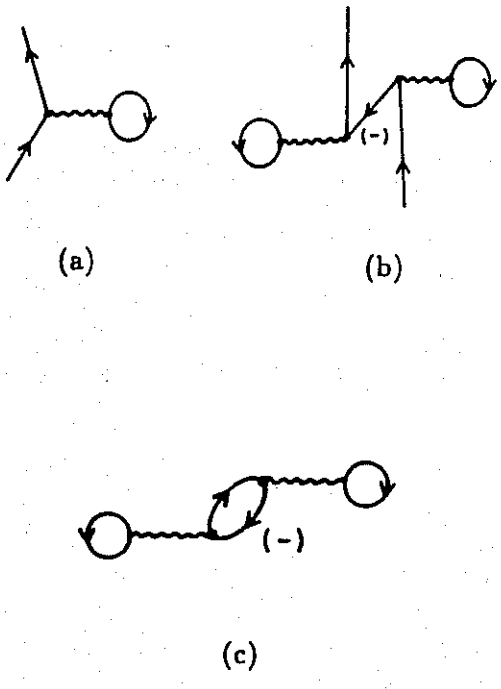

Figure 10.16: **(a) Single particle propagation in nuclear matter with (b) relativistic corrections; (c) is the relativistic correction to the energy** (cf. Fig. 9.2). Virtual antinucleon states (holes in the Dirac sea) are denoted by "(-)", while otherwise the usual many-body graph language is applied (Section 9.3).

Table 10.9: **Results of a relativistic Dirac-Brueckner calculation in comparison to the corresponding non-relativistic one.**

	relativistic					*non-relativistic*			
k_F (fm^{-1})	$\mathcal{E}/A$ (MeV)	$\bar{M}/M$	U_S (MeV)	U_V (MeV)	κ (%)	$\mathcal{E}/A$ (MeV)	$\bar{M}/M$	U_0[a] (MeV)	κ (%)
0.8	−7.02	0.855	−136.2	104.0	23.1	−7.40	0.876	−33.0	26.5
0.9	−8.58	0.814	−174.2	134.1	18.8	−9.02	0.836	−41.0	21.6
1.0	−10.06	0.774	−212.2	164.2	16.1	−10.49	0.797	−49.0	18.5
1.1	−11.18	0.732	−251.3	195.5	12.7	−11.69	0.760	−58.1	14.2
1.2	−12.35	0.691	−290.4	225.8	11.9	−13.21	0.725	−68.5	12.9
1.3	−13.35	0.646	−332.7	259.3	12.5	−14.91	0.687	−80.5	13.1
1.35	−13.55	0.621	−355.9	278.4	13.0	−15.58	0.664	−86.8	13.2
1.4	−13.53	0.601	−374.3	293.4	13.8	−16.43	0.651	−93.2	13.5
1.5	−12.15	0.559	−413.6	328.4	14.4	−17.61	0.618	−106.1	13.0
1.6	−8.46	0.515	−455.2	371.0	15.8	−18.14	0.579	−119.4	12.7
1.7	−1.61	0.477	−491.5	415.1	18.4	−18.25	0.545	−133.2	13.2
1.8	+9.42	0.443	−523.4	463.6	21.9	−17.65	0.489	−147.2	14.3
1.9	25.26	0.418	−546.7	513.5	25.2	−16.41	0.480	−160.7	15.0
2.0	47.56	0.400	−563.6	568.6	27.5	−13.82	0.449	−173.6	15.3
2.1	77.40	0.381	−581.3	640.9	30.2	−9.70	0.411	−186.3	15.7
2.2	114.28	0.370	−591.2	723.5	33.3	−3.82	0.373	−198.1	16.3

As a funtion of the Fermi momentum k_F, it is listed: the energy per nucleon $\mathcal{E}/A$, $\bar{M}/M$, the single-particle scalar and vector potentials U_S and U_V, and the wound integral κ.

[a] U_0 is to be compared to $U_S + U_V$, cf. Eq. (10.24).

Table 10.10: **Partial wave contributions to the energy in nuclear matter (in MeV) for a non-relativistic and a relativistic calculation.**

	$k_F = 1.1$ fm^{-1}		$k_F = 1.35$ fm^{-1}		$k_F = 1.6$ fm^{-1}	
State	non-rel.	relativ.	non-rel.	relativ.	non-rel.	relativ.
$^1S_0$	−10.79	−11.18	−16.01	−16.42	−21.51	−20.36
$^3P_0$	−2.07	−1.48	−3.74	−1.34	−5.61	+2.17
$^1P_1$	1.73	1.77	3.25	3.45	5.33	6.08
$^3P_1$	4.71	5.27	9.77	12.33	17.69	26.65
$^3S_1$	−15.41	−14.16	−20.10	−17.10	−23.77	−17.03
$^3D_1$	0.59	0.57	1.38	1.29	2.64	2.25
$^1D_2$	−0.95	−0.91	−2.28	−2.01	−4.57	−3.39
$^3D_2$	−1.70	−1.62	−4.00	−3.56	−7.71	−5.99
$^3P_2$	−3.10	−2.92	−7.06	−6.28	−13.31	−10.73
$^3F_2$	−0.19	−0.18	−0.54	−0.44	−1.19	−0.67
$^1F_3$	0.32	0.31	0.80	0.75	1.60	1.40
$^3F_3$	0.56	0.55	1.51	1.43	3.20	2.87
$^3D_3$	−0.01	0.00	−0.03	0.00	−0.11	−0.02
$^3G_3$	0.06	0.06	0.20	0.18	0.49	0.41
$J \geq 4$	−0.34	−0.33	−1.07	−0.98	−2.57	−2.13
Total potential energy	−26.61	−24.25	−37.93	−28.72	−49.38	−18.51
Kinetic energy	14.91	13.07	22.35	15.16	31.23	10.05
Total energy	−11.69	−11.18	−15.58	−13.55	−18.14	−8.46

Table 10.11: **Landau parameters at various densities from a non-relativistic and a relativistic nuclear matter calculation.**

k_F (fm^{-1})	density		f_0	f_0'	g_0	g_0'
1.0	$0.4\rho_0$	relativistic	−1.37	0.57	0.22	0.66
		non-relativisic	−1.50	0.62	0.16	0.66
1.35	ρ_0	relativistic	−0.79	0.35	0.28	0.67
		non-relativisic	−1.27	0.38	0.15	0.67
1.7	$2\rho_0$	relativistic	0.56	0.29	0.36	0.68
		non-relativisic	−0.99	0.20	0.14	0.69
2.0	$3.25\rho_0$	relativistic	2.21	0.37	0.38	0.69
		non-relativisic	−0.71	0.09	0.11	0.71

See footnote to Table 10.5.

Table 10.12: **Energy per particle, $\mathcal{E}/A$, Fermi momentum, k_F, and kompression modulus, K, at saturation for nuclear matter with and without relativistic effects.**

	$\mathcal{E}/A$ (MeV)	k_F (fm^{-1})	K (MeV)
relativistic	−13.60	1.37	249
non-relativistic	−18.30	1.66	160

Section 11

Finite Nuclei

In this section, by showing some results for finite nuclei, we shall reveal some striking parallels to nuclear matter. This will underscore the relevance of nuclear matter for nuclear structure physics. As samples we choose the $A = 3$ nucleus and oxygen. The results demonstrate some remarkable successes of meson-theoretic potentials in nuclear structure.

11.1 The Three-Nucleon System

The three-body system is presently the only many-body problem which is amenable to exact solution. For that reason, this system assumes a special role in nuclear structure physics. The results we show in Fig. 11.1 are all obtained in Faddeev calculations (taking 34 channels into account; for more explanations and references to the various results see (Bra+ 88); the Paris energy is from (FGP 88), the charge radius for Potential A from (Kim+ 88)). This figure should be compared with the nuclear matter overview given in Fig. 9.5. This comparison is facilitated by the fact that, in part, the same potentials have been applied to both systems.[1]

For the $A = 3$ system, Fig. 11.1, we plot the energy of the triton versus the invers charge radius of ^3He, the latter quantity being a measure of density, which makes the comparison with nuclear matter graphs easier. As announced, the parallels between the two systems are striking. This is particularly amazing, since three nucleons should be far from being a

[1] References for the potentials are given in Table 9.1; TRS refers to (TRS 75).

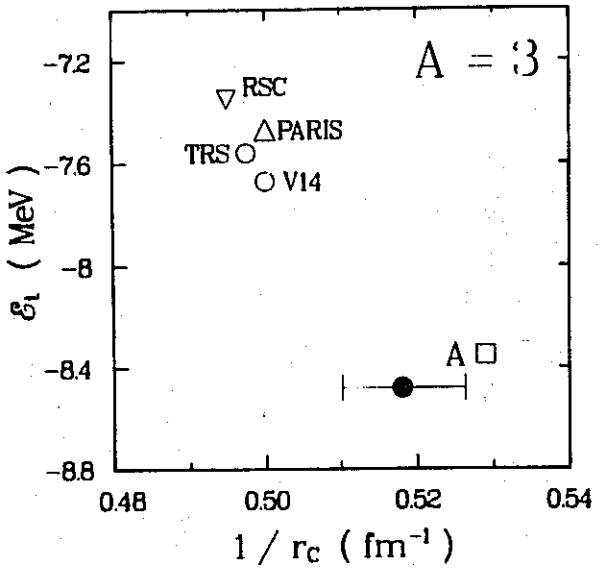

Figure 11.1: Energy of the triton, $\mathcal{E}_t$, versus the invers charge radius of ^{3}He, $1/r_c$, as predicted by various NN potentials. The experimental point is given by the horizontal error bar. [From (Bra+ 88b)]

piece of nuclear matter. Note, however, that for the $A = 3$ system the results have a closer tendency towards experiment: If the energy is right, the radius (density) is also (about) right. This may be attributed to the lower density of the triton.

On the basis of the nuclear matter results of Section 10.5, relativistic effects should be negligibly small at the (very low) average density of the triton. Also, — in contrast to nuclear matter — such additional saturation effects are obviously not need in the three-body system.

Similar to nuclear matter, in the triton the strength of the tensor force (as seen in the %-D-state prediction for the deuteron) rules the binding energy. This is demonstrated in Fig. 11.2 and should be compared with the nuclear-matter Figure 9.6. The reason for this fact is analogous to nuclear matter (cf. Fig. 9.8), with the nuclear matter G-matrix to be replaced by the two-body T-matrix, which is the input to a Faddeev calculation [see

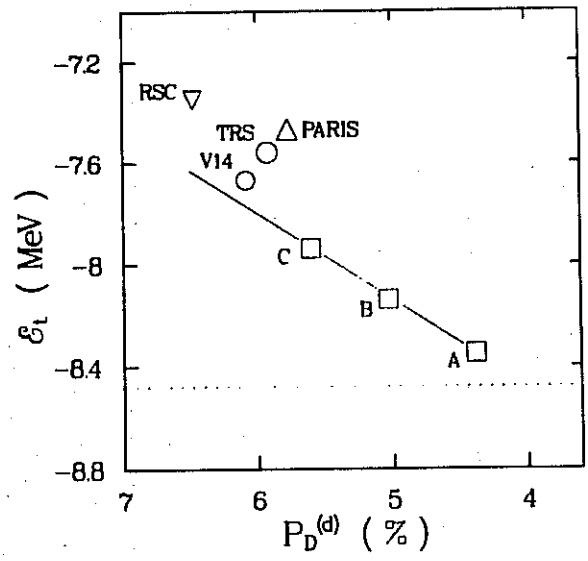

Figure 11.2: **Energy of the triton, $\mathcal{E}_t$, versus the deuteron % D-state $P_D^{(d)}$.** The solid line is a linear (inter-) extra-polation of the results from Potentials *A*, *B*, and *C*. The horizontal dotted line indicates the empirical value for the triton energy of -8.48 MeV. [From (Bra+ 88b)]

(Bra+ 88b) for details].

To give some numbers: for RSC (deuteron D-state probability $P_D^{(d)} = 6.5$ %) the predicted triton binding energy is $\mathcal{B}_t = 7.35$ MeV and the charge radius of ^3He is $r_c = 2.02$ fm; for Potential *A* ($P_D^{(d)} = 4.4$ %) one obtains $\mathcal{B}_t = 8.35$ MeV and $r_c = 1.89$ fm and for Potential B ($P_D^{(d)} = 5.0$ %) $\mathcal{B}_t = 8.14$ MeV. (The given predictions refer to 34-channel calculations; the experimental charge radius for ^3He is $r_c = 1.93 \pm 0.03$ fm; for references see (Bra+ 88b, Kim+ 88).)

In Table 11.1 we give a few important further corrections/contributions to the triton binding energy. The charge-dependence correction is due to the fact that in the triton *np* as well as *nn* pairs interact for which the strength of the nuclear force differs as seen in the different singlet scattering lengths (see Table 6.1). For the charge-independent result (first row

Table 11.1: **Contributions to the triton binding energy, B_t.**

	B_t (MeV)	Reference
Two-body force (2BF)[a]	8.35	Bra+ 88b
Charge-dependence in 2BF	−0.19	Bra+ 88a
Total 2BF	8.16	
Three-body force[b]	0.90	HSS 83
Medium effect on 2BF[c]	−0.60	HSS 83
Total	8.46	
(Experiment)	(8.48)	

[a] Potential A is applied in a 34-channel calculation.
[b] Essentially the contribution from diagram Fig. 10.3a using static π and ρ exchange.
[c] Medium effects on diagram Fig. 10.1.

of Table 11.1 with the result 8.35 MeV) the more attractive np force is used. Results from calculations employing a pp (nn) force are typically less attractive by about 300 keV than those using a np force. Taking charge-dependence into account yields a result that is about $\frac{1}{3}/\frac{2}{3}$ in-between the two charge independent extremes, which can easily be understood in terms of the isospin factors involved (Bra+ 88a).

Similar to nuclear matter (Sections 10.3 and 10.4), a large cancelation between three-body force contributions and medium effects on corresponding two-body force diagrams has been found in the consistent calculations performed for the triton by the Hannover group (HSS 83). In the calculations quoted in Table 11.1 only single-Δ excitation is taken into account. When also double-Δ configurations are included an additional effect of −1.2

MeV on the triton binding energy is obtained which is due to very large dispersive effects in those diagrams (HSY 83).

11.2 The Ground State of Closed-Shell Nuclei

Results from renormalized Brueckner-Hartree-Fock (RBHF) calculations for the ground state of ^{16}O are shown in Fig. 11.3. Open circles represent predictions using static two-body forces (MMF 75). The open triangle is obtained in a calculation which includes effects due to meson and Δ isobar degrees of freedom (Ana+ 78). Finally, the squares refer to a non-relativistic (non-rel.) and a relativistic (relativ.) calculation (MMB 88) using the potential which we applied to nuclear matter in Section 10.5. Roughly speaking the various results resemble much of the corresponding nuclear matter predictions which we discussed in Sects. 9 and 10. However, in ^{16}O it seems to be more difficult to get enough binding energy as compared to nuclear matter. It is not clear in the moment if this is due essentially to the problem of how to choose a reasonable particle spectrum in a finite nucleus calculation. Common choices employ a rather 'high' particle spectrum (harmonic oszillator) causing a large gap relative to the hole states which is known to reduce the binding energy.

For the relativistic calculation the numbers are (with the corresponding non-relativistic results given in parenthesis): $\mathcal{E}/A = -5.62$ MeV (-5.94 MeV) and $r_c = 2.52$ fm (2.36 fm). The experimental values are -7.98 MeV and 2.7 ± 0.05 fm, respectively. Three-body correlations/forces may contribute up to about 1 MeV to the binding energy (Müt 84).

11.3 Excited States

After we have seen that the relativistic effects considerably improve the groundstate properties of nuclei, one may wonder how other nuclear structure properties are influenced. In Fig. 11.4 we show the spectra of two $A = 18$ nuclei (MMB 87). One type of calculation uses only the G-matrix ('g'); the calculation denoted by 'V_{eff}' includes some renormalization terms of the effective many-body Hamiltonian (MMB 87). It is clearly seen that,

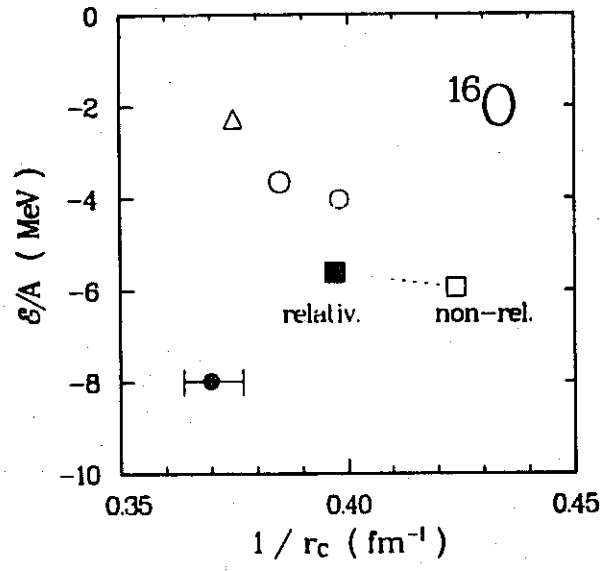

Figure 11.3: **Energy per nucleon in ^{16}O versus the inverse charge radius.** Open symbols from non-relativistic RBHF calculations, the full square from the relativistic Dirac-Brueckner-Hartree-Fock approach. Further explanations are given in the text. The error bar denotes the empirical point.

quite in contrast to the nuclear groundstate, the relativistic effect is rather small for the spectra. This result is quite understandable, since we saw in Section 10.5 that the relativistic effects are strongly density dependent. For small densities they are negligibly small (see Fig. 10.13). The nuclear densities, valence nucleons are exposed to, are certainly very low. Due to the weak tensor force, characteristic for meson-theoretic forces, the non-relativistic result is already quite satisfactory. This is not spoiled by relativistic effects.

As a general balance of just the few nuclear structure results we have given in this section, one may state that meson-theoretic forces allow for a more consistent and quantitative description of nuclear structure properties, as compared to purely phenomenological potentials. Therefore, we like to

strongly encourage further applications of meson-theoretic forces to nuclear structure problems.

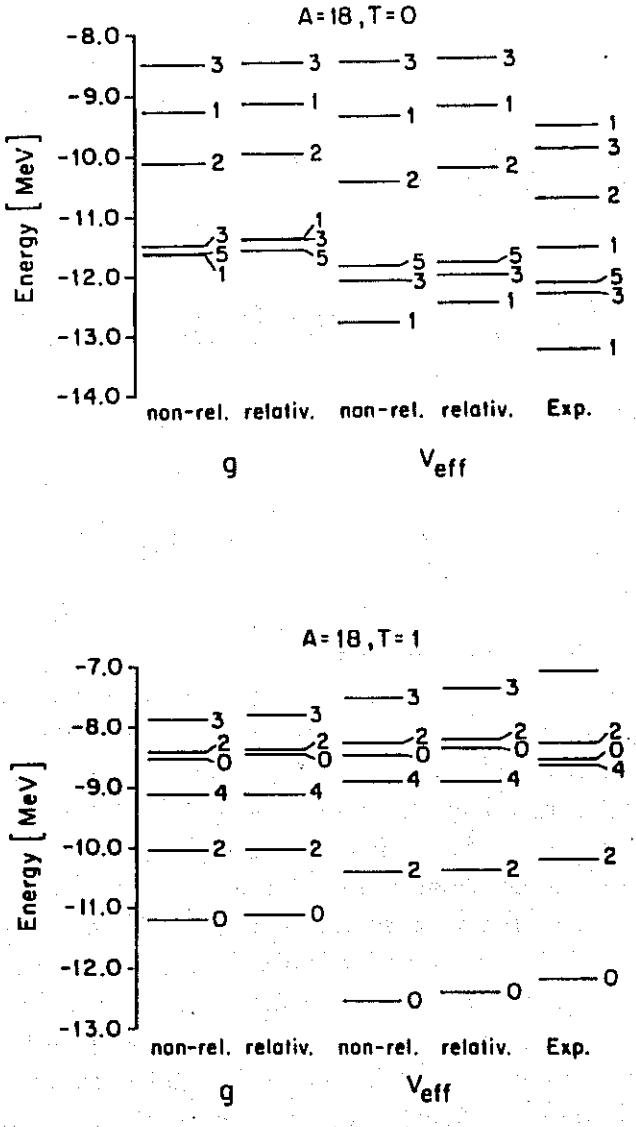

Figure 11.4: Excitation spectrum for nuclei with two valence nucleons in an open shell. The $T = 0$ case refers to ^{18}O, $T = 1$ to ^{18}F. More details are given in the text. 'Exp.' denotes the experimental values. [From (MMB 87)]

Section 12

Summary, Conclusions, and Outlook

Nothing endures but change.
— HERACLITUS

In this article we have been concerned with meson-theoretic approaches to nuclear interactions and nuclear structure. We have reviewed the NN interaction up to about 1 GeV including subtle aspects like charge-asymmetry, charge-dependence and inelasticity. Furthermore, we discussed the many-body problem using meson-theoretic forces. We will not summarize again all the points we have made. However, speaking in general terms, the balance of these considerations is that for the energy range under discussion meson models are quite successfull. At low energy and for the two-nucleon system the description of the data is absolutely quantitative. With increasing energy, the predictions assume a more qualitative character. However, presently it is not clear if this is a pricipal problem, indicating the limitations of meson models, or if it is simply due to the fact that the models for higher energy have not (yet) been worked out as carefully as for low energy. This point deserves further attention in future research. Particularly challenging is the energy region of several GeV in which the inadequacy of traditional models should clearly be revealed. Presently, very little theoretical work exists in that energy range.

In nuclear matter we have studied explicitly meson and Δ degrees of freedom. The inclusion of these degrees of freedom does not improve nuclear saturation; however, it provides a better understanding of the role of many-

body forces in nuclear physics: two- and many-body forces should always be treated consistently; if that is done, there is only a small net effect from many-body forces. We also discussed a relativistic extension of Brueckner theory based on meson-theoretic forces. This approach provides additional saturation such that the empirical properties can be explained. We need, however, a deeper understanding of the relativistic concept behind this method.

Thus, in spite of the well established success of meson theory in nuclear physics, particularly in the low energy regime, there are still many challenging questions for exciting future research.

Acknowledgement

I like to express my deep appreciation to F. Sammarruca for inspiring discussions and substantial advice throughout the writing of this article. It is a great pleasure to thank R. Brockmann, Ch. Elster, and K. Holinde for their collaboration on topics reviewed in this paper. Interesting conversations with M. B. Johnson and R. M. Thaler are greatfully acknowledged. I also like to take this opportunity to thank the Los Alamos National Laboratory, in particular the divisions P-15 and LAMPF, for their outstanding hospitality, and their generous permission to use the facilities.

Appendix A

One-Boson-Exchange Potentials

A.1 Interaction Lagrangians and OBE Amplitudes

Lagrangians for meson-nucleon couplings are

$$\mathcal{L}_{ps} = -g_{ps}\bar{\psi}i\gamma^5\psi\varphi^{(ps)} \tag{A.1}$$

$$\mathcal{L}_{pv} = -\frac{f_{ps}}{m_{ps}}\bar{\psi}\gamma^5\gamma^\mu\psi\partial_\mu\varphi^{(ps)} \tag{A.2}$$

$$\mathcal{L}_{s} = +g_{s}\bar{\psi}\psi\varphi^{(s)} \tag{A.3}$$

$$\mathcal{L}_{v} = -g_{v}\bar{\psi}\gamma^\mu\psi\varphi_\mu^{(v)} - \frac{f_v}{4M}\bar{\psi}\sigma^{\mu\nu}\psi(\partial_\mu\varphi_\nu^{(v)} - \partial_\nu\varphi_\mu^{(v)}) \tag{A.4}$$

with ψ the nucleon and $\varphi_{(\mu)}^{(\alpha)}$ the meson fields (notation and conventions as in BD 64, BD 65, IZ 80; see also Section 3.4). For isospin 1 mesons, $\varphi^{(\alpha)}$ is to be replaced by $\tau\cdot\varphi^{(\alpha)}$ with τ^l $(l = 1,2,3)$ the usual Pauli matrices. *ps*, *pv*, *s*, and *v* denote pseudoscalar, pseudovector, scalar, and vector coupling/field, respectively.

The one-boson-exchange potential (OBEP) is defined as a sum of one-particle-exchange amplitudes of certain bosons with given mass and coupling. We use six bosons. Thus,

$$V_{OBEP} = \sum_{\alpha=\pi,\eta,\rho,\omega,\delta,\sigma} V_\alpha^{OBE} \tag{A.5}$$

with π and η pseudoscalar, σ and δ scalar, and ρ and ω vector particles. The contributions from the iso-vector bosons π, δ and ρ are to be multiplied by a factor of $\tau_1 \cdot \tau_2$.

The Lagrangians mentioned lead to the following (off-shell) OBE amplitudes (Fig. 3.5 and Eq. 3.10):[1]

$$\begin{aligned}
\langle \mathbf{q}'\lambda_1'\lambda_2'|V_{ps}^{OBE}|\mathbf{q}\lambda_1\lambda_2\rangle &= -g_{ps}^2\bar{u}(\mathbf{q}',\lambda_1')i\gamma^5 u(\mathbf{q},\lambda_1)\bar{u}(-\mathbf{q}',\lambda_2')i\gamma^5 u(-\mathbf{q},\lambda_2) \\
&\quad /[(\mathbf{q}'-\mathbf{q})^2+m_{ps}^2] \qquad \text{(A.6)} \\
\langle \mathbf{q}'\lambda_1'\lambda_2'|V_{pv}^{OBE}|\mathbf{q}\lambda_1\lambda_2\rangle &= \frac{f_{ps}^2}{m_{ps}^2}\bar{u}(\mathbf{q}',\lambda_1')\gamma^5\gamma^\mu i(q'-q)_\mu u(\mathbf{q},\lambda_1) \\
&\quad \times\bar{u}(-\mathbf{q}',\lambda_2')\gamma^5\gamma^\mu i(q'-q)_\mu u(-\mathbf{q},\lambda_2) \\
&\quad /[(\mathbf{q}'-\mathbf{q})^2+m_{ps}^2] \\
&= f_{ps}^2\frac{4M^2}{m_{ps}^2}\{\bar{u}(\mathbf{q}',\lambda_1')\gamma^5 u(\mathbf{q},\lambda_1)\bar{u}(-\mathbf{q}',\lambda_2')\gamma^5 u(-\mathbf{q},\lambda_2) \\
&\quad +[(E'-E)/(2M)]^2\bar{u}(\mathbf{q}',\lambda_1')\gamma^5\gamma^0 u(\mathbf{q},\lambda_1)\bar{u}(-\mathbf{q}',\lambda_2')\gamma^5\gamma^0 u(-\mathbf{q},\lambda_2) \\
&\quad +[(E'-E)/(2M)][\bar{u}(\mathbf{q}',\lambda_1')\gamma^5 u(\mathbf{q},\lambda_1)\bar{u}(-\mathbf{q}',\lambda_2')\gamma^5\gamma^0 u(-\mathbf{q},\lambda_2) \\
&\quad +\bar{u}(\mathbf{q}',\lambda_1')\gamma^5\gamma^0 u(\mathbf{q},\lambda_1)\bar{u}(-\mathbf{q}',\lambda_2')\gamma^5 u(-\mathbf{q},\lambda_2)]\} \\
&\quad /[(\mathbf{q}'-\mathbf{q})^2+m_{ps}^2] \qquad \text{(A.7)} \\
\langle \mathbf{q}'\lambda_1'\lambda_2'|V_s^{OBE}|\mathbf{q}\lambda_1\lambda_2\rangle &= -g_s^2\bar{u}(\mathbf{q}',\lambda_1')u(\mathbf{q},\lambda_1)\bar{u}(-\mathbf{q}',\lambda_2')u(-\mathbf{q},\lambda_2) \\
&\quad /[(\mathbf{q}'-\mathbf{q})^2+m_s^2] \qquad \text{(A.8)} \\
\langle \mathbf{q}'\lambda_1'\lambda_2'|V_v^{OBE}|\mathbf{q}\lambda_1\lambda_2\rangle &= \{g_v\bar{u}(\mathbf{q}',\lambda_1')\gamma_\mu u(\mathbf{q},\lambda_1) \\
&\quad +\frac{f_v}{2M}\bar{u}(\mathbf{q}',\lambda_1')\sigma_{\mu\nu}i(q'-q)^\nu u(\mathbf{q},\lambda_1)\} \\
&\quad \times\{g_v\bar{u}(-\mathbf{q}',\lambda_2')\gamma^\mu u(-\mathbf{q},\lambda_2) \\
&\quad -\frac{f_v}{2M}\bar{u}(-\mathbf{q}',\lambda_2')\sigma^{\mu\nu}i(q'-q)_\nu u(-\mathbf{q},\lambda_2)\} \\
&\quad /[(\mathbf{q}'-\mathbf{q})^2+m_v^2] \\
&= \{(g_v+f_v)\bar{u}(\mathbf{q}',\lambda_1')\gamma_\mu u(\mathbf{q},\lambda_1) \\
&\quad -\frac{f_v}{2M}\bar{u}(\mathbf{q}',\lambda_1')[(q'+q)_\mu+(E'-E)(g_\mu^0-\gamma_\mu\gamma^0)]u(\mathbf{q},\lambda_1)\} \\
&\quad \times\{(g_v+f_v)\bar{u}(-\mathbf{q}',\lambda_2')\gamma^\mu u(-\mathbf{q},\lambda_2) \\
&\quad -\frac{f_v}{2M}\bar{u}(-\mathbf{q}',\lambda_2')[(q'+q)^\mu+(E'-E)(g^{\mu 0}-\gamma^\mu\gamma^0)]u(-\mathbf{q},\lambda_2)\} \\
&\quad /[(\mathbf{q}'-\mathbf{q})^2+m_v^2] \qquad \text{(A.9)}
\end{aligned}$$

where λ_i (λ_i') denotes the helicity of an incoming (outgoing) nucleon which is defined

[1]Strictly speaking we give here the potential which is defined as i times the Feynman amplitude Eq. (3.10); furthermore, there is a factor of i in each vertex and meson propagator; as $i^4 = 1$, we can ignore these four factors of i.

as the eigenvalue of the operator $\mathbf{s}\cdot\hat{\mathbf{q}}$ with $\mathbf{s}$ the spin operator and $\hat{\mathbf{q}}=\mathbf{q}/|\mathbf{q}|$ the unit momentum operator of the respective nucleon. $E=\sqrt{M^2+\mathbf{q}^2}$ and $E'=\sqrt{M^2+\mathbf{q}'^2}$. The BbS/Thompson choice (see Section 4.1) for the four-momentum transfer is made, i. e. $(q'-q)=(0,\mathbf{q}'-\mathbf{q})$. The Dirac equation is applied repeatedly in the evaluations for the pv-coupling, the Gordon decomposition (BD 64) is used in the case of the v-coupling (for more details concerning these manipulations see (Mac 86, Section 3.4)). Dirac spinors are normalised covariantly,

$$\bar{u}(\mathbf{q},\lambda)u(\mathbf{q},\lambda)=1. \tag{A.10}$$

with $\bar{u}=u^{\dagger}\gamma^0$. The propagator for vector bosons is

$$i\frac{-g_{\mu\nu}+(q'-q)_\mu(q'-q)_\nu/m_v^2}{-(\mathbf{q}'-\mathbf{q})^2-m_v^2} \tag{A.11}$$

where we drop the $(q'-q)_\mu(q'-q)_\nu$-term which vanishes on-shell, anyhow. The off-shell effect of this term was examined in (HM 75) and was found to be unimportant.

The relation to the S-matrix is

$$\langle p_1'p_2'|S|p_1p_2\rangle=\delta^{(3)}(\mathbf{q}'-\mathbf{q})\delta^{(3)}(\mathbf{q}'-\mathbf{q})-i2\pi\delta^{(4)}(p_1'+p_2'-p_1-p_2)\frac{M^2}{E_q^2}\frac{1}{(2\pi)^3}T(\mathbf{q}',\mathbf{q})$$

with p_i $(i=1,2)$ the initial and p_i' the final four momenta of the two interacting nucleons (i. e. with the notation of Section 4.1: $p_{1/2}^{(\prime)}=\frac{1}{2}P\pm q^{(\prime)}$), and with T as in Eqs. (4.15, 4.20),[2] the V in those equations being defined as in Eqs. (A.6-9).

In practise it is desirable to have the potential represented in partial waves, since the phase shifts of scattering are only defined in such terms and nuclear structure calculations are conventionally performed in an LSJ basis. The further formal developments, necessary to arrive at such a partial wave decomposition for the OBE amplitudes, are presented in all details in (MHE 87, Appendix E) for the ps, s and v coupling.[3] The final result for the pv coupling is given in (Mac 86, Appendix A).

A.2 Relativistic Momentum Space OBEP

We give here two examples of relativistic momentum-space OBEP, which have proven useful in applications in nuclear structure physics. One potential is defined within the BbS equation (Section 4.1) and uses the ps coupling for π and η, Table A.1. Together with "minimal relativity" (Section

[2]Note that the letter T is *not* used consistently throughout this paper; while here and in Section 4 it denotes a covariant scattering amplitude, it denotes e. g. in Section 9.4 a non-relativistic T-matrix.

[3]Note that there is an error in in Eq. (E52.b) of (MHE 87) where it should read: ${}^{34}V_{tt}^J=C_{tt}\{-[q'^2+q^2+4E'E]q'qI_J^{(0)}(m_v)-\ldots$

4.1, Eqs. (4.16-18)) it can be applied in non-relativistic nuclear structure physics. The other potential is formulated in the framework of the Thompson equation (Section 4.1) and uses the *pv* coupling for π and η, Table A.2; it is useful for relativistic nuclear structure calculations as outlined in Section 10.5. As in that relativistic approach pair terms (virtual nucleon-antinucleon intermediate states) are taken into account implicitly (Bro+ 87), the *pv* coupling is necessary; the *ps* coupling leads to unphysically large anti-particle contributions (see Mac 86, Section 8.4).

Note that a formfactor

$$\left(\frac{\Lambda_\alpha^2 - m_\alpha^2}{\Lambda_\alpha^2 + (\mathbf{q}' - \mathbf{q})^2} \right)^{n_\alpha} \tag{A.12}$$

is applied to each meson-nucleon vertex. The coupling constants for the two different couplings for *ps* particles are related by

$$g_{ps} = f_{ps} \frac{2M}{m_{ps}}. \tag{A.13}$$

We use units $\hbar = c = 1$ ($\hbar c = 197.3286$ MeV fm). In the tables, we give the parameters for the ($T = 0$ and $T = 1$) neutron-proton potentials for which the average nucleon mass $M = 938.926$ MeV is used. Proton-proton potentials can be obtained by a minor change of the σ coupling constant (of the $T = 1$ potential); e. g. in the case of the potentials of Table A.1, for $g_\sigma^2/4\pi = 8.713, 8.8557, 8.542$ for potential A, B, C, respectively, the proton-proton singlet scattering length $a_{pp}^C = -7.81$ fm is reproduced (including the Coulomb potential and using the proton mass $M = 938.28$ MeV in the scattering equation[4]).

A.3 Coordinate Space Potentials

The momentum space expressions for the OBE amplitudes given in Appendix A.1 depend on two momentum variables, namely the incoming and outgoing relative momenta $\mathbf{q}$ and $\mathbf{q}'$, respectively. A Fourier transformation of these expressions into coordinate space would yield functions of $\mathbf{r}$ and $\mathbf{r}'$,

[4]Note, that in the potential the average nucleon mass is used in all cases. How charge dependence due to meson and baryon mass differences is calculated properly, is discussed in Section 6.

the relative distance between the two in- and out-going nucleons, i. e. a non-local potential. Because of the complexity of the expressions, this Fourier transformation cannot be done analytically. Both features mentioned are rather inconvenient for r-space calculations. Therefore, it is customary to simplify the momentum space expressions such that an analytic Fourier tranformations becomes possible.[5] This is achieved by using Dirac spinors in the representation

$$u(\mathbf{q},s)=\sqrt{\frac{E+M}{2M}}\begin{pmatrix}1\\ \frac{\boldsymbol{\sigma}\cdot\boldsymbol{q}}{E+M}\end{pmatrix}\chi_s \tag{A.14}$$

(with χ_s a Pauli spinor) for the evaluation of the OBE amplitudes of Appendix A.1 and defining two new momentum variables

$$\mathbf{k} = \mathbf{q}'-\mathbf{q} \tag{A.15}$$

$$\mathbf{p} = \frac{1}{2}(\mathbf{q}'+\mathbf{q}). \tag{A.16}$$

By dropping χ_s the resulting potential is a operator in spin space, as customary. The relativistic energies are expanded in powers of $\mathbf{k}^2$ and $\mathbf{p}^2$ keeping the lowest order. In this way one obtaines the following "reduced" momentum space expressions (for more details concerning the derivation see (Mac 86, Section 3.4)):

$$V_{ps}(\mathbf{k}) = -\frac{g_{ps}^2}{4M^2}\frac{(\sigma_1\cdot\mathbf{k})(\sigma_2\cdot\mathbf{k})}{\mathbf{k}^2+m_{ps}^2} \tag{A.17}$$

$$V_s(\mathbf{k},\mathbf{p}) = -\frac{g_s^2}{\mathbf{k}^2+m_s^2}[1-\frac{\mathbf{p}^2}{2M^2}+\frac{\mathbf{k}^2}{8M^2}-\frac{i}{2M^2}\mathbf{S}\cdot(\mathbf{k}\times\mathbf{p})] \tag{A.18}$$

$$\begin{aligned}V_v(\mathbf{k},\mathbf{p}) = {} & \frac{1}{\mathbf{k}^2+m_v^2}\{g_v^2[1+\frac{3\mathbf{p}^2}{2M^2}-\frac{\mathbf{k}^2}{8M^2}+\frac{3i}{2M^2}\mathbf{S}\cdot(\mathbf{k}\times\mathbf{p})\\ & -\sigma_1\cdot\sigma_2\frac{\mathbf{k}^2}{4M^2}+\frac{1}{4M^2}(\sigma_1\cdot\mathbf{k})(\sigma_2\cdot\mathbf{k})]\\ & +\frac{g_v f_v}{2M}[-\frac{\mathbf{k}^2}{M}+\frac{4i}{M}\mathbf{S}\cdot(\mathbf{k}\times\mathbf{p})-\sigma_1\cdot\sigma_2\frac{\mathbf{k}^2}{M}+\frac{1}{M}(\sigma_1\cdot\mathbf{k})(\sigma_2\cdot\mathbf{k}]\\ & +\frac{f_v^2}{4M^2}[-\sigma_1\cdot\sigma_2\mathbf{k}^2+(\sigma_1\cdot\mathbf{k})(\sigma_2\cdot\mathbf{k}]\}\end{aligned} \tag{A.19}$$

where $\mathbf{S}=\frac{1}{2}(\sigma_1+\sigma_2)$ is the total spin of the two-nucleon system.

[5]Note, however, that the relativistic momentum space expressions of Appendix A.1 allow for a more quantitative description of the NN data, particularly, in the case of a weak tensor force potential; this is discussed and demonstrated in (MHE 87, Section 9.2-3).

These expressions contain nonlocalities due to $\mathbf{p}^2$ and $\mathbf{k} \times \mathbf{p}$ terms. The latter leads to the orbital angular momentum operator $\mathbf{L} = -i\mathbf{r} \times \nabla$ in r-space, whereas the former provides ∇^2-terms.

A quadratic spin-orbit term, $\frac{1}{2}\sigma_1 \cdot L\sigma_2 \cdot L + \sigma_2 \cdot L\sigma_1 \cdot L$, is obtained when terms up to the fourth power in the momentum are retained, leading to substantially more comprehensive potential expressions. However, within the type of meson models considered here, this quadratic spin-orbit term as well as the other terms of higher momenta do not improve the fit to the NN data, but cause serious mathematical problems. If substantial improvements over the expressions Eqs. (A.17-19) are desired, we recommend to use the 'complete' momentum space expressions of Appendix A.1. The role of the quadratic spin-orbit term is different if it is used as a phenomenological term to be fitted to the data. Then, particularly, an improvement of the $^1D_2$ and $^3D_2$ phase shifts can be achieved (HJ 62).

The Fourier transform, $V(\mathbf{r}) = (2\pi)^{-3} \int d^3k e^{i\mathbf{k}\cdot\mathbf{r}} V(\mathbf{k})$, which can now be performed analytically, yields (see (Mac 86, Section 3.4) for details):

$$\begin{aligned}
V_{ps}(m_{ps}, \mathbf{r}) &= \frac{1}{12}\frac{g_{ps}^2}{4\pi} m_{ps} \{(\frac{m_{ps}}{M})^2 [Y(m_{ps}r) - \frac{4\pi}{m_{ps}^3}\delta^{(3)}(\mathbf{r})]\sigma_1 \cdot \sigma_2 \\
&\quad + Z(m_{ps}r) S_{12}\} \qquad \text{(A.20)} \\
V_s(m_s, \mathbf{r}) &= -\frac{g_s^2}{4\pi} m_s \{[1 - \frac{1}{4}(\frac{m_s}{M})^2] Y(m_s r) + \frac{1}{4M^2}[\nabla^2 Y(m_s r) + Y(msr)\nabla^2] \\
&\quad + \frac{1}{2} Z_1(m_s r)\mathbf{L}\cdot\mathbf{S}\} \qquad \text{(A.21)} \\
V_v(m_v, \mathbf{r}) &= \frac{g_v^2}{4\pi} m_v \{[1 + \frac{1}{2}(\frac{m_v}{M})^2] Y(m_v r) - \frac{3}{4M^2}[\nabla^2 Y(m_v r) + Y(m_v r)\nabla^2] \\
&\quad + \frac{1}{6}(\frac{m_v}{M})^2 Y(m_v r)\sigma_1 \cdot \sigma_2 - \frac{3}{2} Z_1(m_v r)\mathbf{L}\cdot\mathbf{S} - \frac{1}{12} Z(m_v r) S_{12}\} \\
&\quad + \frac{1}{2}\frac{g_v f_v}{4\pi} m_v \{(\frac{m_v}{M})^2 Y(m_v r) + \frac{2}{3}(\frac{m_v}{M})^2 Y(m_v r)\sigma_1 \cdot \sigma_2 \\
&\quad - 4Z_1(m_v r)\mathbf{L}\cdot\mathbf{S} - \frac{1}{3} Z(m_v r) S_{12}\} \\
&\quad + \frac{f_v^2}{4\pi} m_v \{\frac{1}{6}(\frac{m_v}{M})^2 Y(m_v r)\sigma_1 \cdot \sigma_2 - \frac{1}{12} Z(m_v r) S_{12}\} \qquad \text{(A.22)}
\end{aligned}$$

with

$$\begin{aligned}
Y(x) &= e^{-x}/x \qquad \text{(A.23)} \\
Z(x) &= (\frac{m_\alpha}{M})^2 (1 + \frac{3}{x} + \frac{3}{x^2}) Y(x) \qquad \text{(A.24)} \\
Z_1(x) &= -(\frac{m_\alpha}{M})^2 \frac{1}{x}\frac{d}{dx} Y(x) \\
&= (\frac{m_\alpha}{M})^2 (\frac{1}{x} + \frac{1}{x^2}) Y(x) \qquad \text{(A.25)}
\end{aligned}$$

and

$$S_{12} = 3\frac{(\sigma_1 \cdot r)(\sigma_2 \cdot r)}{r^2} - \sigma_1 \cdot \sigma_2 \tag{A.26}$$

$$\nabla^2 = \frac{1}{r}\frac{\partial^2}{\partial r^2} r - \frac{\mathbf{L}^2}{r^2} \tag{A.27}$$

Similar to the $\sigma_1 \cdot \sigma_2$ part of the *ps* potential, there are $\delta^{(3)}(\mathbf{r})$ function terms in the central force and spin-spin part of the vector potential which we dropped. They can be found in (BS 69). A formfactor, Eq. (A.12), with $n_\alpha = 1$ can be taken into account by using for each meson potential

$$V_\alpha(\mathbf{r}) = V_\alpha(m_\alpha, \mathbf{r}) - \frac{\Lambda_{\alpha,2}^2 - m_\alpha^2}{\Lambda_{\alpha,2}^2 - \Lambda_{\alpha,1}^2} V_\alpha(\Lambda_{\alpha,1}, \mathbf{r}) + \frac{\Lambda_{\alpha,1}^2 - m_\alpha^2}{\Lambda_{\alpha,2}^2 - \Lambda_{\alpha,1}^2} V_\alpha(\Lambda_{\alpha,2}, \mathbf{r}) \tag{A.28}$$

where $\Lambda_{\alpha,1} = \Lambda_\alpha + \epsilon$ and $\Lambda_{\alpha,2} = \Lambda_\alpha - \epsilon$ with $\epsilon/\Lambda_\alpha \ll 1$ ($\epsilon = 10$ MeV is an appropriate choice). Units $\hbar = c = 1$ are used ($\hbar c = 197.3286$ MeV fm). When using a cutoff of the kind described, the $\delta^{(3)}(\mathbf{r})$-function terms drop out.

The effect of a cutoff can be best seen by considering the simple case of $n_\alpha = 1/2$ in Eq. (A.12). The effect of such a cutoff is obtained by simply subtracting from a meson-exchange potential, Eqs. (A.20-22), the same expression with the meson mass replaced by the cutoff mass (using the same coupling constant), i. e. $V_\alpha(\mathbf{r}) = V_\alpha(m_\alpha, \mathbf{r}) - V_\alpha(\Lambda_\alpha, \mathbf{r})$.

The ∇^2-terms, though moderate in size, are important; without them, it is impossible to fit the $^1S_0$ and the $^3P_2$ phase shifts simultaneously. How to solve the r-space Schrödinger equation for a $\mathbf{p}^2$-dependent potential is explained in (BS 69, Sig 69).

The configuration space OBEP given in Table A.3 are defined in terms of the expressions given here. Note, that the potentials due to the exchanges of the iso-vector bosons π, ρ and δ are to be multiplied by a factor of $\tau_1 \cdot \tau_2$ leading to a factor 1 for the $T = 1$ and a factor (-3) for the $T = 0$ potential. The r-space potentials for the different parts of the nuclear force are plotted for the case of Potential *A* in Figs. 3.6-8.

Table A.1: **Relativistic OBEP using the BbS eq. and the ps coupling for π and η.**

		Potential A		*Potential B* [a]		*Potential C*	
	m_α (MeV)	$g_\alpha^2/4\pi$	Λ_α(GeV)	$g_\alpha^2/4\pi$	Λ_α(GeV)	$g_\alpha^2/4\pi$	Λ_α(GeV)
π	138.03	14.7	1.3	14.4	1.7	14.2	3.0
η	548.8	4	1.5	3	1.5	0	-
ρ	769	0.86	1.95	0.9	1.85	1.0	1.7
ω	782.6	25	1.35	24.5	1.85	24	1.4
δ	983	1.3	2.0	2.488	2.0	4.722	2.0
σ [b]	550	8.8	2.0	8.9437	1.9	8.6289	1.7
	(710–720)	(17.194)	(2.0)	(18.3773)	(2.0)	(17.5667)	(2.0)
$-\epsilon_d$ (MeV)		2.22452		2.22461		2.22459	
P_D (%)		4.38		4.99		5.61	
Q_d (fm^2)		0.274 [c]		0.278 [c]		0.281 [c]	
μ_d (μ_N)		0.8548 [c]		0.8514 [c]		0.8478 [c]	
A_S (fm$^{-1/2}$)		0.8867		0.8860		0.8850	
D/S		0.0263		0.0264		0.0266	
r_d (fm)		1.9693		1.9688		1.9674	
a_{np} (fm)		−23.750		−23.750		−23.751	
r_{np} (fm)		2.71		2.71		2.69	
a_t (fm)		5.427		5.424		5.419	
$r_t = \rho(0,0)$ (fm)		1.763		1.761		1.754	

Given are the are meson, deuteron, and low energy parameters.
For notation and other information see Table 4.1 and 4.2.
It is always used: $f_\rho/g_\rho = 6.1$ and $f_\omega/g_\omega = 0.0$.
$n_\alpha = 1$ except $n_\rho = 2$ and $n_\omega(B) = 2$.
[a] Potential presented in Table 4.1.
[b] The σ parameters given in brackets apply to the $T = 0$ NN potential. Potential A uses 710 MeV, B and C 720 MeV for the σ mass.
[c] Meson-exchange current contributions not included.

Table A.2: **Relativistic OBEP using the Thompson eq. and the pv coupling for π and η.**

		Potential A		*Potential B*		*Potential C*	
	m_α (MeV)	$g_\alpha^2/4\pi$	Λ_α(GeV)	$g_\alpha^2/4\pi$	Λ_α(GeV)	$g_\alpha^2/4\pi$	Λ_α(GeV)
π	138.03	14.9	1.05	14.6	1.2	14.6	1.3
η	548.8	7	1.5	5	1.5	3	1.5
ρ	769	0.99	1.3	0.95	1.3	0.95	1.3
ω	782.6	20	1.5	20	1.5	20	1.5
δ	983	0.7709	2.0	3.1155	1.5	5.0742	1.5
σ	550	8.3141	2.0	8.0769	2.0	8.0279	1.8
$-\epsilon_d$ (MeV)		2.22459		2.22468		2.22450	
P_D (%)		4.47		5.10		5.53	
Q_d (fm^2)		0.274 [a]		0.279 [a]		0.283 [a]	
μ_d (μ_N)		0.8543 [a]		0.8507 [a]		0.8482 [a]	
A_S (fm$^{-1/2}$)		0.8984		0.8968		0.8971	
D/S		0.0255		0.0257		0.0260	
a_{np} (fm)		-23.752		-23.747		-23.740	
r_{np} (fm)		2.69		2.67		2.66	
a_t (fm)		5.482		5.474		5.475	
$r_t = \rho(0,0)$ (fm)		1.829		1.819		1.821	

Given are the meson, deuteron, and low energy parameters.
For notation and other information see Table 4.1 and 4.2.
It is always used: $f_\rho/g_\rho = 6.1$, $f_\omega/g_\omega = 0.0$, and $n_\sigma = 1$.
[a] Meson-exchange current contributions not included.

Table A.3: **Non-relativistic configuration space OBEP.**

		Potential A		*Potential B*	
	m_α (MeV)	$g_\alpha^2/4\pi$	Λ_α(GeV)	$g_\alpha^2/4\pi$	Λ_α(GeV)
π	138.03	14.9	1.3	14.9	2.0
η	548.8	2	1.5	0	–
ρ	769	1.2	1.2	1.7	1.1
ω	782.6	25	1.4	28	1.3
δ	983	2.742	2.0	6.729	2.0
σ^a	550	8.7171	2.0	8.8322	1.4
	(700-710)	(17.6205)	(2.0)	(16.0707)	(2.0)
$-\epsilon_d$ (MeV)		2.2246		2.2246	
P_D (%)		4.75		5.53	
Q_d (fm^2)		0.274 [b]		0.279 [b]	
μ_d (μ_N)		0.8527 [b]		0.8483 [b]	
A_S (fm$^{-1/2}$)		0.8865		0.8860	
D/S		0.0259		0.0263	
a_{np} (fm)		-23.75		-23.75	
r_{np} (fm)		2.69		2.70	
a_t (fm)		5.425		5.423	
$r_t = \rho(0,0)$ (fm)		1.762		1.758	

Given are the meson, deuteron, and low energy parameters.
For notation and other information see Table 4.1 and 4.2.
It is always used: $f_\rho/g_\rho = 6.1$, $f_\omega/g_\omega = 0.0$, and $n_\alpha = 1$.
[a]The σ parameters given in brackets apply to the $T = 0$
NN potential. Potential A uses 710 and B uses 700 MeV for the σ mass.
[b] Meson-exchange current contributions not included.

Appendix B

Models Including Isobar Degrees of Freedom

Interactions between N, Δ, π and ρ are given by the following interaction Lagrangians

$$\mathcal{L}_{N\Delta\pi} = -\frac{f_{N\Delta\pi}}{m_\pi}\bar{\psi}\mathbf{T}\psi^\mu\partial_\mu\varphi^{(\pi)} + h.c. \tag{B.1}$$

$$\mathcal{L}_{N\Delta\rho} = i\frac{f_{N\Delta\rho}}{m_\rho}\bar{\psi}\gamma^5\gamma^\mu\mathbf{T}\psi^\nu(\partial_\mu\varphi_\nu^{(\rho)} - \partial_\nu\varphi_\mu^{(\rho)}) + h.c. \tag{B.2}$$

where ψ_μ is the Rarita-Schwinger field (RS 41b, Lur 68, Dum+ 83) describing the (spin $\frac{3}{2}$) Δ-isobar and $\mathbf{T}$ the isospin transition operator; $h.c.$ stands for hermitean conjugate. $\Delta\Delta$ vertices are disregarded in view of the uncertainties about their form.

The relativistic transition potentials involved in the coupled channel, Eq. (7.3), are determined by these interaction Lagrangians and those of Appendix A.1. For the $NN \to NN$ transition they are given in Appendix A.1. The other two relativistic transition potential, namely $NN \to N\Delta$ and $NN \to \Delta\Delta$, are derived explicitly in (HM 77) for π exchange, and in (Hol+ 78) for ρ exchange. Here, we give three examples of coupled channel models (Table B.1). Model I (which uses relativistic transition potentials) is similar to (HM 77), however with the following extensions: firstly, it includes (besides the pion) also ρ exchange; secondly, in the meson propagators, it takes the mass difference between nucleon and isobar properly into account (see below); and finally, it includes the width of the Δ as given

by the imaginary part of the Δ self-energy (Fig. 7.4b) which produces the inelasticity in these models. Model II is similar, however, uses Thompson-type of relativistic two-baryon propagators and applies the *pv* coupling for π and η.

Model III uses the non-relativistic reductions of the transition potentials. These can be obtained in analogy to the considerations for the $NN \to NN$ transition potentials of Appendix A.3. They are as follows (notation as in Eq. (7.3)) [from (Els 86); cf. (SH 68), (NGS 79), (Dym+ 88)]:

$NN \to N\Delta$:

$$V_{12}^{(\pi)} = -\frac{g_\pi f_{N\Delta\pi}}{2Mm_\pi}(\sigma_1\cdot\mathbf{k})(\mathbf{S}_2\cdot\mathbf{k})\{\frac{1}{2\omega_\pi^2}+\frac{1}{2\omega_\pi(M_\Delta-M+\omega_\pi}\}\tau_1\cdot\mathbf{T}_2 \quad \text{(B.3)}$$

$$\begin{aligned} V_{12}^{(\rho)} = & -\{\frac{(g_\rho+f_\rho)f_{N\Delta\rho}}{2Mm_\rho}(\sigma_1\times\mathbf{k})\cdot(\mathbf{S}_2\times\mathbf{k}) \\ & +\frac{g_\rho f_{N\Delta\rho}}{m_\rho}[4i\mathbf{S}_2\cdot(\mathbf{k}\times\mathbf{p})-(\sigma_2\times\mathbf{k})\cdot(\mathbf{S}_2\times\mathbf{k})]\} \\ & \{\frac{1}{2\omega_\rho^2}+\frac{1}{2\omega_\rho(M_\Delta-M+\omega_\rho}\}\tau_1\cdot\mathbf{T}_2 \end{aligned} \quad \text{(B.4)}$$

$NN \to \Delta\Delta$:

$$V_{13}^{(\pi)} = -\frac{f_{N\Delta\pi}^2}{m_\pi^2}\frac{(\mathbf{S}_1\cdot\mathbf{k})(\mathbf{S}_2\cdot\mathbf{k})}{\omega_\pi(M_\Delta-M+\omega_\pi)}\mathbf{T}_1\cdot\mathbf{T}_2 \quad \text{(B.5)}$$

$$V_{13}^{(\rho)} = -\frac{f_{N\Delta\rho}^2}{m_\rho^2}\frac{(\mathbf{S}_1\times\mathbf{k})\cdot(\mathbf{S}_2\times\mathbf{k})}{\omega_\rho(M_\Delta-M+\omega_\rho)}\mathbf{T}_1\cdot\mathbf{T}_2 \quad \text{(B.6)}$$

where $\mathbf{S}_i$ and $\mathbf{T}_i$ are appropriate spin and isospin transition operators between nucleon and Δ states [see (BW 75, SP 76)], $\omega_\alpha = \sqrt{m_\alpha^2+\mathbf{k}^2}$, and M_Δ(=1232 MeV) denotes the mass of the Δ-isobar.

The analogy between, in particular, the transition potentials Eq. (B.5-6) and the π and ρ $NN \to NN$ potentials discussed in Section 3.4 is obvious. Note, however, that the second term in Eq. (B.4), which deviates from the simple sceme, is important for a quantitative model (Els 86).

The meson propagators given in Eqs. (B.3-6) (which are also used for Model I and II) can be understood in terms of time-ordered perturbation theory neglecting the kinetic energies of the baryons (Hol+ 78,Dur+ 77). The main point is that the mass difference between nucleon and Δ enters the propagator; this is important to obtain a realistic size and range for these transition potentials (Hol+ 78).

In spite of the differences between the three models, the predictions are very similar. Results obtained using Model I are shown in Section 7.

Table B.1: **Coupled channel models for the NN interaction.**

		Model I		*Model II*		*Model III*	
	m_α (MeV)	$g_\alpha^2/4\pi$ or $f_{N\Delta\alpha}^2/4\pi$	Λ_α(GeV)	$g_\alpha^2/4\pi$ or $f_{N\Delta\alpha}^2/4\pi$	Λ_α(GeV)	$g_\alpha^2/4\pi$ or $f_{N\Delta\alpha}^2/4\pi$	Λ_α(GeV
$NN\pi$	138.03	14.4	1.8	14.4	1.6	14.6	1.6
$NN\eta$	548.8	5	2.0	2	1.5	0	-
$NN\rho$	769	0.7	2.2	1.1	1.3	0.9	1.4
$NN\omega$	782.6	22	2.2	23	1.5	24	1.55
$NN\sigma$ [a]	550	4.13	2.0	3.7 [b]	1.5	5.685	2.0
	(550)	(6.32)	(1.5)	(2.5) [b]	(1.5)	(6.1692)	(2.0)
$N\Delta\pi$	138.03	0.35	0.85	0.35	0.9	0.35	0.8
$N\Delta\rho$	769	19	1.3	20.45	1.4	20.45	1.35
$-\epsilon_d$ (MeV)		2.225				2.2245	
P_D (%)		4.92				4.87	
Q_d (fm^2)		0.284 [c]				0.278 [c]	
A_S (fm$^{-1/2}$)		0.8973				0.8954	
D/S		0.0264				0.0257	
a_{np} (fm)		−23.77				−23.78	
r_{np} (fm)		2.70				2.71	
a_t (fm)		5.47				5.46	
$r_t = \rho(0,0)$ (fm)		1.82				1.82	

Given are the are meson, deuteron, and low energy parameters.
It is always used: $f_\rho/g_\rho = 6.1$ and $f_\omega/g_\omega = 0.0$; $M_\Delta = 1232$ MeV.
$n_\alpha = 1$ except $n_{NN\rho}(I) = 2$, $n_\omega(I) = 2$, $n_{N\Delta\rho} = 2$
[a] The σ parameters given in brackets apply to the $T = 0$ NN potential.
[b] Model II uses $m_\sigma = 500$ MeV for $T = 1$ and $m_\sigma = 450$ MeV for $T = 0$.
[c] Meson-exchange current contributions not included.

Appendix C

Deuteron Wave Functions

In this Appendix we present the deuteron wave functions considered in Section 4.2 and shown in Fig. 4.5. The three meson-theoretic potentials which generate these wave functions, denoted by A, B, and C, are defined in Appendix A, Table A.1. They are discussed in Section 4.2. In Table C.1-3 numerical values are given. As customary, $u(r)$ denotes the S-wave, and $w(r)$ the D-wave. The normalization is

$$\int_0^\infty dr[u^2(r) + w^2(r)] = 1. \tag{C.1}$$

Table C.4 presents the coefficients of the following parametrization of the waves (cf. Lac+ 81, MHE 87). The ansatz for the analytic version of the r-space wave functions is

$$u_a(r) = \sum_{j=1}^{n} C_j \exp(-m_j r) \tag{C.2}$$

$$w_a(r) = \sum_{j=1}^{n} D_j \exp(-m_j r)(1 + \frac{3}{m_j r} + \frac{3}{(m_j r)^2}). \tag{C.3}$$

The corresponding momentum space wave functions are

$$\psi_0^a(q) = (2/\pi)^{1/2} \sum_{j=1}^{n} \frac{C_j}{q^2 + m_j^2} \tag{C.4}$$

$$\psi_2^a(q) = (2/\pi)^{1/2} \sum_{j=1}^{n} \frac{D_j}{q^2 + m_j^2} \tag{C.5}$$

with the normalization

$$\int_0^\infty q^2 dq[\psi_0^2(q) + \psi_2^2(q)] = 1. \tag{C.6}$$

The boundary conditions $u_a(r) \to r$ and $w_a(r) \to r^3$ as $r \to 0$ lead to one constraint for the C_j and three constraints for the D_j, namely

$$C_n = -\sum_{j=1}^{n-1} C_j \tag{C.7}$$

$$D_{n-2} = \frac{m_{n-2}^2}{(m_n^2 - m_{n-2}^2)(m_{n-1}^2 - m_{n-2}^2)}[-m_{n-1}^2 m_n^2 \sum_{j=1}^{n-3} \frac{D_j}{m_j^2} + (m_{n-1}^2 + m_n^2) \sum_{j=1}^{n-3} D_j - \sum_{j=1}^{n-3} D_j m_j^2] \tag{C.8}$$

and two other relations obtained by circular permutation of $n-2, n-1, n$. The masses are

$$m_j = \alpha + (j-1)m_0 \tag{C.9}$$

with $m_0 = 0.9$ fm^{-1} and $\alpha = (-\epsilon_d M)^{1/2} = 0.231607$ fm^{-1}.

Note that the parametrization is not very accurate for the D-waves for $r \lesssim 0.5$ fm. If it is expected that results might depend sensitively on the very short range part of the wave function, we recommend to use the numerical values as given in the Tables together with a cubic spline interpolation for $r \lesssim 1$ fm, and the analytic form for the larger r.

Data files for the deuteron wave functions in r-space as well as in *momentum space* can be obtained from the author upon request.

Table C.1: Coordinate-space deuteron wave functions as predicted by Potential A ($P_D = 4.38\%$)

r (fm)	$u(r)$ (fm$^{-1/2}$)	$w(r)$ (fm$^{-1/2}$)	r (fm)	$u(r)$ (fm$^{-1/2}$)	$w(r)$ (fm$^{-1/2}$)
$0.100E-01$	$0.312629E-02$	$0.453076E-05$	$0.270E+01$	$0.457820E+00$	$0.108156E+00$
$0.200E-01$	$0.623445E-02$	$0.215223E-04$	$0.280E+01$	$0.449130E+00$	$0.103666E+00$
$0.300E-01$	$0.933791E-02$	$0.243627E-04$	$0.290E+01$	$0.440381E+00$	$0.992917E-01$
$0.400E-01$	$0.124566E-01$	$-0.535776E-05$	$0.300E+01$	$0.431613E+00$	$0.950588E-01$
$0.500E-01$	$0.155832E-01$	$-0.360107E-04$	$0.320E+01$	$0.414161E+00$	$0.870387E-01$
$0.600E-01$	$0.186992E-01$	$-0.355240E-04$	$0.340E+01$	$0.396980E+00$	$0.796134E-01$
$0.700E-01$	$0.218061E-01$	$-0.221069E-04$	$0.360E+01$	$0.380185E+00$	$0.728083E-01$
$0.800E-01$	$0.249184E-01$	$-0.283813E-04$	$0.380E+01$	$0.363863E+00$	$0.666074E-01$
$0.900E-01$	$0.280402E-01$	$-0.538002E-04$	$0.400E+01$	$0.348079E+00$	$0.609550E-01$
$0.100E+00$	$0.311678E-01$	$-0.821464E-04$	$0.420E+01$	$0.332846E+00$	$0.558184E-01$
$0.200E+00$	$0.633506E-01$	$-0.618530E-03$	$0.440E+01$	$0.318176E+00$	$0.511621E-01$
$0.300E+00$	$0.996283E-01$	$-0.151511E-02$	$0.460E+01$	$0.304087E+00$	$0.469387E-01$
$0.400E+00$	$0.143027E+00$	$-0.160713E-02$	$0.480E+01$	$0.290569E+00$	$0.431054E-01$
$0.500E+00$	$0.193963E+00$	$0.144879E-02$	$0.500E+01$	$0.277602E+00$	$0.396233E-01$
$0.600E+00$	$0.249389E+00$	$0.102994E-01$	$0.520E+01$	$0.265180E+00$	$0.364640E-01$
$0.700E+00$	$0.304556E+00$	$0.257612E-01$	$0.540E+01$	$0.253295E+00$	$0.335964E-01$
$0.800E+00$	$0.355345E+00$	$0.461007E-01$	$0.560E+01$	$0.241924E+00$	$0.309864E-01$
$0.900E+00$	$0.399332E+00$	$0.682102E-01$	$0.580E+01$	$0.231044E+00$	$0.286063E-01$
$0.100E+01$	$0.435599E+00$	$0.892498E-01$	$0.600E+01$	$0.220640E+00$	$0.264365E-01$
$0.110E+01$	$0.464220E+00$	$0.107427E+00$	$0.650E+01$	$0.196609E+00$	$0.218149E-01$
$0.120E+01$	$0.485855E+00$	$0.121929E+00$	$0.700E+01$	$0.175159E+00$	$0.181022E-01$
$0.130E+01$	$0.501436E+00$	$0.132646E+00$	$0.750E+01$	$0.156038E+00$	$0.151155E-01$
$0.140E+01$	$0.511922E+00$	$0.139912E+00$	$0.800E+01$	$0.138991E+00$	$0.126790E-01$
$0.150E+01$	$0.518216E+00$	$0.144256E+00$	$0.850E+01$	$0.123804E+00$	$0.106941E-01$
$0.160E+01$	$0.521129E+00$	$0.146213E+00$	$0.900E+01$	$0.110272E+00$	$0.905039E-02$
$0.170E+01$	$0.521350E+00$	$0.146269E+00$	$0.950E+01$	$0.982167E-01$	$0.769707E-02$
$0.180E+01$	$0.519432E+00$	$0.144865E+00$	$0.100E+02$	$0.874799E-01$	$0.656231E-02$
$0.190E+01$	$0.515822E+00$	$0.142380E+00$	$0.105E+02$	$0.779144E-01$	$0.561693E-02$
$0.200E+01$	$0.510890E+00$	$0.139110E+00$	$0.110E+02$	$0.693956E-01$	$0.482034E-02$
$0.210E+01$	$0.504934E+00$	$0.135277E+00$	$0.115E+02$	$0.618084E-01$	$0.414548E-02$
$0.220E+01$	$0.498184E+00$	$0.131055E+00$	$0.120E+02$	$0.550486E-01$	$0.357714E-02$
$0.230E+01$	$0.490820E+00$	$0.126587E+00$	$0.125E+02$	$0.490305E-01$	$0.309007E-02$
$0.240E+01$	$0.482993E+00$	$0.121990E+00$	$0.130E+02$	$0.436690E-01$	$0.267516E-02$
$0.250E+01$	$0.474821E+00$	$0.117353E+00$	$0.135E+02$	$0.388928E-01$	$0.232197E-02$
$0.260E+01$	$0.466404E+00$	$0.112730E+00$	$0.140E+02$	$0.346412E-01$	$0.201589E-02$

Table C.2: **Coordinate-space deuteron wave functions as predicted by Potential B^a ($P_D = 4.99\%$)**

r (fm)	u(r) ($fm^{-1/2}$)	w(r) ($fm^{-1/2}$)	r (fm)	u(r) ($fm^{-1/2}$)	w(r) ($fm^{-1/2}$)
$0.100E-01$	$0.248747E-02$	$-0.121840E-05$	$0.270E+01$	$0.457732E+00$	$0.110141E+00$
$0.200E-01$	$0.498888E-02$	$-0.451294E-05$	$0.280E+01$	$0.449022E+00$	$0.105426E+00$
$0.300E-01$	$0.749977E-02$	$0.195145E-05$	$0.290E+01$	$0.440256E+00$	$0.100859E+00$
$0.400E-01$	$0.100120E-01$	$0.268024E-04$	$0.300E+01$	$0.431474E+00$	$0.964540E-01$
$0.500E-01$	$0.125335E-01$	$0.603922E-04$	$0.320E+01$	$0.414000E+00$	$0.881510E-01$
$0.600E-01$	$0.150791E-01$	$0.926672E-04$	$0.340E+01$	$0.396803E+00$	$0.805192E-01$
$0.700E-01$	$0.176519E-01$	$0.131441E-03$	$0.360E+01$	$0.379996E+00$	$0.735507E-01$
$0.800E-01$	$0.202476E-01$	$0.189509E-03$	$0.380E+01$	$0.363669E+00$	$0.672180E-01$
$0.900E-01$	$0.228683E-01$	$0.267567E-03$	$0.400E+01$	$0.347882E+00$	$0.614679E-01$
$0.100E+00$	$0.255204E-01$	$0.360556E-03$	$0.420E+01$	$0.332648E+00$	$0.562521E-01$
$0.200E+00$	$0.544739E-01$	$0.227801E-02$	$0.440E+01$	$0.317979E+00$	$0.515285E-01$
$0.300E+00$	$0.896657E-01$	$0.642302E-02$	$0.460E+01$	$0.303893E+00$	$0.472533E-01$
$0.400E+00$	$0.132646E+00$	$0.134377E-01$	$0.480E+01$	$0.290380E+00$	$0.433787E-01$
$0.500E+00$	$0.182917E+00$	$0.241044E-01$	$0.500E+01$	$0.277417E+00$	$0.398610E-01$
$0.600E+00$	$0.237756E+00$	$0.388570E-01$	$0.520E+01$	$0.265000E+00$	$0.366712E-01$
$0.700E+00$	$0.293108E+00$	$0.571739E-01$	$0.540E+01$	$0.253122E+00$	$0.337795E-01$
$0.800E+00$	$0.345058E+00$	$0.774000E-01$	$0.560E+01$	$0.241757E+00$	$0.311497E-01$
$0.900E+00$	$0.390843E+00$	$0.973815E-01$	$0.580E+01$	$0.230882E+00$	$0.287515E-01$
$0.100E+01$	$0.429071E+00$	$0.115299E+00$	$0.600E+01$	$0.220483E+00$	$0.265665E-01$
$0.110E+01$	$0.459489E+00$	$0.130064E+00$	$0.650E+01$	$0.196469E+00$	$0.219159E-01$
$0.120E+01$	$0.482600E+00$	$0.141282E+00$	$0.700E+01$	$0.175032E+00$	$0.181821E-01$
$0.130E+01$	$0.499293E+00$	$0.149052E+00$	$0.750E+01$	$0.155924E+00$	$0.151801E-01$
$0.140E+01$	$0.510570E+00$	$0.153769E+00$	$0.800E+01$	$0.138889E+00$	$0.127322E-01$
$0.150E+01$	$0.517408E+00$	$0.155946E+00$	$0.850E+01$	$0.123713E+00$	$0.107381E-01$
$0.160E+01$	$0.520681E+00$	$0.156081E+00$	$0.900E+01$	$0.110189E+00$	$0.908734E-02$
$0.170E+01$	$0.521124E+00$	$0.154625E+00$	$0.950E+01$	$0.981434E-01$	$0.772802E-02$
$0.180E+01$	$0.519335E+00$	$0.151971E+00$	$0.100E+02$	$0.874143E-01$	$0.658879E-02$
$0.190E+01$	$0.515795E+00$	$0.148447E+00$	$0.105E+02$	$0.778557E-01$	$0.563937E-02$
$0.200E+01$	$0.510897E+00$	$0.144308E+00$	$0.110E+02$	$0.693432E-01$	$0.483954E-02$
$0.210E+01$	$0.504948E+00$	$0.139748E+00$	$0.115E+02$	$0.617616E-01$	$0.416208E-02$
$0.220E+01$	$0.498191E+00$	$0.134921E+00$	$0.120E+02$	$0.550067E-01$	$0.359126E-02$
$0.230E+01$	$0.490811E+00$	$0.129948E+00$	$0.125E+02$	$0.489931E-01$	$0.310235E-02$
$0.240E+01$	$0.482963E+00$	$0.124924E+00$	$0.130E+02$	$0.436356E-01$	$0.268581E-02$
$0.250E+01$	$0.474771E+00$	$0.119919E+00$	$0.135E+02$	$0.388630E-01$	$0.233112E-02$
$0.260E+01$	$0.466335E+00$	$0.114981E+00$	$0.140E+02$	$0.346145E-01$	$0.202388E-02$

[a] Model presented in Section 4, Table 4.1 and 4.2.

Table C.3: Coordinate-space deuteron wave functions as predicted by Potential C ($P_D = 5.61\%$)

r (fm)	$u(r)$ (fm$^{-1/2}$)	$w(r)$ (fm$^{-1/2}$)	r (fm)	$u(r)$ (fm$^{-1/2}$)	$w(r)$ (fm$^{-1/2}$)
$0.100E-01$	$0.155081E-02$	$-0.989515E-07$	$0.270E+01$	$0.457320E+00$	$0.111875E+00$
$0.200E-01$	$0.312905E-02$	$0.462824E-05$	$0.280E+01$	$0.448612E+00$	$0.106979E+00$
$0.300E-01$	$0.473514E-02$	$0.334749E-04$	$0.290E+01$	$0.439847E+00$	$0.102253E+00$
$0.400E-01$	$0.636350E-02$	$0.101252E-03$	$0.300E+01$	$0.431066E+00$	$0.977074E-01$
$0.500E-01$	$0.803105E-02$	$0.201915E-03$	$0.320E+01$	$0.413596E+00$	$0.891696E-01$
$0.600E-01$	$0.976340E-02$	$0.327973E-03$	$0.340E+01$	$0.396405E+00$	$0.813642E-01$
$0.700E-01$	$0.115683E-01$	$0.490328E-03$	$0.360E+01$	$0.379604E+00$	$0.742564E-01$
$0.800E-01$	$0.134417E-01$	$0.704392E-03$	$0.380E+01$	$0.363286E+00$	$0.678096E-01$
$0.900E-01$	$0.153874E-01$	$0.971753E-03$	$0.400E+01$	$0.347510E+00$	$0.619733E-01$
$0.100E+00$	$0.174154E-01$	$0.128722E-02$	$0.420E+01$	$0.332287E+00$	$0.566870E-01$
$0.200E+00$	$0.428078E-01$	$0.709098E-02$	$0.440E+01$	$0.317630E+00$	$0.519027E-01$
$0.300E+00$	$0.778107E-01$	$0.172099E-01$	$0.460E+01$	$0.303557E+00$	$0.475796E-01$
$0.400E+00$	$0.121760E+00$	$0.308644E-01$	$0.480E+01$	$0.290056E+00$	$0.436661E-01$
$0.500E+00$	$0.172999E+00$	$0.474082E-01$	$0.500E+01$	$0.277106E+00$	$0.401147E-01$
$0.600E+00$	$0.228631E+00$	$0.660273E-01$	$0.520E+01$	$0.264701E+00$	$0.368956E-01$
$0.700E+00$	$0.284808E+00$	$0.856365E-01$	$0.540E+01$	$0.252835E+00$	$0.339801E-01$
$0.800E+00$	$0.337741E+00$	$0.104868E+00$	$0.560E+01$	$0.241483E+00$	$0.313303E-01$
$0.900E+00$	$0.384628E+00$	$0.122385E+00$	$0.580E+01$	$0.230619E+00$	$0.289139E-01$
$0.100E+01$	$0.423964E+00$	$0.137187E+00$	$0.600E+01$	$0.220231E+00$	$0.267135E-01$
$0.110E+01$	$0.455405E+00$	$0.148762E+00$	$0.650E+01$	$0.196243E+00$	$0.220322E-01$
$0.120E+01$	$0.479404E+00$	$0.157050E+00$	$0.700E+01$	$0.174830E+00$	$0.182758E-01$
$0.130E+01$	$0.496821E+00$	$0.162280E+00$	$0.750E+01$	$0.155745E+00$	$0.152565E-01$
$0.140E+01$	$0.508667E+00$	$0.164866E+00$	$0.800E+01$	$0.138728E+00$	$0.127957E-01$
$0.150E+01$	$0.515943E+00$	$0.165280E+00$	$0.850E+01$	$0.123570E+00$	$0.107909E-01$
$0.160E+01$	$0.519542E+00$	$0.163968E+00$	$0.900E+01$	$0.110062E+00$	$0.913184E-02$
$0.170E+01$	$0.520218E+00$	$0.161324E+00$	$0.950E+01$	$0.980302E-01$	$0.776546E-02$
$0.180E+01$	$0.518594E+00$	$0.157698E+00$	$0.100E+02$	$0.873134E-01$	$0.662081E-02$
$0.190E+01$	$0.515171E+00$	$0.153371E+00$	$0.105E+02$	$0.777659E-01$	$0.566662E-02$
$0.200E+01$	$0.510352E+00$	$0.148560E+00$	$0.110E+02$	$0.692633E-01$	$0.486288E-02$
$0.210E+01$	$0.504456E+00$	$0.143437E+00$	$0.115E+02$	$0.616904E-01$	$0.418223E-02$
$0.220E+01$	$0.497730E+00$	$0.138140E+00$	$0.120E+02$	$0.549433E-01$	$0.360850E-02$
$0.230E+01$	$0.490372E+00$	$0.132774E+00$	$0.125E+02$	$0.489367E-01$	$0.311731E-02$
$0.240E+01$	$0.482537E+00$	$0.127414E+00$	$0.130E+02$	$0.435853E-01$	$0.269878E-02$
$0.250E+01$	$0.474353E+00$	$0.122118E+00$	$0.135E+02$	$0.388182E-01$	$0.234231E-02$
$0.260E+01$	$0.465921E+00$	$0.116928E+00$	$0.140E+02$	$0.345747E-01$	$0.203364E-02$

Table C.4: **Coefficients for the parametrized deuteron wave functions.** ($n = 11$)

	j	C_j ($\mathrm{fm}^{-1/2}$)	D_j ($\mathrm{fm}^{-1/2}$)
Potential A ($P_D = 4.38$ %) :			
	1	$0.88681402E+00$	$0.23345605E-01$
	2	$-0.27176295E+00$	$-0.57467557E+00$
	3	$-0.38234310E+00$	$0.92159360E+00$
	4	$-0.97399200E+01$	$-0.10072048E+02$
	5	$0.57873078E+02$	$0.21821344E+02$
	6	$-0.21112738E+03$	$-0.34389664E+01$
	7	$0.42789416E+03$	$-0.20707396E+02$
	8	$-0.46272723E+03$	$0.12048237E+02$
	9	$0.25255966E+03$	$-0.18001970E+01$ [b]
	10	$-0.54964903E+02$	$0.43849351E+01$ [b]
	11	$-0.17829662E-03$ [b]	$-0.26061724E+01$ [b]
Potential B ($P_D = 4.99\%$) [a] :			
	1	$0.88611410E+00$	$0.23437728E-01$
	2	$-0.24885006E+00$	$-0.54666750E+00$
	3	$-0.88346659E+00$	$0.51669408E+00$
	4	$-0.46847106E+01$	$-0.73905273E+01$
	5	$0.34755263E+02$	$0.16323355E+02$
	6	$-0.16379524E+03$	$-0.34932110E+01$
	7	$0.38880024E+03$	$-0.12845278E+02$
	8	$-0.46566577E+03$	$0.74194734E+01$
	9	$0.27495507E+03$	$-0.95760909E+00$ [b]
	10	$-0.64119028E+02$	$0.23154287E+01$ [b]
	11	$0.37567807E-03$ [b]	$-0.13651060E+01$ [b]
Potential C ($P_D = 5.61\%$) :			
	1	$0.88507948E+00$	$0.23550301E-01$
	2	$-0.24105451E+00$	$-0.52404123E+00$
	3	$-0.10338683E+01$	$0.15311637E+00$
	4	$-0.29885428E+01$	$-0.50123809E+01$
	5	$0.25258598E+02$	$0.11340227E+02$
	6	$-0.13992344E+03$	$-0.23474968E+01$
	7	$0.36051215E+03$	$-0.81817727E+01$
	8	$-0.45277411E+03$	$0.45534069E+01$
	9	$0.27676633E+03$	$-0.63335941E+00$ [b]
	10	$-0.66461680E+02$	$0.15305094E+01$ [b]
	11	$0.54330150E-03$ [b]	$-0.90175846E+00$ [b]

[a] Model presented in Section 4, Table 4.1 and 4.2.
[b] To obtain a higher numerical accuracy for small r, the last C_j and the last three D_j can be computed from Eq. (C.7) and (C.8), respectively.

References

[Aar 77] R. Aaron, in *Modern Three-Hadron Physics* (A. W. Thomas, ed.), Ch. 5, Springer, Berlin (1977).

[AAY 68] R. Aaron, R. D. Amado, and J. E. Young, *Phys. Rev.* **174**, 2022 (1968).

[Abe+ 86] R. Abegg, D. Bandyopadhyay, J Birchall, E. W. Cairns, H. Coombes, C. A. Davis, N. E. Davison, P. P. J. Delheij, P. W. Green, L. G. Greeniaus, H. P. Gubler, D. C. Healey, C. Lapointe, W. P. Lee, W. J. McDonald, C. A. Miller, G. A. Moss, G. R. Plattner, P. R. Poffenberger, W. D. Ramsay, G. Roy, J. Soukup, J. P. Svenne, R. Tkachuk, W. T. H. van Oers, G. D. Wait, and Y. P. Zhang, *Phys. Rev. Lett.* **56**, 2571 (1986).

[ACS 70] I. R. Afnan, D. M. Clement, and F. J. D. Serduke, *Nucl. Phys.* **A170**, 625 (1970).

[AF 77] H. Arenhövel and W. Fabian, *Nucl. Phys.* **A282**, 397 (1977).

[Ain+ 87] T. L. Ainsworth, E. Baron, G. E. Brown, J. Cooperstein, and M. Prakash, *Nucl. Phys.* **A464**, 740 (1987).

[ALV 60] D. Amati, E. Leader, and B. Vitale, *Nuovo Cim.* **17**, 68; **18**, 409, 458 (1960).

[ALV 63] D. Amati, E. Leader, and B. Vitale, *Phys. Rev.* **130**, 750 (1963).

[AM 83] Y. Avishai and T. Mizutani, *Phys. Rev. C* **27**, 312 (1983).

[Ana+ 78] M. R. Anastasio, A. Faessler, H. Müther, K. Holinde, and R. Machleidt, *Phys. Rev. C* **18**, 2416 (1978).

[Ana+ 79] M. R. Anastasio, A. Faessler, H. Müther, K. Holinde, and R. Machleidt, *Nucl. Phys.* **A322**, 369 (1979).

[Ana+ 83] M. R. Anastasio, L. S. Celenza, W. S. Pong, and C. M. Shakin, *Phys. Reports* **100**, 327 (1983).

[Arn 87] R. A. Arndt, *Interactive Dial-in Program SAID*, version of Fall 1987.

[Arn+ 83] R. A. Arndt, L. D. Roper, R. A. Bryan, R. B. Clark, B. J. VerWest, and P. Signell, *Phys. Rev. D* **28**, 97 (1983).

[AT 74] I. R. Afnan and A. W. Thomas, *Phys. Rev. C* **10**, 109 (1974).

[Aue+ 77] I. P. Auer, E. Colton, D. Hill, K. Nield, B. Sandler, H. Spinka, Y. Watanabe, A. Yokosawa, and A. Beretvas, *Phys. Lett.* **67B**, 113; **70B**, 475 (1977).

[Aue+ 78] I. P. Auer, E. Colton, H. Halpern, D. Hill, H. Spinka, G. Theodosiou, D. Underwood Y. Watanabe, and A. Yokosawa, *Phys. Rev. Lett.* **41**, 354 (1978).

[BA 81] B. Blankleider and I. R. Afnan, *Phys. Rev. C* **23**, 1384; *C* **24**, 1572 (1981).

[Ban 75] M. K. Banerjee, *Electromagnetic Interactions of Nucleons*, University of Maryland Technical Report 75-050 (1975).

[Bar+ 82] J. Bartel, P. Quentin, M. Brack, C. Guet, and H. B. Håkansson, *Nucl. Phys.* **A386**, 79 (1982).

[Bar+ 86] J. Bartel, G. Wenes, M. Waroquier, and J. Ryckebusch, *Modern Physics Letters* **A1**, 509 (1986).

[BB 36] H. A. Bethe and R. F. Bacher, *Rev. Mod. Phys.* **8**, 82 (1936).

[BB 71] J. Binstock and R. A. Bryan, *Phys. Rev. D* **4**, 1341 (1971).

[BB 75] S. Barshay and G. E. Brown, *Phys. Rev. Lett.* **34**, 1106 (1975).

[BBP 63] H. A. Bethe, B. H. Brandow, and A. G. Petschek, *Phys. Rev.* **129**, 225 (1963).

[BC 58] J. S. Ball and G. F. Chew, *Phys. Rev.* **109**, 1385 (1958).

[BC 79] D. M. Bishop and L. M. Cheung, *Phys. Rev. A* **20**, 381 (1979).

[BCP 36] G. Breit, E. Condon, and R. Present, *Phys. Rev.* **50**, 825 (1936).

[BCS 78] R. A. Brandenburg, S. A. Coon, and P. U. Sauer, *Nucl. Phys.* **A294**, 305 (1978).

[BD 64] J. D. Bjorken and S. D. Drell, *Relativistic Quantum Mechanics*, McGraw-Hill, New York (1964).

[BD 65] J. D. Bjorken and S. D. Drell, *Relativistic Quantum Fields*, McGraw-Hill, New York (1965).

[BDR 63] R. A. Bryan, C. R. Dismukes, and W. Ramsey, *Nucl. Phys.* **45**, 353 (1963).

[BDR 79] W. W. Buck, C. B. Dover, and J. M. Richard, *Ann. Phys. (N. Y.)* **121**, 47 (1979).

[Bér+ 73] R. W. Bérard, F. R. Buskirk, E. B. Dally, J. N. Dyer, X. K. Maruyama, R. L. Topping, and T. J. Traverso, *Phys. Lett.* **47B**, 355 (1973).

[Ber+ 85] R. Bertini, P. Birien, K. Braune, W. Brückner, G. Bruge, H. Catz, A. Chaumeaux, J. Ciborowski, H. Döbbeling, J. M. Durand, R. W. Frey, D. Garreta, S. Janouin, T. J. Ketel, K. Kilian, H. Kneis, S. Majewski, B. Mayer, J. C. Peng, B. Povh, R. D. Ransome, R. Szwed, T. A. Shibata, A. Thiessen, M. Treichel, M. Uhrmacher, and T. Walcher, *Phys. Lett.* **158B**, 19 (1985).

[Bet 40] H. A. Bethe, *Phys. Rev.* **57**, 260, 390 (1940).

[Bet 49] H. A. Bethe, *Phys. Rev.* **76**, 38 (1949).

[Bet 53] H. A. Bethe, *Scientific American* **189**, No. 3, p. 58 (1953).

[Bet 56] H. A. Bethe, *Phys. Rev.* **103**, 1353 (1956).

[Bet 71] H. A. Bethe, *Ann. Rev. Nucl. Sci.* **21**, 93 (1971).

[BF 36] G. Breit and E. Feenberg, *Phys. Rev.* **50**, 850 (1936).

[BG 58] K. A. Brueckner and J. L. Gammel, *Phys. Rev.* **109**, 1023 (1958).

[BG 72] R. A. Bryan and A. Gersten, *Phys. Rev. D* **6**, 341 (1972).

[BGB 76] J. P. Blaizot, D. Gogny, and B. Grammaticos, *Nucl. Phys.* **A265**, 315 (1976).

[BGG 53] K. A. Brueckner, M. Gell-Mann, and M. Goldberger, *Phys. Rev.* **90**, 476 (1953).

[BGG 68] G. E. Brown, A. M. Green, and W. J. Gerace, *Nucl. Phys.* **A115**, 435 (1968).

[BGH 85] M. Brack, C. Guet, and H. B. Håkansson, *Phys. Reports* **123**, 275 (1985).

[BH 55] H. A. Bethe and F. de Hoffmann, *Mesons and Fields*, Vol. II, Row, Peterson and Co., Evanston, Ill., U. S. A., (1955).

[Bha 38] H. J. Bhabha, *Proc. Roy. Soc. (London)* **A166**, 501 (1938).

[Bha 39] H. J. Bhabha, *Nature* **143**, 276 (1939).

[BHM 81] X. Bagnoud, K. Holinde, and R. Machleidt, *Phys. Rev. C* **24**, 1143 (1981).

[BHM 84] X. Bagnoud, K. Holinde, and R. Machleidt, *Phys. Rev. C* **29**, 1792 (1984).

[Bie+ 78] E. K. Biegert, J. A. Buchanan, J. M. Clement, W. H. Dragoset, R. D. Felder, J. H. Hoftiezer, K. R. Hogstrom, J. Hudomalj-Gabitzsch, J. D. Lesikar, W. P. Madigan, G. S. Mutchler, G. C. Phillips, J. B. Roberts, T. M. Williams, K. Abe, R. C. Fernow, T. A. Mulera, S. Bart, B. W. Mayes, and L. Pinsky, *Phys. Lett.* **73B**, 235 (1978).

[Bin 71] J. Binstock, *Phys. Rev. D* **3**, 1139 (1971).

[BJ 74] H. A. Bethe and M. B. Johnson, *Nucl. Phys.* **A230**,1 (1974).

[BJ 76] G. E. Brown and A. D. Jackson, *The Nucleon-Nucleon Interaction*, North-Holland, Amsterdam (1976).

[BJK 69] G. E. Brown, A. D. Jackson, and T. T. S. Kuo, *Nucl. Phys.* **A133**, 481 (1969).

[BK 87] F. Bishop and H. G. Kümmel, *Physics Today* **40**, No. 3, p. 52 (1987).

[BL 55] K. A. Brueckner and C. A. Levinson, *Phys. Rev.* **97**, 1344 (1955).

[BL 81] M. Betz and T.-S. H. Lee, *Phys. Rev. C* **23**, 375 (1981).

[BL 82] J. Bystricky and F. Lehar, Nucleon-Nucleon Scattering Data, *Physics Data* **11-1** to **11-3** (1978–1982).

[Bla 80] J. P. Blaizot, *Phys. Reports* **65**, 171 (1980).

[Bli 73] R. J. Blin-Stoyle, in *Fundamental Interaction in Nuclei*, Ch. 11, North-Holland, Amsterdam (1973).

[BLM 54] K. A. Brueckner, C. A. Levinson, and H. M. Mahmoud, *Phys. Rev.* **95**, 217 (1954).

[BLS 80] C. Bourrely, E. Leader, and J. Soffer, *Phys. Reports* **59**, 95 (1980).

[BM 84] R. Brockmann and R. Machleidt, *Phys. Lett.* **149B**, 283 (1984).

[BM 88] R. Brockmann and R. Machleidt, *to be published*, (1988).

[Bol 71] M. Bolsterli, *Ann. Phys. (N. Y.)* **62**, 569 (1971).

[Bor+ 82] I. Borbely, W. Grüebler, V. König, P. A. Schmelzbach, and B. Jenny, *Phys. Lett.* **109B**, 262 (1982).

[BP 68] R. A. Bryan and R. J. N. Phillips, *Nucl. Phys.* **B5**, 201 (1968).

[BPW 70] W. D. Brown, R. D. Puff, and L. Wilets, *Phys. Rev. C* **2**, 331 (1970).

[Bra 64] B. H. Brandow, *Ph. D. thesis*, Cornell University (1964).

[Bra 66] B. H. Brandow, *Phys. Rev.* **152**, 863 (1966).

[Bra 67] B. H. Brandow, *Rev. Mod. Phys.* **39**, 771 (1967).

[Bra 70] B. H. Brandow, *Ann. Phys. (N. Y.)* **57**, 214 (1970).

[Bra 77] B. H. Brandow, *Advances in Quantum Chemistry* **10**, 187 (1977).

[Bra+ 88a] R. A. Brandenburg, G. S. Chulick, Y. E. Kim, D. J. Klepacki, R. Machleidt, A. Picklesimer, and R. M. Thaler, *Phys. Rev. C*, **37**, 781 (1988).

[Bra+ 88b] R. A. Brandenburg, G. S. Chulick, R. Machleidt, A. Picklesimer, and R. M. Thaler, to be published in *Phys. Rev. C* (1988).

[Bre 37] G. Breit, *Phys. Rev.* **51**, 248 (1937).

[Bre 60a] G. Breit, *Proc. Nat. Acad. Sci. (U. S.)* **46**, 746 (1960).

[Bre 60b] G. Breit, *Phys. Rev.* **120**, 287 (1960).

[Bre 62] G. Breit, *Rev. Mod. Phys.* **34**, 776 (1962).

[Bre+ 60] G. Breit, M. H. Hull, K. E. Lassila, and K. D. Pyatt, *Phys. Rev.* **120**, 2227 (1960).

[Bro 79] G. E. Brown, in *Mesons in Nuclei* (M. Rho and D. H. Wilkinson, eds.), Vol. I, p. 330, North-Holland, Amsterdam (1979).

[Bro 81] R. Brockmann, *Phys. Lett.* **104B**, 256 (1981).

[Bro 84] S. J. Brodsky, *Comments Nucl. Part. Phys.* **12**, 213 (1984).

[Bro+ 87] G. E. Brown, W. Weise, G. Baym, and J. Speth, *Comments Nucl. Part. Phys.* **17**, 39 (1987).

[Bru 54] K. A. Brueckner, *Phys. Rev.* **96**, 508 (1954).

[Bru 55] K. A. Brueckner, *Phys. Rev.* **100**, 36 (1955).

[BS 38] G. Breit and J. R. Stehn, *Phys. Rev.* **53**, 459 (1938).

[BS 64] R. A. Bryan and B. L. Scott, *Phys. Rev.* **135**, B434 (1964).

[BS 66] R. Blankenbecler and R. Sugar, *Phys. Rev.* **142**, 1051 (1966).

[BS 69] R. A. Bryan and B. L. Scott, *Phys. Rev.* **177**, 1435 (1969).

[Bug 81] D. V. Bugg, *Prog. Part. Nucl. Phys.* **7**, 47 (1981).

[Bug 85] D. V. Bugg, *Ann. Rev. Nucl. Part. Sci.* **35**, 295 (1985).

[BW 52] J. M. Blatt and V. F. Weisskopf, *Theoretical Nuclear Physics*, Wiley, New York (1952).

[BW 53] K. A. Brueckner and K. M. Watson, *Phys. Rev.* **90**, 699; **92**, 1023 (1953).

[BW 75] G. E. Brown and W. Weise, *Phys. Reports* **C22**, 281 (1975).

[BW 81] R. Brockmann and W. Weise, *Nucl. Phys.* **A355**, 365 (1981).

[Cav+ 87] J. M. Cavedon, B. Frois, D. Goutte, M. Huet, Ph. Leconte, X. H. Phan, S. K. Platchkov, C. N. Papanicolas, S. E. Williamson, W. Boeglin, I. Sick, and J. Heisenberg, *Phys. Rev. Lett.* **58**, 195 (1987).

[CB 87] S. A. Coon and R. C. Barrett, *Phys. Rev. C* **36**, 2189 (1987).

[CC 36] B. Cassen and E. U. Condon, *Phys. Rev.* **50**, 846 (1936).

[CDR 72] M. Chemtob, J. W. Durso, and D. O. Riska, *Nucl. Phys.* **B38**, 141 (1972).

[CG 34] J. Chadwick and M. Goldhaber, *Nature* **134**, 237 (1934).

[CG 81] S. A. Coon and W. Gloeckle, *Phys. Rev. C* **23**, 1790 (1981).

[CH 50] R. S. Christian and E. W. Hart, *Phys. Rev.* **77**, 441 (1950).

[Cha 32] J. Chadwick, *Proc. Roy. Soc. (London)* **A136**, 692 (1932).

[Cha+ 55] O. Chamberlain, E. Segrè, C. Wiegand, T. Ypsilantis, *Phys. Rev.* **100**, 947 (1955).

[Cha+ 57] O. Chamberlain, E. Segrè, R. D. Tripp, C. Wiegand, and T. J. Ypsilantis, *Phys. Rev.* **105**, 288 (1957).

[Che 75] M. Chemtob, in *Interaction Studies in Nuclei* (H. Jochim and B. Ziegler, eds.), p. 487, North-Holland, Amsterdam (1975).

[Che+ 57] G. F. Chew, M. L. Goldberger, F. E. Low, and Y. Nambu, *Phys. Rev.* **106**, 1377 (1957).

[Che 61] G. F. Chew, *S-Matrix Theory of Strong Interactions*, Benjamin, New York (1961).

[Chi 77] S. A. Chin, *Ann. Phys. (N. Y.)* **108**, 301 (1977).

[Chu+ 88] G. S. Chulick, C. Elster, R. Machleidt, A. Picklesimer, and R. M. Thaler, *preprint* (1988).

[CJ 86a] E. D. Cooper and B. K. Jennings, *Nucl. Phys.* **A458**, 717 (1986).

[CJ 86b] E. D. Cooper and B. K. Jennings, *Phys. Rev. D* **33**, 1509 (1986).

[CK 60] F. Coester and H. Kümmel, *Nucl. Phys.* **17**, 477 (1960).

[Cla+ 73] B. C. Clark, R. L. Mercer, D. G. Ravenhall, and A. M. Saperstein, *Phys. Rev. C* **7**, 466 (1973).

[Cla 86] B. C. Clark, in *Relativistic Dynamics and Quark-Nuclear Physics* (M. B. Johnson and A. Picklesimer, eds.), p. 302, Wiley, New York (1986).

[Clo 79] F. Close, *Introduction to Quarks and Partons*, Academic Press, London (1979).

[CM 86] C. Y. Cheung and R. Machleidt, *Phys. Rev. C* **34**, 1181 (1986).

[CM 87] G. A. Crawford and G. A. Miller, *Phys. Rev. C* **36**, 2569 (1987).

[Coe 58] F. Coester, *Nucl. Phys.* **7**, 421 (1958).

[Coe+ 70] F. Coester, S. Cohen, B. D. Day, and C. M. Vincent, *Phys. Rev. C* **1**, 769 (1970).

[Coo+ 79] S. A. Coon, M. D. Scadron, P. C. McNamee, B. R. Barrett, D. W. E. Blatt, and B. H. J. McKellar, *Nucl. Phys.* **A317**, 242 (1979).

[Coo+ 87] E. D. Cooper, B. K. Jennings, P. Guichon, and A. W. Thomas, *Nucl. Phys.* **A468**, 717 (1987).

[Côt+ 82] J. Côté, M. Lacombe, B. Loiseau, B. Moussallam, and R. Vinh Mau, *Phys. Rev. Lett.* **48**, 1319 (1982).

[CP 50] K. M. Case and A. Pais, *Phys. Rev.* **80**, 203 (1950).

[CPP 47] M. Conversi, E. Pancini, and O. Piccioni, *Phys. Rev.* **71**, 209, 557 (1947).

[CS 72] X. Campi and D. W. L. Sprung, *Nucl. Phys.* **A194**, 401 (1972).

[CS 82a] S. A. Coon and M. D. Scadron, *Phys. Rev. C* **26**, 562 (1982).

[CS 82b] S. A. Coon and M. D. Scadron, *Phys. Rev. C* **26**, 2402 (1982).

[CS 86a] L. S. Celenza and C. M. Shakin, *Relativistic Nuclear Physics: Theories of Structure and Scattering*, Lecture Notes in Physics, Vol. 2, World Scientific, Singapore (1986).

[CS 86b] G. Co' and J. Speth, *Phys. Rev. Lett.* **57**, 547 (1986).

[CSB 75] S. A. Coon, M. D. Scadron, and B. R. Barrett, *Nucl. Phys.* **A242**, 467 (1975).

[CSM 77] S. A. Coon, M. D. Scadron, and P. C. McNamee, *Nucl. Phys.* **A287**, 381 (1977).

[Czi+ 59] P. Cziffra, M. H. MacGregor, M. J. Moravcsik, and H. P. Stapp, *Phys. Rev.* **114**, 880 (1959).

[Dan 71] M. Danos, *Ann. Phys. (N. Y.)* **63**, 319 (1971).

[Day 67] B. D. Day, *Rev. Mod. Phys.* **39**, 719 (1967).

[Day 78] B. D. Day, *Rev. Mod. Phys.* **50**, 495 (1978).

[Day 81a] B. D. Day, *Phys. Rev. C* **24**, 1203 (1981).

[Day 81b] B. D. Day, *Phys. Rev. Lett.* **47**, 226 (1981).

[DBS 84] J. W. Durso, G. E. Brown, and M. Saarela, *Nucl. Phys.* **A430**, 653 (1984).

[DC 76] B. D. Day and F. Coester, *Phys. Rev. C* **13**, 1720 (1976).

[DFM 82] W. H. Dickhoff, A. Faessler, and H. Müther, *Nucl. Phys.* **A389**, 492 (1982).

[DG 79] M. Danos and V. Gillet, in *Mesons in Nuclei* (M. Rho and D. Wilkinson, eds.) Vol. III, p. 839, North-Holland, Amsterdam (1979).

[DG 80] J. Dechargé and D. Gogny, *Phys. Rev. C* **21**, 1568 (1980).

[Die+ 75] R. Diebold, D. S. Ayres, S. L. Kramer, A. J. Pawlicki, and A. B. Wicklund, *Phys. Rev. Lett.* **35**, 632 (1975).

[Dil 75] W. Dilg, *Phys. Rev. C* **11**, 103 (1975).

[DJV 80] J. W. Durso, A. D. Jackson, and B. J. VerWest, *Nucl. Phys.* **A345**, 471 (1980).

[DKS 82] J. Dubach, W. M. Kloet, and R. R. Silbar, *J. Phys. G* **8**, 475 (1982).

[DKS 87] J. Dubach, W. M. Kloet, and R. R. Silbar, *Nucl. Phys.* **A466**, 573 (1987).

[DL 68] C. B. Dover and R. H. Lemmer, *Phys. Rev.* **165**, 1105 (1968).

[DL 69] C. B. Dover and R. H. Lemmer, *Phys. Rev.* **183**, 908 (1969).

[Dov 84] C. B. Dover, *Nucl. Phys.* **A416**, 313c (1984).

[Dov 86] C. B. Dover, *Phys. Rev. Lett.* **57**, 1207 (1986).

[Dov+ 86] C. B. Dover, A. Gal, L. Klieb, and D. J. Millener, *Phys. Rev. Lett.* **56**, 119 (1986).

[DR 79] C. B. Dover and J. M. Richard, *Ann. Phys. (N. Y.)* **121**, 70 (1979).

[DR 80] C. B. Dover and J. M. Richard, *Phys. Rev. C* **21**, 1466 (1980).

[DR 82] C. B. Dover and J. M. Richard, *Phys. Rev. C* **25**, 1952 (1982).

[Dub+ 81] J. Dubach, W. M. Kloet, A. Cass, and R. R. Silbar, *Phys. Lett.* **106B**, 29 (1981).

[Dub+ 82] R. Dubois, D. Axen, R. Keeler, M. Comyn, G. A. Ludgate, J. R. Richardson, N. M. Stewart, A. S. Clough, D. V. Bugg, and J. A. Edington, *Nucl. Phys.* **A377**, 554 (1982).

[Due 56] H. P. Duerr, *Phys. Rev.* **103**, 469 (1956).

[Dum+ 83] O. Dumbrajs, R. Koch, H. Pilkuhn, G. C. Oades, H. Behrens, J. J. de Swart, and P. Kroll, *Nucl. Phys.* **B216**, 277 (1983).

[Dur+ 77] J. W. Durso, M. Saarela, G. E. Brown, and A. D. Jackson, *Nucl. Phys.* **A278**, 445 (1977).

[Dut+ 86] A. K. Dutta, J. P. Arcoragi, J. M. Pearson, R. Behrman, and F. Tondeur, *Nucl. Phys.* **A458**, 77 (1986).

[DW 85] B. D. Day and R. B. Wiringa, *Phys. Rev. C* **32**, 1057 (1985).

[Dym+ 88] R. Dymarz, C. J. Morningstar, R. Gourishankar, and F. C. Khana, *preprint, University of Alberta at Edmonton*, Alberta THY-5-88 (1988).

[ECM 85] R. G. Ellis, S. A. Coon, and B. H. J. McKellar, *Nucl. Phys.* **A438**, 631 (1985).

[Els 86] Ch. Elster, *Ph. D. thesis*, University of Bonn, W. Germany (1986).

[Els+ 87] Ch. Elster, K. Holinde, D. Schütte, and R. Machleidt, *preprint, University of Bonn* (1987).

[EM 83] T. E. O. Ericson and G. A. Miller, *Phys. Lett.* **132B**, 32 (1983).

[EO 31] P. Ehrenfest and J. Oppenheimer, *Phys. Rev.* **37**, 333 (1931).

[ER 83] T. E. O. Ericson and M. Rosa-Clot, *Nucl. Phys.* **A405**, 497 (1983).

[ER 85] T. E. O. Ericson and M. Rosa-Clot, *Ann. Rev. Nucl. Part. Sci.* **35**, 271 (1985).

[Eri 84] T. E. O. Ericson, *Comments Nucl. Part. Phys.* **13**, 157 (1984).

[Erk 74] K. Erkelenz, *Phys. Reports* **13C**, 191 (1974).

[Erw+ 61] A. R. Erwin, R. March, W. D. Walker, and E. West, *Phys. Rev. Lett.* **6**, 628 (1961).

[Eul 37] H. Euler, *Z. Physik* **105**, 553 (1937).

[EW 41] L. Eisenbud and W. Wigner, *Proc. Natl. Acad. Sci. (U. S.)* **27**, 281 (1941).

[Fea 87] H. W. Fearing, *Nucl. Phys.* **A463**, 95c (1987).

[Fer 34] E. Fermi, *Z. Physik* **88**, 161 (1934).

[Fer 54] E. Fermi, *Nuovo Cim.* **11**, 407 (1954).

[FF 59] W. R. Frazer and J. R. Fulco, *Phys. Rev. Lett.* **2**, 365 (1959).

[FF 60] W. R. Frazer and J. R. Fulco, *Phys. Rev.* **117**, 1609 (1960).

[FGP 84] J. L. Friar, B. F. Gibson, and G. L. Payne, *Ann. Rev. Nucl. Part. Sci.* **34**, 403 (1984).

[FGP 88] J. L. Friar, B. F. Gibson, and G. L. Payne, *Los Alamos preprint* LA-UR-88-96 (1988).

[FK 35] E. Feenberg and J. K. Knipp, *Phys. Rev.* **48**, 906 (1935).

[FK 81] R. C. Fernow and A. D. Krisch, *Ann. Rev. Nucl. Part. Sci.* **31**, 107 (1981).

[FK 87] G. Fink and H. O. Klages, *private communication* (1987).

[FLM 80] C. Fayard, G. H. Lamot, and T. Mizutani, *Phys. Rev. Lett.* **45**, 524 (1980).

[FM 57] J. I. Fujita and H. Miyazawa, *Prog. Theor. Phys.* **17**, 360 (1957).

[FM 77] B. A. Freedman and L. D. McLerran, *Phys. Rev. D* **16**, 1169 (1977).

[FN 73] G. Faí and J. Németh, *Nucl. Phys.* **A208**, 463 (1973).

[FP 87] B. Frois and C. N. Papanicolas, *Ann. Rev. Nucl. Part. Sci.* **37**, 133 (1987).

[FS 80] W. Ferchländer and D. Schütte, *Phys. Rev. C* **22**, 2536 (1980).

[FT 75] J. Fleischer and J. A. Tjon, *Nucl. Phys.* **B84**, 375 (1975).

[FT 77] J. Fleischer and J. A. Tjon, *Phys Rev. D* **15**, 2537 (1977).

[FT 80] J. Fleischer and J. A. Tjon, *Phys Rev. D* **21**, 87 (1980).

[FT 84] E. E. van Faassen and J. A. Tjon, *Phys. Rev. C* **30**, 285 (1984).

[FT 86] E. E. van Faassen and J. A. Tjon, *Phys. Rev. C* **33**, 2105 (1986).

[Gal 85] A. Gal, *Nucl. Phys.* **A434**, 381c (1985).

[Gar 55] S. Gartenhaus, *Phys. Rev.* **100**, 900 (1955).

[Gar 82] H. Garcilazo, *Phys. Rev. Lett.* **48**, 577 (1982).

[Gar 87] H. Garcilazo, *Phys. Rev. C* **35**, 1804, 1820 (1987).

[GCT 57] J. L. Gammel, R. S. Christian, and R. M. Thaler, *Phys. Rev.* **105**, 311 (1957).

[GH 74] A. M. Green and P. Haapakoski, *Nucl. Phys.* **A221**, 429 (1974).

[GK 62] N. K. Glendenning and G. Kramer, *Phys. Rev.* **126**, 2159 (1962).

[GK 80] W. Grein and P. Kroll, *Nucl. Phys.* **A338**, 332 (1980).

[GKT 82] R. P. Goddard, L. D. Knutson, and J. A. Tostevin, *Phys. Lett.* **118B**, 241 (1982).

[GL 48] E. Gardner and C. M. G. Lattes, *Science* **107**, 270 (1948).

[GL 60] M. Gell-Mann and M. Lévy, *Nuovo Cim.* **16**, 705 (1960).

[GL 79] P. Grangé and A. Lejeune, *Nucl. Phys.* **A327**, 335 (1979).

[GN 75] A. M. Green and J. A. Niskanen, *Nucl. Phys.* **A249**, 493 (1975).

[GN 84] A. M. Green and J. A. Niskanen, *International Review of Nuclear Physics* **2** (1984).

[GNS 78] A. M. Green, J. A. Niskanen and M. E. Sainio, *J. Phys. G* **4**, 1055 (1978).

[Gol 57] J. Goldstone, *Proc. Roy. Soc. (London)* **A239**, 267 (1957).

[Gol 60] M. L. Goldberger, *Proc. Midwestern Conf. on Theor. Phys.*, p. 50, Purdue University, Lafayette, Ind., U.S.A. (1960).

[Gol+ 87] T. Goldman, G. J. Stephenson, K. R. Maltman, and K. E. Schmidt, Los Alamos *preprint* LA-UR-87-3922 (1987).

[Gre 67] A. E. S. Green, *Rev. Mod. Phys.* **39**, 495 (1967).

[Gre 77] W. Grein, *Nucl. Phys.* **B131**, 255 (1977).

[Gre 79] A. M. Green, in *Mesons in Nuclei* (M. Rho and D. Wilkinson, eds.), p. 227, North-Holland, Amsterdam (1979).

[Gro 69] F. Gross, *Phys. Rev.* **186**, 1448 (1969).

[GS 65] A. E. S. Green and R. D. Sharma, *Phys. Rev. Lett.* **14**, 380 (1965).

[GS 67] A. E. S. Green and R. D. Sawada, *Nucl. Phys.* **B2**, 267 (1967).

[GS 72] A. M. Green and T. H. Schucan, *Nucl. Phys.* **A188**, 289 (1972).

[GS 79] A. M. Green and M. E. Sainio, *J. Phys. G* **5**, 503 (1979).

[GT 57] J. L. Gammel and R. M. Thaler, *Phys. Rev.* **107**, 291, 1339 (1957).

[GT 60] J. L. Gammel and R. M. Thaler, *Prog. Elem. Part. Cosmic Ray Phys.* **5**, 97 (1960).

[GTG 71] A. Gersten, R. Thompson, and A. E. S. Green, *Phys. Rev. D* **3**, 2076 (1971).

[GV 83] J. H. Gruben and B. J. VerWest, *Phys. Rev. C* **28**, 836 (1983).

[HA 78] G. Horlacher and H. Arenhövel, *Nucl. Phys.* **A300**, 348 (1978).

[Har+ 85] J. W. Harris, R. Bock, R. Brockmann, A. Sandoval, R. Stock, H. Stroebele, G. Odyniec, H. G. Pugh, L. S. Schroeder, R. E. Renfordt, D. Schall, D. Bangert, W. Rauch, and K. L. Wolf, *Phys. Lett.* **153B**, 377 (1985).

[Hei 32] W. Heisenberg, *Z. Physik* **77**, 1 (1932).

[Hen 69] E. M. Henley, in *Isospin in Nuclear Physics* (D. H. Wilkinson, ed.), p. 16, North-Holland, Amsterdam (1969).

[HGB 83] E. Hadjimichael, B. Goulard, and R. Bornais, *Phys. Rev C* **27**, 831 (1983).

[HH 29] W. Heitler and G. Herzberg, *Naturwiss.* **17**, 673 (1929).

[Hid+ 77] H. Hidaka, A. Beretvas, K. Nield, H. Spinka, D. Underwood, Y. Watanabe, and A. Yokosawa, *Phys. Lett.* **70B**, 479 (1977).

[Hip 88] T. Hippchen, *Ph. D. thesis*, University of Bonn (1988).

[HJ 62] T. Hamada and I. D. Johnston, *Nucl. Phys.* **34**, 382 (1962).

[HJS 49] O. Haxel, J. H. D. Jensen, and H. E. Suess, *Phys. Rev.* **75**, 1766 (1949).

[HKM 83] E. M. Henley, L. S. Kisslinger, and G. A. Miller, *Phys. Rev. C* **28**, 1277 (1983).

[HLM 61] N. Hoshizaki, I. Lin, and S. Machida, *Prog. Theor. Phys.* **26**, 680 (1961).

[HM 62] N. Hoshizaki and S. Machida, *Prog. Theor. Phys. (Kyoto)* **27**, 288 (1962).

[HM 75] K. Holinde and R. Machleidt, *Nucl. Phys.* **A247**, 495 (1975).

[HM 76] K. Holinde and R. Machleidt, *Nucl. Phys.* **A256**, 479, 497 (1976).

[HM 77] K. Holinde and R. Machleidt, *Nucl. Phys.* **A280**, 429 (1977).

[HM 79] E. M. Henley and G. A. Miller, in *Mesons in Nuclei* (M. Rho and D. H. Wilkinson, eds.), Vol. I, p. 406, North-Holland, Amsterdam (1979).

[HM 81] K. Holinde and R. Machleidt, *Nucl. Phys.* **A372**, 349 (1981).

[HM 84] I. Hulthage and F. Myhrer, *Phys. Rev.* **30**, 298 (1984).

[HM 87] B. ter Haar and R. Malfliet, *Phys. Reports* **149**, 207 (1987).

[Höh+ 76] G. Höhler, E. Pietarinen, I. Sabba-Stefanesu, F. Borkowski, G. G. Simon, V. H. Walther, and R. D. Wendling, *Nucl. Phys.* **B114**, 505 (1976).

[Höh+ 79] G. Höhler, F. Kaiser, R. Koch, and E. Pietarinen, Handbook of Pion-Nucleon Scattering, *Physics Data* **12-1** (1979).

[Hol+ 78] K. Holinde, R. Machleidt, M. R. Anastasio, A. Faessler, and H. Müther, *Phys Rev C* **18**, 870 (1978).

[Hol+ 79] K. Holinde, R. Machleidt, M. R. Anastasio, A. Faessler, and H. Müther, *Phys Rev C* **19**, 948 (1979).

[Hol+ 81] K. Holinde, R. Machleidt, M. R. Anastasio, A. Faessler, and H. Müther, *Phys Rev C* **24**, 1159 (1981).

[Hos 68] N. Hoshizaki, Prog. Theor. Phys. (Kyoto), Supplement **42**, 107 (1968).

[Hou 71] T. L. Houk, *Phys. Rev. C* **3**, 1886 (1971).

[HP 75] G. Höhler and E. Pietarinen, *Nucl. Phys.* **B95**, 210 (1975).

[HS 57] L. Hulthén and M. Sugawara, *Encyclopedia of Physics* **39**, 1 (1957).

[HS 81] C. J. Horowitz and B. D. Serot, *Nucl. Phys.* **A368**, 503 (1981).

[HS 87] C. J. Horowitz and B. D. Serot, *Nucl. Phys.* **A464**, 613 (1987).

[HSS 83] C. Hajduk, P. U. Sauer, and W. Strueve, *Nucl. Phys.* **A405**, 581 (1983).

[HSY 83] C. Hajduk, P. U. Sauer, and S. N. Yang, *Nucl. Phys.* **A405**, 605 (1983).

[HT 70] M. I. Haftel and F. Tabakin, *Nucl. Phys.* **A158**, 1 (1970).

[HT 71] M. I. Haftel and F. Tabakin, *Phys. Rev. C* **3**, 921 (1971).

[IH 56] J. Iwadare and S. Hatano, *Prog. Theor. Phys. (Japan)* **15**, 185 (1956).

[IJL 73] F. Iachello, A. D. Jackson, and A. Landé, *Phys. Lett.* **B43**, 191 (1973).

[Iwa+ 55] J. Iwadare, S. Otsuki, R. Tanagaki, and R. Watari, *Prog. Theor. Phys. (Kyoto)* **15**, 86 (1955).

[Iwa+ 56] J. Iwadare, S. Otsuki, R. Tanagaki, and R. Watari, *Prog. Theor. Phys. (Kyoto)* **16**, 455 (1956).

[IZ 80] C. Itzykson and J. B. Zuber, *Quantum Field Theory*, McGraw-Hill, New York (1980).

[Jas 51] R. Jastrow, *Phys. Rev.* **81**, 165 (1951).

[Jas 55] R. Jastrow, *Phys. Rev.* **98**, 1479 (1955).

[JH 44] J. M. Jauch and N. Hu, *Phys. Rev.* **65**, 289 (1944).

[JLM 75] J. P. Jeukenne, A. Lejeune, and C. Mahaux, *Nucl. Phys.* **A245**, 411 (1975).

[JLM 76] J. P. Jeukenne, A. Lejeune, and C. Mahaux, *Phys. Reports* **25**, 83 (1976).

[JRK 83] A. D. Jackson, M. Rho, and E. Krotschek, *Nucl. Phys* **A407**, 495 (1983).

[JRV 75] A. D. Jackson, D. O. Riska, and B. Verwest, *Nucl. Phys.* **A249**, 397 (1975).

[Käl 64] G. Källen, *Elementary Particle Physics*, Addison-Wesley, Reading, Mass., U.S.A. (1964).

[KB 66] T. T. S. Kuo and G. E. Brown, *Nucl. Phys.* **85**, 40 (1966).

[KD 69] A. Kallio and B. D. Day, *Nucl. Phys.* **A124**, 177 (1969).

[Kel+ 39] J. Kellog , I. Rabi, N. F. Ramsey, and J. Zacharias, *Phys. Rev.* **55**, 318; **56**, 728 (1939).

[Kel+ 40] J. Kellog , I. Rabi, N. F. Ramsey, and J. Zacharias, *Phys. Rev.* **57**, 677 (1940).

[Kem 38a] N. Kemmer, *Proc. Roy. Soc. (London)* **A166**, 127 (1938).

[Kem 38b] N. Kemmer, *Proc. Cambridge Phil. Soc.* **34**, 354 (1938).

[Kem 39] N. Kemmer, *Proc. Roy. Soc. (London)* **A173**, 91 (1939).

[Kim+ 88] Kr. T. Kim, Y. E. Kim, D. J. Klepacki, R. A. Brandenburg, E. P. Harper, and R. Machleidt, *Purdue University preprint*, PNTG-88-1 (1988).

[Kit+ 86] P. Kitching, D. A. Hutcheon, K. Michaelian, R. Abegg, G. H. Coombes, W. K. Dawson, H. Fielding, G. Gaillard, P. Green, L. G. Greeniaus, M. Hugi, C. A. Miller, G. C. Neilson, W. C. Olson, J. Soukup, N. R. Stevenson, J. Wesick, H. W. Fearing, and R. L. Workman, *Phys. Rev. Lett.* **19**, 2363 (1986).

[Kla+ 86] S. Klarsfeld, J. Martorell, J. A. Oteo, M. Nishimura, and D. W. L. Sprung, *Nucl. Phys.* **A456**, 373 (1986).

[Kle 58] A. Klein, *Prog. Theor. Phys. (Kyoto)* **20**, 357 (1958).

[KLZ 78] H. Kümmel, K. H. Lührmann, and J. G. Zabolitzky, *Phys. Reports* **36**, 1 (1978).

[KMS 76] K. Kotthoff, R. Machleidt, and D. Schütte, *Nucl. Phys.* **A264**, 484 (1976).

[KMS 84] S. Klarsfeld, J. Martorell, and D. W. L. Sprung, *J. Phys. G: Nucl. Phys.* **10**, 165 (1984).

[Koe 75] H. S. Koehler, *Phys. Reports* **18**, 217 (1975).

[Kot+ 75] K. Kotthoff, K. Holinde, R. Machleidt, and D. Schütte, *Nucl. Phys.* **A242**, 429 (1975).

[Koo+ 87] N. Koori *et al.*, in *Proc. of the XI. International Conference on Few Body Systems in Particle and Nuclear Physics*, Contributed Papers, Contribution 6-7, Tokyo and Sendai (Japan), August 1986.

[KP 80] R. Koch and E. Pietarinen, *Nucl. Phys.* **A336**, 331 (1980).

[Kri 85] A. D. Krisch, Lecture at the *School on High Energy Spin Physics*, Lake Louise, Canada (1985).

[Kro 81] P. Kroll, *Physics Data* **22-1**, Fachinformationszentrum, Karlsruhe, W. Germany (1981).

[KS 69] M. W. Kermode and D. W. L. Sprung, *Nucl. Phys.* **A135**, 535 (1969).

[KS 80] W. M. Kloet and R. R. Silbar, *Nucl. Phys.* **A338**, 281, 317 (1980).

[KS 81] W. M. Kloet and R. R. Silbar, *Nucl. Phys.* **A364**, 346 (1981).

[KT 75] T. E. Kalogeropoulos and G. S. Tzanakos, *Phys. Rev. Lett.* **34**, 1047 (1975).

[KW 86] B. Keister and R. Wiringa, *Phys. Lett.* **B173**, 5 (1986).

[LA 82] C. van der Leun and C. Alderliesten, *Nucl. Phys.* **A380**, 261 (1982).

[Lac+ 75] M. Lacombe, B. Loiseau, J. M. Richard, R. Vinh Mau, P. Pires, and R. de Tourreil, *Phys. Rev. D* **12**, 1495 (1975).

[Lac+ 80] M. Lacombe, B. Loiseau, J. M. Richard, R. Vinh Mau, J. Côté, P. Pires, and R. de Tourreil, *Phys. Rev. C* **21**, 861 (1980).

[Lac+ 81] M. Lacombe, B. Loiseau, J. M. Richard, R. Vinh Mau, J. Côté, P. Pires, and R. de Tourreil, *Phys. Lett.* **B101**, 139 (1981).

[Las+ 62] K. E. Lassila, M. H. Hull, H. M. Ruppel, F. A. McDonald, and G. E. Breit, *Phys. Rev.* **126**, 881 (1962).

[Lee 83] T.-S. H. Lee, *Phys. Rev. Lett.* **50**, 1571 (1983).

[Lee 84] T.-S. H. Lee, *Phys. Rev. C* **29**, 195 (1984).

[LG 86] J. M. Lina and B. Goulard, *Phys. Rev. C* **34**, 714 (1986).

[Lin 65] I. Lindgren, in *Alpha-, Beta-, Gamma-Spectroscopy* (K. Siegbahn, ed.), Vol. II, p. 1623, North-Holland, Amsterdam (1965).

[Lom 76] E. L. Lomon, *Phys. Rev. D* **14**, 2402 (1976).

[Lom 77] E. L. Lomon, *Phys. Lett.* **B68**, 419 (1977).

[Lom 80a] E. L. Lomon, *Phys. Rev. D* **22**, 229 (1980).

[Lom 80b] E. L. Lomon, *Ann. Phys. (N. Y.)* **125**, 309 (1980).

[Lom 82] E. L. Lomon, *Phys. Rev. D* **26**, 576 (1982).

[LOP 47] C. M. G. Lattes, G. P. S. Occhialini, and C. F. Powell, *Nature* **160**, 453, 486 (1947).

[LP 81] I. E. Lagaris and V. R. Pandharipande, *Nucl. Phys.* **A359**, 349 (1981).

[LSS 86] M. P. Locher, M. E. Sainio, and A. Švarc, in *Advances in Nuclear Physics* (J. W. Negele and E. Vogt, eds.), Vol. 17, p. 47, Plenum Press, New York (1986).

[LT 63] A. A. Logunov and A. N. Tavkhelidze, *Nuovo Cim.* **29**, 380 (1963).

[Lur 68] D. Lurié, *Particles and Fields*, Interscience, New York (1968).

[Mac 67] S. Machida, *Prog. Theor. Phys. (Kyoto), Supplement* **67**, 91 (1967).

[Mac 82] R. Machleidt, *unpublished* (1982).

[Mac 86] R. Machleidt, in *Relativistic Dynamics and Quark-Nuclear Physics* (M. B. Johnson and A. Picklesimer, eds.), p. 71, Wiley, New York (1986).

[Mag+ 61] B. C. Maglić, L. W. Alvarez, A. H. Rosenfeld, and M. L. Stevenson, *Phys. Rev. Lett.* **7**, 178 (1961).

[Mah 79] C. Mahaux, *Nucl. Phys.* **A328**, 24 (1979).

[Maj 33] E. Majorana, *Z. Physik* **82**, 137 (1933).

[Man 58] S. Mandelstam, *Phys. Rev.* **112**, 1344 (1958).

[Man 62] S. Mandelstam, *Rep. Prog. Phys.* **25** (1962).

[Mar 61] A. Martin, *Phys. Rev.* **124**, 614 (1961).

[MAS 78] P. J. G. Mulders, A. T. M. Aerts, and J. J. de Swart, *Phys. Rev. Lett.* **40**, 1543 (1978).

[MAW 69] M. H. MacGregor, R. A. Arndt, and R. A. Wright, *Phys. Rev.* **182**, 1714 (1969).

[May 49] M. G. Mayer, *Phys. Rev.* **75**, 1969 (1949).

[MB 85] R. Machleidt and R. Brockmann, *Phys. Lett.* **160B**, 364 (1985).

[Mcc 60] J. McConnell, *Prog. Elem. Part. Cosmic Ray Phys.* **5**, 205 (1960).

[MEH 74] R. Machleidt, K. Erkelenz, and K. Holinde, *Nucl. Phys.* **A232**, 398 (1974).

[MG 78] W. Manzke and M. Gari, *Nucl. Phys.* **A312**, 457 (1978).

[MH 80] R. Machleidt and K. Holinde, *Nucl. Phys.* **A350**, 396 (1980).

[MH 85] R. Machleidt and K. Holinde, *Phys. Lett.* **152B**, 295 (1985).

[MHE 87] R. Machleidt, K. Holinde, and C. Elster, *Phys. Reports* **149**, 1 (1987).

[MHN 75] R. Machleidt, K. Holinde, and J. Németh, *Nucl. Phys.* **A251**, 93 (1975).

[MJ 55] M. G. Mayer and J. H. D. Jensen, *Elementary Theory of Nuclear Shell Structure*, John Wiley and Sons, New York (1955).

[ML 86] A. Matsuyama and T.-S. H. Lee, *Phys. Rev. C* **34**, 1900 (1986).

[MMB 87] H. Müther, R. Machleidt, and R. Brockmann, *Phys. Lett.* **198B**, 45 (1987).

[MMB 88] H. Müther, R. Machleidt, and R. Brockmann, *Phys. Lett.* **202B**, 483 (1988).

[MMF 75] R. Machleidt, H. Müther, and A. Faessler, *Nucl. Phys.* **A241**, 18 (1975).

[MMM 87] R. Machleidt, T. Mizutani, and F. Myhrer, *unpublished* (1987).

[Mor 63] M. J. Moravcsik, *The Two-Nucleon Interaction*, Clarendon Press, Oxford (1951).

[Mor 72] M. J. Moravcsik, *Rep. Prog. Phys.* **35**, 587 (1972).

[MR 40] C. Møller and L. Rosenfeld, *Kgl. Danske Vid. Selskab, Math.-Fys. Medd.* **17**, No. 8 (1940).

[MR 79] B. H. J. McKellar and R. Rajaraman, in *Mesons in Nuclei* (M. Rho and D. Wilkinson, eds.), Vol. I, p. 357, North-Holland, Amsterdam (1979).

[MRV 80] L. Montanet, G. C. Rossi, and G. Veneziano, *Phys. Reports* **63**, 149 (1980).

[MS 60] S. A. Moskowski and B. L. Scott, *Ann. Phys. (N. Y.)* **11**, 65 (1960).

[MS 69] W. D. Myers and W. J. Swiatecki, *Ann. Phys. (N. Y.)* **55**, 395 (1969).

[MT 76] F. Myhrer and A. W. Thomas, *Phys. Lett.* **64B**, 59 (1976).

[MTW 86] G. A. Miller, A. W. Thomas, and A. G. Williams, *Phys. Rev. Lett.* **56**, 2567 (1986).

[Müt 84] H. Müther, *Prog. Part. Nucl. Phys.* **14**, 123 (1984).

[MZ 86] U. G. Meissner and I. Zahed, in *Advances in Nuclear Physics* (J. W. Negele and E. Vogt, eds.), Vol. 17, p. 143, Plenum Press, New York (1986).

[NA 37] S. H. Neddermeyer and C. D. Anderson, *Phys. Rev.* **51**, 884 (1937).

[Nak 69] N. Nakanishi, *Prog. Theor. Phys. (Kyoto), Supplement* **43**, 1 (1969).

[Nam 57] Y. Nambu, *Phys. Rev.* **106**, 1366 (1957).

[NDT 76] *Atomic Data and Nuclear Data Tables* **17**, Nos. 5-6 (1976).

[Neg 70] J. W. Negele, *Phys. Rev. C* **1**, 1260 (1970).

[Neg 71] J. W. Negele, *Nucl. Phys.* **A165**, 305 (1971).

[Neg 74] J. W. Negele, *Comments Nucl. Part. Phys.* **6**, 15 (1974).

[Neg 82] J. W. Negele, *Rev. Mod. Phys.* **54**, 913 (1982).

[Neg 85] J. W. Negele, *Comments Nucl. Part. Phys.* **14**, 303 (1985).

[NGS 79] G. H. Niephaus, M. Gari, and B. Sommer, *Phys. Rev. C* **20**, 1096 (1979).

[NKS 84] K. Nakayama, S. Krewald, and J. Speth, *Nucl. Phys.* **A431**, 419 (1984).

[Noy 72] H. P. Noyes, *Ann. Rev. Nucl. Sci.* **22**, 465 (1972).

[NRS 73] M. M. Nagels, T. A. Rijken, and J. J. de Swart, *Ann. Phys. (N. Y.)* **79**, 338 (1973).

[NRS 78] M. M. Nagels, T. A. Rijken, and J. J. de Swart, *Phys. Rev. D* **17**, 768 (1978).

[NRS 79] M. M. Nagels, T. A. Rijken, and J. J. de Swart, *Phys. Rev. D* **20**, 1633 (1979).

[NS 69] J. A. Nolen, Jr., and J. P. Schiffer, *Ann. Rev. Nucl. Sci.* **19**, 471 (1969).

[Nut 76] W. T. Nutt, *Ann. Phys. (N. Y.)* **100**, 490 (1976).

[NW 75] W. T. Nutt and L. Wilets, *Phys. Rev. D* **7**, 110 (1975).

[Nym 79] E. M. Nyman, in *Mesons in Nuclei* (M. Rho and D. H. Wilkinson, eds.), Vol. III, p. 889, North-Holland, Amsterdam (1979).

[Occ+ 47] G. P. S. Occhialini, C. F. Powell, C. M. G. Lattes, and H. Muirhead, *Nature* **159**, 186, 694 (1947).

[OCR 54] C. L. Oxley, W. F. Cartwright, and J. Rouvina, *Phys. Rev.* **93**, 806 (1954).

[Oga+ 67] S. Ogawa, S. Sawada, T. Ueda, W. Watari, and M. Yonezawa *Prog. Theor. Phys. (Kyoto), Supplement* **39**, 140 (1967).

[OM 58] S. Okubo and R. E. Marshak, *Ann. Phys. (N. Y.)* **4**, 166 (1958).

[PA 86] B. C. Pearce and I. R. Afnan, *Phys. Rev. C* **34**, 991 (1986).

[Pau 46] W. Pauli, *Meson Theory of Nuclear Forces*, Interscience, New York (1946).

[Pav+ 78] P. Pavlopoulos, G. Backenstoss, P. Blüm, K. Fransson, R. Guigas, N. Hassler, M. Izycki, H. Koch, A. Nilsson, H. Poth, M. Suffert, L. Tauscher, and K. Zioutas, *Phys. Lett.* **72B**, 415 (1978).

[PDG 74] Particle Data Group, *Phys. Lett.* **50B**, 6, 74 (1974).

[PDG 76] Particle Data Group, *Rev. Mod. Phys.* **48**, S26, S114 (1976).

[PDG 84] Particle Data Group, *Rev. Mod. Phys.* **56**, S1 (1984).

[Pet 84] H. R. Petry, in *Quarks and Nuclear Structure* (K. Bleuler, ed.), Lecture Notes in Physics Vol. **197**, p. 236, Springer, New York (1984).

[PFG 80] G. L. Payne, J. L. Friar, and B. F. Gibson, *Phys. Rev. C* **22**, 832 (1980).

[PH 39] H. Primakoff and H. Holstein, *Phys. Rev.* **55**, 1218 (1939).

[Phi 59] R. J. N. Phillips, *Rep. Prog. Phys.* **22**, 562 (1959).

[Phi 67] R. J. N. Phillips, *Rev. Mod. Phys.* **39**, 681 (1967).

[Pir 79] H. J. Pirner, *Phys. Lett.* **85B**, 190 (1979).

[PL 70] M. H. Partovi and E. L. Lomon, *Phys. Rev. D* **2**, 1999 (1970).

[PL 72] M. H. Partovi and E. L. Lomon, *Phys. Rev. D* **5**, 1192 (1972).

[Pro 36] A. Proca, *J. Phys. Radium* **7**, 347 (1936).

[PSZ 87] H. Pöpping, P. U. Sauer, and Zhang, Xi-Zhen, *Nucl. Phys.* **A474**, 557 (1987). University of Hannover (1987).

[PW 79] V. R. Pandharipande and R. B. Wiringa, *Rev. Mod. Phys.* **51**, 821 (1979).

[RB 67] R. Rajaraman and H. A. Bethe, *Rev. Mod. Phys.* **39**, 745 (1967).

[RC 74] D. O. Riska and Y. H. Chu, *Nucl. Phys.* **A235**, 499 (1974).

[Rei 68] R. V. Reid, *Ann. Phys. (N. Y.)* **50**, 411 (1968).

[Rin 83] A. S. Rinat, *Nucl. Phys.* **A397**, 381 (1983).

[RK 86] N. L. Rodning and L. D. Knutson, *Phys. Rev. Lett.* **57**, 2248 (1986).

[Ros 45] L. Rosenfeld, *Nature* **145**, 141 (1945).

[Ros 48] L. Rosenfeld, *Nuclear Forces*, North-Holland, Amsterdam (1948).

[RS 41a] W. Rarita and J. Schwinger, *Phys. Rev.* **59**, 436, 556 (1941).

[RS 41b] W. Rarita and J. Schwinger, *Phys. Rev.* **60**, 61 (1941).

[RT 77] A. S. Rinat and A. W. Thomas, *Nucl. Phys.* **A282**, 365 (1977).

[Rut 11] E. Rutherford, *Phil. Mag.* **21**, 669 (1911).

[RV 75] R. V. Reid and M. L. Vaida, *Phys. Rev. Lett.* **34**, 1064 (1975).

[RW 79] M. Rho and D. H. Wilkinson, eds., *Mesons in Nuclei*, Vol. I–III, North-Holland, Amsterdam (1979).

[Sak 60a] J. J. Sakurai, *Ann. Phys. (N. Y.)* **11**, 1 (1960).

[Sak 60b] J. J. Sakurai, Phys. Rev. **119**, 1784 (1960).

[Sak 60c] J. J. Sakurai, *Nuovo Cim.* **16**, 388 (1960).

[Sam 88] F. Sammarruca, *Ph. D. thesis*, Virginia Polytechnical Institute and State University, Blacksburg, Virginia (1988).

[Saw+ 62] S. Sawada, T. Ueda, W. Watari, and M. Yonezawa, *Prog. Theor. Phys.* **28**, 991 (1962).

[SB 51] E. E. Salpeter and H. A. Bethe, *Phys. Rev.* **84**, 1232 (1951).

[SC 63] M. Sobel and A. Cromer, *Phys. Rev.* **132**, 2698 (1963).

[Sch 42] J. Schwinger, *Phys. Rev.* **61**, 387 (1942).

[Sch 51] L. I. Schiff, *Phys. Rev.* **84**, 1, 10 (1951).

[Sch 61] S. S. Schweber, *An Introduction to Relativistic Quantum Field Theory*, Row, Peterson and Co., Evanston, Ill., U.S.A. (1961).

[Sch 72] G. Schierholz, *Nucl. Phys.* **B40**, 335 (1972).

[Sch 74] D. Schütte, *Nucl. Phys.* **A221**, 450 (1974).

[Sch 83] D. Schütte, *Nucl. Phys.* **A411**, 369 (1983).

[Seg 58] E. Segrè, *Ann. Rev. Nucl. Sci.* **8**, 127 (1958).

[Seg 77] E. Segrè, *Nuclei and Particles*, Benjamin, London (1977).

[Ser 63] R. Serber, *Phys. Rev. Lett.* **10**, 357 (1963).

[SF 74] A. de Shalit and H. Feshbach, *Theoretical Nuclear Physics*, Vol. I, Wiley, New York (1974).

[SH 68] H. Sugawara and F. von Hippel, *Phys. Rev.* **172**, 1764 (1968).

[Sha 36] S. S. Share, *Phys. Rev.* **50**, 488 (1936).

[Sha 78] I. S. Shapiro, *Phys. Reports* **C35**, 129 (1978).

[SHS 83] W. Strueve, C. Hajduk, and P. U. Sauer, *Nucl. Phys.* **A405**, 620 (1983).

[Sie 70] P. J. Siemens, *Nucl. Phys.* **A141**, 225 (1970).

[Sig 69] P. Signell, in *Advances in Nuclear Physics* (J. W. Negele and E. Vogt, eds.), Vol. 2, p. 223, Plenum Press, New York (1969).

[Sim 83] M. Simonius, *Nucl. Phys.* **A396**, 203c (1983).

[Sim 87] M. Simonius, *Nucl. Phys.* **A463**, 283c (1987).

[Sky 59] T. H. R. Skyrme, *Nucl. Phys.* **9**, 615 (1959).

[Sla 87] I. Šlaus, in *Few-Body Systems, Supplement 1*, Proc. European Workshop on Few-Body Physics (C. Ciofi degli Atti, O. Benhar, E. Pace, and G. Salmè, eds.), p. 160, Springer, Wien (1987).

[SM 58] P. Signell and R. Marshak, *Phys. Rev.* **109**, 1229 (1958).

[SZM 58] P. Signell, R. Zinn, and R. Marshak, *Phys. Rev. Lett.* **1**, 416 (1958).

[Spr 72] D. W. L. Sprung, in *Advances in Nuclear Physics* (J. W. Negele and E. Vogt, eds.), Vol. 5, p. 225, Plenum Press, New York (1972).

[SP 76] R. A. Smith and V. R. Pandharipande, *Nucl. Phys.* **A256**, 327 (1976).

[SS 37] J. C. Street and E. C. Stevenson, *Phys. Rev.* **51**, 1005A (1937).

[SSW 81] G. G. Simon, Ch. Schmitt, and V. H. Walther, *Nucl. Phys.* **A364**, 285 (1981).

[Sto+ 82] R. Stock, R. Bock, R. Brockmann, J. W. Harris, A. Sandoval, H. Stroebel, and K. L. Wolf, *Phys. Rev. Lett.* **49**, 1236 (1982).

[Sup 55] *Prog. Theor. Phys. (Kyoto), Supplement* **1** and **2** (1955).

[Sup 56] *Prog. Theor. Phys. (Kyoto), Supplement* **3** (1956).

[Sup 67] *Prog. Theor. Phys. (Kyoto), Supplement* **39** (1967).

[SW 63] A. Scotti and D. Y. Wong, *Phys. Rev. Lett.* **10**, 142 (1963).

[SW 65] A. Scotti and D. Y. Wong, *Phys. Rev.* **138**, 145 (1965).

[SW 86] B. D. Serot and J. D. Walecka, in *Advances in Nuclear Physics* (J. W. Negele and E. Vogt, eds.), Vol. 16, p. 1, Plenum Press, New York (1986).

[Swa 87] J. J. de Swart, *private communication* (1987).

[SYM 57] H. P. Stapp, T. J. Ypsilantis, and N. Metropolis, *Phys. Rev.* **105**, 302 (1957).

[TG 87] G. F. de Téramond and B. Gabioud, *Phys. Rev. C* **36**, 691 (1987).

[THH 36] M. Tuve, N. Heydenburg, and L. Hafstad, *Phys. Rev.* **50**, 806 (1936).

[Thi 86] M. Thies, *Phys. Lett.* **166B**, 23 (1986).

[Tho 13] J. J. Thompson, *Rays of Positive Electricity*, Longmans, Green (1913).

[Tho 70] R. H. Thompson, *Phys. Rev. D* **1**, 110 (1970).

[Tho 83] A. W. Thomas, in *Advances in Nuclear Physics* (J. W. Negele and E. Vogt, eds.), Vol. 13, p. 1, Plenum Press, New York (1983).

[TMM 85] R. Tegen, T. Mizutani, and F. Myhrer, *Phys. Rev. D* **32**, 1672 (1985).

[TMO 52] M. Taketani, S. Machida, and S. Onuma, *Prog. Theor. Phys. (Kyoto)* **7**, 45 (1952).

[TNS 51] M. Taketani, S. Nakamura, and M. Sasaki, *Proc. Theor. Phys. (Kyoto)* **6**, 581 (1951).

[TRS 75] R. de Tourreil, B. Rouben, and D. W. L. Sprung, *Nucl. Phys.* **A242**, 445 (1975).

[TS 73] R. de Tourreil and D. W. L. Sprung, *Nucl. Phys.* **A201**, 193 (1973).

[TSS 84] P. H. Timmers, W. A. van der Sanden, and J. J. de Swart, *Phys. Rev. D* **29**, 1928 (1984).

[UNG 73] T. Ueda, M. Nack, and A. E. S. Green, *Phys. Rev. C* **8**, 2061 (1973).

[Vin 79] R. Vinh Mau, in *Mesons in Nuclei* (M. Rho and D. H. Wilkinson, eds.), Vol. I, p. 151, North-Holland, Amsterdam (1979).

[Vin+ 73] R. Vinh Mau, J. M. Richard, B. Loiseau, M. Lacombe, and W. N. Cottingham, *Phys. Lett.* **44B**, 1 (1973).

[WA 52] L. Wolfenstein and J. Ashkin, *Phys. Rev.* **85**, 947 (1952).

[Wal 74] J. D. Walecka, *Ann. Phys. (N. Y.)* **83**, 491 (1974).

[Wal 87] S. J. Wallace, *Ann. Rev. Nucl. Part. Sci.* **37**, 267 (1987).

[Wat 53] K. M. Watson, *Phys. Rev.* **89**, 575 (1953).

[Wei 35] C. F. von Weizäcker, *Z. Physik* **96**, 431 (1935).

[Wei 67] S. Weinberg, *Phys. Rev. Lett.* **18**, 188 (1967).

[Wen 49] G. Wenzel, *Quantum Theory of Fields*, Interscience, New York (1949).

[WF 86] R. L. Workman and H. W. Fearing, *Phys. Rev. C* **34**, 780 (1986).

[WHW 83] M. Waroquier, K. Heyde, and G. Wenes, *Nucl. Phys.* **A404**, 269 (1983).

[Wic 38] G. Wick, *Nature* **142**, 993 (1938).

[Wig 33] E. Wigner, *Phys. Rev.* **43**, 252 (1933).

[Wil 63] R. Wilson, *The Nucleon-Nucleon Interaction*, Interscience, New York (1963).

[Wil 69] D. H. Wilkinson, ed., *Isospin in Nuclear Physics*, North-Holland, Amsterdam (1969).

[Wil 79] L. Wilets, in *Mesons in Nuclei* (M. Rho and D. H. Wilkinson, eds.), Vol. III, p. 791, North-Holland, Amsterdam (1979).

[WJ 72] R. Woloshyn and A. D. Jackson, *Nucl. Phys.* **A185**, 131 (1972).

[WJ 73] R. Woloshyn and A. D. Jackson, *Nucl. Phys.* **B64**, 269 (1973).

[Wol 56] L. Wolfenstein, *Ann. Rev. Nucl. Sci.* **6**, 43 (1956).

[Won 59] D. Y. Wong, *Phys. Rev. Lett.* **2**, 406 (1959).

[Won 86] C. W. Wong, *Phys. Reports* **136**, 1 (1986).

[WSA 84] R. B. Wiringa, R. A. Smith, and T. L. Ainsworth, *Phys. Rev. C* **29**, 1207 (1984).

[Yae 71] R. J. Yaes, *Phys. Rev. D* **3**, 3086 (1971).

[Yam 87] T. Yamazaki, *Nucl. Phys.* **A463**, 39c (1987).

[Yan 84] S. N. Yang, in *Few Body Problems in Physics* (B. Zeitnitz, ed.), Vol. II, p. 111, North-Holland, Amsterdam (1984).

[Ynd 83] F. J. Ynduráin, *Quantum Chromodynamics*, Springer, New York (1983).

[Yok 80] A. Yokosawa, *Phys. Reports* **64**, 47 (1980).

[You+ 77] D. H. Youngblood, C. M. Rozsa, J. M. Moss, D. R. Brown, and J. D. Bronson, *Phys. Rev. Lett.* **39**, 1188 (1977).

[YS 37] H. Yukawa and S. Sakata, *Proc. Phys. Math. Soc. Japan* **19**, 1084 (1937).

[YST 38] H. Yukawa, S. Sakata, and M. Taketani, *Proc. Phys. Math. Soc. Japan* **20**, 319 (1938).

[Yuk 35] H. Yukawa, *Proc. Phys. Math. Soc. Japan* **17**, 48 (1935).

[Yuk 37] H. Yukawa, *Proc. Phys. Math. Soc. Japan* **19**, 712 (1937).

[Yuk+ 38] H. Yukawa, S. Sakata, M. Kobayasi, and M. Taketani, *Proc. Phys. Math. Soc. Japan* **20**, 720 (1938).

[ZB 86] I. Zahed and G. E. Brown, *Phys. Reports* **142**, 1 (1986).

[ZT 81] M. J. Zuilhof and J. A. Tjon, *Phys. Rev. C* **24**, 736 (1981).